

STRENGTHENING PERFORMANCE OF REINFORCED
CONCRETE BEAM USING COMBINED EXTERNALLY
BONDED AND NEAR SURFACE MOUNTED TECHNIQUES

KH. MAHFUZ UD DARAIN

FACULTY OF ENGINEERING
UNIVERSITY OF MALAYA
KUALA LUMPUR

2016

**STRENGTHENING PERFORMANCE OF
REINFORCED CONCRETE BEAM USING COMBINED
EXTERNALLY BONDED AND NEAR SURFACE
MOUNTED TECHNIQUES**

KH. MAHFUZ UD DARAIN

**THESIS SUBMITTED IN FULFILMENT OF THE
REQUIREMENTS FOR THE DEGREE OF DOCTOR OF
PHILOSOPHY**

**FACULTY OF ENGINEERING
UNIVERSITY OF MALAYA
KUALA LUMPUR**

2016

UNIVERSITY OF MALAYA
ORIGINAL LITERARY WORK DECLARATION

Name of Candidate: Kh Mahfuz ud Darain

Registration/Matric No: KHA120024

Name of Degree: Doctor of Philosophy (PhD)

Title of Project Paper/Research Report/Dissertation/Thesis (“this Work”):

**STRENGTHENING PERFORMANCE OF REINFORCED
CONCRETE BEAM USING COMBINED EXTERNALLY BONDED
AND NEAR SURFACE MOUNTED TECHNIQUES**

Field of Study: Structural Engineering and Materials

I do solemnly and sincerely declare that:

- (1) I am the sole author/writer of this Work;
- (2) This Work is original;
- (3) Any use of any work in which copyright exists was done by way of fair dealing and for permitted purposes and any excerpt or extract from, or reference to or reproduction of any copyright work has been disclosed expressly and sufficiently and the title of the Work and its authorship have been acknowledged in this Work;
- (4) I do not have any actual knowledge nor do I ought reasonably to know that the making of this work constitutes an infringement of any copyright work;
- (5) I hereby assign all and every rights in the copyright to this Work to the University of Malaya (“UM”), who henceforth shall be owner of the copyright in this Work and that any reproduction or use in any form or by any means whatsoever is prohibited without the written consent of UM having been first had and obtained;
- (6) I am fully aware that if in the course of making this Work I have infringed any copyright whether intentionally or otherwise, I may be subject to legal action or any other action as may be determined by UM.

Candidate’s Signature

Date:

Subscribed and solemnly declared before,

Witness’s Signature

Date:

Name:

Designation:

ABSTRACT

Structural strengthening is a technique to upgrade and improve existing structural systems to carry additional loads and prolong design life. Various structural strengthening techniques are now being used in the construction industry. Among these techniques, the externally bonded reinforcement (EBR) technique is the most common. However, it has a tendency to fail by debonding failure at the plate curtailment location. This is due to interfacial shear stress, which increases with increasing plate thickness. The near surface mounted (NSM) technique is comparatively new and more efficient. Nevertheless, it exhibits premature failure when multiple grooves are used within a narrow cross-sectional width.

The aim of this research was to develop a strengthening solution to improve the structural performance of RC beams while avoiding premature failure. To achieve this objective, this study proposed a combination of the EBR and NSM techniques, calling it the combined externally bonded and near surface mounted (CEBNSM) technique. In this study, the performance of RC beams strengthened with the CEBNSM technique were investigated experimentally. An artificial intelligence technique was used to predict the serviceability behavior of these strengthened beams. The finite element method (FEM) was also used to simulate the structural behavior of the strengthened beams.

The experimental test matrix consisted of a total of twenty-seven RC beams divided into four groups. Round steel or CFRP bars were used in the NSM grooves for the CEBNSM-B beams, whereas rectangular CFRP strips were inserted into the CEBNSM-S beams. In both cases, CFRP fabric was externally bonded at the tension face of the beam soffit. NSM and EBR strengthened beams were also tested in order to compare results with the CEBNSM technique. Fuzzy logic expert system (FLES) was used as an

artificial intelligence (AI) tool to predict the serviceability behavior of the strengthened beams. Incremental static load and variable NSM bar length were the input parameters and the outputs were deflection and crack width of the strengthened beams. Applying expert knowledge using *if-then* rules, the input and output variables were expressed linguistically as well as in numeric values. FEM was applied to develop a numerical model to verify the experimental results of the strengthened RC beams. The plastic damage behavior of concrete, elasto-plastic behavior of steel reinforcement and material nonlinearity were considered in developing the FEM model.

Beams strengthened with NSM CFRP showed greater increment in strength, although they failed prematurely, in contrast to the flexural failure of steel bar NSM beams whose stiffness and cracking behavior were superior as well. For CEBNSM beams, the ultimate capacity increased from 32% to 176%, depending on the variation in strengthening reinforcement ratio. The failure mode, serviceability and stiffness of the beams also improved considerably. The output of the AI models excellently predicted the deflection and crack width of the strengthened beams. In evaluating the FLES prediction model, it was found that the relative error of the predicted deflection and crack width values were within the acceptable limit (5%) and the goodness of fit of the predicted values was close to 1.0. The results simulated by the FEM model satisfactorily agreed with the load-deflection and strain values of the CEBNSM strengthened RC beams. The simulated damage pattern of the beams also matched well with the experimental beams.

ABSTRAK

Pengukuhan struktur adalah teknik untuk memperelokkan dan memperbaiki sistem struktur sedia ada untuk menerima beban tambahan dan menambah jangka hayatnya. Pelbagai jenis teknik pengukuhan struktur telah digunakan dalam industri pembinaan. Antara teknik-teknik yang ada, pengukuhan terikat luaran (EBR) adalah yang paling biasa digunakan. Namun, teknik ini selalunya gagal disebabkan nyah-ikatan pada lokasi hujung plat. Ini disebabkan tegasan ricih antara muka, yang meningkat dengan peningkatan ketebalan plat. Teknik pemasangan berhampiran permukaan (NSM) adalah satu teknik yang agak baru dan lebih efisien. Namun, teknik ini juga menunjukkan kegagalan pra-matang apabila beberapa alur digunakan dalam satu keratan rentas kelebaran yang sempit.

Kajian ini bertujuan untuk mengahaislkan satu teknik pengukuhan yang akan meningkatkan prestasi struktur dan mengelakkan kegagalan pra-matang untuk rasuk RC. Untuk mencapai matlamat ini, kajian ini mencadangkan gabungan teknik-teknik EBR dan NSM, yang akan dipanggil teknik gabungan terikat luaran dan pemasangan dekat permukaan (CEBNSM). Dalam kajian ini, prestasi rasuk CEBNSM akan disiasat secara ujikaji makmal. Teknik kecerdasan buatan akan digunakan untuk meramal tingkah laku ketika servis bagi rasuk-rasuk yang diperkukuhkan ini. Kaedah unsur terhingga (FEM) juga akan digunakan untuk mensimulasi tingkah laku struktur rasuk yang diperkukuhkan.

Matriks ujikaji makmal terdiri daripada dua puluh tujuh rasuk RC yang dibahagikan kepada empat kumpulan. Keluli atau CFRP berbentuk bulat telah digunakan dalam alur NSM untuk rasuk CEB-NSM-B, manakala CRP berbentuk empat segi telah dimasukkan ke dalam rasuk CEBNSM-S. Dalam kedua-dua kes ini, fabrik CFRP telah dipasang secara terikat luaran ke atas muka tegangan di permukaan bawah rasuk. Rasuk NSM

dan EBR yang diperkukuhkan juga telah diuji untuk membandingkan keputusan dengan teknik CEBNSM. Sistem fuzzy logik pakar (FLES) telah digunakan sebagai alat kecerdasan buatan (AI) untuk meramalkan tingkah laku ketika servis bagi rasuk-rasuk yang diperkukuhkan. Beban statik yang ditambah secara bertingkat dan panjang bar NSM yang berubah-ubah adalah parameter-parameter input yang digunakan manakala keputusan pula adalah pesongan dan lebar retakan untuk rasuk-rasuk yang diperkukuhkan. Penggunaan pengetahuan pakar dengan peraturan-peraturan jika-maka, input dan keputusan pembolehubah itu diungkapkan dengan ungkapan linguistik berserta dengan nilai-nilai numerik. FEM telah digunakan untuk membangunkan model berangka untuk mengesahkan keputusan ujikaji rasuk-rasuk RC yang diperkukuhkan. Tingkah laku kerosakan plasti bagi kontrit, tingkah laku elasto-plastik bagi tetulang keluli dan sifat ketaklurusan bahan telah dipertimbangkan untuk membangunkan model FEM ini.

Rasuk-rasuk yang diperkukuhkan dengan NSM CFRP menunjukkan kenaikan yang lebih besar dari segi kekuatan, walaupun mereka gagal secara pra-matang, berbanding dengan kegagalan lenturan bagi bar NSM keluli yang mempunyai kekakuan dan sifat retakan yang lebih bagi juga. Bagi rasuk-rasuk CEBNSM, keupayaan muktamad meningkat daripada 32% kepada 176%, bergantung kepada perubahan dalam mengukuhkan nisbah tetulang. Mod kegagalan, kebolehhidmatan dan kekukuhan rasuk juga bertambah baik dengan ketara. Keputusan model AI meramalkan dengan baik pesongan dan retak lebar bagi rasuk-rasuk yang diperkukuhkan. Untuk penilaian FLES, didapati bahawa kesilapan relatif pesongan yang diramalkan dan retak nilai lebar adalah dalam had yang boleh diterima (5%) dan kebaikan patut bagi nilai-nilai yang diramalkan adalah berhampiran dengan 1.0. Simulasi FEM memberikan keputusan yang memuaskan bagi ramalan beban-pesongan dan ketegangan nilai bagi rasuk-rasuk RC

yang diperkukuhkan dengan CEBNSM. Corak kerosakan bagi rasuk-rasuk yang telah disimulasi juga padan dengan baik dengan rasuk-rasuk tersebut.

University of Malaya

ACKNOWLEDGEMENTS

In the Name of Allah, The Beneficent, The Merciful, I would like to express my utmost gratitude and thanks to the almighty Allah (s.w.t) for the help and guidance that he has given me through all these years.

I would like to express my sincere appreciation and gratitude to my supervisor, Prof. Ir. Dr. Mohd Zamin Jumaat for his excellent supervision, guidance, encouragement and financial supports in carrying out this research work. I am deeply indebted to him.

Sincere and great appreciation goes to University Malaya High Impact Research Grant under Grant Account No: UMC/HIR/MOHE/ENG/36 (D000036-160001) for funding this research work.

I would like to thank all of the post graduate student of UM for their help, support, encouragement and standing beside me like a family member throughout the whole course.

Nothing would have been possible if I do not have the encouragement and blessing of my late parents and in-laws. My two sons are my inspiration in this whole endeavor. Last but not the least; the love, sympathy and constant support provided by my wife. Thank you all for your love and sacrifices.

TABLE OF CONTENTS

Abstract	ii
Abstrak	iv
Acknowledgements	vii
Table of Contents	viii
List of Figures	xv
List of Tables	xxi
List of Notations	xxii
List of Acronyms	xxv
CHAPTER 1: INTRODUCTION	1
1.1 Prelude	1
1.2 Background	1
1.3 Statement of the Problem	3
1.4 Arguments for the CEBNSM Technique	4
1.5 Research Questions	6
1.6 Objectives of the Study	7
1.7 Justification of the Research	7
1.8 Scope	9
1.9 Research Methodology	9
1.10 Outline of Thesis	10
CHAPTER 2: LITERATURE REVIEW	12
2.1 Methods of Strengthening	13
2.2 Externally Bonded Reinforcement (EBR) Strengthening Technique	14
2.2.1 Performance of EBR Strengthened RC Beam	18
2.2.2 Debonding Behavior of EBR Strengthened RC Beam	22
2.2.3 Anchorage Performance of EBR Strengthened RC Beam	26

2.3 Near Surface Mounted (NSM) Technique	29
2.3.1 Important Factors for NSM	30
2.3.1.1 Concrete Class	31
2.3.1.2 FRP Material	33
2.3.1.3 Groove Dimension	35
2.3.2 Performance of Near Surface Mounted (NSM) Strengthened RC Beam.....	36
2.3.3 Assessment of Bond Behavior of NSM Strengthening Technique	41
2.3.4 Debonding Failure Modes of NSM Strengthening Technique.....	43
2.3.5 Ductility Performance Using NSM Technique	44
2.3.6 Flexural Behavior of NSM Technique	46
2.4 Recent Works on Strengthening Materials and Techniques	49
2.4.1 Alternative Strengthening Materials	49
2.4.2 Other Options of Strengthening Techniques	53
2.4.3 Combination of Different Strengthening Techniques	55
2.4.3.1 T-Shaped NSM and EBR CFRP Strips	55
2.4.3.2 Hybrid Bonding Technique	56
2.5 Artificial Intelligence (AI) Technique	57
2.5.1 FLES Application in Structural Strengthening	57
2.6 Finite Element Modelling (FEM)	59
2.6.1 Application of FEM on Strengthened RC Beam.....	60
2.7 Summary of the Findings	64
CHAPTER 3: METHODOLOGY OF EXPERIMENTAL PROGRAM	67
3.1 Test Matrix	67
3.2 Material Properties	71
3.2.1 Concrete	72
3.2.2 Steel	72

3.2.3 CFRP Bar and Fabric	73
3.2.4 Epoxy Adhesive	74
3.3 Specimen Configuration and Preparation	74
3.3.1 Configuration of Control and Strengthened RC beam	74
3.3.2 Fabrication of RC Beam.....	76
3.3.3 Strengthening Procedure	79
3.3.3.1 Near Surface Mounted (NSM) Strengthening Procedure.....	79
3.3.3.2 EBR Strengthening Procedure	81
3.3.3.3 CEBNSM Strengthening Procedure.....	82
3.3.4 Test Setup and Instrumentation.....	84
3.3.4.1 Deflection Measurement	86
3.3.4.2 Strain Value.....	86
3.3.4.3 Crack Width Determination	87
3.3.4.4 Data Acquisition System.....	87
CHAPTER 4: EXPERIMENTAL RESULTS AND DISCUSSIONS.....	89
4.1 Experimental results.....	89
4.1.1 Control Beam for Group-A	89
4.1.2 NSM Strengthened Beams	92
4.1.2.1 Load Carrying Capacity	93
4.1.2.2 Load Deflection Curve	95
4.1.2.3 Failure Modes.....	97
4.1.2.4 Cracking Behavior.....	100
4.1.2.5 Ductility Analysis.....	107
4.1.2.6 Stiffness Assessment	111
4.1.2.7 Strain Measurement.....	116
4.1.3 Control Beam for Group B, C and D	118

4.1.4 Externally Bonded Strengthening with CFRP Fabric	120
4.1.4.1 Load Deflection Curve	121
4.1.4.2 Cracking Behavior.....	122
4.1.4.3 Failure Modes.....	124
4.1.4.4 Strain Measurement.....	126
4.1.5 CEBNSM-B Technique with CFRP and Steel NSM Bar	128
4.1.5.1 Load Carrying Capacity	128
4.1.5.2 Load Deflection Curve	130
4.1.5.3 Failure Modes.....	133
4.1.5.4 Cracking Behavior.....	138
4.1.5.5 Ductility Analysis.....	142
4.1.5.6 Stiffness Assessment.....	144
4.1.5.7 Strain Measurement.....	147
4.1.6 CEBNSM-S Technique with CFRP Strip	150
4.1.6.1 Load Carrying Capacity	150
4.1.6.2 Load Deflection Curve	152
4.1.6.3 Failure Modes.....	154
4.1.6.4 Cracking Behavior.....	157
4.1.6.5 Ductility Analysis.....	159
4.1.6.6 Stiffness Assessment.....	160
4.1.6.7 Strain Measurement.....	162
4.2 Parametric Analysis of Experimental Results.....	166
4.2.1 NSM Strengthened Beam.....	166
4.2.1.1 Effect of Bond Length.....	166
4.2.1.2 Effect of Strengthening Materials	167
4.2.2 CEBNSM-B Strengthened Beam	167

4.2.2.1	Effect of Area of Strengthening Materials	167
4.2.2.2	Effect of NSM Materials	168
4.2.2.3	Effect of EB CFRP Thickness.....	168
4.2.2.4	Effect of NSM Diameter	169
4.2.2.5	Effect of U-Wrap Anchorage	170
4.2.3	Comparison between EB and CEBNSM-B beams	171
4.2.4	CEBNSM-S Strengthened Beam	172
4.2.4.1	Effect of Area of Strengthening Materials	172
4.2.4.2	Effect of Number of Groove	173
4.2.4.3	Effect of Groove Dimension	173
4.2.5	Comparison between EB and CEBNSM-S beams.....	174
4.2.6	Comparison between CEBNSM-B and CEBNSM-S beams.....	175
4.3	Analytical Prediction Approach.....	177
4.3.1	Deflection Prediction.....	177
4.3.2	Deflection Prediction Model for NSM Strengthened RC beam.....	180
4.3.3	Optimum Bond Length of NSM Bar.....	187
4.3.4	Crack Width	188
CHAPTER 5: ARTIFICIAL INTELLIGENCE TECHNIQUE		191
5.1	Fuzzy Logic Expert System (FLES)	191
5.2	Basic Theory of FLES.....	192
5.2.1	Fuzzification.....	197
5.2.2	Rule base	198
5.2.3	Inference.....	198
5.2.4	Defuzzification	199
5.3	Serviceability Prediction Model Using FLES.....	200
5.3.1	FLES Model Development.....	200

5.3.2 Numerical Error Determination	205
5.3.3 Results of FLES Model	206
5.3.4 Model Validation.....	209
CHAPTER 6: FINITE ELEMENT MODELLING.....	212
6.1 Basic Steps of FEM.....	212
6.2 FEM Model Construction of CEBNSM-B beams	215
6.2.1 Material Properties and Constitutive Laws	216
6.2.1.1 Concrete	216
6.2.1.2 Internal Steel Bar.....	221
6.2.1.3 FRP	221
6.2.1.4 CFRP-Concrete Interface	222
6.2.2 Model Geometry	222
6.2.3 Loads	225
6.2.4 Mesh Sensitivity Analysis.....	226
6.3 Results of FEM simulation of CEBNSM-B beams	228
6.3.1 Load-deflection Comparison.....	229
6.3.2 Load-Strain Comparison	234
CHAPTER 7: CONCLUSIONS.....	239
7.1 NSM and EBR Strengthened RC Beams	239
7.2 Serviceability Prediction Model Using Fuzzy Logic	239
7.3 Combined Externally Bonded and Near Surface Mounted RC Beam	240
7.4 Performance of CEBNSM-B Strengthened RC Beam.....	240
7.5 Finite Element Analysis	241
7.6 Recommendation.....	241
REFERENCE	243
APPENDIX A	254

APPENDIX B	259
APPENDIX C	264
APPENDIX D	270
PUBLICATION	274

University of Malaya

LIST OF FIGURES

Figure 1.1: Methodology of the thesis	10
Figure 2.1: Reasons for strengthening of existing structure (Badawi, 2007).....	12
Figure 2.2: Ultimate capacity increment and cost variation of different strengthening technique (Hassan, 2002)	19
Figure 2.3: Single, double shear and pullout bending (Cruz, 2005) test configuration ..	23
Figure 2.4: Bilinear bond slip relationship (Ulaga et al., 2003).....	24
Figure 2.5: Bond-slip curve (Oller et al., 2011).....	25
Figure 2.6: Various anchorage schemes for FRP strengthened RC beams(Kotynia et al., 2008)	27
Figure 2.7: Type I, II and III anchorage device (Grelle & Sneed, 2013).....	28
Figure 2.8: Effect of concrete strength on failure load and FRP debonding strain(Soliman et al., 2010)	32
Figure 2.9: NSM groove dimension and nomenclatures by different authors (De Lorenzis & Teng, 2007; Parretti & Nanni, 2004)	36
Figure 2.10: Failure modes of the NSM strengthened test specimen (De Lorenzis & Nanni, 2001a).....	37
Figure 2.11: NSM groove geometry and effect of geometric parameters on FRP strain efficacy(Kalayci et al., 2010)	38
Figure 2.12: Force vs. Displacement of the tested beams under monotonic loading (Sena-Cruz et al., 2012)	39
Figure 2.13: Groove geometry and failure modes (Al-Mahmoud, F. et al., 2011).....	40
Figure 2.14: Average bond- slip curves of NSM CFRP (Sharaky et al., 2013).....	42
Figure 2.15: (a) Typical brittle response of FRP beam (b) response of all tested beams (Rasheed et al., 2010).....	44
Figure 2.16: Optimum ductility of un-fatigued and fatigued beam(Oudah, F. & El-Hacha, R., 2012).....	45
Figure 2.17: Load vs. Deflection of NSM CFRP rebar & strip and comparison of EBR & NSM(El-Hacha, R. & Rizkalla, S. H., 2004).....	47

Figure 2.18: Failure modes of the strengthened beams(Rahal & Rumaih, 2011).....	51
Figure 2.19: Rectangular and T-shaped CFRP strip (Lim, 2009).....	56
Figure 2.20: Detail modelling strategy of NSM bar and main reinforcement (Hawileh, 2011)	62
Figure 3.1: Steel bar used for specimen preparation.....	72
Figure 3.2: CFRP bar used for strengthening of RC beam	73
Figure 3.3: CFRP fabric used for strengthening of RC beam.....	74
Figure 3.4: (a) Beam dimension, (b) beam cross-section and reinforcement and (c) NSM groove details of series A beam	75
Figure 3.5: Preparation and casting of RC beam	77
Figure 3.6: Strengthening process of RC beam with NSM technique	80
Figure 3.7: Sequence of specimen preparation and strengthening.....	83
Figure 3.8: Instrumentation and loading setup.....	86
Figure 4.1: Load-deflection diagram of control beams for Group A.....	90
Figure 4.2: Failure modes of control beams for Group A.....	91
Figure 4.3: Steel strain value of control beams for Group A.....	92
Figure 4.4: Concrete strain of control beams for Group A	92
Figure 4.5: Percentile increment of different load levels of NSM beams.....	94
Figure 4.6: Percentile decrement of ultimate deflection of NSM beam	95
Figure 4.7: Load-deflection curve for NSM-CFRP strengthened beams.....	97
Figure 4.8: Load-deflection curve for NSM-steel strengthened beams	97
Figure 4.9: Failure mode of (a) N1.6F (b) N1.8F and (c) N1.9F RC beam.....	99
Figure 4.10: Failure mode of (a) N1.6S (b) N1.8S and (c) N1.9S RC beam.....	99
Figure 4.11: Crack spacing details of NSM beams.....	102
Figure 4.12: Crack pattern of the NSM strengthened beams	103

Figure 4.13: Load versus crack width of NSM strengthened RC beams	105
Figure 4.14: Deflection versus crack width of NSM strengthened RC beams	105
Figure 4.15: Crack width at 1 st crack and service load of NSM strengthened beams...	107
Figure 4.16: Various ductility index of NSM strengthened RC beam.....	108
Figure 4.17: Deformability and energy index of NSM strengthened beams	111
Figure 4.18: Yield and ultimate curvature of the NSM strengthened beam	112
Figure 4.19: Bending stiffness of the control and NSM strengthened beams.....	113
Figure 4.20: Comparison of concrete strain of NSM strengthened beams at 15,40 and 60 kN service load.....	116
Figure 4.21: Comparison of steel strain of NSM strengthened beams at 15,40 and 60 kN service load.....	117
Figure 4.22: Tensile strain at NSM CFRP and steel bar	118
Figure 4.23: Load-deflection curve of control beams for Group B, C and D	119
Figure 4.24: Failure modes of control beams for Group B, C and D.....	120
Figure 4.25: Load-deflection curve of EB strengthened beams.....	122
Figure 4.26: Crack spacing details of control and EB strengthened beams.....	123
Figure 4.27: Crack width details of control and EB strengthened beams	124
Figure 4.28: Failure modes of EB strengthened beams	125
Figure 4.29: Steel tensile strain of control and EB strengthened beams.....	126
Figure 4.30: CFRP fabric tensile strain profile of EBP1 beam.....	127
Figure 4.31: CFRP fabric tensile strain profile of EBP2 beam.....	127
Figure 4.32: Percentile increment of different load levels of CEBNSM-B beams over the control RC beam.....	129
Figure 4.33: Load-deflection curve of CEBNSM-B strengthened beams with CFRP bar	131
Figure 4.34: Load-deflection curve of CEBNSM-B beams with steel bar	132

Figure 4.35: Deflection reduction of CEBNSM-B strengthened beam	133
Figure 4.36: Failure modes of CEBNSM-B beams (a) to (g)	135
Figure 4.37: Crack spacing details of control and CEBNSM-B beams	138
Figure 4.38: Load vs. crack width diagram of CEBNSM-B beams.....	140
Figure 4.39: Various ductility index for CEBNSM-B beams	143
Figure 4.40: Bending stiffness of CFRP bar strengthened CEBNSM-B beams	144
Figure 4.41: Bending stiffness of steel bar strengthened CEBNSM-B beams	145
Figure 4.42: Comparison of concrete strain of CEBNSM-B beam at 15, 30 and 39 kN service load.....	147
Figure 4.43: Comparison of steel tensile strain of CEBNSM-B beam at 15, 30 and 39 kN service load.....	148
Figure 4.44: NSM CFRP strain of CEBNSM-B beams	149
Figure 4.45: NSM steel strain of CEBNSM-B beams	149
Figure 4.46: Percentile increment of different load levels of CEBNSM-S beams	151
Figure 4.47: Load-deflection curve of CEBNSM-S beams	152
Figure 4.48: Deflection reduction of CEBNSM-S beams.....	153
Figure 4.49: Failure modes of CEBNSM-S beams	155
Figure 4.50: Crack spacing details of control and CEBNSM-S beams	157
Figure 4.51: Load vs. crack width diagram of CEBNSM-S beams	158
Figure 4.52: Bending stiffness variation of CEBNSM-S beams	161
Figure 4.53: Comparison of concrete strain of CEBNSM-S beam at 15, 40 and 60 kN service load.....	163
Figure 4.54: Load-steel strain curve of CEBNSM-S beams	164
Figure 4.55: Comparison of steel tensile strain of CEBNSM-S beam at 15, 40 and 60 kN service load.....	164
Figure 4.56: NSM CFRP strip strain of CEBNSM-S beams	165

Figure 4.57: EB CFRP fabric strain of CEBNSM-S beams	165
Figure 4.58: Effect of bond length of NSM bar	166
Figure 4.59: Effect of area of CEBNSM-B strengthening materials	167
Figure 4.60: Effect of NSM strengthening materials on CEBNSM-B beams	168
Figure 4.61: Effect of EB CFRP fabric thickness on CEBNSM-B beams	169
Figure 4.62: Effect of variable diameter of NSM bar on CEBNSM-B beams	169
Figure 4.63: Effect of U-Wrap anchorage on CEBNSM-B beams	170
Figure 4.64: Comparison between EBP1 and single ply CEBNSM-B beams	171
Figure 4.65: Comparison between EBP1 and double ply CEBNSM-B beams	172
Figure 4.66: Effect of area of strengthening materials on CEBNSM-S beams	172
Figure 4.67: Effect of number of groove on CEBNSM-S beams	173
Figure 4.68: Comparison between EBP1 and single ply CEBNSM-S beams	175
Figure 4.69: Comparison between EBP2 and double ply CEBNSM-S beams	175
Figure 4.70: Typical moment of inertia variation with various moment	178
Figure 4.71: Strain and stress distribution of NSM strengthened beam	182
Figure 4.72: Experimental and analytical load-deflection diagram of N1.8F, N1.8S, N1.9F and N1.9S beams	185
Figure 4.73: Bending moment diagram with optimum length of NSM bar	187
Figure 5.1: Crisp set for hot temperature	194
Figure 5.2: Fuzzy set for hot temperature	194
Figure 5.3: Triangular membership function for input variables	195
Figure 5.4: Trapezoidal membership function for input variables	195
Figure 5.5: Flow chart of knowledge based approach	197
Figure 5.6: Fuzzy inference mechanisms	199

Figure 5.7: Membership functions of input variables a) load – F (kN) and b) NSM length – L (mm)	203
Figure 5.8: Rule viewer of fuzzy inference system.....	207
Figure 5.9: Control surfaces for steel bar.....	208
Figure 5.10: Control surfaces for CFRP bar	209
Figure 5.11: Experimental and predicted load deflection graphs for NSM steel beams	210
Figure 5.12: Experimental and predicted load deflection graphs for NSM CFRP beams	211
Figure 6.1: Response of concrete to uniaxial loading in tension (Abaqus documentation)	217
Figure 6.2: Response of concrete to uniaxial loading in compression (Abaqus documentation).....	217
Figure 6.3: Fracture energy cracking model (Abaqus documentation).....	219
Figure 6.4: Plane stress concrete failure surface (Abaqus documentation)	220
Figure 6.5: Elasto-plastic model for reinforcement	221
Figure 6.6: 3D non-linear finite element model of reinforcements	223
Figure 6.7: 3D finite element mesh of RC strengthened specimen.....	224
Figure 6.8: Applied Loading in the model.....	225
Figure 6.9: Comparison between the experimental and FE analysis for different mesh size.....	227
Figure 6.10: Tensile damage behavior of control beam with (a) 25, (b) 35 and (c) 35 mesh size	228
Figure 6.11: Comparison between experimental and FEM load-deflection behavior for control and CEBNSM-B strengthened RC beam (a) to (g)	230
Figure 6.12: load-strain behavior of CFRP fabric for control and CEBNSM-B strengthened RC beam (a) to (h)	234

LIST OF TABLES

Table 2.1: Methods of strengthening	14
Table 2.2: Failure modes of EBR strengthened RC beam (Obaidat, 2011; Smith & Teng, 2002a).....	16
Table 2.3: Usual mechanical properties of steel and FRP in different guidelines	33
Table 3.1: Test matrix of the experimental program.....	68
Table 4.1: Summary of experimental test results of NSM beams	94
Table 4.2: Experimental maximum, minimum and average crack spacing of NSM beams.....	102
Table 4.3: Summary of different ductility index of NSM beams	107
Table 4.4: Summary of experimental test results of EB beams	121
Table 4.5: Experimental maximum, minimum and average crack spacing of EB beams	123
Table 4.6: Summary of experimental test results of CEBNSM-B beams.....	129
Table 4.7: Experimental maximum, minimum and average crack spacing of CEBNSM-B beams	139
Table 4.8: Service load and corresponding crack width of CEBNSM-B beams	142
Table 4.9: Summary of different ductility index of CEBNSM-B beams.....	142
Table 4.10: Summary of experimental test results of CEBNSM-S beams	151
Table 4.11: Experimental maximum, minimum and average crack spacing of CEBNSM-S beams	157
Table 4.12: Summary of different ductility index of CEBNSM-S beams	160
Table 5.1: Fuzzy inference rules	202
Table 6.1: Mesh sensitivity analysis for FEM model with different mesh size.....	226
Table 6.2: Comparison between experimental and FEM output for CEBNSM-B beams	229

LIST OF NOTATIONS

a	:	The shear span of beam
a_b	:	Thickness of NSM CFRP strip
a_e	:	Edge clearance
a_g	:	Clear spacing of NSM grooves
A_s	:	Cross sectional area of steel bar
A_f	:	Cross sectional area of NSM reinforcement
b	:	Width of the concrete beam specimen
b_g	:	Width of NSM groove
c	:	Depth of neutral axis
d	:	Effective depth of concrete beam specimen
d_b	:	Nominal diameter of round NSM bar
d_c	:	Depth of concrete cover
d_x	:	Depth of compressive force carried out by concrete
E_c	:	Modulus elasticity of concrete
E_f	:	Modulus elasticity of CFRP bar
E_s	:	Modulus elasticity of steel bar
f_{ck}	:	Characteristic strength of concrete
f_{fu}	:	Failure strength of NSM CFRP bar
f_t	:	Tensile strength of concrete
f_y	:	Yield strength of steel bar
F_c	:	The force carried by the concrete
F_f	:	The force carried by the NSM bar
F_s	:	The force carried by the internal steel bar
h	:	Height of the concrete beam specimen

I	:	Moment of inertia
I_{cr}	:	Cracked moment of inertia
I_{eff}	:	Effective moment of inertia
I_g	:	Gross moment of inertia
l	:	Span length
K_e	:	Effective pre-yield stiffness of RC beams
L_c	:	Critical length of the strengthening bar
M	:	Moment
m	:	Meter
M_r	:	Resisting bending moment
$M_{r,b}$:	Balance moment of resistance
P	:	Applied load
s_{r0}	:	Minimum crack spacing
t_f	:	Thickness of the CFRP fabric
w	:	Crack width
z	:	Lever arm
β_1	:	An empirical constant, depends on concrete compressive strength
Δ	:	Deflection
ε	:	Strain
ε_{bi}	:	Existing state of strain on strengthened beam soffit
ε_c	:	Strain of concrete
ε_{cu}	:	Ultimate strain of concrete
ε_{fd}	:	Design strain of CFRP accounting debonding failure mode
ε_{fe}	:	Effective level of strain in NSM strengthening bar
ε_{fu}	:	The ultimate strain of NSM FRP bar
ε_s	:	Strain of main tensile steel

φ	:	Curvature at a given strain increment
κ_m	:	Reduction factor for the tensile strain in NSM FRP reinforcement
μ	:	Fuzzy membership function
ρ_f	:	Reinforcement ratio of FRP
ρ_s	:	Reinforcement ratio of internal steel
σ_c	:	Normal stress in the concrete
τ	:	Interfacial shear stress; average bond stress
τ_f	:	Peak bond stress
τ_{max}	:	Shear strength

University of Malaya

LIST OF ACRONYMS

ACI	:	American Concrete Institute
AI	:	Artificial Intelligence
CEBNSM	:	Combined Externally Bonded and Near Surface Mounted
CEBNSM-B	:	Combined Externally Bonded and Near Surface Mounted -Bar
CEBNSM-S	:	Combined Externally Bonded and Near Surface Mounted -Strip
CFRP	:	Carbon Fiber Reinforced Polymer
EBR	:	External Bonded Reinforcement
FEA	:	Finite Element Analysis
FEM	:	Finite Element Modeling
FLES	:	Fuzzy Logic Expert System
FRP	:	Fiber Reinforced Polymer
JSCE	:	Japan Society of Civil Engineering
LVDT	:	Linear Variable Displacement Transducer
NSM	:	Near Surface Mounting
RC	:	Reinforced Concrete

CHAPTER 1: INTRODUCTION

1.1 Prelude

Sustainability of construction is an important issue throughout the world and construction industries face a significant number of challenges in the effort of improving the rate of sustainability of construction (Ochsendorf, 2005). The engineering community around the globe comes across a policy to treat the issue from a different standpoint; that is, by discouraging new constructions rather than extending the design life of the existing structure. With the pace of time, transportation structures like bridges, culverts and overpasses need to cope with the increased traffic load, upgradation of existing code, and the extension of design life (Toutanji et al., 2006). In the past, the service load was lighter compared to the heavy requirements of the present. Many transportation structures which were built in the late '60s are now deteriorating and underperforming due to various man-made and environmental reasons. Impact loads due to accidents can damage bridges leading to a deficiency in structural capacity that may not be able to carry the existing service load. Moreover, sometimes, mistakes or construction errors may result in an inadequate load carrying capacity in the structure.

1.2 Background

With regard to the aforementioned problem, the engineers and policy makers are more interested to recover or upgrade the existing structures with the structural strengthening measures. This technique can be considered a part of Green Technology as the demolition of old structures to erect new ones consumes huge amounts of energy and adds to environmental pollution, eventually increasing the carbon footprint of the globe.

Structural strengthening is not a new concept. This approach has been used by many countries from distant past using different materials and techniques. The common materials used in strengthening include spray concrete, ferro-cement and steel. Classical structural strengthening approaches include section enlargement, external pre-stressing, and externally bonded steel plate. Even, reports say, a deficient bridge slab was strengthened during 1947 in Finland using slotted steel bar with cement grout.

Since the last decade, Fiber Reinforced Polymer (FRP) has largely substituted conventional strengthening materials like steel and concrete due to its high strength to weight ratio, resistance to corrosion and low density (ACI, 2002; fib, 2001). Externally Bonded Reinforcement (EBR) and Near Surface Mounted (NSM) are the two strengthening techniques that have gained the greatest attention in the structural strengthening research community. The former system consists of one or multiple FRP laminates that are placed on the tension side of the member to be strengthened. The NSM technique entails the insertion of FRP strips or rods into grooves cut into the concrete cover of the member, which are afterwards filled with epoxy adhesive (De Lorenzis & Teng, 2007). This contemporary technique offers a higher level of strengthening performance, is less prone to premature debonding failure and enhances protection against fire, mechanical damage, aging effects and vandalism acts. It also demonstrates better durability, stress sharing mechanisms and fatigue performance as the reinforcement is located inside the structural element (Rosenboom & Rizkalla, 2006).

1.3 Statement of the Problem

The main problem with the EBR method is failure due to premature debonding as a result of high interfacial shear stresses between the FRP and the concrete substrate at the FRP curtailment location. The thickness of FRP composites plays an important role in this issue as the reduction of plate thickness which drives down the magnitude of stress concentration at the plate ends (Lousdad et al., 2010). Many researchers have proposed different solutions to resolve this problem. The solutions can be categorized into two main groups based on material and geometry of the joint. Al-Emrani et al. (2007), Haghani et al. (2008) and Bouchikhi et al. (2010) proposed a selection of appropriate materials (e.g. softer adhesive or stiffer plate) to reduce the stress concentration at the plate extremities. However, other researchers have argued that these measures may limit the optimization of the material as an effective tool in reducing the stresses in the adhesive joints (Lousdad et al., 2010). Another proposed solution has suggested changes in the depth of the adhesive film or the FRP or the joint configuration by tapering the plate or using adhesive fillets (Tsai & Morton, 1995).

For a fixed FRP ratio, the debonding potential increases significantly with increasing FRP thickness (Garden et al., 1997). Oehlers (1992) proposed a formula based on the interaction between the flexural and shear capacities of the beam where the debonding failure moment is inversely proportional to the FRP sheet thickness. Ziraba et al. (1994) presented a model based on the shear capacity of the beam where debonding shear force decreases with steel plate thickness. Hassanen and Raoof (2001) proposed that the design strain on the plate is inversely proportional to plate thickness. Most codes of practice (ACI, 2002; fib, 2001) also recommend limiting the design strain on the FRP sheet to eliminate debonding. Other studies (Lu et al., 2007; Maruyama & Ueda, 2001; Shehata et al., 2001; Teng et al., 2003) have confirmed similar limits. In most cases, the

design debonding strains are inversely proportional to the FRP composite thickness. Therefore, reducing FRP composite thickness at the curtailment location of EB strengthening materials is an effective way to prevent debonding failure.

In the NSM method, the width of the beam may not be wide enough to provide the necessary edge clearance and clear spacing between two adjacent NSM grooves. ACI has proposed a minimum edge clearance and clear spacing between two adjacent NSM grooves based on the research works of De Lorenzis (2002), Blaschko (2003) and Parretti and Nanni (2004). This strengthening technique requires a thicker concrete cover to allow enough space for grooves to be cut without any possibility of damaging the steel. However, many existing structures have inadequate concrete cover due to faulty construction or other reasons, which poses a major challenge for this technique. Moreover, debonding failure may still occur with this technique, although it is less likely compared to the EBR technique. The influencing parameters which can trigger this debonding problem include the internal steel reinforcement ratio, the FRP reinforcement ratio, the cross-sectional shape and the surface configuration of the NSM reinforcement, and the tensile strengths of both the epoxy and the concrete (De Lorenzis & Teng, 2007).

1.4 Arguments for the CEBNSM Technique

Considering the limitations of the NSM and EBR techniques, this study proposes a new strengthening system which joins the EBR technique with the NSM technique for strengthening RC beams. Previous research has shown that a reduction in CFRP fabric thickness diminishes the degree of stress concentration at the fabric edge (Lousdad et al., 2010). Rizkalla and Hassan (2001) have found that among several strengthening techniques, externally bonded CFRP sheet/fabric was the cheapest strengthening material but exhibited the higher ultimate load carrying capacity.

By combining NSM and EBR techniques, it is possible to reduce the CFRP fabric thickness by transferring a part of the required total strengthening area of CFRP fabric material from the EBR to the NSM technique. Consequently, the NSM bar or strip size can also be reduced through sharing with the EBR strengthening material and thus can provide sufficient space for edge clearance and groove clear spacing. Besides, by means of this combination, both systems will complement each other and reciprocally reduce their limitations.

The proposed combination technique enhances bond performance between strengthening materials and the concrete substrate, especially useful when increasing the flexural strength of RC members with limited cross-sectional width. If the thickness of the FRP fabric is reduced then the remaining required strengthening reinforcement is transferred to the NSM system. The possibility of debonding failure becomes less because of the reduced interfacial shear stress at the fabric cut-off location. Moreover, the NSM groove itself creates more contact surface area between the FRP composites and the concrete substrate at the cross-section. As stress is equal to load divided by corresponding surface area, an increase in surface area will decrease interfacial stress.

Lim (2009) used T-shaped CFRP plates at the tension face of several RC T-beams which increased the flexural capacity but demonstrated debonding failure mode. Similar result with enhanced flexural strength and debonding failure mode was reported by Rahman et al. (2015), where a combination technique was introduced with steel NSM bar and externally bonded steel plate. The present research applied CFRP fabric as externally bonded reinforcement along with NSM reinforcement. This decision was influenced by the research findings of Hassan (2002) where it was mentioned that the highest efficiency was achieved with least strengthening cost by externally bonded CFRP fabric among several other strengthening techniques. Besides, the thin cross-

sectional thickness of CFRP fabric was suitable for limiting the interfacial shear stress at the curtailment location which could reduce the possibility of debonding failure. Furthermore, the addition of adhesive in the NSM grooves in the Combined Externally Bonded and Near Surface Mounted (CEBNSM) system further improves bond performance between the strengthening CFRP fabric and the concrete substrate.

In this study the proposed CEBNSM technique has been divided into two types: (a) CEBNSM-B and (b) CEBNSM-S. The former type consists of steel and CFRP round bars inside the NSM groove with CFRP fabric bonded at the beam soffit. The CEBNSM-S type uses CFRP rectangular strips inside the NSM groove with CFRP fabric externally fixed to the beam soffit. Several other beams were strengthened using the EBR technique with variable CFRP fabric thickness in order to compare with the proposed CEBNSM technique. Several beams were also strengthened with only the NSM technique. These beams investigated the effect of bond length of strengthening bar and the possibility of using steel bars as NSM strengthening material. The findings from studying these parameters were utilized in investigating the proposed CEBNSM technique.

1.5 Research Questions

This study is concerned with developing a structural strengthening technique. An experimental program is conducted and its outcome answer the following research questions:

- i. What is the influence of strengthening material type (bar, strip and fabric) on the performance of the CEBNSM strengthening technique?
- ii. How effective is the performance of the CEBNSM technique compared to the EBR and NSM methods?

- iii. How effectively do AI techniques predict the serviceability behavior of the strengthened RC beams?

1.6 Objectives of the Study

The aim of the research is to develop effective strengthening solutions which will enhance the flexural performance of RC beams, ensure full composite action, and avoid premature failure. The objectives of the research are as follows:

- i. verifying the performance of RC beam using NSM and EBR strengthening techniques
- ii. developing a model for predicting the serviceability of NSM strengthened RC beam using Fuzzy logic
- iii. proposing a strengthening solutions which combine the EBR with NSM technique
- iv. assessing the performance of the CEBNSM technique
- v. assessing the flexural behavior of CEBNSM strengthened RC beams using FEM model.

1.7 Justification of the Research

Structural strengthening is now an influential branch of structural engineering as its research outcomes directly contribute to society. Newly developed materials and techniques enrich this area of research day by day. In this context, an endeavor to explore the efficiency of the proposed CEBNSM technique as a valid alternative strengthening option to the currently available techniques (NSM and EBR) is relevant and timely.

In this research, the structural performance of the NSM and EBR techniques was assessed along with the CEBNSM technique. In this way, the shortcomings of those systems were again identified under the current research and their effectiveness compared with the proposed CEBNSM technique. The experimental program consisted of four groups, namely: i) NSM, ii) EBR, iii) CEBNSM-B and iv) CEBNSM-S strengthened RC beams. The load-deflection, serviceability, stiffness, failure modes, ductility and strain behavior were evaluated separately for each group to compare their effectiveness. A parametric analysis was done which incorporated the variable parameters of the tested specimens. Theories related to failure modes and strength models were evaluated based on comparison with the test data.

An analytical prediction model was developed to compare the predicted load-deflection behavior with the experimental results. The theoretical model used in this study expanded on previous research conducted on the EBR strengthening technique. Despite good agreement with experimental results, further improvement can be possible, which led to another major research issue. A simple but effective artificial intelligence based technique was therefore applied to predict serviceability behavior. In this case, a Fuzzy Logic expert system was used. This system does not rely on analytical equations or mechanics based approaches. Instead, it depended solely on expert appraisal of particular behaviors of strengthened beams. The developed model enabled faster and simpler predictions of the deflection and crack width of steel or CFRP strengthened RC beams with variable inputs. This will allow users to optimize the number of experiments that will need to be conducted, which will eventually save significant amounts of time and expense.

Finally, an FEM model was developed using actual material properties, geometrical dimensions and loading conditions to simulate the load-deflection and strain behavior of

the CEBNSM-B strengthened RC beams. The simulated beams showed good agreement with the experimental results.

1.8 Scope

The research work reported in this thesis comprised of experimental tests of RC beam strengthened with EB, NSM and CEBNSM strengthening methods to evaluate and compare their strengthening efficiency. Finite Element Method (FEM) was applied to verify the experimental output and Artificial Intelligence (AI) based model was developed to predict the serviceability behavior of the strengthened beams. Application of these strengthening techniques to old pre-cracked concrete structure, and long term durability issues were not in the scope of this research. The rectangular RC beams designed with under-reinforced condition (steel ratio, $\rho = A_s/bd = 0.0085$) were considered in this study for strengthening. Strengthening effects on over-reinforced beam or varying steel ratio of the RC beams were also out of the scope of this research.

1.9 Research Methodology

Figure 1.1 demonstrates the methodology of this research in brief. To fulfill the proposed objectives, three approaches have been adopted in this research. They are: i) laboratory based experimental test of the RC beams using the proposed strengthening technique; ii) development of AI based serviceability prediction model and iii) development of FEM based numerical model to compare the experimental output.

The first, third and fourth objectives mentioned in section 1.6 were achieved by the experimental outcome of the strengthened RC beams. The second objective of this study regarding the development of serviceability prediction model of strengthened RC beams was fulfilled using the AI technique. The last objective was attained by using an FEM based software (ABAQUS) to assess the experimental results of the strengthened RC

beam behavior under static load. Besides, theoretical analysis was performed to explain and validate the experimental results.

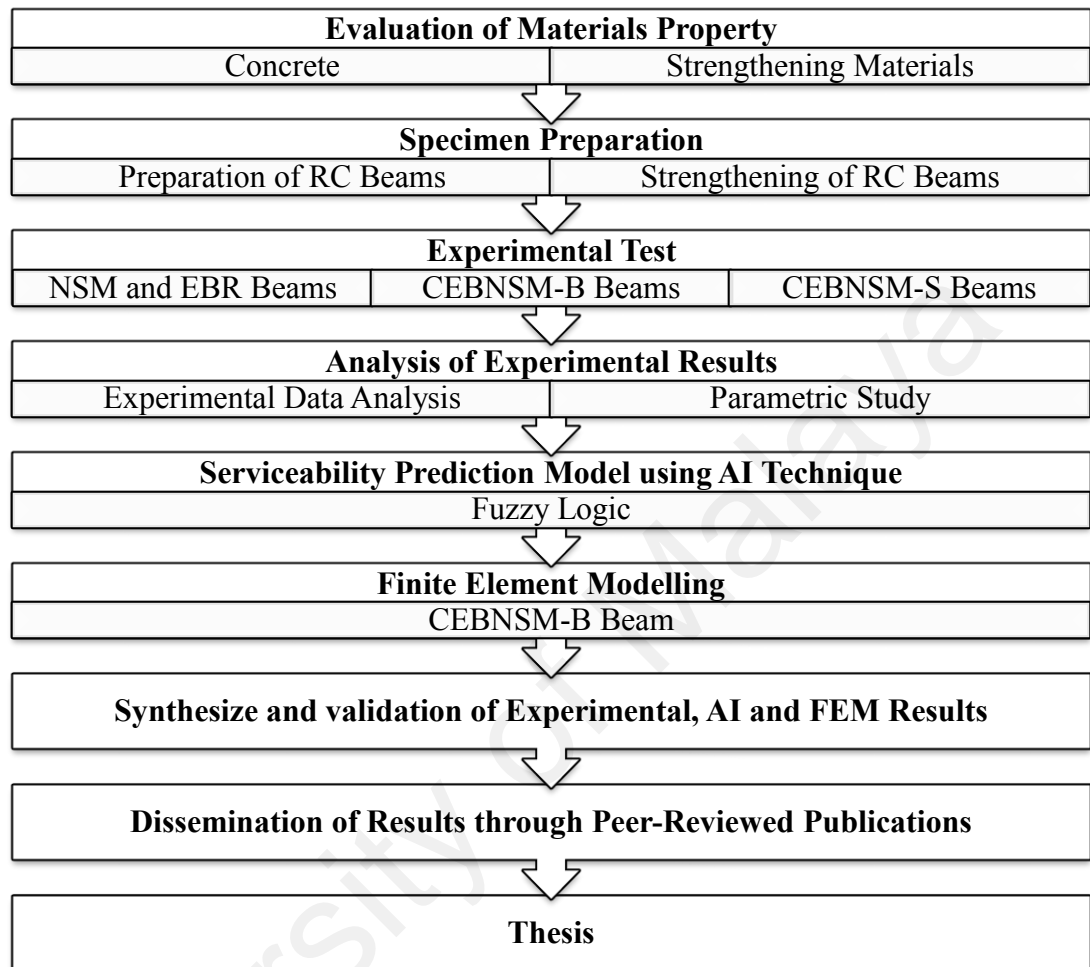


Figure 1.1: Methodology of the thesis

1.10 Outline of Thesis

Seven main chapters are incorporated in this thesis where the first chapter briefly explains the research background, problem statements, objectives, justification, scope and outline of the thesis.

Chapter 2 reviews the main aspects of different strengthening techniques and their key attributes. The factors which influenced the efficiency of the techniques are also remarked. The AI and FEM based research on structural strengthening issues are discussed. Addressing the features, research gaps are identified and summarized at the end of the chapter.

Chapter 3 describes the experimental test methodology adopted to fulfill the research objectives. Only the methodology of the experimental test program is discussed in this chapter elaborately. The material's mechanical properties, specimen fabrication, strengthening process, specimen instrumentation and test setup are discussed in this chapter.

Chapter 4 presents the experimental result and a critical discussion on their outputs. Deflection behavior, cracking pattern, stiffness, ductility and failure modes of the control and strengthened beams are described and analyzed. Strain response of concrete, steel and strengthening materials are critically investigated. A parametric and analytical study was performed with the experimental results.

Chapter 5 discusses about the development of artificial intelligence based serviceability prediction model and their simulated output. Fuzzy logic was utilized as the AI technique to develop and assess the prediction model with expert knowledge derived from the experimental output. The basics of the fuzzy logic along with their application in the structural area were pointed out as a background study to have a clear picture of them. Finally, the accuracy of their simulated output was verified with the standard statistical computation.

Chapter 6 represents the FE based modelling strategy, simulation technique and their simulated output. The basic of finite element, their application in structural strengthening research, and material property are discussed in detail in this section. The FEM simulation is critically analyzed with the help of experimental output to verify the accuracy of the developed model.

Chapter 7 sums up the main findings of this research work and proposes several recommendations for future works in this research area.

CHAPTER 2: LITERATURE REVIEW

Globally, structural engineering is facing significant challenges in the effort to improve the sustainability of construction. Sustainability refers to effective material consumption, economical use of resources and leaving quality resources for future generations. The structural engineering community is improving sustainability of built environment by improving the lifespan of existing structures rather than constructing new structures. All over the world, significant number of transportation structures (e.g. bridges, flyovers, etc.) and buildings were built in the late 60s when loading requirements were less severe compared to what they are now.

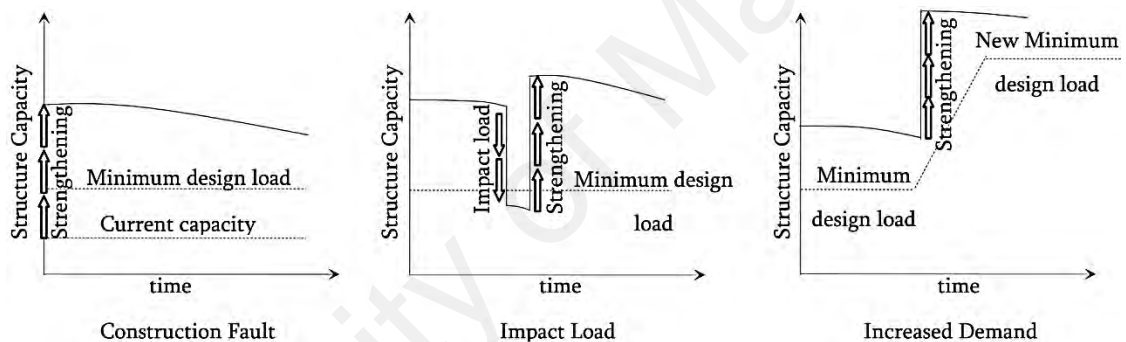


Figure 2.1: Reasons for strengthening of existing structure (Badawi, 2007)

Most of the existing transportation structures are overloaded with increasing number of vehicles which also amplify the impact load on the structures. Human mistakes can also be occurred at the design phase or during execution of the structures. Besides, several structures which are still maintaining their serviceability state need to be upgraded because of non-compliance of the currently developed code of practice for structural design to extend their design service life. The reasons for structural deficiency are graphically illustrated in Figure 2.1.

Structural strengthening can upgrade current structural systems to improve performance under existing loads or increase the strength of structural components to carry additional loads. This technique can be considered as a part of green technology

because the demolition of old structures and the erection of new ones consume much energy and cause environmental pollution. Strengthening of existing RC structure has been considered by the researchers as a great challenge since the concrete demonstrates quasi-brittle characteristics with lower tensile strain capacity under monotonic service loading. Concrete exhibits deterioration which eventually forms larger cracks before their design service life expires. Therefore, structures which are experiencing deterioration or are under threat of increasing live load can be rehabilitated using structural strengthening techniques.

This literature review chapter presents an appraisal of the research to date on the topic of static performance of RC strengthened structures using several strengthening techniques with their advantages and shortcomings. An overall description of the behavior of Externally Bonded Reinforcement (EBR) FRP strengthened beams under static conditions is presented. Therefore, a critical explanation of the performance of Near Surface Mounted (NSM) FRP strengthened beams with their bond behavior, debonding characteristics, ductility performance, and flexural behavior is described. Lastly, the other strengthening approaches with different materials and techniques are demonstrated with their opportunities and limitations.

2.1 Methods of Strengthening

There are many methods for strengthening, such as: section enlargement, steel plate bonding, and external post tensioning method, epoxy bonded (EB) system, unbounded anchored system and near-surface mounted (NSM) system. General methods for strengthening are summarized in Table 2.1. The basic concept of strengthening is to improve the strength and stiffness of concrete members by adding reinforcement to the concrete surface.

Table 2.1: Methods of strengthening

Methods	Description
(a) Section Enlargement	“Bonded” reinforced concrete is added to an existing structural member in the form of an overlay or a jacket.
(b) Steel plate bonding	Steel plates are glued to the concrete surface by epoxy adhesive to create a composite system and improve flexural strength.
(c) External post tensioning system	Active external forces are applied to the structural member using post-tensioned cables to improve flexural strength.
(d) Externally bonded reinforcement (EBR) system	FRP composites are bonded to the concrete surface by using epoxy adhesive to improve the flexural strength. FRP material could be in the form of sheets or plates.
(e) Near-surface mounted (NSM) system	FRP bars or plates are inserted into a groove on the concrete surface and bonded to the concrete using epoxy adhesive.
(f) Unbounded /mechanically fastened system	This method uses a powder-actuated fastener gun to install mechanical fasteners and fender washers through holes in the FRP predrilled into the concrete substrate, "nailing" the FRP in place.

2.2 Externally Bonded Reinforcement (EBR) Strengthening Technique

Externally bonded reinforcement (EBR) technique increases the flexural capacity by introducing steel plate or unidirectional fiber reinforced polymer plate or fabric at the maximum tensile region of RC beam. At first, during the 60’s, this EBR technique was launched to strengthen concrete structures with steel plate to glue with epoxy and/or anchor which was popular due to economical aspect. Despite limited manufacturing technology, this epoxy bonded steel plate was popular within Europe for the last three decades (Beber et al., 2001). However, due to heavy self-weight, extreme corrosiveness, and installation difficulties, researchers introduced FRP which is lightweight, non-corrosive and easy to install. This was a scientific breakthrough in literature; the ultimate flexure capacity increment was reported as 160% (Meier & Kaiser, 1991; Ritchie et al., 1991). However, the percentage increase had been limited to 40% due to ductility and serviceability limitations. The use of Fiber Reinforced Polymer (FRP) to strengthen reinforced concrete (RC) structures has grown in popularity and established

itself as an acceptable engineering practice in recent years. In particular, using FRP as external reinforcement is a widely used technique for structural rehabilitation.

Due to the desirable properties of FRP, numerous studies have looked at many aspects of using externally applied FRP for structural strengthening. However, one of the key concerns with externally bonded FRP is premature loss of bond between the concrete substrate and the externally bonded FRP laminate. Premature debonding in the present context means loss of bond before the FRP laminate can reach its expected capacity based on a perfect bond.

To strengthen the structure, the FRP must transfer its resistance contribution to the concrete section via shear stresses through the epoxy adhesive and the epoxy adhesive-concrete interface. Therefore, a sufficient bond between the epoxy adhesive and the concrete is critical for the strengthening of the structure. If the bond between the concrete and epoxy adhesive remains intact, stress can be transferred from concrete to FRP, and vice versa, and full composite action between the FRP and the unstrengthened RC beam will prevail. If premature debonding occurs, the composite action is lost, thus the RC beam cannot reach the theoretical ultimate capacity of the composite beam.

If an FRP-plated beam retains its composite action, there are two possible failure modes (Saxena et al., 2008) : (1) compressive concrete crushing prior to, or after, tensile steel yielding and (2) flexural failure due to rupture of the FRP. When premature debonding occurs between the FRP plate and concrete, the composite action of the beam is lost. The loss of composite action is characterized by the following four failure modes: (1) concrete cover separation (2) plate end debonding, (3) Shear crack induced debonding and (4) intermediate crack (IC) debonding (Table 2.2).

Table 2.2: Failure modes of EBR strengthened RC beam (Obaidat, 2011; Smith & Teng, 2002a)

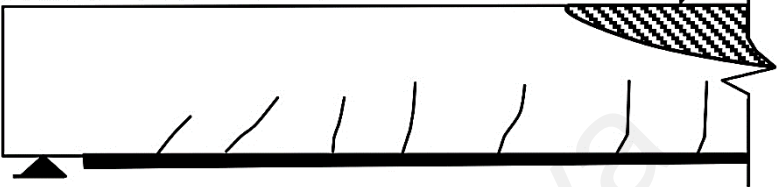
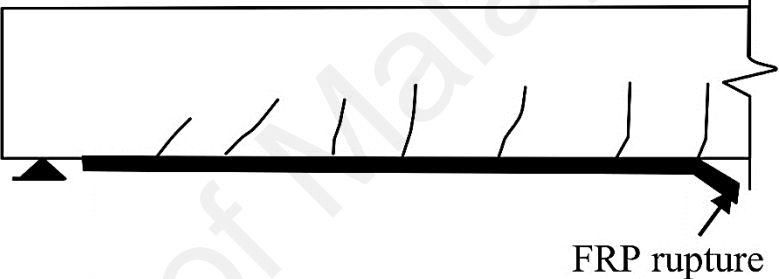
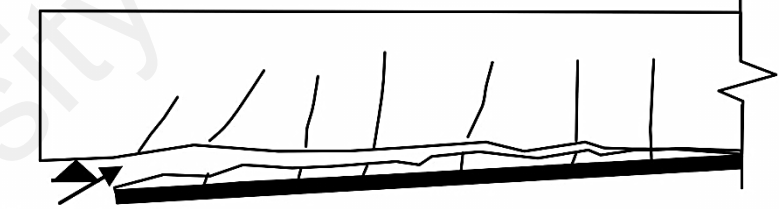
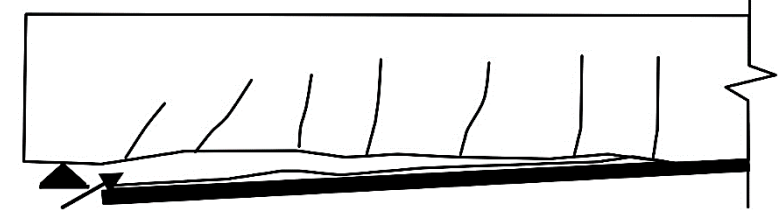
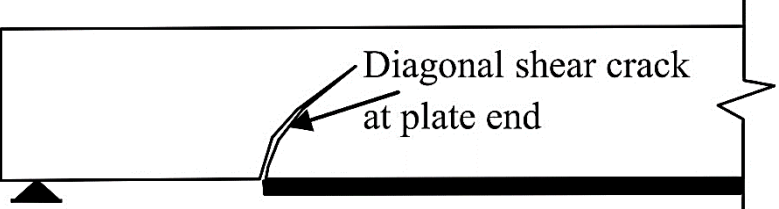
Failures	Failure types	Failure Modes
<p>Case I Full composite action</p>	<p>Concrete Crushing</p>	 <p>Compression failure</p> <p>The diagram shows a cross-section of a beam with a triangular shaded area at the top right corner, indicating concrete crushing. An arrow points to this area with the label 'Compression failure'. The beam is supported at the bottom left by a triangle and has several vertical lines representing reinforcement bars extending upwards.</p>
	<p>FRP rupture</p>	 <p>FRP rupture</p> <p>The diagram shows a cross-section of a beam with a jagged, broken line at the bottom right corner, representing the rupture of the FRP plate. An arrow points to this area with the label 'FRP rupture'. The beam is supported at the bottom left by a triangle and has several vertical lines representing reinforcement bars.</p>
<p>Case II Premature failure</p>	<p>End cover separation</p>	 <p>Crack initiation</p> <p>The diagram shows a cross-section of a beam with a jagged, broken line at the bottom left corner, representing the separation of the end cover. An arrow points to this area with the label 'Crack initiation'. The beam is supported at the bottom left by a triangle and has several vertical lines representing reinforcement bars.</p>
	<p>End interfacial delamination</p>	 <p>Crack initiation</p> <p>The diagram shows a cross-section of a beam with a jagged, broken line at the bottom left corner, representing delamination at the interface. An arrow points to this area with the label 'Crack initiation'. The beam is supported at the bottom left by a triangle and has several vertical lines representing reinforcement bars.</p>
	<p>Shear crack induced debonding</p>	 <p>Diagonal shear crack at plate end</p> <p>The diagram shows a cross-section of a beam with a diagonal crack at the bottom right corner, representing shear crack induced debonding. An arrow points to this area with the label 'Diagonal shear crack at plate end'. The beam is supported at the bottom left by a triangle and has several vertical lines representing reinforcement bars.</p>

Table 2.2, continued: Failure modes of EBR strengthened RC beam (Obaidat, 2011; Smith & Teng, 2002a)

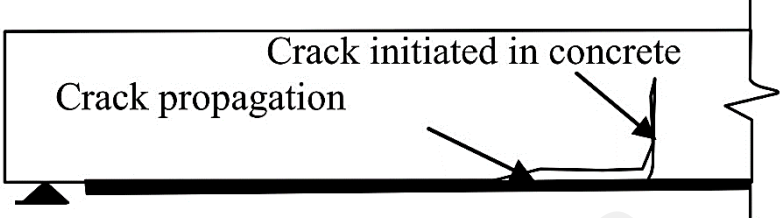
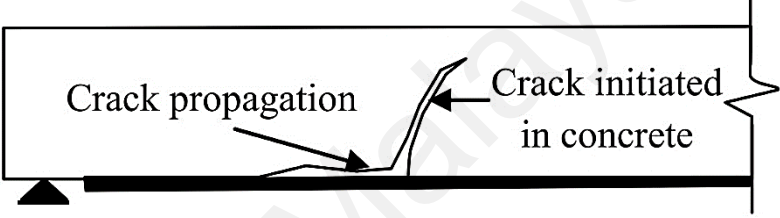
Failures	Failure types	Failure Modes
	Flexural crack induced (IC) debonding	
	Flexural-shear crack induced IC debonding	

Plate end debonding is caused by high normal and shear stresses developed at the laminate ends during loading. When the stresses exceed the strength of the weakest element, failure occurs. Upon failure, the FRP will debond from the concrete, usually within the concrete, at one end of the beam/slab leading to failure of the specimen. Concrete cover separation is caused by a crack developing at the laminate end propagating upwards to the level of the steel tensile reinforcement and horizontally along the reinforcement. The extension of the crack along the tensile reinforcement leads to concrete cover separation and the failure of the specimen. This type of failure typically occurs in members with relatively thinner cover, larger internal reinforcing bars and a stronger FRP-concrete interface. Failure of the concrete cover is initiated by the formation of a crack at or near the plate end due to high interfacial shear and normal stresses caused by the abrupt termination of the plate.

Intermediate Crack (IC) debonding occurs when flexural or flexural-shear cracks develop in an RC beam or slab, releasing tensile stress to the adjacent FRP. High strain

in the FRP plate is necessary to accommodate the high local interfacial stress across the crack. This high strain causes the propagation of cracks along the FRP-concrete interface. This high strain causes the propagation of cracks along the FRP-concrete interface. The growth of these cracks toward the region of less moment leads to premature debonding of FRP in the form of IC debonding. The cracks commonly occur in the concrete below the concrete-epoxy interface because the tensile strength of the epoxy adhesive is much higher than that of the concrete. The vertical displacement on either side of a flexural-shear crack can also cause a peeling force on one side of the crack which also contributes to IC debonding. However, the peeling force is considered less significant than the widening of cracks in causing IC debonding (Chen & Teng, 2001).

2.2.1 Performance of EBR Strengthened RC Beam

Hassan (2002) tested five different strengthening techniques and compared their structural efficiency with construction cost. The strengthening techniques were NSM with Leadline bars, C-BAR CFRP bars, and CFRP strips as well as EB CFRP sheet and strips. Three half-scale models were prepared and experimented in simple span with double cantilever arrangement. In Figure 2.2, the cost analysis with ultimate flexure capacity increment of various strengthening scheme was demonstrated. The EB CFRP strips showed only 11% increment of flexural capacity compared to the control beam which was the least among other strengthening schemes. However, the construction cost was expensive compared to its flexural capacity enhancement. The NSM lead line bar and C-BAR CFRP bar demonstrated almost the same flexural capacity with full composite action. The NSM CFRP strips displayed better ultimate capacity enhancement, though its construction cost was higher compared to other NSM strengthening materials. The beam with externally bonded CFRP sheet displayed 44% increase of the ultimate capacity and its stiffness was 3.3 times higher than those

properties of control beam specimen. From Figure 2.2, it is clear that EB CFRP sheets was the most efficient technique in terms of strength enhancement and construction expenditure. Its cost was only 25% compared to NSM strip technique.

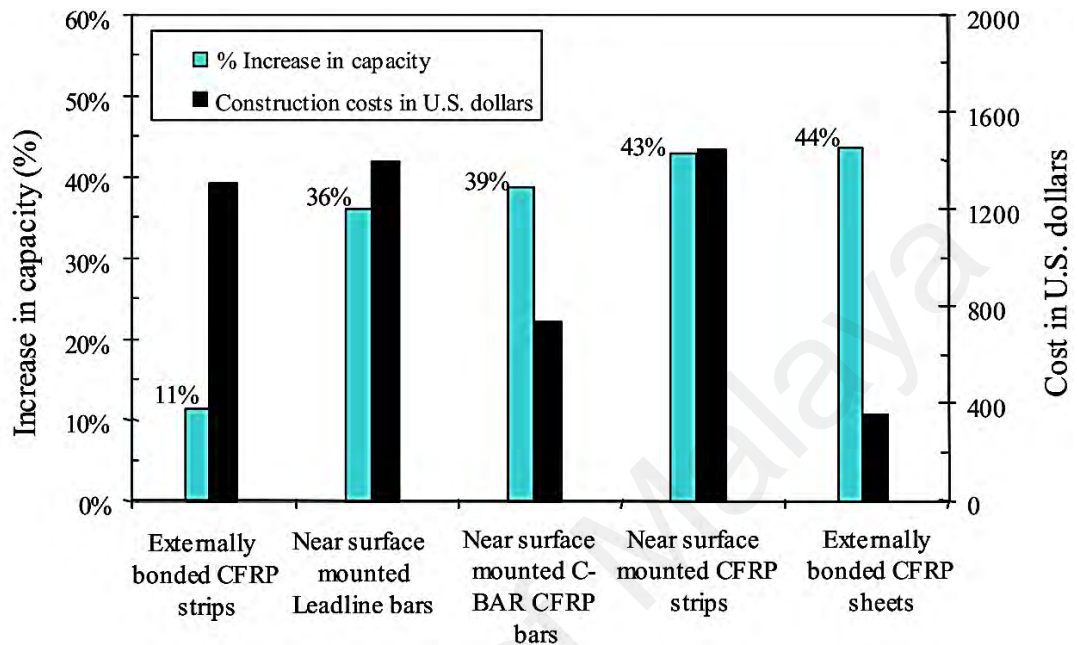


Figure 2.2: Ultimate capacity increment and cost variation of different strengthening technique (Hassan, 2002)

Oehlers (1992) performed an experimental study in order to provide a better understanding of the shear peeling of reinforced concrete beams having steel plates glued to their bottoms. In addition, the researcher's aim of study was to observe the interaction between shear and flexure peeling and to produce a design procedure for preventing plate debonding. Twenty-six beams strengthened in shear were tested. The beams' cross-sectional width and depth were 130mm and 175mm respectively. The tested beams comprised different shear spans which can be termed as distance from load point to support reactions. Two predominant failure modes resulted from the test: shear failure and flexure failure. The results showed that the cracks which cause peeling depend on the M/V ratio, where M is the moment and V is the shear force at the plate end. It was found that extending the steel plates does not affect the shear strength of the beams with no internal shear stirrups. Also, it was observed that the shear peeling is a

function of the concrete beam without the internal stirrups. The formation of diagonal shear cracks has been noticed as a major factor influencing debonding. Moreover, debonding due to shear and flexure has strong interaction. As a result, design guidelines for beams strengthened with steel plates were stated to provide procedure for preventing debonding due to peeling.

Triantafillou (1998) conducted an experimental and analytical study to improve the database of shear strengthening for reinforced concrete beams and to develop a model for the design within the modern codes. Eleven beams deficient in shear were tested under four-point bending at an effective span of 800mm. Two beams were used as control. The rest nine beams were strengthened against shear using CFRP sheets in different fractions of area and configurations. CFRP debonding was the predominant failure mode. The analytical study showed that the effective strain of FRP decreases with the increase of axial rigidity of the FRP. The experimental study in this research and other previous studies supported this result. The FRP sheets contribution to shear capacity of strengthened beams has a linear relationship with FRP axial rigidity. These results have been found useful for the design of FRP reinforcement.

Maalej and Bian (2001) investigated the CFRP thickness effect on interfacial shear stress concentration at plate curtailment and failure mode. They also evaluated the CFRP efficiency ratio as a function of plate thickness. The researchers tested 5 beams in their experimental work. One beam was considered as a control beam and the other four were strengthened with CFRP laminates with different layers. The beams were tested under four-point bending over a simply supported span of 1350 mm. The thickness and width of the CFRP laminate used in the research were 0.111mm and 115mm respectively. All beams failed by concrete cover ripping except beam 2 which failed by rupture of CFRP plate. The results showed that the load-carrying capacity of beams was

increased after adding the CFRP plates. The deflection capacity was more for the beams with lesser number of CFRP layers. Beam 3 with two layers of CFRP showed the maximum load-carrying capacity. In addition, the results showed that interfacial shear stress has its maximum value at the plate cut-off and it decreases as the distance from the plate cut-off increases. Maximum shear stresses exist in beams with thicker layers of CFRP. The CFRP external reinforcement becomes less effective as the thickness of CFRP is increased. The premature failure was started by flexure-shear cracks at the CFRP cut-off and it continued to reach the tension steel reinforcement causing the ripping of the concrete cover. The results were compared to some theoretical models obtained from previous studies.

Ali et al. (2001) conducted an experimental study to compare the mechanisms of shear and flexural debonding of steel and FRP plated beams. A total of thirteen beams were tested in this research. Eight beams were used to study the flexural peeling resistance of FRP with steel plates. Plate thickness was the major parameter varied in the experiment specimens. Five beams were bonded with plates to their tension faces whereas the other three beams were bonded to their sides. The other five beams were used to study the shear peeling of side plates. In all five beams, one portion was bonded with FRP plates and the other portion was bonded with steel plates. The test results showed that FRP plates have a lower possibility of detaching as a result of flexural peeling than steel plates having the same size. Also, it was found that FRP plates have more resistance to shear peeling than the steel plates in spite of the fact that they have the same mechanism. In addition, the researchers found that as the longitudinal elastic modulus of plate decreases, the shear peeling strength increases.

Mohamed Ali et al. (2006) studied the debonding behavior of steel plates bonded to the compression face of reinforced concrete beams and compared it to that in the tension

face plated beams. All beam specimens had the same cross-section 200×370 mm and were tested on 4700mm effective span. The plates were placed either at the tension or on the compression faces of beams. The results showed that in the case of tension plates, the CDC was caused by the formation of a critical diagonal crack. A sudden horizontal crack was then formed at the level of reinforcement. For the compression plates, the CDC debonding occurred in three stages: in the first stage, there was formation of shear diagonal crack, then propagation of the crack towards the point of load application, in the last stage, the CDC debonding was completed by extending the crack simultaneously to form a new diagonal crack. The CDC debonding of the compression face plate was 30% more than that of the tension face plates. In addition, it was found that the compression face plate is about 2.3% more resistant to FEP debonding than the tension face plates.

2.2.2 Debonding Behavior of EBR Strengthened RC Beam

The efficacy of the EBR technique depends on the bond between the concrete surface and the FRP material where epoxy stands as the interface element between them. Most of the researchers argued about the surface preparation and concrete quality as the dominant factors of a good bond (Bizindavyi & Neale, 1999; Chajes et al., 1996). The surface preparation is dependent on the type of strengthening material, whether it is FRP plate or fabric (Fanning & Kelly, 2001; Triantafillou & Plevris, 1992). It is important to maintain the uniform thickness (recommended thickness = 3 mm) of the epoxy when it is applied on the roughened strengthening surface according to the manufacturer's guidelines.

It is important to evaluate the bond strength of concrete to steel/FRP interface for designing the strengthening of concrete structure with externally bonded reinforcement technique. Standard experimentations have been executed using numerous test-setups,

comprising single and double shear tests along with pullout bending test as shown in Figure 2.3 (Bizindavyi & Neale, 1999; Chajes et al., 1996; Sena-Cruz, 2005; Van Gemert, 1980).

In single and double shear test, in-plane pullout force is applied to the FRP/concrete interface at FRP plane. Generally, the uniaxial tensile force is applied in the longitudinal direction of the FRP fiber orientation. The shear strain is recorded along the interface which is subsequently utilized to develop the bond-slip relationship. This relation is applied to develop the prediction model of debonding failure across the FRP-concrete interface. Typically, the bond-slip curve area of the FRP-concrete system is denoted as the mode II fracture energy, G_F . In practical case, both shear and normal stresses exist at the crack tips, though the shear test only assume the interfacial shear stress along the FRP-concrete interface. Hence, several studies have utilized pullout bending tests to perform more realistic feedback for the debonding failure of FRP-strengthened concrete beams.

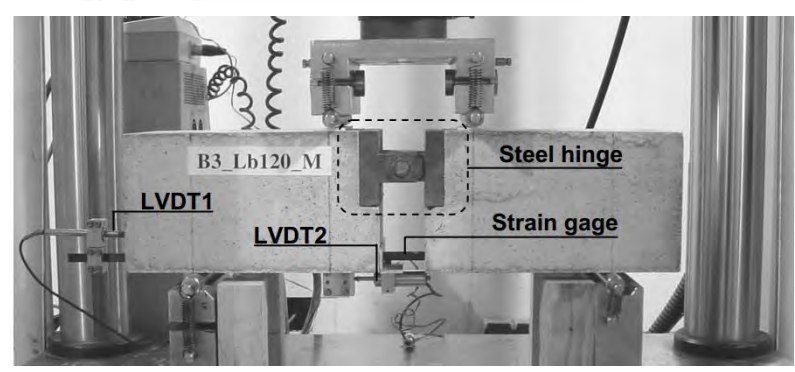
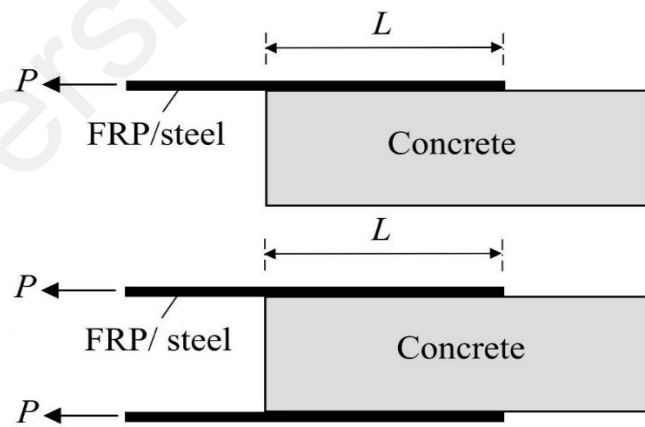


Figure 2.3: Single, double shear and pullout bending (Cruz, 2005) test

Smith and Teng (2002a) classified debonding models of several researchers into three categories based on their approach namely (1) shear capacity based models; (2) concrete tooth models and (3) interfacial stress based models. Some of the models were developed for steel plated beams and some of them were modeled dedicatedly for FRP strengthened beams. Smith and Teng (2002b) discussed the performance of these models using a huge experimental database. They concluded that concrete cover separation was more usual failure mode compared to plate end failure. All FRP plate based strength models demonstrated poor performance compared to the steel plated one. Among the three approaches, shear capacity based model displayed superior performance. The prediction model of Oehlers (1992) showed safe projection about debonding strength and it could be incorporated in design, though it was conservative.

Ulaga et al. (2003) developed a simple bilinear bond-slip relationship (Figure 2.4) where the curve is subdivided into three zones. The curve denotes the relative displacement between reinforcement and support where Zone I, Zone II and Zone III represent the upward branch, downward branch and horizontal branch respectively. This bilinear bond-slip relation can be stated by equation 2.1.

$$s(x) = \begin{cases} \frac{s_{LM}}{\tau_{LM}} \tau(x) & (\text{Zone I}) \\ s_{LM} + \frac{s_{L0} - s_{LM}}{\tau_{LM}} (\tau_{LM} - \tau(x)) & (\text{Zone II}) \end{cases} \quad (2.1)$$

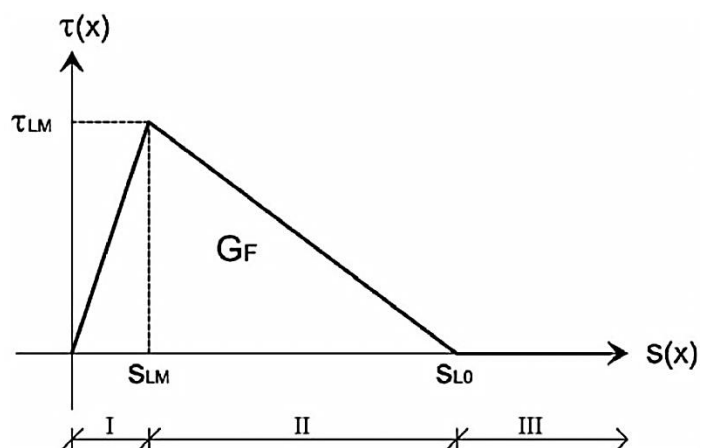


Figure 2.4: Bilinear bond slip relationship (Ulaga et al., 2003)

Oller et al. (2011) reviewed laminate debonding process where he mentioned about the bond-slip relationship where FRP laminate was considered pure shear medium. The relative displacement or slip between concrete and FRP maintains the constitutive relation of the interface demonstrated by the bond-slip curve in Figure 2.5. Three distinct zones were displayed in the curve where:

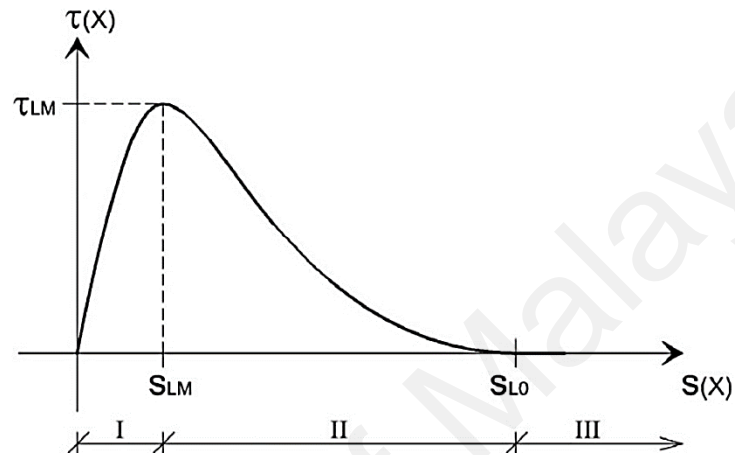


Figure 2.5: Bond-slip curve (Oller et al., 2011)

- Zone I shows increasing shear stress which represents the adhesive deformation.
- Zone II represents the decreasing function of the shear stress and also the post-peak behavior. Though micro cracks are developing in this stage, the shear stress transfer still continues due to aggregate interlock.
- Zone III demonstrates higher slip value than S_{L0} and almost zero shear stress. The joint is supposed to be cracked with the initiation of an interfacial macro crack.

Täljsten (1994) worked out that the external work done by a force P will be stored as strain energy in the laminate, in the support and in the joint. If an interfacial crack grows within a differential length da , the energy stored in the laminate will vary by a certain amount given by equation 2.2

$$dU_L = \frac{1}{2} \frac{P^2}{E_L t_L b_L} da \quad (2.2)$$

Where, b_L and t_L are the width and thickness of the bonded laminate respectively, and E_L is the laminate modulus of elasticity. The energy release during the crack enlarges, a differential da can be written as a function of the fracture energy, G_F

$$dW = G_F b_L da \quad (2.3)$$

The critical values of applied force P_{max} (equation 2.4) can be obtained from equation 2.3 and 2.4.

$$P_{max} = b_L \sqrt{2G_F E_L t_L} \quad (2.4)$$

2.2.3 Anchorage Performance of EBR Strengthened RC Beam

Plate end debonding can be prevented using the FRP anchorage system. It also enhances the ultimate load capacity by providing a vertical stiffness against peeling off stresses. Compared to the un-anchorage strengthened RC beam, the plate end FRP anchorage showed superior ductility ratios and increased ultimate capacity in Figure 2.6 (Breña & Macri, 2004; Ritchie et al., 1990).

FRP anchorage sheet is also used along the beam length to delay the Intermediate crack debonding. Chicoine (1997) tested FRP strengthened beams which failed due to debonding at their end. After this result, he developed two different configurations with FRP anchorage to prevent the premature failures (Figure 2.6). The 1st arrangement consisted of U-shaped FRP anchorage which was fixed at the end of two main FRP laminate. In the other configuration, unidirectional transverse strips were used along the FRP laminate. The first and second configurations enhanced the flexural capacity of the strengthened RC beam by 32.0% and 46.0% respectively compared to the un-strengthened beam. The second configuration changed the failure mode from debonding to flexure failure (rupture of FRP laminate). A similar observation was also reported by (Kotynia et al., 2008; Ritchie et al., 1990; Spadea et al., 1998)

The splitting of concrete cover can be prevented using the FRP anchor with transverse reinforcement. The FRP U-wrap is an efficient device which can be clamped at plate end. The area of this transverse clamping reinforcement A_f can be ascertained using the following equation 2.5 (Reed et al., 2005).

$$A_{f\ anchor} = \frac{(A_f f_{fu})_{longitudinal}}{(E_f \kappa_v \epsilon_{fu})_{anchor}} \quad (2.5)$$

Leung, 2006 found in his study that the FRP anchorage away from the plate end sometimes demonstrated better performance and the use of the plate end anchorage was not so successful always.

Kotynia et al. (2008) did not extend the FRP U-shaped anchorage sheet to the end of the FRP laminates. The study found that the debonding initiated just after the end of the continuous FRP anchorage laminates and propagated towards the plate ends at load level similar to the failure load of the un-anchored beam.

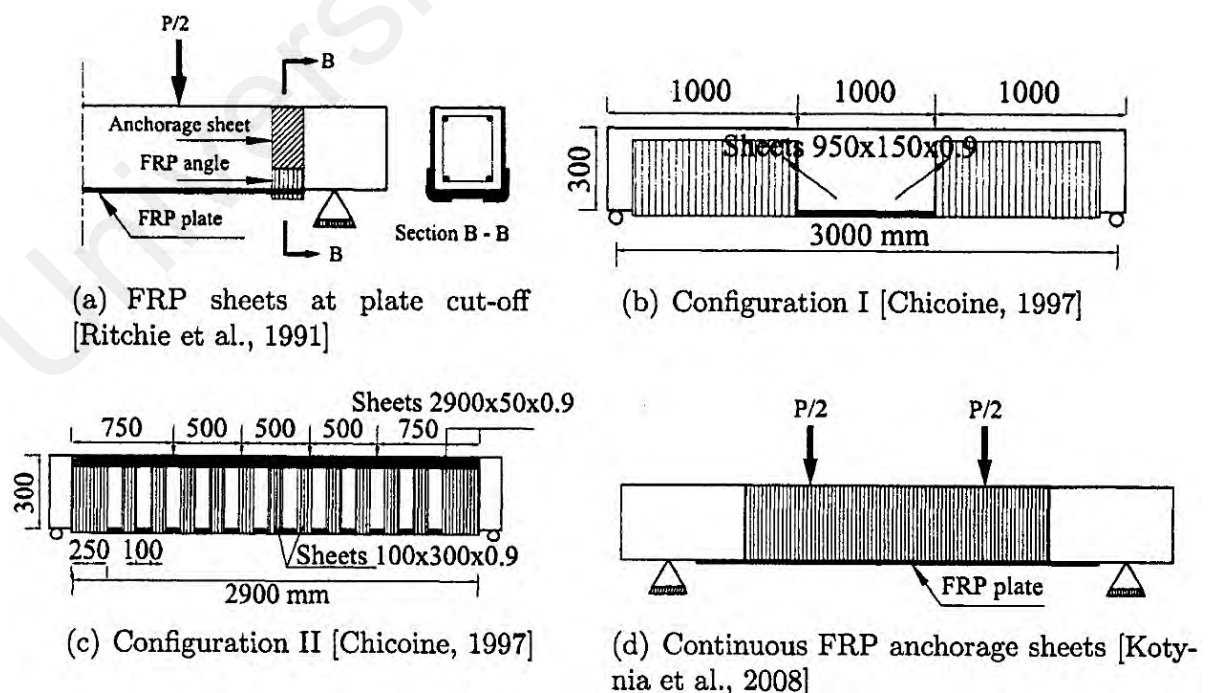


Figure 2.6: Various anchorage schemes for FRP strengthened RC beams (Kotynia et al., 2008)

The basic reasons behind anchorage usage in externally bonded reinforcement techniques are: a) to delay or avoid interfacial crack initiation; b) to enhance the interfacial shear stress reassignment; c) to develop a shear transfer process if the bond length is not available beyond the critical section. Based on this anchorage behavior, Grelle and Sneed (2013) categorized type I, II, and III anchorage device (Figure 2.7).

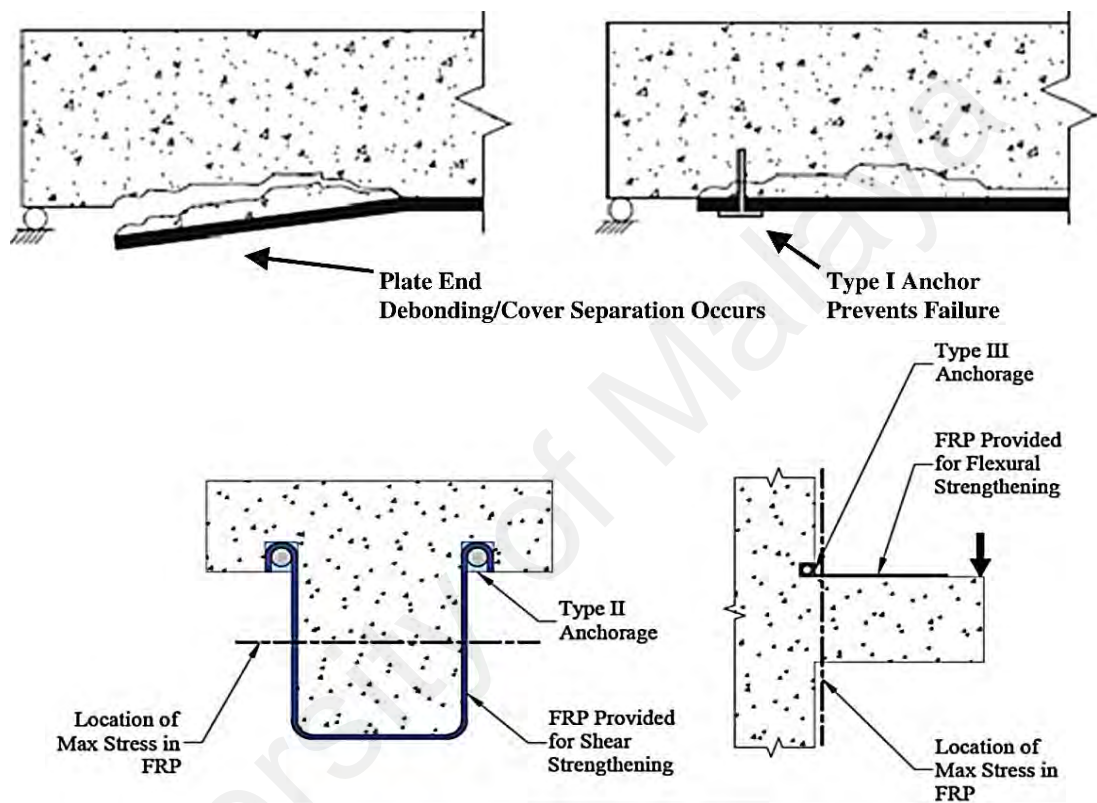


Figure 2.7: Type I, II and III anchorage device (Grelle & Sneed, 2013)

Type I anchorage will prevent the plate end interfacial debonding or concrete cover separation. A typical example of this anchorage is the mechanical anchor provided at the FRP laminate end. Type II anchorage improves the interfacial shear stress transfer mechanism. It is needed when the effective bond length is more than the transfer length because of the geometric configuration of the structural member. Type III is used where no bond length is available beyond the critical section. This condition applies when the critical design section is located at a sheet or plate end, or near an abrupt change in fiber direction, such as at the location of an interface between two orthogonal structural members. U-anchor is used to represent the type II and III anchorage (Figure 2.7). The

author suggested performing an independent full scale anchor test data to incorporate the anchorage system in the design code.

Kalfat et al. (2011) reviewed several anchorage devices to achieve superior fiber utilization to delay or prevent debonding failure. Known anchorage devices for FRP-to-concrete applications comprise FRP U-jackets, FRP spike anchors, patch anchors, nailed metal plates, near-surface mounted rods, mechanical fastening, concrete embedment, and mechanical substrate strengthening. FRP U-jackets are non-invasive and their easy installation procedure makes ideal choice for flexurally strengthened RC beams. It was obtained that inclined U-jackets were 74% more effective than vertically orientated U-jacket anchors, and the subsequent anchorage efficiency was $k_{fab} = 1.36$. FRP anchors demonstrated 46% more efficiency than vertically positioned U-jackets and marginally less efficiency than inclined U-jackets.

2.3 Near Surface Mounted (NSM) Technique

Despite the numerous studies found in the literature and real life applications, Strengthening using EB-FRP composite exhibits some drawbacks: surface preparation, occurrence of debonding, and exposure to the external environment. Strengthening using NSM FRP offers an innovative alternative to EB FRP laminates. The strengthening procedure involves embedding CFRP reinforcement inside a pre-cut groove filled with epoxy. Following are some of its advantages over EB technique (De Lorenzis & Nanni, 2002):

- i. Feasibility of anchoring into members adjacent to the one to be strengthened
- ii. Excellent for strengthening in the negative moment regions, where external reinforcement would be subjected to mechanical and environmental damage
- iii. Better fire performance
- iv. Less likely to debond near ultimate capacity

- v. Limited surface preparation work
- vi. Protection of the strengthening material from external damage such as vehicle impact
- vii. Less coverage of the concrete surface, which reduces the built-in moisture, hence, avoids freeze-thaw problems.

It should be noted that the NSM technique is more suitable for outdoor structures, such as bridges, than for indoor structures with normally less concrete cover (Nordin & Täljsten, 2006). Several factors and concerns should be taken into account when strengthening RC structures using the NSM technique (De Lorenzis & Teng, 2007):

- i. Type of FRP reinforcement: The choice of FRP material with higher tensile capacity and modulus of elasticity such as CFRP would allow the use of smaller FRP and groove cross-sectional areas, hence, less risks of interfering with the internal reinforcement.
- ii. Groove filler: In terms of structural behavior, its most relevant mechanical properties are the tensile and shear strengths.
- iii. Groove dimension: the groove, width, depth, net distance between two adjacent grooves, and the net distance between a groove and the beam edge are all relevant construction parameters which can influence the bond performance.

2.3.1 Important Factors for NSM

The important factors that affect NSM strengthening technique are: concrete class, FRP material and groove dimension. The details are discussed in the following sections.

2.3.1.1 Concrete Class

Increase in the concrete compressive strength causes the rise in intensity of the demanding loads. Hassan and Rizkalla (2003) found that increasing compressive strength of concrete reduces the development length of FRP and increases the debonding load in NSM strengthened RC beam. Hassan, Tarek K and Rizkalla, Sami H (2004) reported that using high-strength concrete increases the resistance to concrete split failure.

Sena-Cruz and Barros (2004) carried out pull out bending test considering concrete class as one of the test variables and the compressive strength was selected as 30, 45 and 70 MPa. The concrete strength had not shown any significant effect on the loaded end slip at peak pullout force and was also independent of the ratio between the maximum tensile stress recorded on CFRP and its tensile strength.

After testing NSM CFRP strengthened RC beam with variable concrete strength (30 MPa and 60 MPa), Al-Mahmoud, Firas et al. (2009) came to a conclusion that concrete plays an important role on ultimate strength of a beam when conventional failure mode occurs. However, no substantial changes had been observed due to concrete class on load-carrying capacity of beam when it failed by NSM system failure.

Al-Mahmoud, Firas et al. (2011) conducted pullout test where they had verified that resin was one of the key factors to achieve higher ultimate capacity irrespective of the groove width and concrete strength. Tension member test revealed that concrete strength had no particular significance of changing the transfer length for FRP rods embedded in concrete.

Kotynia (2012) found that superior concrete strength delays CFRP debonding and increases debonding CFRP strain. On the other hand, it posed an insignificant influence

on the ultimate load of strengthening beam. This parameter also affects the CFRP bond strain of the beam which had discontinued steel bar at mid-span.

Godat et al. (2012) applied 20.7 MPa and 42.7 MPa concrete as test specimen and revealed that bond strength is proportionately varied with concrete strength. The result also confirmed that debonding can be prevented using higher class concrete. Concrete splitting is the dominant failure mode of lower strength concrete, whereas high strength concrete exhibited the pullout mode of failure.

From Figure 2.8 it can be seen that the debonding load and debonding strain level in the NSM-FRP bars were proportionally enhanced with the increasing concrete compressive strength. Until 20 MPa of concrete compressive strength, there was no significant change of bearing capacity which started rising from 30 to 50 MPa with a capacity increment from 10% to 17%. Therefore, NSM FRP strengthened beam showed better efficiency with stronger concrete up to a threshold limit, beyond which it would not improve (Soliman et al., 2010).

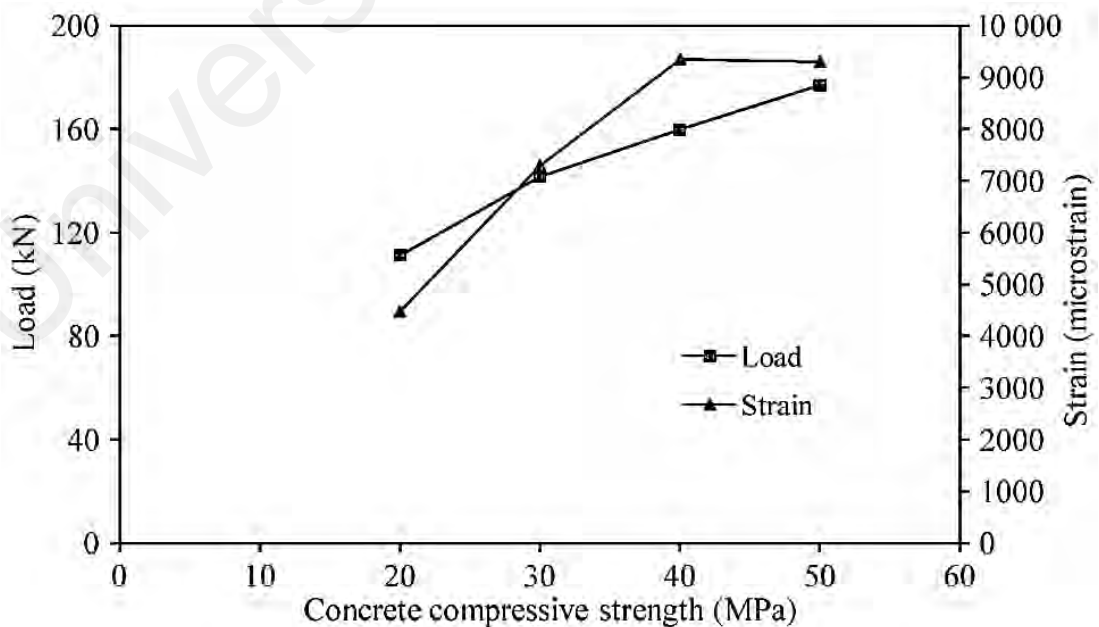


Figure 2.8: Effect of concrete strength on failure load and FRP debonding strain(Soliman et al., 2010)

2.3.1.2 FRP Material

After the invention of the Fiber Reinforced Polymer (FRP) it has gained widespread acceptance from the engineering community to strengthen Reinforced Concrete (RC), steel, masonry and timber structure. The properties which make it as a unique product for structural strengthening are corrosion resistance, high strength to weight ratio and easy application. Carbon, glass and aramid fibers are embedded in thermoset or thermoplastic resin to manufacture the FRP composites.

Table 2.3: Usual mechanical properties of steel and FRP in different guidelines

Guidelines	Mechanical properties	Steel	CFRP	GFRP	AFRP
ACI, 440.1R-06	Nominal yield stress (MPa)	276 to 517	N/A	N/A	N/A
	Tensile strength (MPa)	483 to 690	600 to 3690	483 to 1600	1720 to 2540
	Elastic Modulus (GPa)	200	120 to 580	35 to 51	41 to 125
	Yield Strain (%)	0.14 to 0.25	N/A	N/A	N/A
	Rupture Strain (%)	6.0 to 12.0	0.5 to 1.7	1.2 to 3.1	1.9 to 4.4
	Density (g/cm ³)	7.9	1.5 to 1.6	1.25 to 2.1	1.25 to 1.4
	Coefficient of thermal expansion- Longitudinal(°C)	11.7 ×10 ⁻⁶	(-9 to 0)×10 ⁻⁶	(6 to10) ×10 ⁻⁶	(-6 to -2) ×10 ⁻⁶
	Coefficient of thermal expansion- Transverse(°C)	11.7 ×10 ⁻⁶	(74 to 104) ×10 ⁻⁶	(21 to 23) ×10 ⁻⁶	(60 to 80) ×10 ⁻⁶
ISIS Canada 2007a	Tensile strength (MPa)	483 to 690	780 to 4000	1800 to 4900	2800 to 4210
	Elastic Modulus (GPa)	200 to 210	200 to 800	70 to 87	74 to 179
	Elongation (%)	1.4 to 2.5	0.4 to 2.5	2.0 to 5.6	1.9 to 4.6
	Coefficient of thermal expansion(°C)	11.7×10 ⁻⁴	(-1.6 to -0.1) ×10 ⁻⁴	(2.9 to 5.0) ×10 ⁻⁴	-2.0 ×10 ⁻⁴
	Poisson's ratio	0.3	-0.2	0.2 to 0.22	0.35
CNR-DT 200/2004	Tensile strength (MPa)	350 to 600	2400 to 5100	2000 to 4800	3600 to 3800
	Elastic Modulus (GPa)	206	240 to 760	70 to 90	62 to 180
	Rupture Strain (%)	20 to 30	0.5 to 1.73	3.5 to 5.5	1.9 to 5.5
	Density (g/cm ³)	7.8	1.75 to 1.9	2.46 to 2.6	1.44 to 1.47
	Coefficient of thermal expansion(°C)	10.4 ×10 ⁻⁶	(-0.6 to -1.45) ×10 ⁻⁶	(1.6 to 5.4) ×10 ⁻⁶	-2×10 ⁻⁶

Among the three types of FRP composites, CFRP has been widely used for NSM strengthening in all the structure like RC, masonry and timber. In literature it is found that, as a strengthening material, few researchers prefer CFRP for concrete structure and

GFRP for masonry and timber structure (De Lorenzis & Teng, 2007). The mechanical properties of different NSM strengthening materials are tabulated in Table 2.3.

Among the three types of FRP composites, CFRP has been widely used for NSM strengthening in all the structure like RC, masonry and timber. In literature it is found that, as a strengthening material, few researchers prefer CFRP for concrete structure and GFRP for masonry and timber structure (De Lorenzis & Teng, 2007). The mechanical properties of different NSM strengthening materials are tabulated below in Table 2.3.

Glass fiber posed good impact resistance and its weight is more than carbon or aramid fiber. Composites originated from this fiber reveal superior electrical and thermal insulation properties. The usage of GFRP bar is limited in concrete structure and not usually recommended as a pre-stressing or post-tensioning element. The cost of glass fiber is comparatively lesser than the carbon fiber product. Carbon fiber offers an excellent combination of high strength, low weight and high modulus (Hollaway & Leeming, 1999). Due to the superior tensile strength and modulus of elasticity, CFRP bar requires less cross-sectional area compared to GFRP bar for the similar tensile capability (De Lorenzis & Teng, 2007). High stiffness carbon fiber is generally used for rehabilitation of RC structural members. However, due to low value of ultimate strain, ultra-high stiffness carbon fiber composite is not normally used to upgrade RC structures. Carbon fibers can cause galvanic corrosion when used next to metals. A barrier material such as glass and resin is used to prevent this occurrence. Aramid fibers are organic and anisotropic in nature which may be sensitive to moisture and possibly will degrade after extensive exposure to sunlight. However, this fiber can withstand both static and dynamic loading and pose good fatigue performance and effective tensile elastic characteristics. It possesses ductile compressive characteristic, though their ultimate compressive strength is small (Hollaway & Teng, 2008).

FRP bars and strips are commercially available in the market for NSM strengthening. FRP bars are available in round, square, rectangular and oval shapes with different textures such as sand-blasted, sand-coated, spirally wound with a fiber tow, or roughened with a peel ply (ACI 440, 2006). Narrow FRP strips necessitate more groove filler and hence lessen the debonding behavior by improving the surface area-to-sectional area ratio (El-Hacha, Raafat & Rizkalla, Sami H, 2004; Hassan & Rizkalla, 2002).

2.3.1.3 Groove Dimension

The preliminary and most important job is to fix the groove dimension of the NSM system. Figure 2.9 shows the details of the groove geometry of FRP strips, square bar and round bars separately with FRP strips and round bar combined in the same image (De Lorenzis & Teng, 2007; Parretti & Nanni, 2004).

From the bond test of round bars, De Lorenzis (2002) defined, $k = b_g/d_b$, where, b_g = groove width and d_b = nominal diameter of a round bar. She proposed $k = 1.5$ and 2 for smooth or lightly sand-blasted bars and deformed bar respectively. Other researchers (De Lorenzis & Nanni, 2001b; Hassan & Rizkalla, 2003) also supported this proposition that NSM groove should be at least $1.5d_b$ for round bars. For FRP strip, the suggested minimum groove dimension is $3.0a_b \times 1.5b_b$, where a_b is the least of the strip dimension and b_b stands for the largest one (ACI, 2008).

ACI also suggests that the least possible clear groove spacing for NSM FRP bars should be greater than twice the depth of the NSM groove to avoid overlapping of the tensile stresses around the NSM bars. Furthermore, a clear edge distance of four times the depth of the NSM groove should be provided to minimize the edge effects that could accelerate debonding failure (Hassan & Rizkalla, 2003).

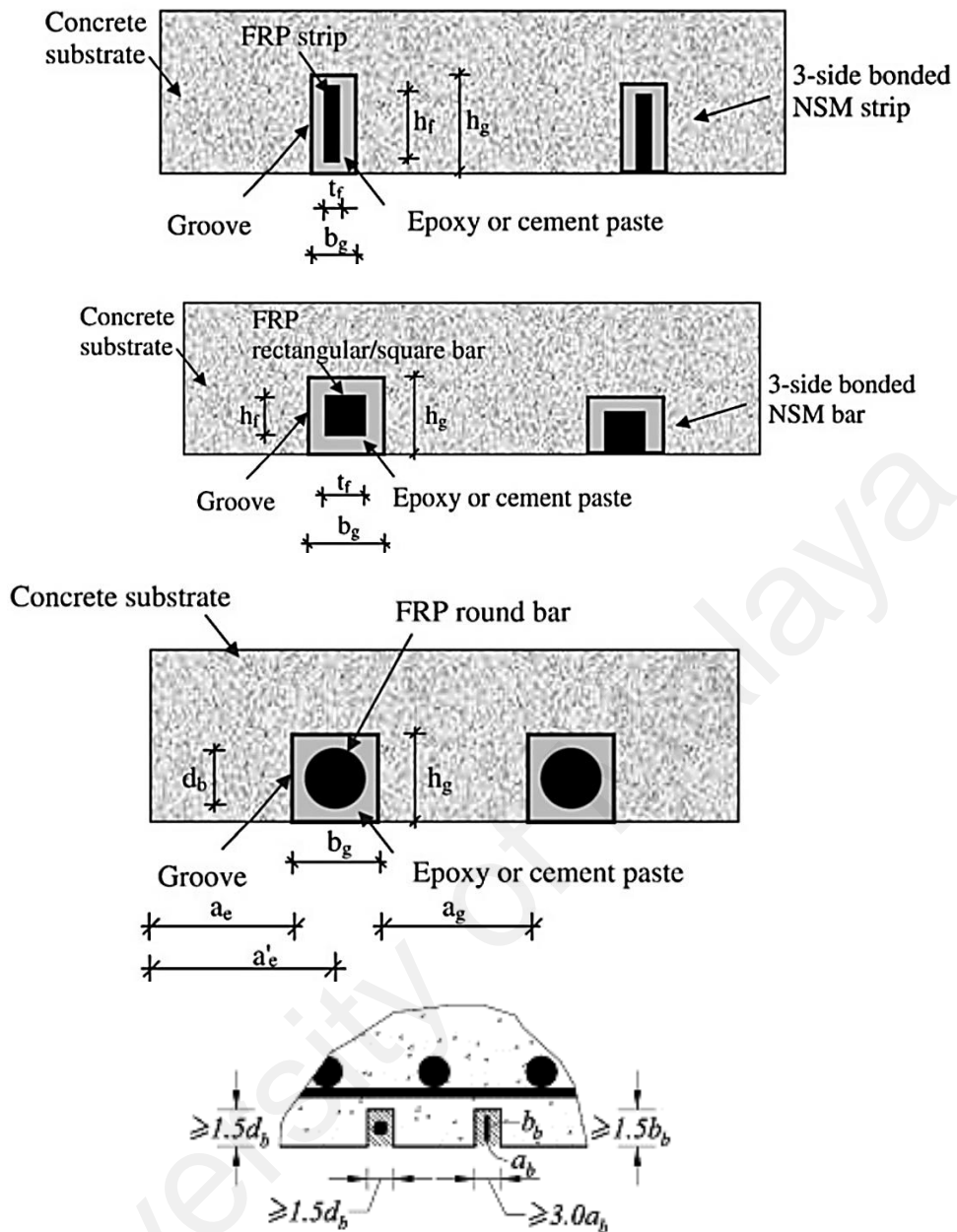


Figure 2.9: NSM groove dimension and nomenclatures by different authors (De Lorenzis & Teng, 2007; Parretti & Nanni, 2004)

2.3.2 Performance of Near Surface Mounted (NSM) Strengthened RC Beam

De Lorenzis and Nanni (2001a) characterized material property, sub-system (groove geometry), structural member level (shear capacity), design approach (compared test results with predictions). Tensile test was performed on CFRP No. 3 deformed rods according to JSCE 1997 using grouted anchor to avoid premature local failure during the test. 5 beam pull-out tests were adopted with variable bonded length and groove size to observe the bond performance. Average values of tensile strength, elastic modulus,

and ultimate strain were 1,875 MPa, 104.8 GPa, and 1.79% respectively which showed tensile failure occurred away from anchor.

In Figure 2.10, two significant bond failure modes were observed depending on the groove size: splitting of the epoxy cover and cracking of the concrete surrounding the groove. Shear capacity was enhanced by applying NSM FRP rod. Predictions of a simple design approach had shown a reasonable agreement with the experimental results.

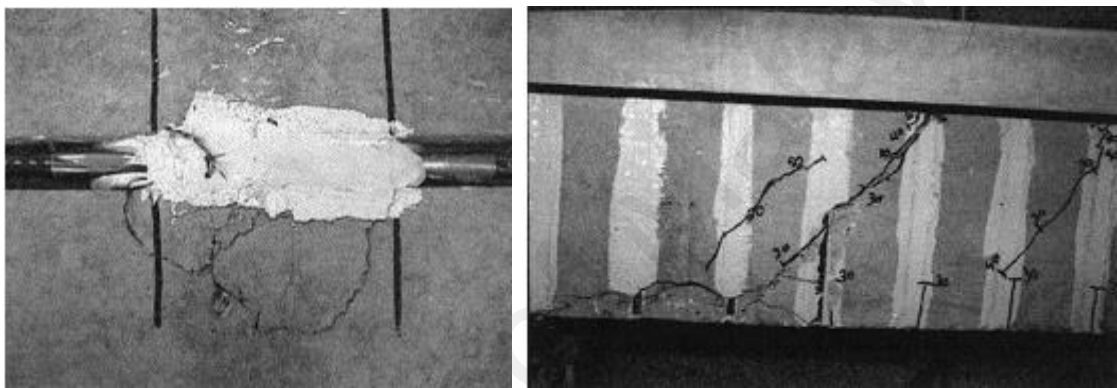


Figure 2.10: Failure modes of the NSM strengthened test specimen (De Lorenzis & Nanni, 2001a)

Kalayci et al. (2010) performed a study to ascertain the upper limit of NSM FRP system's groove size and to further investigate the effects of design parameters such as the multiple bars or strips, groove width and depth, concrete compressive strength, and the type of FRP and epoxy (Figure 2.11). Twelve 2.1 m long T-section beams with a clear span of 2 m were tested in three-point bending. Half of the beams were retrofitted with FRP strips (rectangular groove) and the other half with FRP bars (square groove). Longitudinal steel reinforcement consisted of 2 No. 10M bars in compression and 2 No. 16M bars in tension. Shear reinforcement included No. 10M stirrups at 127 mm on center. The total length of the FRP strips or bars used was 1715 mm.

Sena-Cruz et al. (2012) had done a comparative research to assess the FRP strengthening efficiency among EBR, NSM and MF-EBR beam. Externally Bonded

Reinforcement (EBR) or Near Surface Mounted (NSM) FRP strengthening systems allow the epoxy to fix the FRP in the concrete cover region which is susceptible to premature failure due to its great exposure to atmosphere. The Mechanically Fastened and Externally Bonded Reinforcement (MF-EBR) is a new concept which includes insertion of mechanical fasteners over the glued multidirectional CFRP laminates.

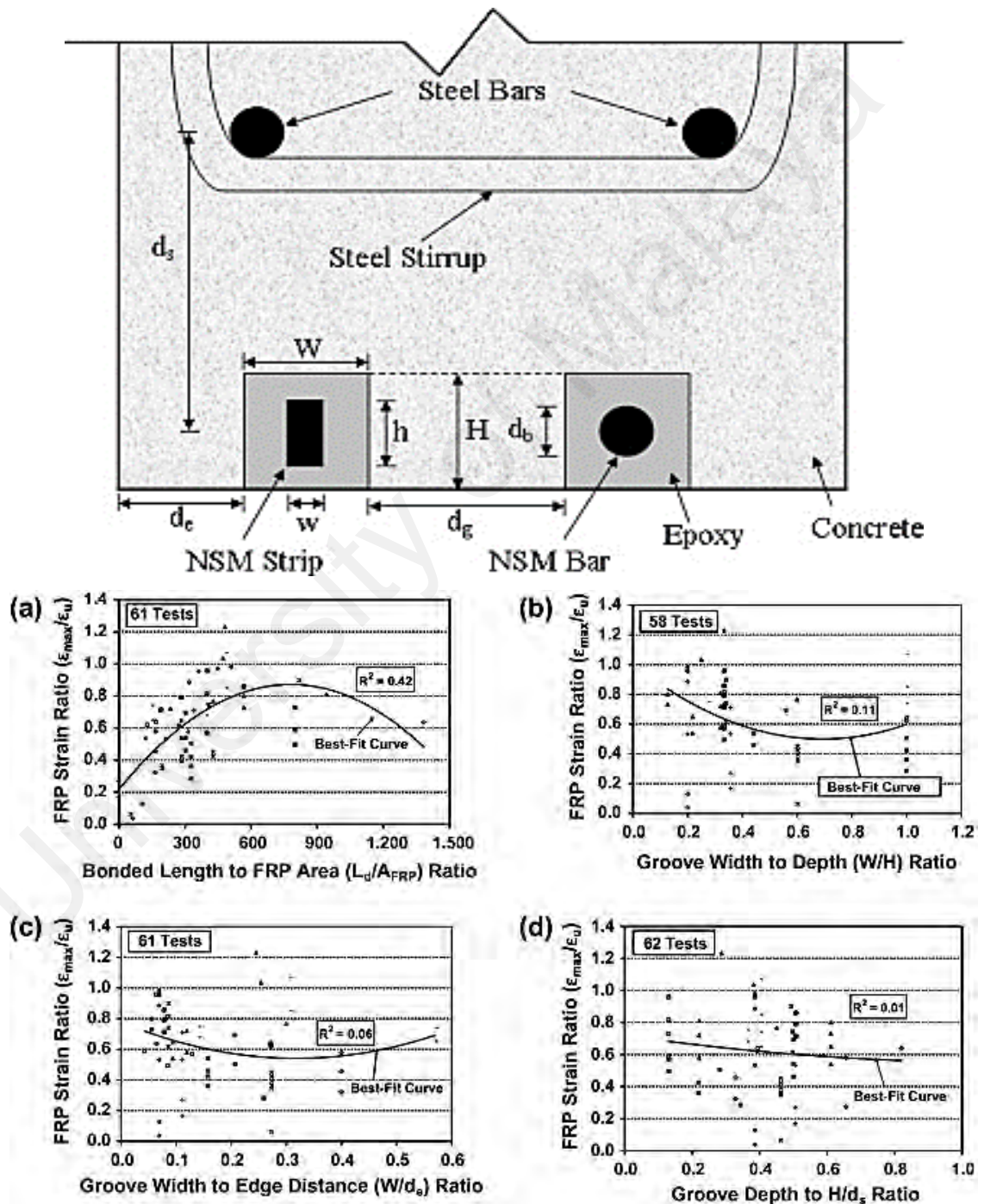


Figure 2.11: NSM groove geometry and effect of geometric parameters on FRP strain efficacy (Kalayci et al., 2010)

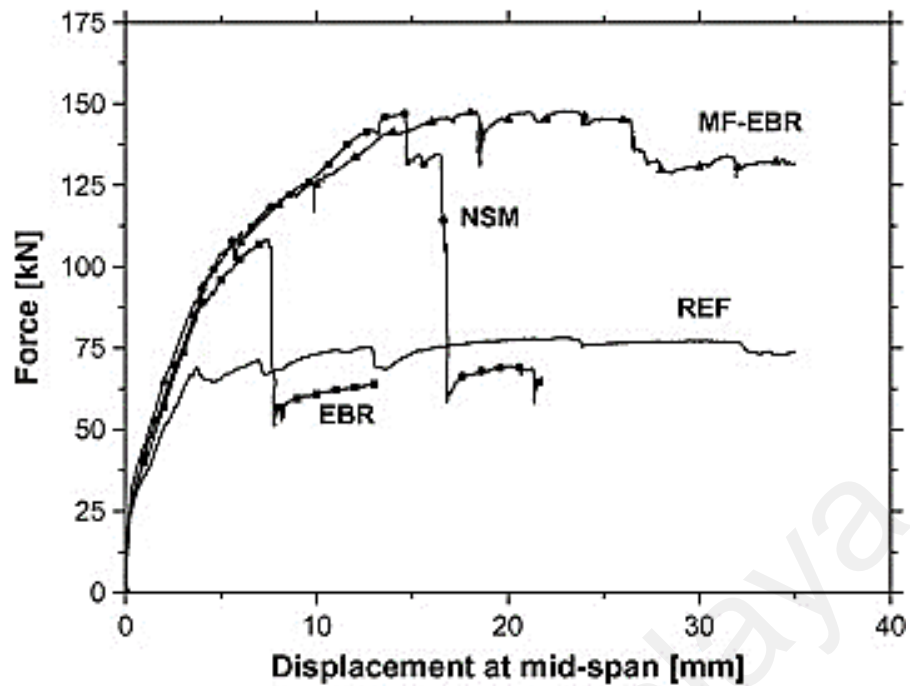


Figure 2.12: Force vs. Displacement of the tested beams under monotonic loading (Sena-Cruz et al., 2012)

In Figure 2.12, two series of above mentioned beams were tested to monotonic and fatigue loading tests where reference beams were included. In monotonic test the load carrying capacities of EBR, MF-EBR and NSM strengthened bars have been significantly improved by 37%, 87% and 86%, respectively, in comparison to the reference beam. Ductility performance of MF-EBR is superior to any other beams. Normalized deflection capacity at maximum load (δ_{max}/δ_y) of MF-EBR was 4.35, which is higher compared to EBR (1.8) and NSM (2.98). Ductile failure mode has been monitored for MF-EBR beam.2. During post fatigue monotonic tests, NSM was detected as the most efficient strengthening system in terms of maximum load (101%) and ultimate deflection capacity. Its highest normalized deflection capacity at maximum load is 6.7 which is the highest in comparison to MF-EBR (3.5) and EBR (2.4).

FEM analysis was performed to validate the results and to extend the study about other geometric and physical parameters. Groove size tolerance has little or no influence on the performance of NSM FRP system. All test specimens failed by premature debonding either in the form of epoxy or as concrete splitting. When the no. of bars was

increased, it did not show any improvement and FRP strain efficacy decreased with it. Using high modulus FRP did not significantly increase the load capacity and higher modulus epoxy increased the overall stiffness of the system. Bonded length is the most significant parameter that affects the FRP strain efficacy.

Study of Al-Mahmoud, Firas et al. (2011) involved the effects of concrete strength, filling material, groove dimensions, and groove surface preparation for such CFRP rods used in the NSM technique (Figure 2.13). Concentration on the specific problems of NSM: reduction of contact surface area between filling material and concrete and eccentricity of FRP rods.

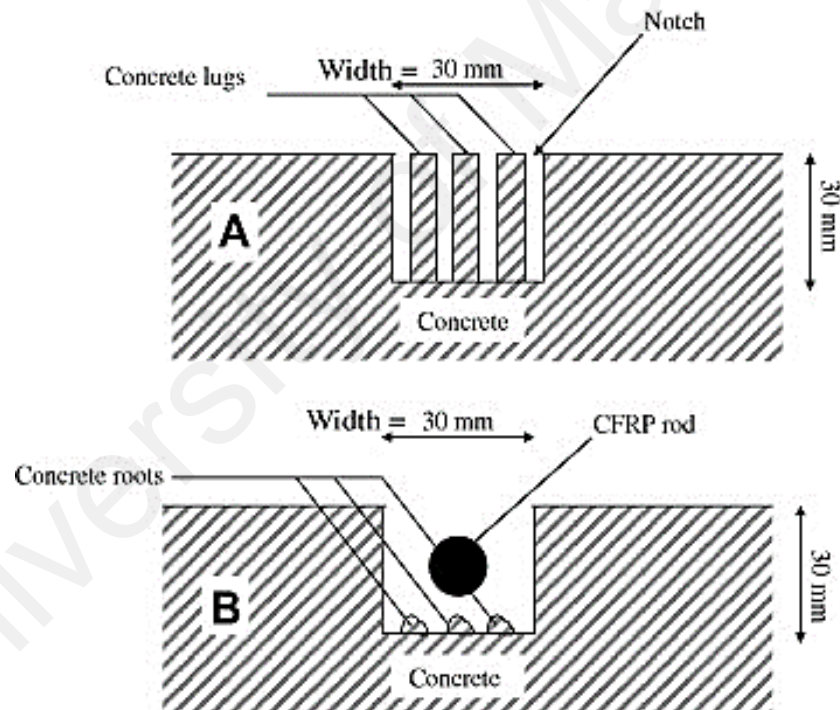


Figure 2.13: Groove geometry and failure modes (Al-Mahmoud, F. et al., 2011)

Two interfaces are involved in the NSM technique: one between the reinforcing composite rod and the filling material, and the other between this material and the old concrete. The coupling between the two interfaces was studied through two mechanical tests: the usual pull-out test, which assessed the anchoring capacity of the CFRP rods, and the tension member test, which simulated the behavior of the CFRP rod bond in the

tensile zone of an RC-structural element. A groove width to nominal rod diameter ratio between 1.7 and 2.5 appears to be optimal. For pull-out test, ultimate load was always higher for resin embedded CFRP rod than that of concrete embedded CFRP rod because of debonding failure at the mortar–concrete interface. For tension member tests, in both systems the transfer length was similar and there was no significant effect of the mechanical behavior on the tension members due to presence of the filling material.

2.3.3 Assessment of Bond Behavior of NSM Strengthening Technique

Wahab et al. (2010) conducted bond tests on concrete beams strengthened with near-surface-mounted NSM non pre-stressed and pre-stressed CFRP rods under static loading by four-point bending test of RC beam. Six concrete beams were tested. The test variables included presence of internal tension steel reinforcement (unreinforced and reinforced), use of NSM CFRP strengthening (non pre-stressed and pre-stressed), and type of CFRP Rod (spirally wound and sand blasted). For pre-stressing applications, the sand blasted rods had a shorter transfer length than the spirally wound rods. For failure mode, spirally wound CFRP rods failed by pull-out of the CFRP rod from the epoxy in the region close to the support and the other one was pull out from the epoxy that initiated as debonding at mid-span and progressed to the region close to the supports. At failure, the beams strengthened with a given rod type exhibited the same CFRP strain at sections close to the support.

Muhamad et al. (2010) used partial interaction theory to develop generic closed form solutions for crack spacing and widths, the load to cause primary, secondary cracks and subsequent cracks. Four different types of interface bond characteristics (τ - δ) were considered: a linear for serviceability; a linear descending for ultimate limit state; a nonlinear bond slip and the CEB-FIP Model Code 90. Authors developed a fundamental mechanics that govern the tension stiffening behavior for short term loads as it is

starting position for precisely calculating long term deflection. From comparison between mechanics and empirical models it has been showed that empirical research has identified the major parameters that affect tension stiffening but that the mechanics equations are too complex to be derived empirically.

Sharaky et al. (2013) studied about the modified pullout test (adapted to NSM reinforcement) which was used to analyze the effect of groove surface, groove geometry (dimensions and shapes), FRP bar type (material and surface treatment), bond length and groove–concrete system. Twenty-six C-shaped concrete blocks (outside dimension-350x350mm, inside dimension-170x180mm and height-300 mm) were tested as modified pullout test with variation of two types of groove surface (pre-formed and saw cut). The test variables were groove surface (pre-formed and saw cut), groove geometry (dimensions and shapes), FRP type (carbon and glass), bar diameter ($d_b=8, 9.05, 9.28, 12$ mm), modulus of elasticity (41, 64, 134, 170 GPa), bond length, and the incorporation of different modifications in the NSM–concrete interaction (transverse interlocking with or without shear connectors, covering plate with shear connectors and confinement of surrounding concrete).

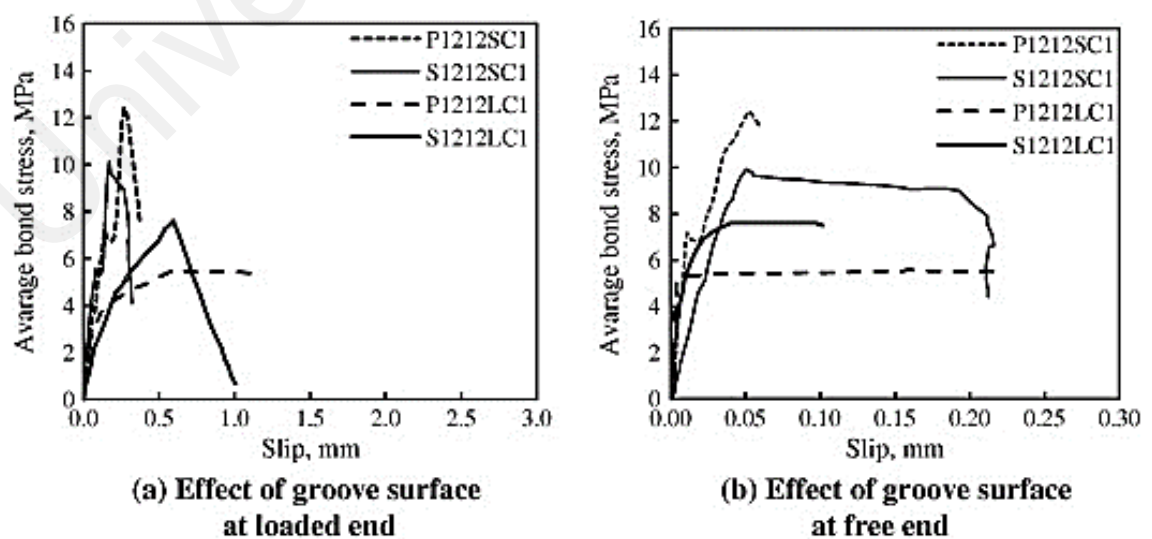


Figure 2.14: Average bond- slip curves of NSM CFRP (Sharaky et al., 2013)

In Figure 2.14 average bond-slip curves are shown for the different FRP materials. The specimens with medium bond lengths and smooth surface texture attained the best average bond stress distribution along their bond lengths. For square grooves, increasing the groove size from $1.5d_b$ to $2d_b$ delayed the bar–epoxy interface failure and increased the failure load by 14.8%. Failure load of textured surface bar increased by 34% than smoother surface bar. The use of mechanical interlocking in the epoxy–concrete interface slightly increased the failure loads by approximately 8.67%.

2.3.4 Debonding Failure Modes of NSM Strengthening Technique

Teng et al. (2006) conducted some preliminary bond tests to characterize the local bond-slip behavior of the NSM system. Flexural strengthened RC beams using NSM CFRP strip were tested to observe debonding failure mechanism where the test variable was the embedment length of the NSM strip. Load-deflection curves, failure modes, strain distributions in the CFRP strip, and local bond stresses at the CFRP–epoxy interface from the tests were examined in detail and results were compared with a predictive simple analytical model. The debonding failure mode of NSM CFRP strips in bond tests was interfacial debonding at the FRP–epoxy interface. Of the four embedment lengths investigated, all but the shortest one led to a notable increase in the load-carrying capacity and to a lesser extent, in the post-cracking stiffness of the beam. Debonding was found to be the primary failure mode in all cases except for the beam with the longest embedment length. No simple or direct relationship exists between the debonding failure mode observed in the bond tests and that observed in the beams.

More recently, Oehlers et al. (2010) proposed a unified approach for reinforced concrete beams retrofitted with FRP reinforcement hinging on the separation of the behavior within reinforced concrete specimens between undisturbed regions controlled by conventional moment-curvature analyses and disturbed regions defined by discrete

rotations. The discrete-rotation model depends on three fundamental principles: linear rigid-body displacements, shear friction or aggregate interlock, and IC theory—the partial-interaction behavior (interface slip) from the commencement of crack widening to debonding. The researchers theorized that this approach could be used to produce specific models to deal with the behavior of FRP-strengthened concrete structures regarding flexure, shear, moment redistribution, ductility, and confinement.

2.3.5 Ductility Performance Using NSM Technique

Rasheed et al. (2010) showed a higher strength increment and relatively more ductile flexural behavior by using transverse FRP U-wraps to anchor the longitudinal composite systems (Figure 2.15). A controlled debonding failure mode up to ultimate flexural capacity was also visualized in their tests. Six beams with cross-sectional dimension of 254x457 mm with clear span of 4.88 m, flexural reinforcement of 4 nos.19 mm, compression steel of 2 nos. 9mm and 9 mm stirrup at a spacing of 152.4 mm were tested in three-points bending using four composite-based strengthening systems, namely: externally bonded CFRP sheets, NSM prefabricated CFRP strips, externally bonded steel reinforced polymer (SRP) sheets and NSM stainless steel bars.

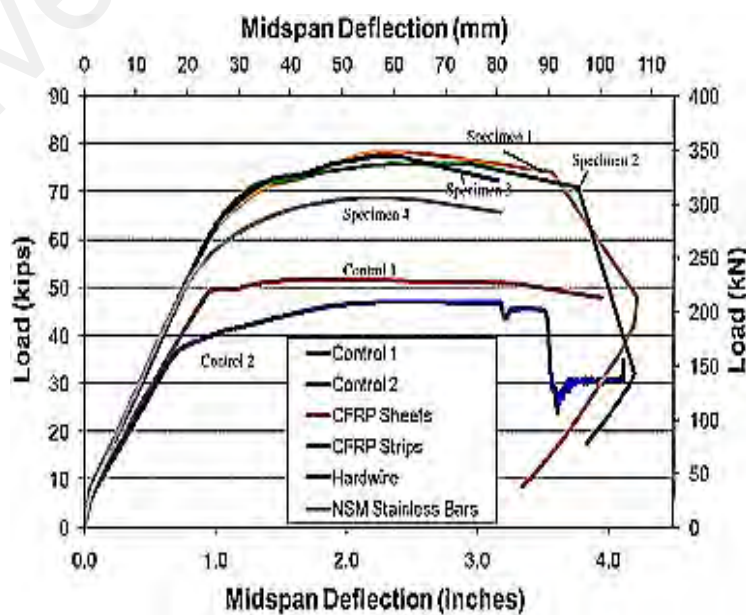


Figure 2.15: Response of tested FRP beams (Rasheed et al., 2010)

Equivalent flexural strengthening designs, for the four different systems, were developed using a nonlinear analysis program. The flexural failure mode predicted by initial analysis was crushing of the unconfined concrete at a compressive strain of 0.003. A more ductile behavior was observed as a result of transverse strengthening and concrete confinement effects (Figure 2.16). Accordingly, an increase of approximately 50% in flexural strength is accomplished and flexural performance is similar despite the different failure modes encountered. Concrete confinement by using closed stirrup allowed for better utilization of the high strength properties of the various strengthening systems. The experimental results were in close agreement with the theoretical response curves. The analytical ductility values under-predicted the actual ductility numbers.

FRP reinforcement demonstrates linear elastic response which is responsible for the lower ductile quality of FRP reinforced RC beam. (Oudah, Fadi & El-Hacha, Raafat, 2012) proposed a new ductility model which considered the deformability of FRP strengthened RC structure and the energy dissipation. It counted both the static and fatigue loading.

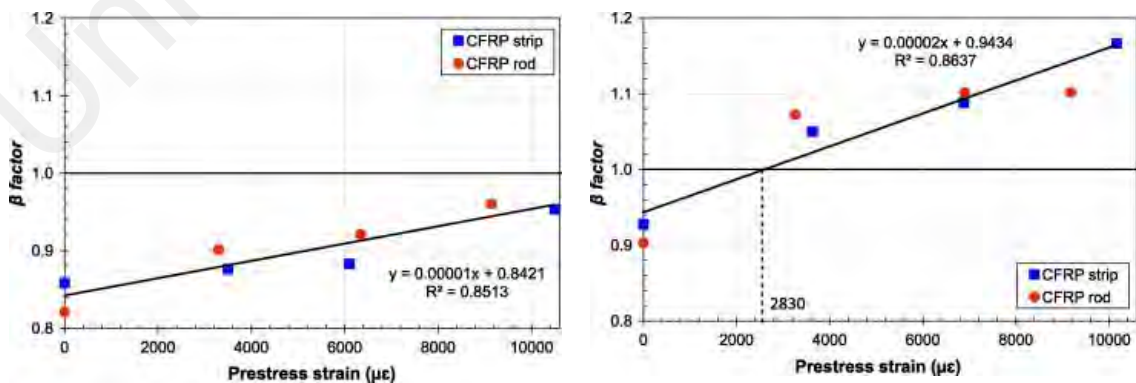


Figure 2.16: Optimum ductility of un-fatigued and fatigued beam(Oudah, F. & El-Hacha, R., 2012)

This new ductility expression was derived considering the deformability of a structure to the amount of energy dissipated and the lack of a general ductility expression. The ductility model was validated with the experimental result which is shown in Figure 2.16 (fatigued and un-fatigued beam). Five beams were cast (one control and rests were strengthened with different levels of NSM pre-stressed CFRP rods). The span of the beams was 5000 mm with 200x400 mm dimension. All beams were tested under fatigue loading condition which survived the 3 million fatigue cycles and then submitted to monotonic tests up to failure in order to examine the effect of fatigue loading on the post-fatigue mono-tonic behavior. The derived ductility model can correlate the deformability of the beam and the energy dissipated. This model can be applied to RC or FRP strengthened RC beam for both fatigued and un-fatigued loading. The obtained pre-stress strain was $2830\mu\epsilon$ for optimum ductility index of fatigued NSM CFRP strengthened beams; whilst no optimum ductility index could be attained for the un-fatigued beam. The proposed pre-stress strain is constrained by the design of the strengthened beams (i.e. mechanical properties of constitutive materials, beam geometry, amount of reinforcement, pre-stressing, etc.)

2.3.6 Flexural Behavior of NSM Technique

El-Hacha, R. and Rizkalla, S. H. (2004) compared the behavior and effectiveness of the materials that were used for various NSM and externally bonded FRP strengthening systems. The structural performance and modes of failure of the tested beams were presented and discussed in their study. A total of eight, simply supported, 2.7 m long, concrete T-beams were constructed and tested under a monotonically increasing concentrated load applied at mid-span of the beam using displacement-control mode at a loading rate of 1.07 mm/min.

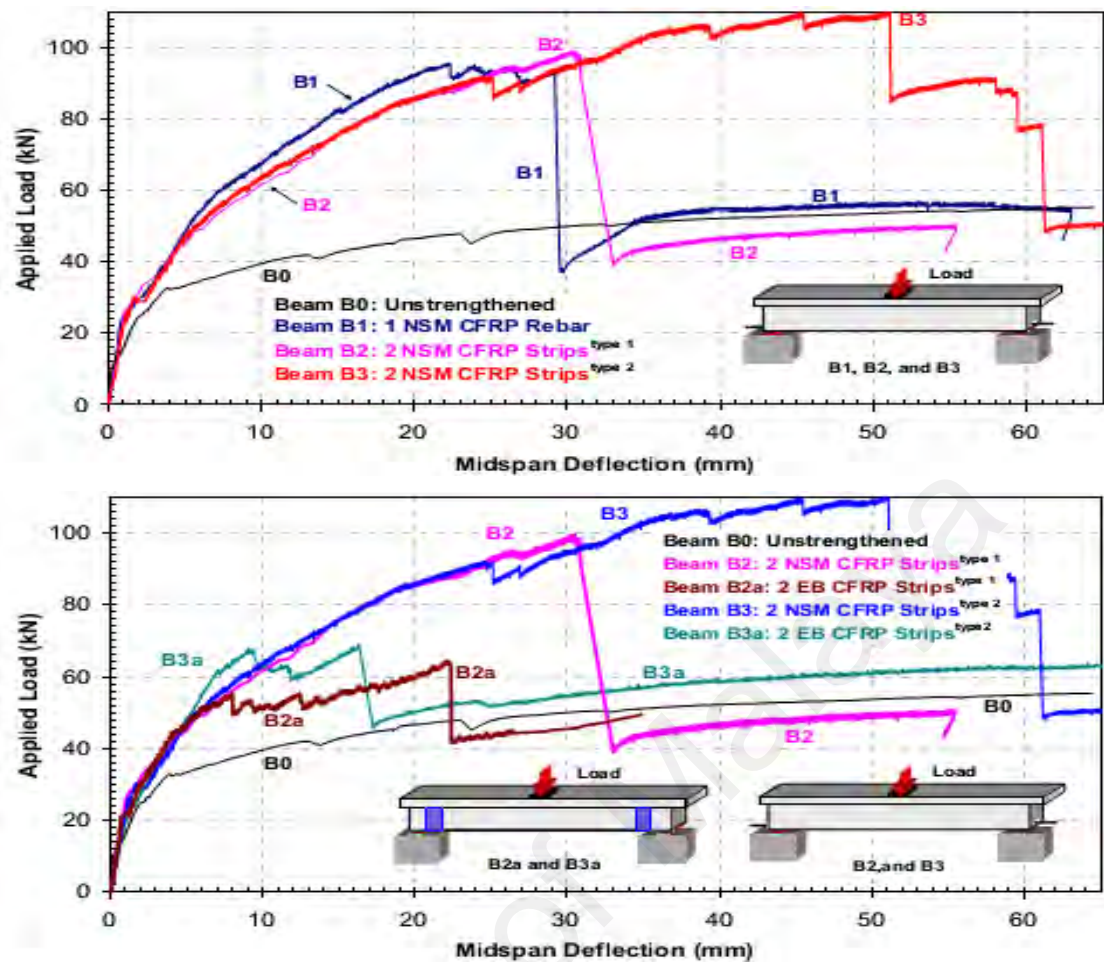


Figure 2.17: Load vs. Deflection of NSM CFRP rebar & strip and comparison of EBR & NSM (El-Hacha, R. & Rizkalla, S. H., 2004)

The bottom tension reinforcement consisted of 2 nos. 13mm with 2 nos. 16 mm deformed steel bars in such a manner that the flexural failure of the strengthened beams would always occur at the mid-span section, and simulate field conditions where the bottom steel reinforcement was corroded or damaged. In their research, NSM FRP reinforcement achieved higher ultimate load than beams strengthened with externally bonded FRP reinforcement. This was due to the high utilization of the tensile strength of the FRP reinforcement. The NSM FRP strips had doubled the bond area compared to externally bonded FRP strips. Failure modes of NSM were as follows: (a) NSM CFRP strips failed by tensile rupture, NSM CFRP rebar failed by FRP-epoxy-split failure at rebar-epoxy interface, NSM GFRP thermoplastic strips failed by Concrete-split failure. Failure of externally bonded CFRP or thermoplastic GFRP strips was due to debonding

between the strips and the concrete. From the Figure 2.17 it was visible that NSM CFRP strips showed more load carrying capacity compared to similar beams strengthened with NSM CFRP rebar having same axial stiffness. This was possibly due to the early debonding failure that occurred at the CFRP rebar-epoxy interface.

Ashour (2006) reported test results of 12 concrete beams reinforced with glass fiber-reinforced polymer (GFRP) bars subjected to a four point loading system. Simplified methods for predicting the flexural and shear capacities of beams tested were presented with numerical analysis. Twelve GFRP-reinforced concrete beams having f_{cu} of 34 MPA and 59MPa with the same length and width of 2100 and 150 mm were taken under experimentation. Three beam depths were examined, namely 200, 250 and 300 mm. For each depth, two types/ varieties of GFRP reinforcement were used; one for under-reinforced case and the other for over-reinforced case. All beams had neither vertical links nor compression reinforcement. Under-reinforced beams failed in flexural mode due to GFRP bar rupture whereas shear failure occurred for over-reinforced beams. Beams failed in flexure exhibited excessive deflection compared with the same depth beams failed in shear. The proposed analytical prediction model showed a good correlation with experimental results. Existing methods for calculating shear capacity showed inconsistency and conservative in nature.

Yost, J.R. et al. (2007) documented the behavior of full-scale test beams strengthened in flexure with NSM CFRP strips and tested to failure in four-point bending. They had evaluated strength and ductility of steel reinforced concrete beams strengthened with near surface mounted CFRP strips. Three control beams and twelve CFRP strengthened simply supported full-scale concrete beams were tested in flexure. All test beams had shear-span-to-steel-reinforcement-depth ratio a_v/d_s of 8.4 so that ultimate strength would be controlled by flexural failure and not shear failure.

Experimental variables included three different ratios of steel reinforcement ρ_s and two different ratios of CFRP reinforcement ρ_{frp} . Yield and ultimate strengths, flexural failure modes, and ductility were discussed based on measured load, deflection, and strain data. The strengthened beams failed in flexure as predicted according to the amounts of steel and CFRP reinforcement. Specimens with two CFRP strips failed by steel yield followed by concrete crushing where specimens with one CFRP strip failed by steel yield followed by CFRP rupture. In all cases, no debonding of the CFRP was detected. All beams strengthened with CFRP failed at loads greater than their respective control beams.

2.4 Recent Works on Strengthening Materials and Techniques

Several researchers attempted to introduce alternative strengthening materials and techniques to achieve better structural functioning and superior performance against debonding problem.

2.4.1 Alternative Strengthening Materials

The NSM technique is considered as a contemporary technique, though NSM steel bars have been successfully applied in a faulty concrete bridge deck in Lapland, Finland since 1947. Steel plate has been widely used as a strengthening material at the tension zone of the structures. The main drawback of the technique is the self-weight and the corrosive nature of the steel plate. However, the example of steel bar inside the groove was rare except Asplund's effort. Steel bar with cement grout was occasionally used in different countries to repair RC structure. However, this approach was not widely popular in the scientific community due to steel's corrosive behavior within the cement mortar or grout.

Currently, the researchers are curious about the usage of steel as strengthening material inside epoxy adhesive. This is promising as the modern specialized epoxy

creates hindrance of moisture penetration inside epoxy around the steel bar which would create the oxidation process and will eventually causes corrosion. Several researchers are experimenting using steel inside the NSM groove. Cost of strengthening material plays very important role in the decision making process as (GangaRao et al., 2006) stated the FRP's cost was around 30 times more than the conventional steel reinforcement. Whereas (Rahal & Rumaih, 2011) documented only 7%–10% shear capacity improvement by CFRP strengthened test region over the steel strengthened test region and their performance was comparatively analogous.

Wu et al. (2010) examined mechanical performance and performance of steel-fiber reinforce polymer (SFCB). Uniaxial and cyclic test exhibited that SFCB has a high elastic modulus, a stable post-yield modulus and a high ultimate strength. The factors that influence the failure mode of pullout test were steel/FRP ratio, effective bond length, and concrete strength. Section stiffness at service stage and bearing capacity in the ultimate stage was significantly improved by introducing NSM-SFCB strengthening system in flexure members.

Sun, Z. Y. et al. (2011) presented a comparative study which presented static loading result of NSM reinforced RC beam using steel bars, CFRP bars, and four different types of Steel Fiber Reinforced Polymer Composite Bars (SFCB). Seven NSM reinforced RC beams having X-sectional dimension of 300x150 mm with 1800 mm length had been tested under four-point bending load. Test matrix was 1 control beam, 1 Steel-NSM beam (14 mm diameter), 4 SFCB-NSM beams and 1 CFRP-NSM Beam (2-8mm diameter). Two identical rectangular grooves with the lengths of 1700mm, widths of 20mm and depth of 20 mm were cut on the beam soffit. The clear spacing between the grooves was 50mm. SFCB-NSM beam showed enhanced stiffness and bearing capacity. Failure mode of Steel-NSM was crushing of concrete after yielding of steel bar. The

beam with CFRP-NSM bar failed due to debonding of concrete cover. The SFCB-NSM beams showed debonding of concrete cover with high FRP/Steel ratio and ductile concrete crushing occurred after the rupture of the SFCB's outer FRP with lower FRP/Steel ratio. It showed anticorrosion like CFRP with lower strengthening cost.

Rahal and Rumaih (2011) studied the shear strengthening performance of four large scale RC T-beams using CFRP and steel reinforced NSM technique. It focused on the factors such as the anchorage in the flange concrete, orientation and type of NSM reinforcement. Among the four beams, one was control and the other three were NSM strengthened for shear which contained two testing region each, one strengthened with CFRP and the other with conventional steel. The beams were 3 m long, 500 mm deep, $d=430$ mm, flange width= 380 mm and flange depth = 100 mm. The shear span $a = 1290$ mm gives a shear span to depth ratio a/d of 3. Between the two testing regions, left side was strengthened with conventional $\phi 8$ mm deformed steel bars, while the right side was strengthened with 8 mm ϕ deformed CFRP bars. Among these three beams, strengthening reinforcement of anchorage was with or without extension to the flange and 45° oriented to the axis of beam. NSM grooves were cut 25 mm deep and 25 mm wide in the cast concrete.



Figure 2.18: Failure modes of the strengthened beams(Rahal & Rumaih, 2011)

By strengthening shear was increased from 37% to 92%. In Figure 2.18, the failure modes of the strengthened beam are presented. Through orienting the NSM

reinforcement at 45° , it shows most efficient increment. It also showed improvement of ductility. Only 7%–10% shear capacity improvement was observed in CFRP strengthened test region over the steel strengthened test region and their performance was comparatively analogous. The NSM reinforcement minimized the diagonal crack width and improved the cracking shear force which ranged between 23% and 85%.

Sun, Z. et al. (2011) studied flexural behavior of a novel reinforcement named Steel-FRP Composite Bar (SFCB) under static loading. RC beams were strengthened by SFCB, CFRP bars and ordinary steel bars and then tested. Test variables of SFCB were the types of FRP used (CFRP and basalt FRP) and steel/FRP ratio. NSM-SFCB exhibited increase in stiffness. NSM-CFRM beam showed crushing after steel bar yielded and CFRP beam was failed by debonding. With a high FRP/steel ratio, NSM-SFCB failed by debonding of concrete cover while lower ratio confirmed concrete crushing failure. NSM-CFRM is economical than CFRP maintaining anti-corrosiveness.

Godat et al. (2012) developed an experimental and analytical model for FRP shear strengthened RC beams to assess bond behavior of embedded through section (ETS). Direct-shear test specimens were prepared with variable parameters like concrete strength, hole diameter, bar diameter, bar surface area, and bar bond length. Results show that debonding can be avoided by providing a sufficient bar length and high concrete strength. A new equation that accounts for concrete compressive strength and bar diameter is provided to estimate the development length.

Ferrier et al. (2012) developed of new composite fiber cement internally reinforced with FRP rod (CFCIR-CFRP or CFCIR-GFRP) were tested to assess mechanical performance (increasing bearing capacity & reducing crack propagation). Four-point bending test was conducted to get load–displacement curve, bending stiffness, cracking load, yield strength and failure load. Using the new composites, both EBR and NSM

system exhibits good results in terms of bearing capacity (63% increased) and reducing crack width in same proportion to traditional solution (NSM-CFRP).

Jalali et al. (2012) evaluated manually made FRP rod's (MMFRP) efficacy for shear strengthening. A series of test were done with and without a new end anchorage system with MMFRP. The proposed end anchorage improved ductility performance of the beam as well as increased shear capacity by 25% to 48% over the control specimen.

2.4.2 Other Options of Strengthening Techniques

Eshwar et al. (2008) presented the study of two FRP based anchor systems named, NSM end anchor and spike anchor to observe the effectiveness of these systems against premature peeling and to determine their bond length. 16 NSM end anchor and 19 spike anchor specimen were tested. For NSM anchor system the study focused on the location, groove size, and anchor bar size and for spike anchor system, the location and embedment of the spike anchors were taken into account. Both of the systems demonstrated a superior efficacy with hindering FRP delamination. Bond-dependent coefficients of 0.90 (K_m) and 0.25 (K_v) are recommended when using these anchors for flexural and shear strengthening applications

Chaallal et al. (2011) examined the shear strengthening performance of new method Embedded through Section (ETS) over the existing shear strengthening method (EB, NSM) using FRP. T-beams were prepared which consists of control beam, EB-CFRP, NSM-FRP and ETS-FRP and the variables of experimental test matrix were effectiveness of strengthening methods, presence of internal steel stirrups and spacing of the steel stirrups. The average increase of shear capacity reached 23% for EB U jacket sheet, 31% for NSM-FRP and 60% for ETS-FRP rod. EB failed by FRP sheet debonding and NSM failed by side cover of stirrups, while ETS failed by flexure.

Authors suggested studying the effects of spacing, cross-section area, and different types of FRP rods, and developing a design model at last.

Razaqpur et al. (2011) tested a new self-anchored NSM CFRP bar to visualize their efficacy of delaying the onset of delamination from substrate. Two control beams (NSM-CFRP) and 4 self-anchored NSM-CFRP beams (flexure & shear strengthened) were tested under 4 point bending to visualize and compare the beams' strength, failure mode, deformability, and ductility. The new system exhibited at least 45% increment of failure load, 90% rise of tensile strain over the unanchored specimen and also delayed delamination. Displacement ductility and energy ductility were also increased by 34% and 42%, respectively, corresponding to 20% strength degradation.

Nardone et al. (2011) developed the numerical analysis of flexural behavior at both serviceability and ultimate limit states for an alternative mechanically fastened FRP (MF-FRP) system where steel anchors nailed the adhesive bonded FRP laminate to the substrate. Actually this was an extension of the research of Bank, 2004; Rizzo, 2005 and Elsayed et.al., 2009. Its advantages are quick installation, minimal surface preparation and immediate use of the strengthened structures. Along with the benefits, this system also creates concrete damage during fastener installation and brittle failure modes.

Mostofinejad and Shamel (2013) proposed experimental test of an improved strengthening technique named EBROG method which was an advanced approach over EBR. The researchers placed FRP sheets (one, two & three) in groove at tension face with wet-lay-up application then subjected to 4-point bending test. It demonstrated an increased ultimate limit over EBR. Higher failure loads and less displacement was resulted using EBROG method with multiple FRP sheets.

Babaeidarabad et al. (2014) explored the possibility of an external strengthening technique using fabric-reinforced cementitious-matrix (FRCM) materials in RC members. It is a composite material consisting of one or more layers of cement-based matrix reinforced with dry-fiber fabric. 18 FRCM flexurally strengthened RC beams were tested with one and four fabric reinforcement arrangement. Subject to the quantity of FRCM, 13% to 92% of flexural capacity was increased. Based on the reinforcement, two failure modes were observed, namely: fabric slippage within the matrix, and FRCM delamination from the substrate. However, the pseudo-ductility reduced with the increasing amount of the flexural capacity.

2.4.3 Combination of Different Strengthening Techniques

2.4.3.1 T-Shaped NSM and EBR CFRP Strips

Lim (2009) studied the flexural strengthening performance of RC T-beam reinforced with combination of NSM and EBR CFRP strips. Nine RC T-beams were tested by 4-point bending load test where two groups were formed. One group consisted of only NSM strengthened beam and the other group comprised joint reinforced of EBR and NSM system. By using epoxy, two CFRP strips were glued perpendicularly at middle to form a T-shape strip which was believed to enhance the serviceability performance (Figure 2.19). The main test variables were number and spacing of NSM strips, and the number and width of EBR CFRP strips. Combined strengthened beam demonstrated enhanced flexural strength and stiffness compared to NSM series. Its flexural strength was increased up to 347% compared with control beam. In this combination system, EBR strip showed initial debonding failure, later which succeeded to NSM strip failure. This system can resist applied load as well as redistribute total stress from RC beam. Author suggested increasing sufficient side concrete cover thickness from the NSM strip to the concrete surface to full use of the tensile strength of NSM CFRP strip. The maximum tensile strains measured in the NSM and EBR CFRP strips of the beam

reinforced with T-shape strips were seen to be in the range of 8200–11 600 $\mu\epsilon$ and 7000–8900 $\mu\epsilon$, respectively. This result shows that the T-shaped strips have good combination to resist applied load and the combined reinforcement with NSM and EBR strips can redistribute appropriately the total stress subjected to the concrete beam to the EBR and NSM strips.

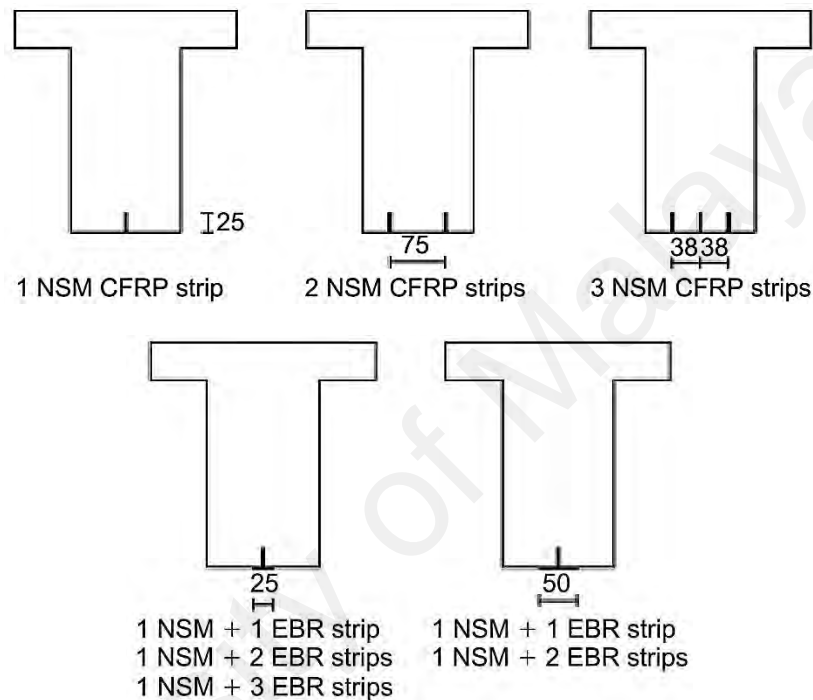


Figure 2.19: Rectangular and T-shaped CFRP strip (Lim, 2009)

Lim (2010) Investigated the efficacy of shear strengthening of NSM-CFRP and EBR-CFRP strengthened RC beam. Combined NSM and EBR strengthened CFRP expressively heightened the shear stiffness and strength in comparison to the control beam. This combination system can resist applied load and redistribute total stress of the RC beam.

2.4.3.2 Hybrid Bonding Technique

Rahman et al. (2015) presented the experimental results of hybrid bonding technique. The system included the externally bonded steel plate with slotted deformed steel bar.

Seven beams (one control and six strengthened) were tested where the test variables were, geometrical dimensions of the plate and number of grooves or NSM bars. Four point bending load was applied on the tested specimens. All the beams were failed due to debonding where the concrete cover was separated. The ultimate load capacity of the strengthened beam was increased by 27% to 65% compared to the control beam. Hybrid bonding method improved 32% failure load compared to the corresponding plate bonding method. A negative impact was noticed when the number of groove was increased which may adversely influence the efficiency of the hybrid bonding method. Ductility was not improved by using this technique and its value was less than the unstrengthened beam.

2.5 Artificial Intelligence (AI) Technique

Artificial Intelligence (AI) technique pursues the computer or machines to behave as intelligent as human being. In 1956, John McCarthy first coined this word at the Massachusetts Institute of Technology (MIT). He defined this term as “The science and engineering of making intelligent machines, especially intelligent computer programs”. Its goal is to develop expert systems which can learn, behave and execute decisions intelligently just like the human perform.

In this research, Fuzzy Logic Expert System (FLES) is the particular area of interest in the branch of AI technique. Very few researches on structural strengthening works were reported which incorporated the implementation of these AI technique to forecast the performance of any specific parameters. Some of the researchers’ works are reported in the following sections.

2.5.1 FLES Application in Structural Strengthening

After realizing the promising applicability of fuzzy logic, it has been used as embedded controller in different machine or electrical equipment. Its application in civil

engineering area is also getting popularity and researchers are looking for its new usage in different areas of this branch of engineering. However, in structural strengthening area, very few applications are reported so far in literature.

Aydin and Kisi (2014) investigated the appropriateness of using a new fuzzy genetic fused system to identify the damage in Timoshenko beam-type structures. The crack location and extent was identified by this hybrid system. Fuzzy logic was the backbone of this investigation where the membership function was tuned by genetic algorithm. The developed model can be used as a non-destructive structural health monitoring procedure in real beam type structures.

Irani and Kamal (2014) reported about the intelligent system and their solution in the construction industry. They came across 514 publications extracted from Scopus database. According to the authors, construction project operations and building construction projects were the mostly used context category where several intelligent systems were used. During 1990 to 2012, the USA, Taiwan, UK and Canada were the principal research region in intelligent systems. Among several other AI techniques, fuzzy logic also contributed significantly.

Güler et al. (2012) presented a fuzzy approach to model the stress-strain behavior of high strength concrete under uni-axial loading. The model could simulate the stress-strain behavior correctly considering different parameters. The fuzzy output excellently conformed to the experimental and analytical results. Both normal and high strength concrete could be simulated with slight modification of the fuzzy approximation.

Şen (2010) categorized existing buildings of Istanbul, Turkey against seismic hazard with the help of fuzzy logic. Several visual assessable parameters (e.g. story number, cantilever extension, soft story, and peak ground velocity) were used as input variables

where earthquake hazard category was the only output variable. The developed fuzzy model played an excellent role as a decision tool of the municipality to identify the buildings vulnerable to earthquake. They authority could again categorize those building as “not-demolishable” or “demolishable”.

Cevik (2011) applied several soft computing techniques, such as neuro- fuzzy, genetic programming, stepwise regression and neural network to model the influence of FRP on confined concrete cylinders. The model was based on collected experimental data from open literature, which showed superior accuracy. Their formulation also conforms to the existing 10 models.

Zheng et al. (2011) predicted the delamination size and location of glass/epoxy laminate beams using a combination of fuzzy logic theory, neural networks and genetic algorithms. Modal frequencies were obtained from finite element analysis and the parameters were fed in this genetic fuzzy hybrid learning algorithm. The model demonstrated robust and promising applications in the structural health monitoring system.

Nasrollahzadeh and Basiri (2014) developed a model to predict the shear strength of FRP reinforced RC structures using the Fuzzy Inference System (FIS). The study samples were 197 RC beams and slabs for which they utilized the subtractive clustering approach for partitioning the numerical data. The output of their model was only compared with the shear design guidelines (e.g., ACI and CAN/CSA).

2.6 Finite Element Modelling (FEM)

The finite element method is the prevailing discretization method in structural mechanics. In this analysis, any complex structure can be modelled mathematically comprising a system of point called node. The finite elements are connected with the

help of these nodes which contain the information of the specific material and its property to define its behavior under certain condition (e.g. applied load, temperature etc.). The process was operated by several sets of algebraic equations and the number of degrees of freedom. To express a particular engineering problem, a set of governing equations are assigned with specific boundary conditions.

2.6.1 Application of FEM on Strengthened RC Beam

Finite element analysis of FRP strengthened RC beams attracts attention of the researchers in the recent decades. Experimental analyses of the FRP strengthened structures are extremely costly and several uncertainties (construction error, mishandling, material property discrepancy) are involved during experiments which make the experimental results questionable. FEM provides an alternative approach to simulate the actual behavior of a strengthened structure under variable loading. Several researchers performed finite element analysis to confirm their experimental findings.

Hu et. al., 2004 developed an FE model using ABAQUS to predict the ultimate capacity of FRP strengthened RC beams. Proper constitutive models were used to model the nonlinearities of the concrete, steel and FRP. Short and long beams are studied with low and high steel ratio to study the influence of beam length, reinforcement ratio and fiber orientation under uniformly distributed load. Only $\frac{1}{4}$ th of the beam was modeled where symmetric boundary condition was applied along two symmetric planes. The numerical results showed that beams with low steel ratio significantly affected with the length of beam. However, the high steel ratio did not exhibit such relation with beam length. The beam with high steel ratio displayed more cracks at the mid-span region, whereas the low steel ratio beams showed more cracks at the support area.

De Lorenzis et al., 2004 presented the mechanics of bond of NSM FRP bar with concrete using current and previous test results. They also developed a three dimensional FEM model and calibrated with experimental results. The test variables of experimental test series were bar type, groove size, bonded length, and groove-filling material. The NSM reinforcement was modelled having two interfaces: the bar-epoxy and the epoxy-concrete interface which differed from the regular internal steel bar bond with concrete. The epoxy concrete interface was modeled with a Coulomb frictional model. On principle, the interface element has a relation with the traction and displacement. The concrete, epoxy, and FRP bar were all modeled with solid elements. After calibrating the FEM model with some of the experimental beams, it was capable to simulate the failure mode, ultimate load and the load-deflection behavior. Even this model gave the bond-slip behavior as output rather than an input.

Soliman et. al., 2010 assessed flexural performance of RC beam strengthened by NSM-FRP bars. Test variables included internal steel reinforcement ratio, type of NSM-FRP bars, FRP bar diameter, bonded length, and groove size. Displacement controlled nonlinear three-dimension FEM analysis was performed in ADINA software to observe the flexure behavior of the tested beam. Concrete, CFRP, and epoxy layers were modeled using eight node brick elements and steel bars were simulated with two node truss element. The general multi-axial stress-strain relations are derived from the nonlinear uniaxial stress-strain relation. After comparing the experimental and numerical findings, a parametric study was done which included the factors of internal steel reinforcement ratio, concrete compressive strength, bonded length and area, and the Young's modulus of NSM-FRP bars. Worthy agreement was established between experiment and analysis in terms of load-deflection and load-strain relationships, ultimate capacities, and modes of failure. Due to the full bond consideration between

the adhesive and the FRP, the numerical model demonstrated 5% higher debonding strain compared to the experimental one.

Hawileh, 2011 developed three dimensional nonlinear FEM model through ANSYS finite element software based on the experimental result of Al-Mahmoud et al., 2009. The nonlinear model predicts load-deflection and failure mode by measuring the effect of carrying capacity and response of NSM-CFRP strengthened RC beam under four-point bending test. Figure 2.20 showed the modelling strategy which counted the nonlinear constitutive concrete material property, yielding of steel reinforcement, cracking of the filler materials, bond slip of the steel and NSM reinforcements with the adjacent concrete surfaces, and bond at the interface between the filling materials and concrete. This experiment validated the numerical results with other researcher's experimental result. Validated model was used for further study of the effect of NSM bar type and size.

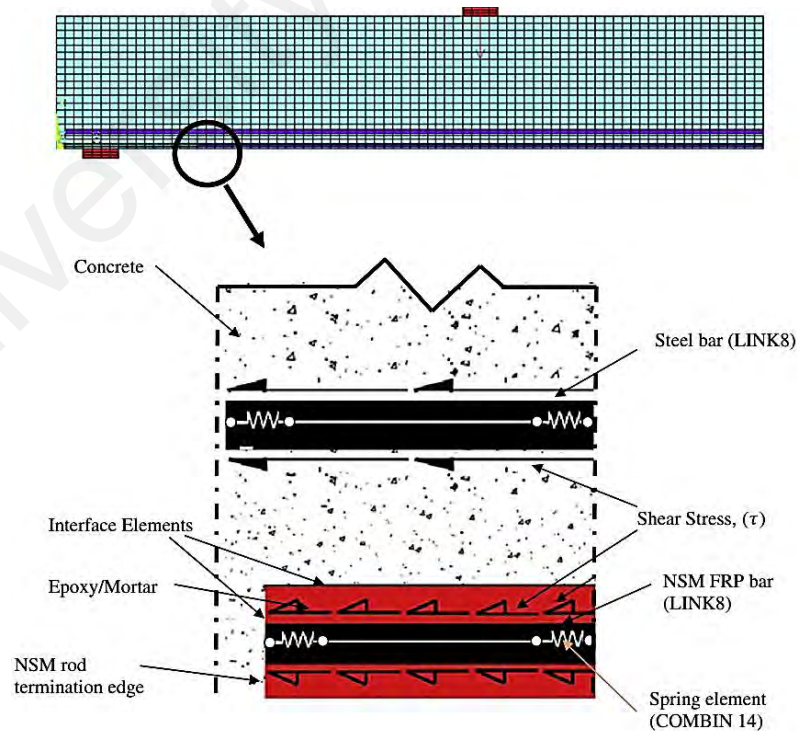


Figure 2.20: Detail modelling strategy of NSM bar and main reinforcement (Hawileh, 2011)

Sasmal et. al., 2013 performed a three dimensional FEM analysis for bond-slip relations of NSM CFRP bars under displacement controlled pullout test. Test variables were rib diameter, rib spacing and epoxy strength. Shear stress along length, fracture energy and tension stiffening were considered with material nonlinear properties. The ATENA software was used for FE analysis where three dimensional solid regions called macro-elements were used in this study. Perfect bonding was considered for contact between epoxy and concrete, though, a 3D interface element was defined between epoxy and NSM CFRP bar. The results found that, the higher the epoxy strength, the lower the bond strength. The rib spacing of 0.8 times the bar diameter and rib's diameter of 1.2 times the bar diameter was the most efficient to increase the bond strength. The model conformed to experimental result and a good relationship was established to develop a reliable bond slip model for useful practice in designing strengthening scheme.

Zhang and Teng, 2013 described the interaction forces between RC beam and NSM bar. The theoretical study was based on the closed form solution of Smith and Teng, 2001 about the tangential and normal interaction forces of EBR strengthened beam. In this study, it included NSM FRP rectangular bar and strip and compared the results with three dimensional FEM model. ABAQUS software had been used for FEM analysis. Maintaining the geometry, a quarter of the beam was modeled using eight-node brick element to save the computational cost. From FE result, approximate equations were derived for the tangential stiffness parameter and the normal stiffness parameter. Both the analytical and FEM studies confirm the high interaction forces at bar end region due to the debonding failure. The authors described this approach as a generic solution which could be applicable to circular and elliptical shaped NSM bars.

Almusallam, 2013 tested NSM- Steel & GFRP flexure strengthened RC beams under monotonic load and nonlinear FEM analysis was conducted using LS-DYNA finite element program. Considering corrosion and loosing strength of the beam, different schemes of NSM steel and GFRP strengthened RC beam were designed. Only half of the strengthened RC beam was modeled considering the overall beam geometry. Concrete and epoxy adhesive were modeled using 8-node solid hexahedron elements. The software can control the undesirable hourglass modes by applying three dimensional algorithms. The problem solving issue was dependent on explicit time integration algorithms and the displacement controlled operation fixed a pace rate of 1 mm/min to match with the experimental rate. The FE simulated failure mode was nicely matched with the experimental failures. The load-deflection curves were also in good agreement with a little variation (8% to 11%) of ultimate strength prediction. In experiment, NSM-steel or GFRP bar didn't show any debonding failure. Steel NSM was a successful technique for flexure strengthening and the flexural capacity and effective pre-yield stiffness was increased due to increased NSM reinforcement ratio. Though the result exhibited efficient flexure capacity, however, effective stiffness of NSM-FRP beams were reduced due to using lower modulus FRP.

2.7 Summary of the Findings

Based on the review of the existing literature, the following comments can be constituted on the strengthened RC beam.

- i. Steel plate has been widely used as strengthening material in EBR in spite of its limitations like corrosion and high density. However, the research on steel bar as a strengthening material inside NSM groove was less unexplored which is a particular research interest in area of strengthening.

- ii. In EBR technique, thickened or multiple layers of laminates are much susceptible to plate end debonding. The development of high interfacial shear stresses at the CFRP sheet ends could cause the premature debonding failure without utilizing its full capacity. An efficient technique is needed to avoid such failures.
- iii. It is identified that the drop in CFRP fabric thickness diminishes the degree of stress concentration at the plate edge. The remedial solution could be either the variation of thickness of adhesive layer of the FRP plate or the joint geometry by tapering the plate or using adhesive fillets which is quite complex, time consuming and requires more cost.
- iv. In NSM method, often, the width of the beam may not be wide enough to provide necessary edge clearance and clear spacing between two adjacent NSM grooves. Furthermore, it requires more concrete cover to the existing reinforcement to allocate the grooves to be cut exclusive of the possibility of damaging the steel.
- v. A thin CFRP fabric at outer layer with NSM steel or CFRP reinforcement inside could be a better alternative to increase the flexural strength with less debonding possibility for a RC beam having less beam width. With the combination of these two techniques, the effective bond surface area would be increased, which ultimately would decreased the interfacial shear stress and the possibility of debonding.
- vi. The review of existing literature reveals that a complete theoretical deflection prediction model of NSM or other newly strengthened RC structures is scarce. The existing analytical models are either based on the classical RC beam theory or are modified version for EBR strengthened beam. The AI based techniques could solve this problem which had a

proven track record of developing prediction model in other branch of sciences. Even, several prediction models on shear strengthening and other structural engineering related problems were successfully solved by the AI based Fuzzy logic approach.

- vii. At present, FEM models on various structural strengthening techniques were developed by different researchers. The FEM is an effective tool to predict the behavior of the original structure under applied load. Hence, it is desired to assess the behavior of the proposed strengthening technique with the FEM and verify the experimental results.

From the findings it can be concluded that both the EBR and NSM systems have some limitations. Combination technique is capable of making it possible to reduce the plate thickness by transferring a portion of plate material from plate bonding to NSM technique. Consequently, the NSM bar size can also be reduced through shearing with plate bonding method and thus provide sufficient space of edge clearance and groove clear spacing. Furthermore, the FEM model is needed to compare the experimental results of the strengthened RC beams. The FLES techniques are able to develop a serviceability prediction model where the predicted values could be achieved shortly, which, in turn, would make it possible for a large number of alternative strengthening configurations to be evaluated, and thus beam specifications could be easily optimized for future use.

CHAPTER 3: METHODOLOGY OF EXPERIMENTAL PROGRAM

The methodology of the experimental test program is presented in this chapter. The main goal of this research was to develop an effective strengthening system which could increase the flexural performance as well as delay the debonding failure. The experimental program was designed to meet the objectives of the research. Four different groups were categorized according to their strengthening schemes which are listed in the Table 3.1. The materials which were used for preparing the concrete beam and its strengthening are discussed in detail. These supplementary test results are reported in the appendix chapter. The strengthening process for different strengthening scheme is discussed thoroughly to understand their construction sequences. The strain gauge, linear measurement, crack monitoring equipment and acquisition systems are explained along with their necessary features. The test setup along with the necessary instrumentation procedure for the experiments is described at the end of this chapter.

3.1 Test Matrix

Twenty-seven RC beams were prepared for experimental test based on the test matrix provided in Table 3.1. There were mainly four groups: i) Near Surface Mounted strengthened beams with CFRP/steel bar, ii) Externally Bonded with CFRP fabric, iii) CEBNSM-B strengthened beams with CFRP/steel bar and iv) CEBNSM-S strengthened beams with CFRP strip as well as control unstrengthened specimens. All the specimens in the four groups were tested under monotonic load. All the RC beams were designed with under-reinforced condition to be failed in flexure (concrete crushing after yielding the internal steel). The detailed design of RC beams is described in Appendix A. The beam notation is explained in the subsequent paragraphs.

Table 3.1: Test matrix of the experimental program

Sl. No.	Notation	Description	Strengthening dimension
Group A: NSM strengthened RC beams under static loading			
1	CB	Control RC beam	-
2	N1.6F	12 mm NSM CFRP bar	Bond length=1600 mm
3	N1.6S	12 mm NSM steel bar	Bond length=1600 mm
4	N1.8F	12 mm NSM CFRP bar	Bond length=1800 mm
5	N1.8S	12 mm NSM steel bar	Bond length=1800 mm
6	N1.9F	12 mm NSM CFRP bar	Bond length=1900 mm
7	N1.9S	12 mm NSM steel bar	Bond length=1900 mm
Group B: 06 nos.)			
1	CB	Control unstrengthened beam	-
2	CB	Control unstrengthened beam	-
3	EBP1	EB 1 ply CFRP fabric	CFRP fabric: 2900×125×0.17 mm ³
4	EBP2	EB 2 ply CFRP fabric	CFRP 1st fabric: 2900×125×0.17 mm ³ CFRP 2nd fabric: 2700×125×0.17 mm ³
Group C: CEBNSM-B beams with CFRP/steel bar in NSM groove			
1	CBC8P1	NSM CFRP bar and EB 1 ply CFRP fabric	CFRP bar: 1-8mm ϕ (length=2900 mm) CFRP fabric: 2900×125×0.17 mm ³
2	CBC8P2	NSM CFRP bar and EB 2 ply CFRP fabric	CFRP bar: 1-8mm ϕ (2900 mm) CFRP 1st fabric: 2900×125×0.17 mm ³ CFRP 2nd fabric: 2700×125×0.17 mm ³
3	CBC10P1	NSM CFRP bar and EB 1 ply CFRP fabric	CFRP bar: 1-10mm ϕ (2900 mm) CFRP fabric: 2900×125×0.17 mm ³
4	CBC10P2	NSM CFRP bar and EB 2 ply CFRP fabric	CFRP bar: 1-10mm ϕ (2900 mm) CFRP 1st fabric: 2900×125×0.17 mm ³ CFRP 2nd fabric: 2700×125×0.17 mm ³
5	CBS8P1	NSM steel bar and EB 1 ply CFRP fabric	Steel bar: 1-8mm ϕ (2900 mm) CFRP fabric: 2900×125×0.17 mm ³
6	CBS8P2	NSM steel bar and EB 2 ply CFRP fabric	Steel bar: 1-8mm ϕ (2900 mm) CFRP 1st fabric: 2900×125×0.17 mm ³ CFRP 2nd fabric: 2700×125×0.17 mm ³
7	CBS10P1	NSM steel bar and EB 1 ply CFRP fabric	Steel bar: 1-10mm ϕ (2900 mm) CFRP fabric: 2900×125×0.17 mm ³
8	CBS10P2	NSM steel bar and EB 2 ply CFRP fabric	Steel bar: 1-10mm ϕ (2900 mm) CFRP 1st fabric: 2900×125×0.17 mm ³ CFRP 2nd fabric: 2700×125×0.17 mm ³
9	CBC10P2A	NSM CFRP bar, EB 2 ply CFRP fabric and 2 ply U-wrap end anchorage	CFRP bar: 1-10 mm ϕ (2900 mm) CFRP fabric: 2900×125×0.34 mm ³ CFRP U-wrap anchorage: 2 ply (625×125×0.34 mm ³)
10	CBS10P2A	NSM steel bar, EB 2 ply CFRP fabric and 2 ply U-wrap end anchorage	Steel bar: 1-10mm ϕ (2900 mm) CFRP fabric: 2900×125×0.34 mm ³ CFRP U-wrap anchorage: 2 ply (625×125×0.34 mm ³)

Table 3.1, continued: Test matrix of the experimental program

Sl. No.	Notation	Description	Strengthening dimension
Group D: CEBNSM-S beams with CFRP strips in groove			
1	CS1G1P2	Single grooved 1 no. CFRP NSM strip and EB 2 ply CFRP fabric	CFRP strip: 1 no.2900×15×1.4 mm ³ CFRP 1 st fabric: 2900×125×0.17 mm ³ CFRP 2nd fabric: 2700×125×0.17mm ³
2	CS2G2P2	Double grooved 2 nos. CFRP NSM strips and EB 2 ply CFRP fabric	CFRP strip: 2 no.2900×15×1.4 mm ³ CFRP 1 st fabric: 2900×125×0.17mm ³ CFRP 2nd fabric: 2700×125×0.17mm ³
3	CS2G1P1	Single grooved 2 nos. CFRP NSM strips and EB 1 ply CFRP fabric	CFRP strip: 2 nos.2900×15×1.4 mm ³ CFRP fabric: 2900×125×0.17 mm ³
4	CS2G2P1	Double grooved 2 nos. CFRP NSM strips and EB 1 ply CFRP fabric	CFRP strip: 2 nos.2900×15×1.4 mm ³ CFRP fabric: 2900×125×0.17 mm ³
5	CS3G3P1	Triple grooved 3 nos. CFRP NSM strips and EB 1 ply CFRP fabric	CFRP strip: 3 nos.2900×15×1.4 mm ³ CFRP fabric: 2900×125×0.17 mm ³
6	CS4G2P1	Double grooved 4 nos. CFRP NSM strips and EB 1 ply CFRP fabric	CFRP strip: 4 nos.2900×15×1.4 mm ³ CFRP fabric: 2900×125×0.17 mm ³

Seven beams were tested under Group A which is composed of one control beam and six NSM strengthened RC beams. The main testing variables were the bond length of the NSM reinforcement (1600, 1800, and 1900 mm) and the type of NSM reinforcement (CFRP and steel). The beam notation can be explained with an example of N1.9F and N1.9S beams. Here, N = NSM technique, 1.9 = bond length of NSM bar in meter, F= CFRP NSM bar, S= steel NSM bar. The bond lengths of the NSM reinforcement were 1600 mm, 1800 mm, and 1900 mm. The diameter of steel and CFRP bar was 12 mm for the strengthening material. 2-part epoxy adhesive (Sika 30) was used to affix the NSM strengthening material into the groove at the beam soffit. The dimension of the groove was fixed as 24 mm× 24 mm which was twice the strengthening bar diameter. This dimension was considered as optimal for round deformed rod according to (De Lorenzis & Nanni, 2002; Yost, J. R. et al., 2007).

Group B held four beams where two unstrengthened beams were tested to be the control beam of Group B, C and D. The other two beams were strengthened using the

EBR technique where the width of the EB CFRP fabric was fixed as 125 mm. The only test variable was the thickness of the CFRP fabric which varied from single layer (0.17 mm thickness) to double layer (0.34 mm thickness). The length of the single ply fabric was 2900 mm. However, in case of double layer, the inner ply length was maintained as 2900 mm and the outermost layer was 2600 mm to avoid the end peeling failure due to the increased interfacial shear stress and normal stress developed at the curtailment end of the CFRP fabric (Roberts and Haji-Kazemi 1989; Malek et al. 1998 and ACI-440.2R.08). These strengthened beams were tested with a goal to compare the experimental result with the CEBNSM-B and CEBNSM-S series beams as they consisted of both single and double layer at their exterior beam soffit face.

Group C comprised of the CEBNSM-B beams which were strengthened with the combination of NSM bar and EB CFRP fabric. The main testing variables were the types of NSM bar (CFRP and steel), the diameter of the NSM bar (8 mm and 10 mm) and the thickness of the external CFRP fabric (single layer or double layers) and the anchorage at curtailment location. Besides, the length of the CFRP fabric was also varied. For single-ply, 2900 mm long CFRP fabric was bonded at the beam soffit. However, for double-ply condition, the second layer was 2600 mm. The detail test matrix is shown in Table 3.1. The beam notation can be explained as follows with an example of CBC10P2A and CBS10P2A beams. Here, C = combination technique, BC = bar as NSM CFRP reinforcement, BS = bar as steel NSM reinforcement, 8 = 8mm diameter NSM bar, P2 = 2 ply CFRP fabric through EBR technique and A = Anchorage. Besides, inside the literature, the CBC series would mean the beams with NSM CFRP reinforcement and CBS stands for beams having NSM steel bar.

The CEBNSM-B strengthened series (Group C) consisted of ten beams. The first eight RC beams were strengthened using steel or CFRP NSM bar plus externally

bonded CFRP fabric and the remaining two beams were tested with CEBNSM-B plus CFRP U-anchorage technique. 8 mm or 10 mm diameter CFRP or steel bars were used as NSM strengthening material. These strengthening materials were inserted and fixed to the slot at the beam soffit with the help of a commercial epoxy adhesive (Sika 30). After proper curing, the concrete surface was prepared and CFRP fabric was glued over the entire width of beam using another two-part adhesive (Sika 330).

For Group D, six CEBNSM-S strengthened RC beams were tested under monotonic loading where rectangular CFRP strips were inserted at the NSM groove along with the externally bonded CFRP fabric at beam soffit. Table 3.1 shows the detail description and strengthening dimension of those beams. The main test variables were the number of NSM CFRP strip (1, 2, 3 and 4 nos.), number of grooves (single or double), dimensions of the groove (5 mm × 25 mm and 10 mm × 25 mm) and thickness of EB CFRP fabric layer (single or double layer). The beam notation can be explained as follows with an example of CS4G2P1 beam. Here, C = combination technique, S4= four CFRP strip as NSM reinforcement, G2= two grooves, P1= 1 ply CFRP fabric through EBR technique. In this series, the highest four CFRP strips were used in double NSM grooves where the groove dimensions were bigger. Maximum three CFRP strips were used in three separate single NSM grooves where the grooves were smaller in size. The thickness of the CFRP fabric varied to single and double layer where the bonded length was 2900 mm (for 1st layer) and 2600 mm (for 2nd layer).

3.2 Material Properties

The main ingredients to prepare the test specimens were concrete and steel. Besides, Carbon Fiber Reinforced Polymer (CFRP) bar, fabric and epoxy adhesive were used for strengthening purposes. Different mechanical properties of concrete and steel were

determined in the laboratory. The properties of CFRP bar, fabric and epoxy were supplied by the concerned manufacturers.

3.2.1 Concrete

Ready mixed concrete was used for the construction of the RC beam specimens. Crushed stone, 20 mm in diameter, was used as coarse aggregate and natural river sand was used as fine aggregate. The 28 days cube compressive strength of 2.3 m beams was 43.24 MPa and the flexural strength was 5.01 MPa. For 3.3 m beams, cube compressive strength and flexural strength were 50.1 MPa and 5.5 MPa respectively. The compressive and flexural strengths of the concrete were determined according to (ASTM, 2014; EN, BS 2009; EN, BS, 2009). The dimensions of the cube, cylinder and prism were 100 mm × 100 mm × 100 mm, 200 mm × 100 mm diameter and 500 mm × 100 mm × 100 mm, respectively.

3.2.2 Steel

Deformed steel bars, 12 mm in diameter, were used for internal longitudinal reinforcement in the beams (Figure 3.1). The deformed bars were tested in the laboratory for tensile strength to confirm the mechanical properties supplied by the manufacturer. The yield stress and modulus of elasticity were found to be 400 MPa and 200 GPa, respectively. 8 mm steel bars with yield stress of 380 MPa and modulus of elasticity of 200 GPa were used as shear reinforcement. 12 mm deformed steel bars with yield stress and modulus of elasticity of 520 MPa and 200 GPa, respectively, were used for NSM strengthening.



Figure 3.1: Steel bar used for specimen preparation

3.2.3 CFRP Bar and Fabric

Carbon-epoxy pultruded FRP (CFRP) bars, 12 mm in diameter with a density of 1.65 g/mm² were used for NSM strengthening in this study (Figure 3.2). These CFRP bars demonstrated linear elastic behavior up to failure. According to the manufacturer's product result (LAMACO), the ultimate strength of the bars was found to be 2400 MPa and the modulus of elasticity was 165 GPa. The surfaces of the CFRP bars was sand-coated to enhance bond performance.



Figure 3.2: CFRP bar used for strengthening of RC beam

SikaWrap Hex 230C uni-directional carbon fiber fabric was used to strengthen the concrete beams, prestressed to 40% and 60%, at the location of steel brackets. Sidatur® 330 was used to bond the CFRP sheets onto the concrete surface. The average cured laminate properties were as follows: tensile strength of 894 MPa, tensile modulus of 65.4 GPa, and tensile elongation of 1.33% (Sika, 2011).

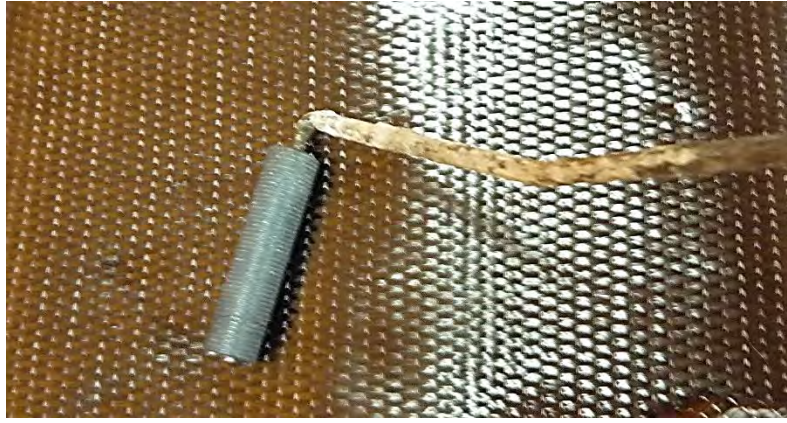


Figure 3.3: CFRP fabric used for strengthening of RC beam

3.2.4 Epoxy Adhesive

An epoxy adhesive, Sikadur® 30, was used to bond the NSM reinforcements to the concrete substrate for superior bond strength. The adhesive is composed of two components, resin and hardener, which were blended together in a ratio of 3:1 until an even grey color was attained. According to the manufacturer's results, the density was 1.65 kg/liter at 23⁰ C. The bond strength with steel was 21MPa according to DIN EN 24624 and with concrete it was 4MPa. The compressive, tensile and shear strengths of this adhesive were 85-95 MPa, 26-31 MPa and 16-19 MPa respectively at 7 days curing time and at 35⁰ C temperature (Sikadur®-30).

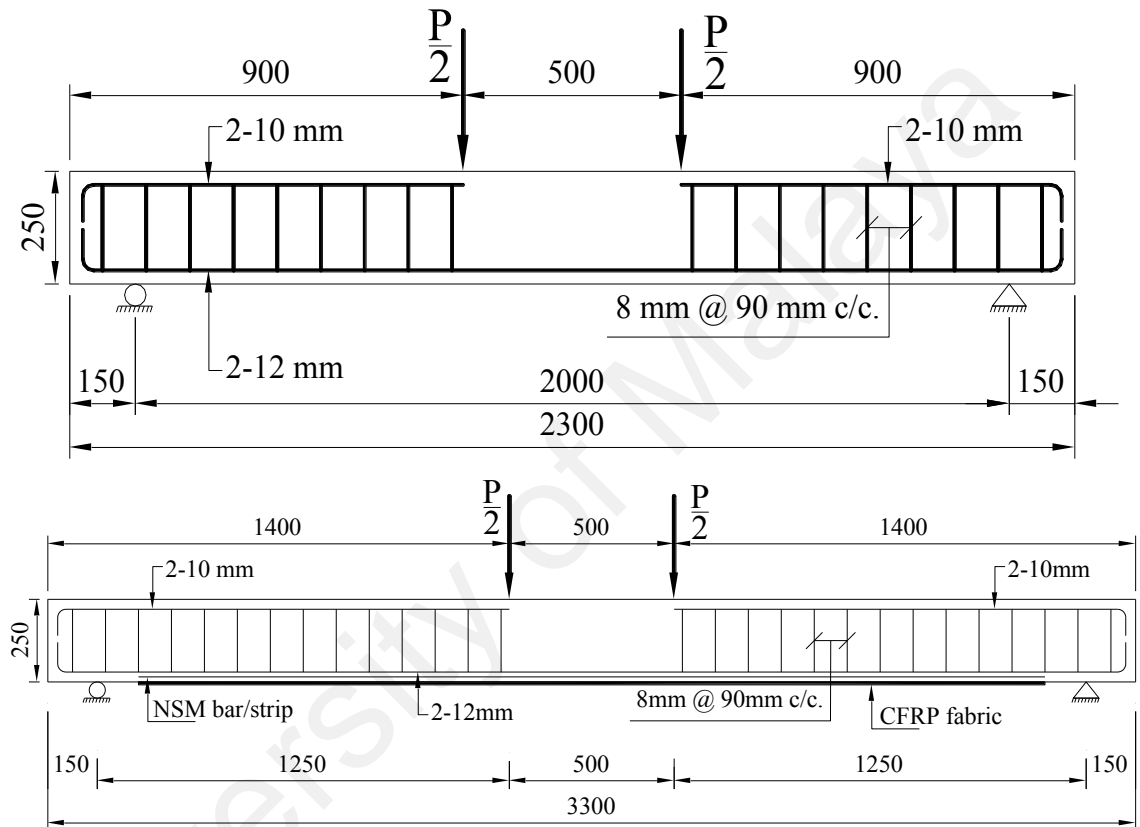
Sikadur® 330 is a two-component (4:1 by weight) epoxy resin used primarily for dry lay-up process. The mechanical properties of the epoxy were as follows: tensile strength of 30 MPa, elongation at break of 1.5%, and modulus of elasticity of 3.8 GPa (Sika, 2010a).

3.3 Specimen Configuration and Preparation

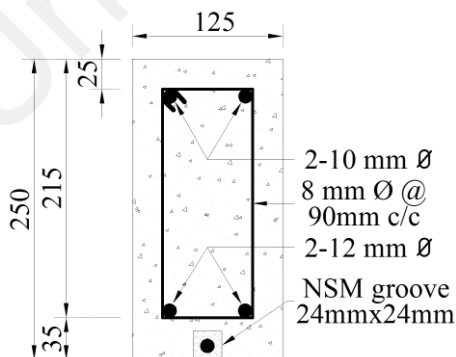
3.3.1 Configuration of Control and Strengthened RC beam

The beams in group A were 2.3 m long with effective spans of 2 m and rectangular cross-sections with dimension of 125 mm × 250 mm. Group B, C and D had beam dimension of 3300 mm × 125 mm × 250 mm with a clear span of 3000 mm. The control and strengthened beam specimens of group A were cast in the laboratory using

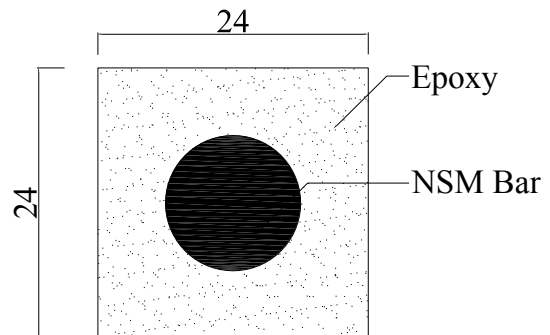
conventional concrete mixer. However, all the RC beams for group B, C and D were cast in the construction yard of a reputed precast concrete company named Eastern Pretech Sdn Bhd in order to maintaining the consistent quality of concrete and internal steel. The bottom clear cover was 35 mm to provide sufficient space for groove preparation and CFRP insertion. The side and top clear cover was maintained at 25 mm.



(a) Dimension and longitudinal main reinforcement of RC beams (All dimensions are in 'mm')



(b) Beam cross-section



(c) NSM groove detail

Figure 3.4: (a) Beam dimension, (b) beam cross-section and reinforcement and (c) NSM groove details of series A beam (All dimensions are in 'mm')

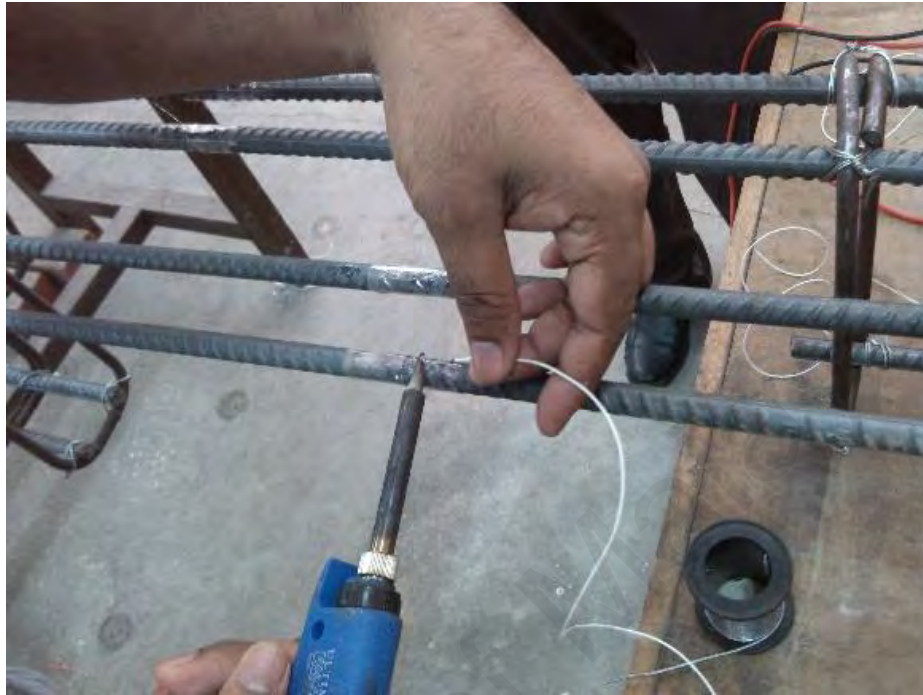
The tension reinforcements consisted of two 12 mm diameter ribbed bars with a ninety-degree bend at both ends. Two 10 mm diameter ribbed bars were used in the compression zone as hanger bars. There is no top bar at the middle portion of the beam where the moment was the maximum and shear was zero. The shear reinforcements were made with 8 mm diameter ribbed steel bars spaced 90 mm apart to make sure that there should not be any shear failure during the test.

The beams were designed as under reinforced ($\rho = A_s/bd = 0.0085$) beams to initiate failure in flexure in accordance with the EC2 code. Figure 3.4 displays the details of the beam configuration. For NSM strengthened beams, a 24 mm \times 24 mm groove was cut at the soffit of the RC beam using a diamond cutter and hand chisel. 12 mm diameter CFRP and steel rod is inserted in the groove for Group A specimen. For CEBNSM-B and CEBNSM-S strengthened beams (Group C and D), 8 mm and 10 mm diameter CFRP and steel bars were used as strengthening material in the slotted RC specimens.

3.3.2 Fabrication of RC Beam

The steel cages for the RC beams was prepared according to the design and dimension provided in the Figure 3.4. As there was no compression reinforcement at the top of the cage, only bottom tensile reinforcement's strain was measured using 5 mm strain gauge. Before installing these strain gauges, these two 12 mm steel bars were grinded carefully to flatten the bottom part of the bar and were cleaned properly using acetone from dirt. During wiring the strain gauge, proper care was taken to avoid the contact of strain gauge wire with the steel bar. After wiring, the strain gauges were covered with silicon to protect from moisture and damage during casting of concrete. The steel molds were prepared carefully with proper lubrication and were sealed at the bottom to avoid leakage during concrete casting. After concrete pouring, the specimens

were covered with polythene sheets and the standard curing was maintained according to the code requirement. The whole construction sequence is presented in Figure 3.5.



(a) Wiring of strain gauge on steel



(b) Application of silicon on strain gauge
Figure 3.5: Preparation and casting of RC beam



(c) Prepared steel mold for casting



(d) Concrete casting and compaction process

Figure 3.5, continued: Preparation and casting of RC beam

3.3.3 Strengthening Procedure

Four different types of strengthening techniques were adopted in the research. They were: NSM, EBR, CEBNSM-B and CEBNSM-S strengthening technique. In this section, procedures of these strengthening techniques are described in detail.

3.3.3.1 Near Surface Mounted (NSM) Strengthening Procedure

All the strengthened beam specimens had a single groove (24 mm × 24 mm) cut along the beam length to accommodate a 12 mm diameter steel or CFRP bar. The beam soffit was marked according to the bond length (1600, 1800 and 1900 mm) of the strengthening material.

A special concrete saw with a diamond blade was used to create parallel cuts as deep as the required NSM grooves in the longitudinal direction on the tension side of the RC beam. Throughout the cutting process, a hosepipe was connected to the diamond blade to ensure a constant water flow. The water was used to minimize the dust generated from the cutting and prevented over-heating of the cutting blade. A hammer and a hand chisel were used to remove any remaining concrete lugs in the groove and to create a rough surface inside it. Debris and fine particles were also removed from the groove using wire brush and high pressure air jet. These steps were done to ensure appropriate bonding between the epoxy adhesive and the concrete. Acetone was applied on the groove (Figure 3.6) and also to the outer surface of the CFRP and steel bar for cleaning purposes. The groove was filled with epoxy adhesive up to around 2/3 of its depth. The CFRP or steel bar was gently inserted into the groove and pressed lightly to ensure that the bar was in the midway of the groove depth and the epoxy fully covered the bar. The remaining space in the groove was filled with epoxy and the surface was leveled with spatula. This arrangement was left for one week in order to allow the epoxy to achieve full strength.



(a) Cutting groove with diamond cutter blade



(b) Removing dirt from groove by air jet



(c) Cleaning the groove with acetone

Figure 3.6: Strengthening process of RC beam with NSM technique



(d) Mixing of two-part epoxy



(e) Pressing strengthening bar in epoxy



(f) Application of epoxy in groove



(g) Finishing of the beam soffit

Figure 3.6, continued: Strengthening process of RC beam with NSM technique

3.3.3.2 EBR Strengthening Procedure

The RC beams in Group B were strengthened with externally bonded CFRP fabric. The standard wet lay-up practice was exercised for binding the CFRP fabric on the surface of beams. First, the surface was prepared using an abrasive blast cleaning

equipment to remove cement laitance, loose and friable material to achieve a profiled open textured surface. All dust, loose and friable materials were removed from the prepared surface. Acetone was used to clean the concrete surface against oil, grease, coatings and any other dirt.

The two part epoxy (Sikadur 330) was mixed with a 1:4 ratio as per the manufacturer's instruction. A mechanical stirrer was used to stir these two parts to maintain the homogeneity of the epoxy. After achieving a homogeneous gray color, the epoxy was spread over the surface. During application proper care was taken to fill up the small voids within the concrete surface for ensuring proper bonding between epoxy and the CFRP sheet. The amount of epoxy spread over the surface was around 1.4 kg/m² according to the manufacturer's requirement. A special roller provided by the manufacturer was also used to squeeze the resin through the fibers. The strengthened RC beam was placed for one week for curing of the epoxy according to the manufacturer's recommendations.

3.3.3.3 CEBNSM Strengthening Procedure

CEBNSM Strengthening technique offers increased flexural capacity as well as less debonding possibilities in Reinforced Concrete (RC) structures. In this section, the strengthening procedure of both CEBNSM-B and CEBNSM-S are described in detail.

In CEBNSM-B technique, CFRP bar or steel bar was inserted in a groove which was cut using concrete cutter with diamond blade. The specimen preparation and strengthening process is demonstrated in Figure 3.7.

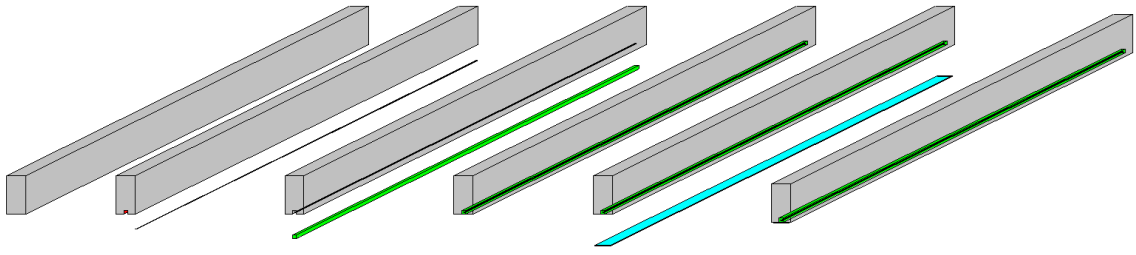


Figure 3.7: Sequence of specimen preparation and strengthening

The groove dimension was dependent on the strengthening material's (CFRP or steel bar) texture and bond capacity. Generally, it varies from 1.5 to 2.0 times the CFRP/steel bar diameter (De Lorenzis and Teng, 2007; Parretti and Nanni, 2004). In the present experiment, steel bars of two different diameters were used (8 mm diameter and 10 mm diameter). Both steel and CFRP bar were used with variable diameters, as strengthening material inside the slot at beam soffit. The groove dimension was selected as 2.0 times the diameter of steel or CFRP bar.

After using the cutter, the concrete lugs were manually taken out with a hand chisel and hammer. The remaining rough concrete surface was cleaned using a high pressure air jet. Acetone was applied on this surface to remove any fine dust particles, and any oily substances present in the groove in order to make a good bonding surface for strengthening. Masking tape was affixed along the ridge of the groove line to ensure the proper placement of epoxy inside the groove and neat finishing of the epoxy surface. Nearly 2/3 of the groove was then filled with epoxy (Sikadur® 30) which was prepared according to the manufacturer's directions. The NSM steel or CFRP bar was properly cleaned and gently pressed inside the groove until surrounded by equal dimension of epoxy. A spatula was then used to level the surface and clean the area. The whole preparation was left for standard curing time prescribed by the manufacturer.

In CEBNSM-S technique CFRP strip was inserted in a groove which was cut using concrete cutter with diamond blade. According to Blaschko (2003), the height and breadth of the groove should be 3 mm larger than the height and thickness of the

corresponding CFRP strip. Parretti and Nanni (2004) suggested that the groove width should not be less than three times the thickness of CFRP strip and the groove height should not be less than 1.5 times the height of the CFRP strip. Conforming to these recommendations, the groove dimension for the CEBNSM-S technique was fixed as 5 mm × 25 mm for single strip in one groove. To accommodate double strips in single groove, the dimension was fixed as 10 mm × 25 mm. The CFRP strip thickness and height was selected as 1.4 mm and 16 mm respectively.

Two component epoxy was used as groove filler which surrounded the strengthening bar or strip and transferred the stress from FRP to concrete. After maintaining the standard curing time of the groove filler, the concrete surface was cleaned and prepared by mechanical abrasion for the next phase of external strengthening with FRP fabric. The surface was prepared smooth according to the manufacturer's instruction. After preparing the concrete surface, another two-part epoxy was applied over the concrete face and FRP fabric was affixed with the help of a roller. The beam specimens were to be kept one week for epoxy to cure and achieve full strength.

3.3.4 Test Setup and Instrumentation

Loading condition in a test can be classified into two categories; a) Static and b) Dynamic. A load is said to be static when any given force is steadily applied to some object without changing its position. It is a mechanical force which can be applied slowly to an assembly or object. This test is useful in identifying the mechanical properties of materials and in determining the maximum allowable loads on engineering structures. It is possible to visualize the flexure and shear stress behavior under this loading condition. Generally, three point or four-point bending test are carried out to observe these behaviors in Reinforced Concrete (RC) beam. In three-point test, the testing instrument localized its peak stress at mid-point of the specimen with less stress

elsewhere. Whereas, in four-point test, the machine generated peak stress along an extended area of the sample thus exposing a larger span of the specimen with more possibility for flaw and defects to be highlighted. Within the static loading condition numerous researchers use the above mentioned tests to observe the performance of their strengthened RC beam/slab over the control un-strengthened specimen.

In this experiment, a closed-loop Instron universal testing machine of 500kN capacity was used to apply four-point loading on the prepared specimens. Monotonic load was directed through a servo-hydraulic actuator reacting against a steel frame anchored to the laboratory's strong floor. The load was distributed equally by a steel spreader beam which transferred the applied load to two points along the beam, hence, achieving four point bending. The spreader beam transmitted the applied load through steel bars which were encircled by thick steel boxes and rested over the beam. A thick rubber pad was placed beneath the steel box to spread the load homogeneously in case of any surface irregularities. The beams were rested on a roller and hinge support which resembled the same configuration to those steel boxes placed beneath the steel spreader beam. The only difference of the supports was the increased dimension of those boxes to carry more loads. The machine was operated under load control mode with a loading rate of 5 kN/min up to yielding of the internal reinforcement of the RC beam specimens. After yielding, displacement control was applied up to failure with a rate of 1.8 mm/min.

The instrumentation for the different series of control and strengthened beams was intended to capture the reliable and maximum amount of deflection, strain and cracking data. The instrumentation detail of a typical strengthened beam is shown in Figure 3.8.

glue. Proper care was taken to avoid the steel contacting with the output wire coming from the strain gauge. After installation the strain gauges were covered with a silicon based water proof coating to avoid moisture. 30 mm length strain gauges were placed on the top smooth concrete surface of the RC beam to measure concrete compressive strains. In the CEBNSM strengthening technique, 30 mm strain gauges were fixed on the extreme CFRP fabric surface at different locations to capture the strain profile of the externally bonded CFRP fabric.

3.3.4.3 Crack Width Determination

A digital microscope was used to measure micro cracks on the surface of the beams. The brand name of the digital microscope was Dino-Lite which was manufactured by AnMo Electronics Corporation. The equipment was operated with software named DinoCapture 2.0 which was installed in a laptop. During the operation, the laptop was with the equipment where the real-time crack width images were taken and stored in the system.

3.3.4.4 Data Acquisition System

An independent data acquisition system was used to capture the load, displacement and strain readings from different parts of the specimen during the experiment. The model name of the equipment was TDS-530 which was manufactured by TML. It has the capacity to receive 30 channels with a display capacity of 10 channels during operation. The equipment was set to capture the data in each channel at every single second.

The experimental test program is presented in this chapter. First, the testing matrix is described where the strengthening schemes are tabulated. The detail drawings of each beam are presented at the appendix for clarity of the experimental program. The properties of the materials which were used for specimen preparation and strengthening

are also described. The strengthening procedure along with its surface preparation process is explained in detail to understand the proper procedure of CEBNSM strengthening technique. Finally, the experimental setup along with the instrumentation and data acquisition is explicated. The ancillary test process and the test results are arranged in the appendix.

University of Malaya

CHAPTER 4: EXPERIMENTAL RESULTS AND DISCUSSIONS

The research was an aggregation of four different groups of control and strengthened RC beams. First two groups were strengthened by means of NSM and EBR techniques to compare their flexural performance with the proposed CEBNSM strengthening technique which was covered by the last two groups. The experiment was carried out with the monotonic four-point bending load. The proposed technique was based on the combination and hybridization of both EBR and NSM techniques, thus, their outcome had marked a significance on the CEBNSM result. Several parameters were considered to assess the performance of the strengthening scheme, namely: load-deflection behavior, failure modes, crack spacing, crack width, ductility and the strain profile of the different components of the experimental specimens. The following sections elaborately discussed the experimental results of different strengthening techniques used in this research.

4.1 Experimental results

4.1.1 Control Beam for Group-A

The control beam described in this section was considered as a reference beam to assess the NSM strengthened beams of Group-A. The length was 2300 mm for two control beams which were tested to get the flexural response to make comparison with other beams. Finally, one beam was chosen from the two to compare the result with the strengthened beams. All the beams were designed to be under-reinforced with a steel ratio of 0.0085. The beams were tested under four-point bending load in Instron universal testing machine using load control mode at a rate of 5 kN/min until it reaches to the yield point. The machine controller was then changed to displacement mode at a rate of 2 mm/min up to the full failure of the beam. The load-deflection diagram of the two control beams was shown in Figure 4.1.

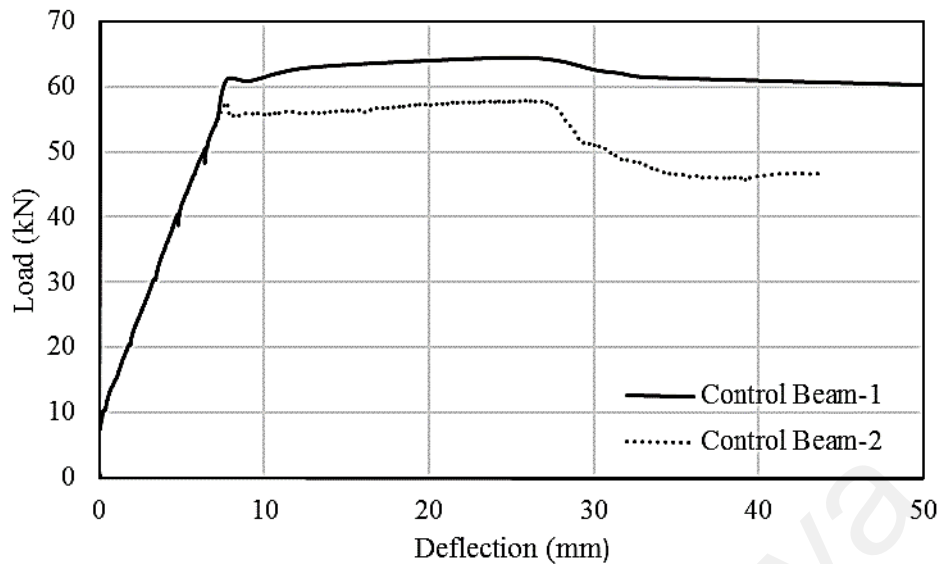
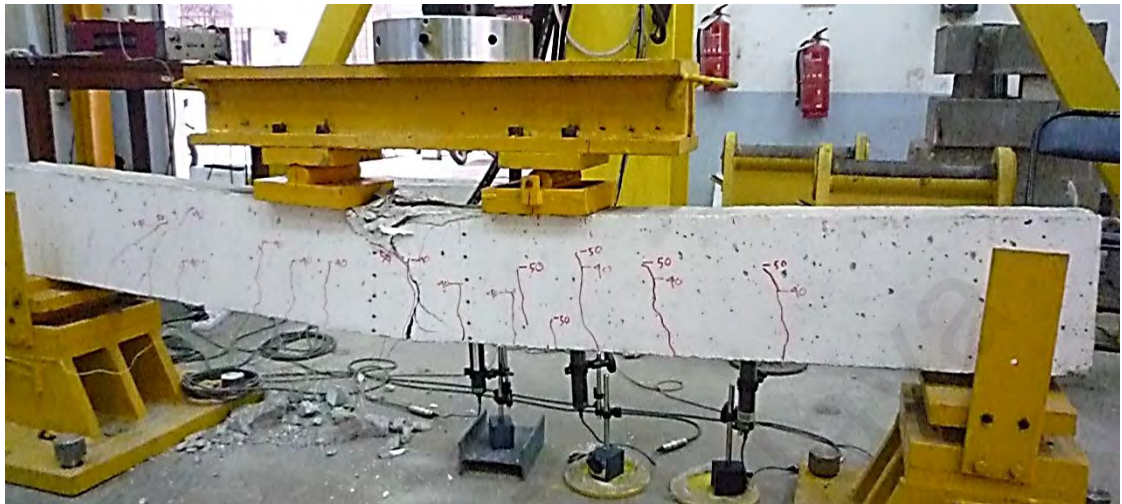


Figure 4.1: Load-deflection diagram of control beams for Group A

The diagram in Figure 4.1 followed a typical RC beam's load deflection curve. The curve can be subdivided into three parts. First crack appeared at 10.6 kN and 7.5 kN for the control beam 1 and 2, respectively. The 1st portion of the curve could be distinguished until first crack which indicated a stiffer response followed by an elastic linear path up to the yield point. Both the control beams showed same response until their internal steel reached to their yield point at 61 kN and 54 kN (Figure 4.3). After crossing the yield point, the 3rd portion of the curve maintained a plateau up to the ultimate capacity at 64 kN and 58 kN for the corresponding control beam 1 and 2. Beyond this point both the beams demonstrated concrete crushing failure (Figure 4.2) at the top mid-span portion and the load-deflection curve was moving downward which exhibited a softening behavior followed by the formation of wedge at the compression zone.

Figure 4.3 and Figure 4.4 showed the internal steel and concrete strain values of the control beams 1 and 2. The indication of 1st crack load can be easily identified from these two figures. The changes of the slope of the load-strain curve gave an indication of changes of load-level. However, the first crack was too prominent for the control beam-2 which indicated the value as 7.5 kN. The yield point can be obtained from these

figures where the strain value varied with negligible load and the slope of the load-strain curve drastically marked this fluctuation.



(a) Control beam 1



(b) Control beam 2

Figure 4.2: Failure modes of control beams for Group A

Both the beams had similar characteristics of the load-deflection and the strain value of steel and concrete. However, the ultimate load capacity of control beam 1 is higher than that of control beam 2. If the control beam 2 was considered as reference, then the difference of control and strengthened beam would be higher. Therefore, to make a justifiable and reasonable comparison with the strengthened NSM beam, control beam 1 was chosen as the reference control beam throughout this study.

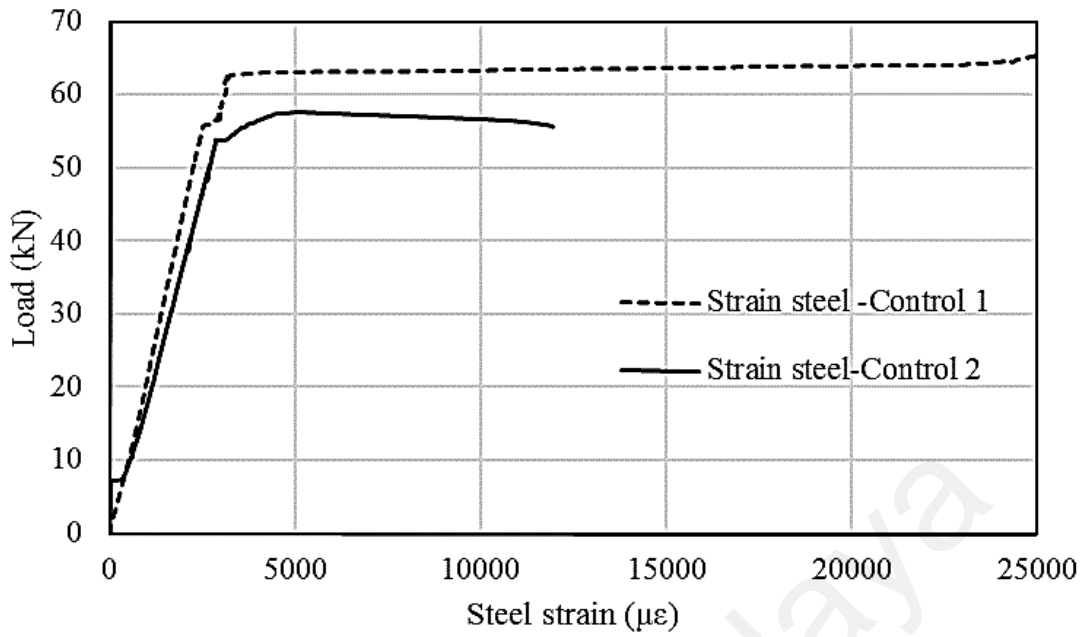


Figure 4.3: Steel strain value of control beams for Group A

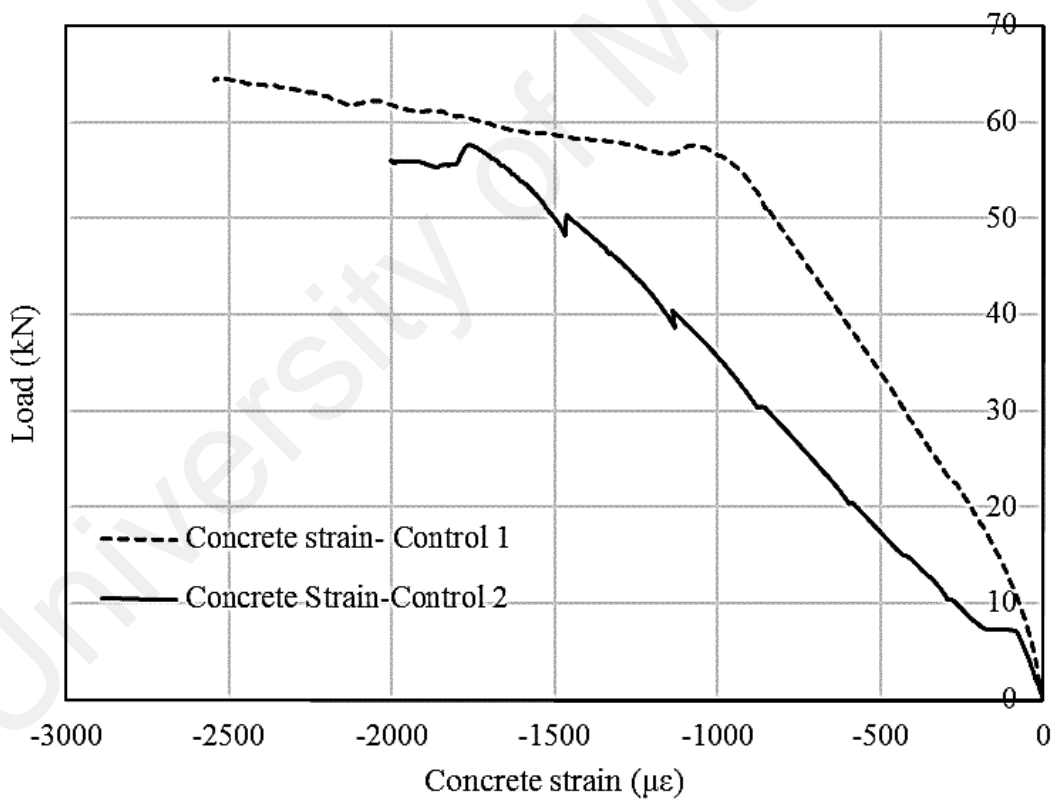


Figure 4.4: Concrete strain of control beams for Group A

4.1.2 NSM Strengthened Beams

Table 4.1 presents the flexural behavior of the RC beams strengthened with NSM steel or CFRP bar. The parameters identified for the tested specimens were first crack load, yield load and ultimate load with their respective deflections. Stiffness was also

measured to understand the improvement in flexural behavior after strengthening. Strains were also observed in the internal steel reinforcement, NSM steel or CFRP bar and concrete to comprehend behavior under static monotonic loading and failure mechanisms.

4.1.2.1 Load Carrying Capacity

Table 4.1 demonstrated the gist of the experimental finding of the NSM strengthened RC beams. It listed the corresponding load and deflection of first crack, yield and ultimate capacity of the control and NSM strengthened beams along with their failure modes. Addition of the NSM strengthening material to the RC beams caused superior load carrying capacity at the first crack, yield and ultimate load level as well as a considerable reduction of ultimate deflection. The ultimate load capacity was increased by 46%, 70%, 55%, 103%, 61% and 107% for the N1.6S, N1.6F, N1.8S, N1.8F, N1.9S and N1.9F strengthened beams, respectively. From the result it is evident that the bond length of the NSM strengthening material has a significant effect on the flexural capacity as well as the serviceability improvement. The result also has presented a comparison between two different strengthening materials (CFRP and steel) regarding their structural performance.

The percentile increment of the 1st cracking, yield and ultimate load of NSM strengthened beam was compared with the control RC beam which was depicted in the Figure 4.4. All the strengthened beams showed significant improvement of carrying capacity at 1st crack, yield and ultimate load level. The first crack load is tremendously improved by 117% in case of N1.9S beam which was strengthened using steel bar. The higher first crack load was desirable as the early crack development can lead towards an additional damage of structures by the surrounding environment. The steel NSM beam also demonstrated the higher effective pre-yield stiffness compared to the CFRP NSM

beam at the same bond length. The stiffness is directly associated with the modulus of elasticity of the strengthening reinforcement. As the steel's modulus was higher than the CFRP, so the stiffness of steel is greater than CFRP which was a reasonable consequence which was supported by Almusallam et al. (2013).

Table 4.1: Summary of experimental test results of NSM beams

Beam ID	P_{cr} (kN)	Δ_{cr} (mm)	P_y (kN)	Δ_y (mm)	K_e (kN/m)	$\% \Delta K_e$	P_u (kN)	Δ_u (mm)	Failure mode
CB	10.6	0.3	61.0	7.7	7922	-	64.4	24.7	FF
N1.9F	15.0	0.3	104.5	10.7	9766	23	133.2	19.2	CCS
N1.9S	23.0	0.7	101.3	10.0	10130	28	103.8	12.4	FF
N1.8F	14.0	0.6	110.6	13.0	8508	7	130.8	18.6	CCS
N1.8S	15.5	1.0	94.7	10.8	8769	11	99.6	16.8	FF
N1.6F	17.5	0.4	83.6	8.5	9835	24	109.5	13.6	CCS
N1.6S	14.4	0.7	88.7	8.3	10687	35	94.1	9.4	CCS

*Where P_{cr} = first crack load; P_y = yield load; K_e = effective pre-yield stiffness; $\% \Delta K_e$ = percent increase in effective pre-yield stiffness over the control beam; P_u = ultimate load; Δ_{cr} = deflection at 1st crack; Δ_y = deflection at yield of steel; Δ_u = mid-span deflection at ultimate load, FF = flexural failure (concrete crushing after steel yielding), CCS = concrete cover separation.

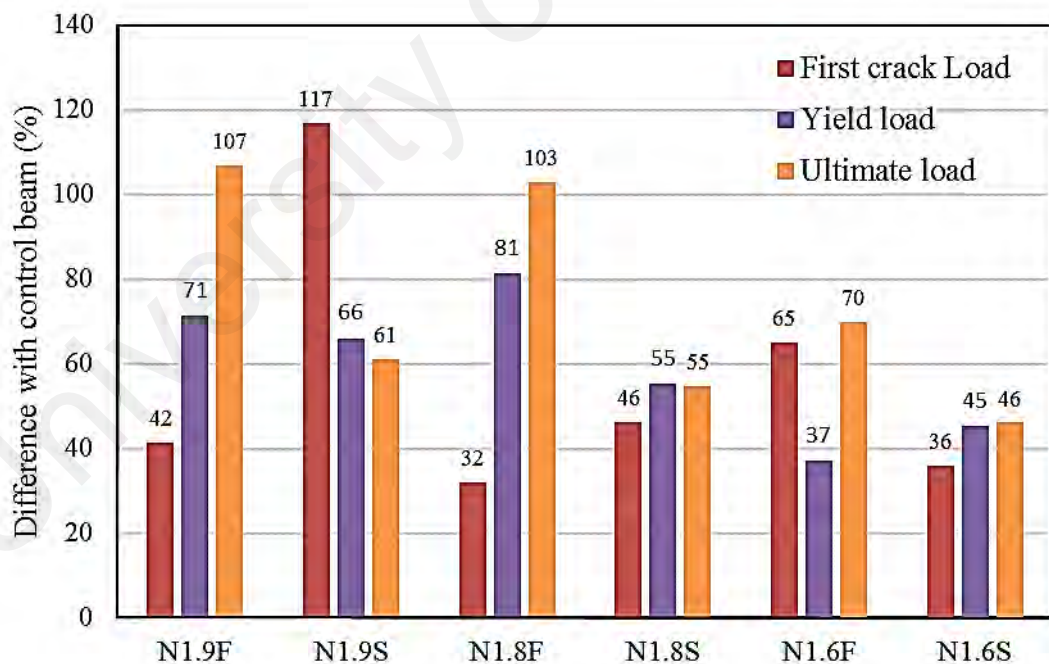


Figure 4.5: Percentile increment of different load levels of NSM beams

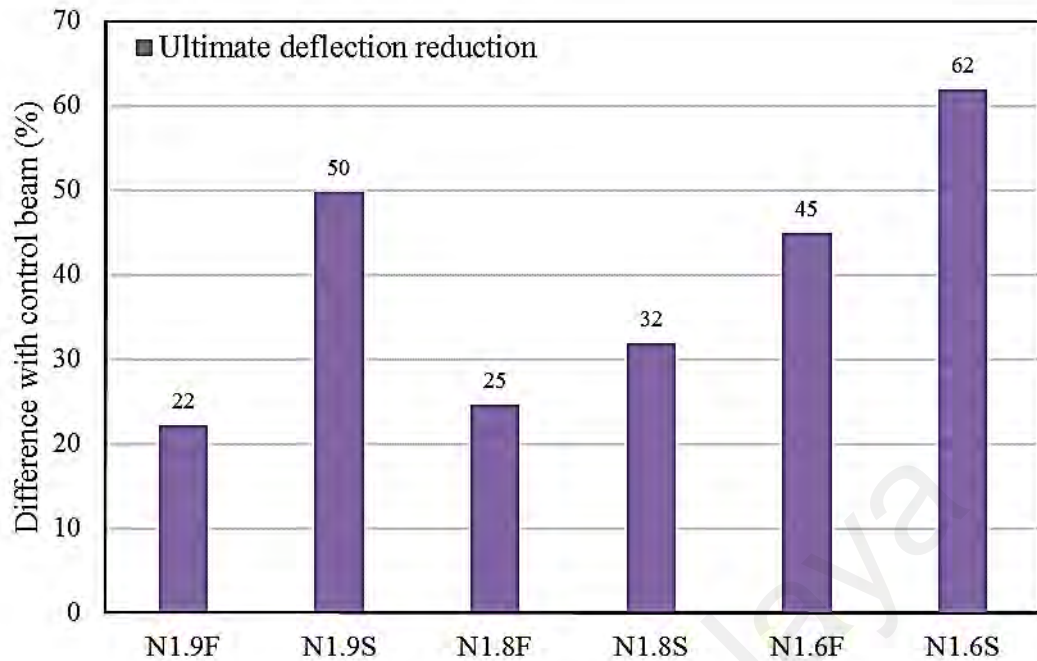


Figure 4.6: Percentile decrement of ultimate deflection of NSM beam

Figure 4.6 showed the reduction percentage of deflection at ultimate load for the NSM strengthened beams compared to the control beam. All the strengthened beams demonstrated lower ultimate deflection. The N1.9F showed the least reduction whereas the N1.6S depicted the highest decrease of the ultimate deflection. In all cases, the steel NSM beam demonstrated higher reduction of deflection compared to the CFRP NSM beams. According to Hosen et al. (2014), the possible reason behind the fact was the higher stiffness of steel NSM beam compared to their CFRP counterpart. The higher stiffness restricted those beams from deflecting too much at their ultimate capacity.

4.1.2.2 Load Deflection Curve

As shown in Figure 4.7, the load-deflection diagram of the NSM CFRP strengthened beams demonstrates a nearly tri-linear response. The first segment of the curves linearly varies with negligible deflection up to the 1st cracking. In this portion the stiffness increment of the beams was quite low. However, strengthening increased the 1st crack load for all strengthened beams. The second phase was the post cracking to yielding of the internal reinforcement of the beams. In this stage a considerable stiffness

improvement was noticeable in strengthened beams compared to the unstrengthened control beam. The NSM CFRP bar prevented further increment of flexural cracks, which increased the moment of inertia of the cracked section. The third portion of the load deflection behavior extended from yielding up to failure, and this portion displayed greatly improved strength and stiffness in the strengthened specimens. The load deflection curves for the NSM steel strengthened beams showed (Figure 4.8) a bi-linear response up to the yielding stage. Beyond this region the behavior of the specimens was totally nonlinear.

All the strengthened beams demonstrated superior first cracking loads compared to the control beam. However, this incremental trend was better for the NSM steel strengthened beams compared to the NSM CFRP strengthened beams. An especially dramatic improvement of around 117% was seen in the 1st cracking load of the N1.9S beam. In addition, from Figure 4.7 and Figure 4.8, it can be seen that the slope of the load deflection curve for steel is quite a bit steeper than that of the curve for FRP strengthened beams. It is also evident from Table 4.1 that the effective pre-yield stiffness of the NSM steel strengthened beams is higher than the NSM CFRP strengthened beams.

For the NSM steel strengthened beams, the N1.8S beam showed more deflection compared to the N1.6S beam when tested under similar load conditions from the first cracking until steel yielding (Figure 4.7). The N1.9S beam exhibited the least deflection among the three bonded lengths within the same load range. In the case of NSM CFRP strengthened beams, the pattern of deflection for the N1.6F, N1.8F and N1.9F beams was similar to the behavior of the previously mentioned NSM steel strengthened beams. Similar behavior was found by the other researchers (Almusallam et al., 2013; Rahal & Rumaih, 2011).

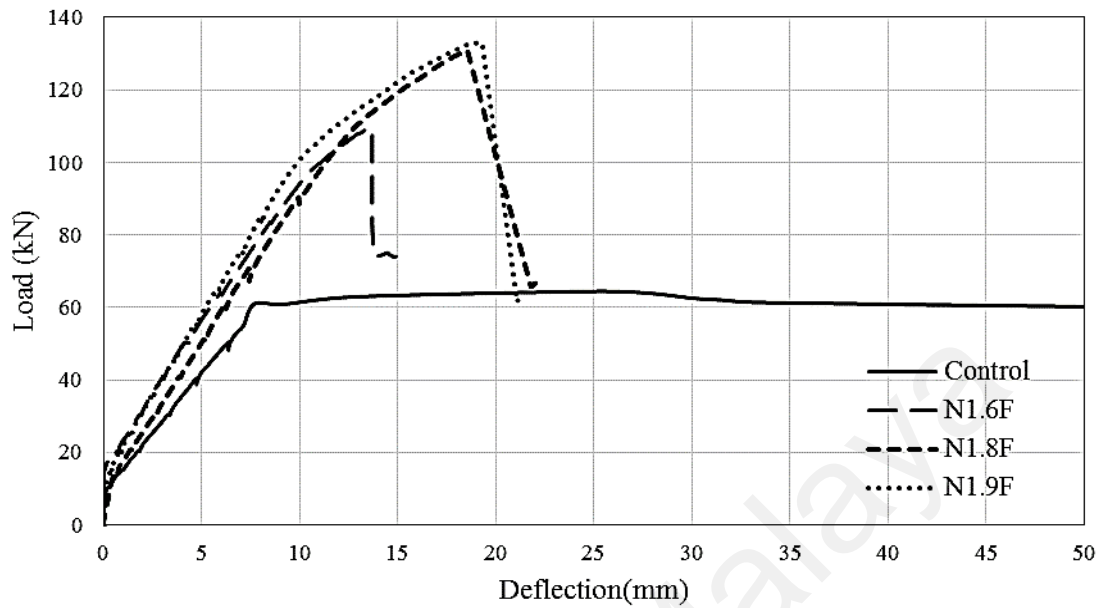


Figure 4.7: Load-deflection curve for NSM-CFRP strengthened beams

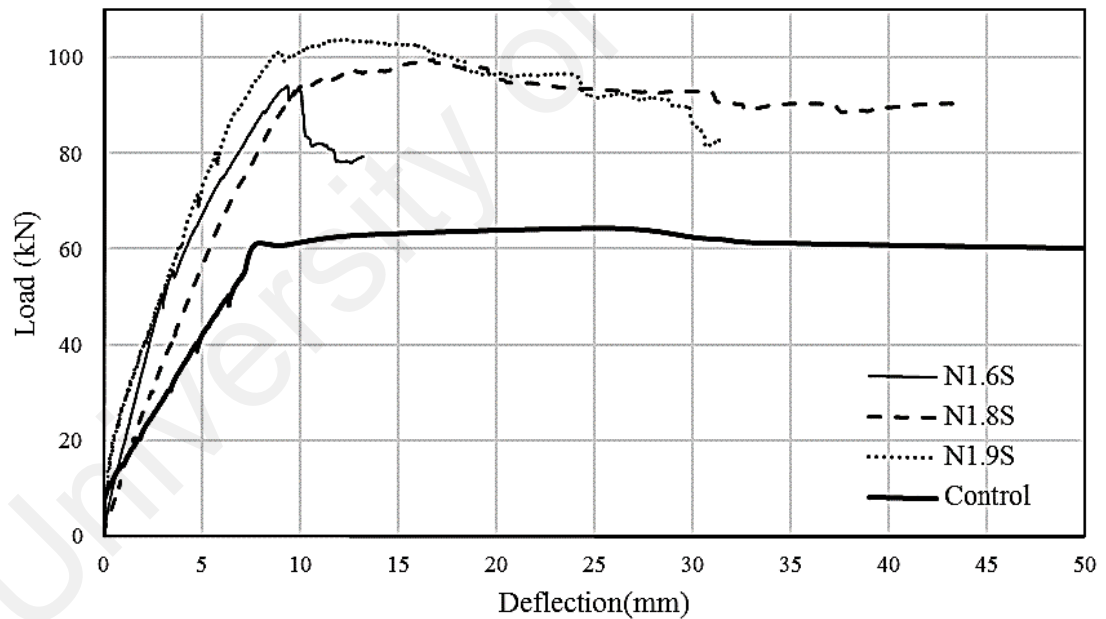


Figure 4.8: Load-deflection curve for NSM-steel strengthened beams

4.1.2.3 Failure Modes

The control beam failed by concrete crushing at the top mid-span after the internal tensile steel yielding. All the NSM CFRP strengthened beams failed due to premature debonding problem (Figure 4.9). Failure of N1.6F beam occurred due to concrete cover separation that initiated at the tip of NSM bar cut-off region (Figure 4.9a). Several tiny

shear cracks, which were very close to the support, were formed after the internal steel yielding of this beam. The debonding failure occurred slowly after formation of these shear cracks. The shear crack at the end of NSM CFRP rod triggered the failure mechanism where a bending crack further aggravated the problem (Ceroni, 2010). Combination of these cracks was further guided by horizontal cracks formed at the level of internal steel and put forward along the beam mid-span which ensued final failure. After the failure, the beam was investigated critically and it was found that the bottom cover along with the end of CFRP bar was completely detached from the adjacent concrete part. The angle of the concrete failure plane was around 22° with the horizontal plane.

The rip-off failure occurred in case of N1.8F strengthened beam (Figure 4.9b). However, for this beam, the failure was sudden and catastrophic. Almost half of the total beam's concrete cover was detached drastically due to this premature failure. After yielding of the internal steel shear cracks were visible at the support end. With the increase in time, the width of these cracks also increased. The failure was initiated at the last crack just beside the support, and not at the NSM bar end which was unlike the N1.6F beam case. The crack development path was propagated approximately 29° with horizontal level which moved further to the internal steel bar level. Afterwards, the concrete cover was completely ripped along the steel bar level horizontally towards the mid-span. Similar failure pattern was observed by other researcher (De Lorenzis, 2002).

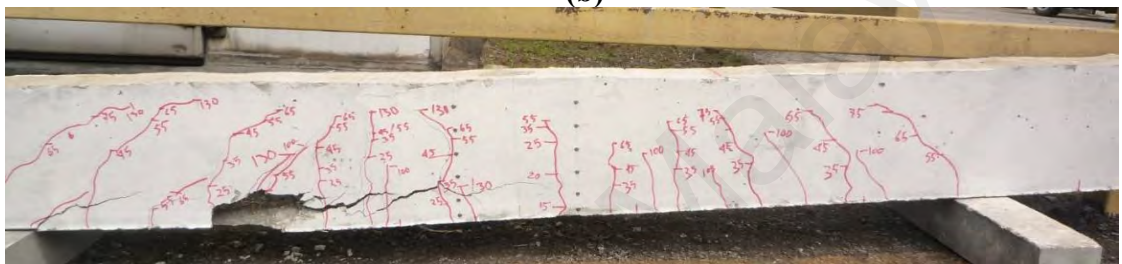
The failure mode of N1.9 F was quite different from the other NSM strengthened RC beam (Figure 4.9c). The beam sustained against the maximum moment compared to other specimens. Firstly, the NSM FRP-epoxy matrix was detached from the surrounding concrete before at the bar end. In course of time the prism formed by CFRP bar and surrounding epoxy was detached having a variable thin layer of concrete.



(a)

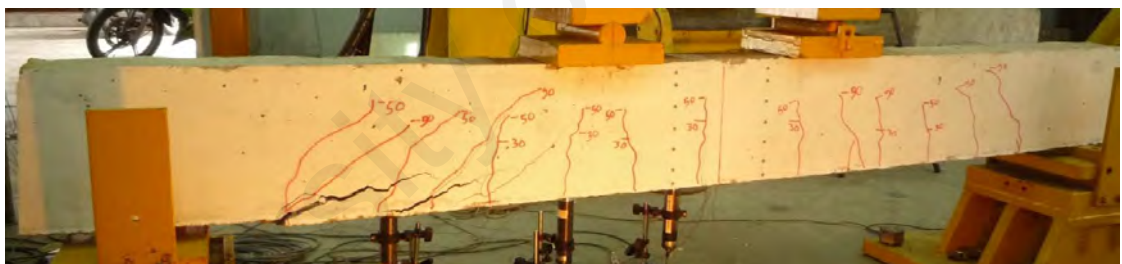


(b)

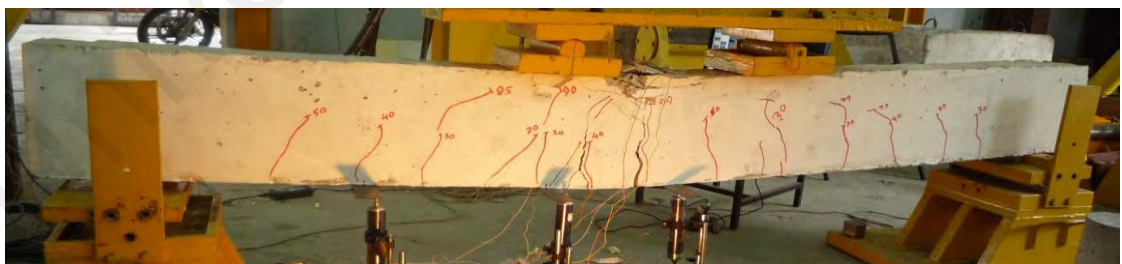


(c)

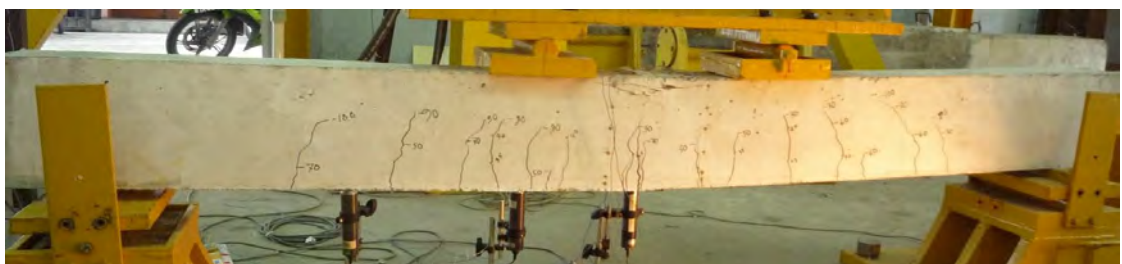
Figure 4.9: Failure mode of (a) N1.6F (b) N1.8F and (c) N1.9F RC beam



(a)



(b)



(c)

Figure 4.10: Failure mode of (a) N1.6S (b) N1.8S and (c) N1.9S RC beam

Finally, a significant portion of concrete cover was detached due to the splitting action by the CFRP-epoxy prism. Horizontal cracks were also visible at the internal steel level which ended almost at the center of the beam. The failure mode of NSM steel strengthened RC beams were depicted in Figure 4.10. Except N1.6S, other two steel strengthened beams failed due to concrete crushing after internal reinforcement yielding, which is a very desirable mode of failure in case of any strengthened RC beam. It also demonstrated that full composite action was ensured for N1.9S and N1.8S beams during application of monotonic loading up to ultimate capacity of the strengthened RC beam.

Similar behavior was observed by Almusallam et al. (2013) where the GFRP and steel bar were used as NSM reinforcement. From Figure 4.8, it is also revealed that the ductility of these two beams was also improved compared to the control beam and a good bonding was detected between the strengthen NSM steel and concrete. The failure mode of N1.6S is quite similar to that of N1.6F beam. N1.6S failed due to concrete crushing which was triggered at the tip of NSM steel bar's cut-off region. The debonding was ensued from several tiny shear cracks close to the support of the beam. These diagonal shear cracks moved slightly upward horizontally and these cracks became wider and separated the concrete cover (Figure 4.10a).

4.1.2.4 Cracking Behavior

During the experimental test, cracks were measured using a digital crack microscope named DinoLite and the data was stored in a laptop. The cracks were documented after appearance of the first crack, and the subsequent crack formation were also recorded at different load levels. The first primary crack was located and documented at the internal steel level in central portion of the maximum moment region.

According to the strain compatibility, the minimum crack (s_{r0}) spacing can be expressed as the nearest point of a present crack at which fresh crack can develop where concrete again reach the tensile strength (equation 4.1). It can be expressed as

$$s_{r0} = \frac{f_{ctm} \phi_s}{4\tau_{bm}\rho_{ef}} = \left(\frac{f_{ctm} A_{c,eff}}{\tau_{bm} \sum u} \right) \quad (4.1)$$

Where, f_{ctm} = mean tensile strength of concrete; ϕ_s = nominal diameter of reinforcement; τ_{bm} = average bond stress along the disturbed zone; ρ_{ef} = effective reinforcement ratio; $A_{c,eff}$ = effective concrete area in tension and $\sum u$ = (sum of) perimeter(s) of reinforcing bar(s).

According to Borosnyói (2002) crack spacing was supposed to fluctuate between $s_{r,min} = s_{r0}$ and $s_{r,max} = 2s_{r0}$. Various researchers proposed different values of average (mean) crack spacing which varied from 1.33 to 1.54 times the minimum value, whilst maximum crack spacing can be expressed as $s_{r,max} = 2s_{r,min}$.

$$\frac{s_{r,min}}{s_{r,mean}} = 0.67 \text{ to } 0.77 \quad (4.2)$$

$$\frac{s_{r,max}}{s_{r,mean}} = 1.33 \text{ to } 1.54 \quad (4.3)$$

Figure 4.11 depicted the ratios of minimum to average and maximum to average crack spacing of the control and NSM strengthened RC beams. The average values of the maximum and minimum ratios were 1.54 and 0.61, respectively, which conformed well to the prediction in equation 4.2 and 4.3.

Table 4.2 showed the maximum, minimum and average crack spacing along with the number of cracks appeared on the tested beams. The minimum and maximum crack spacing was observed as 50 mm and 183 mm for the beams N1.9F and N1.8F respectively. The average crack spacing maintained a range between 81 mm to 120 mm.

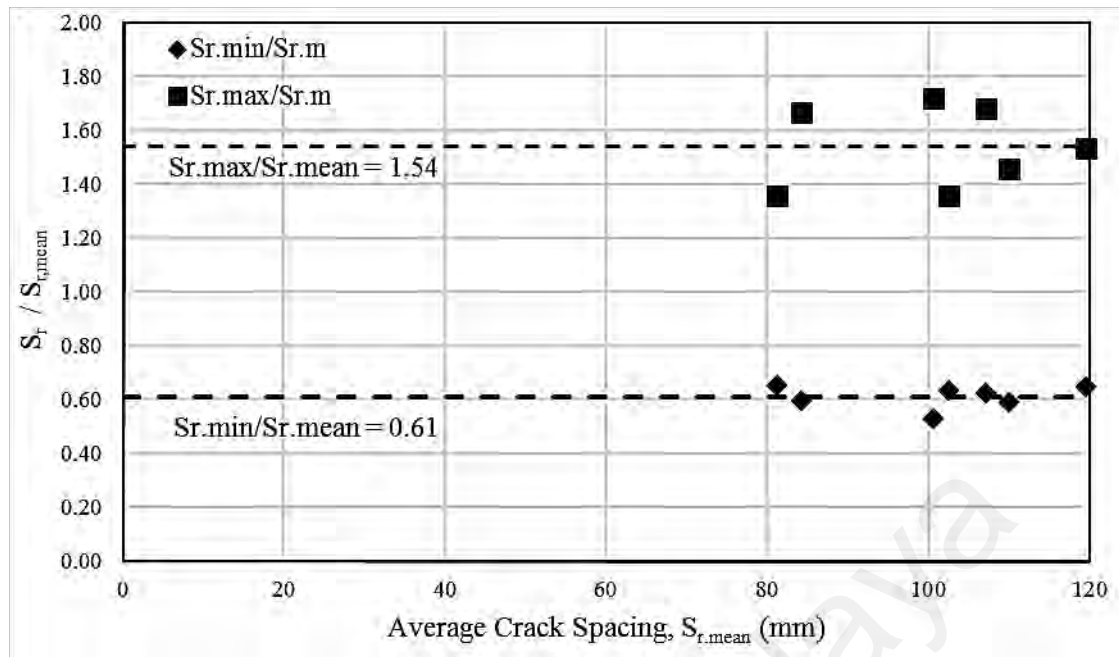


Figure 4.11: Crack spacing details of NSM beams

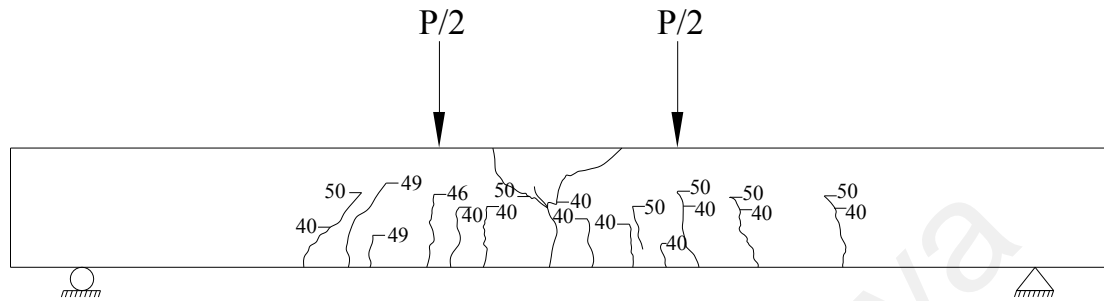
The number of cracks appeared on the control and strengthened beam were almost same and its average was around 16 numbers. The N1.9F beams demonstrated the highest number of cracks (21 nos.), whereas the N1.6S showed the least cracks (13 nos.).

Table 4.2: Experimental maximum, minimum and average crack spacing of NSM beams

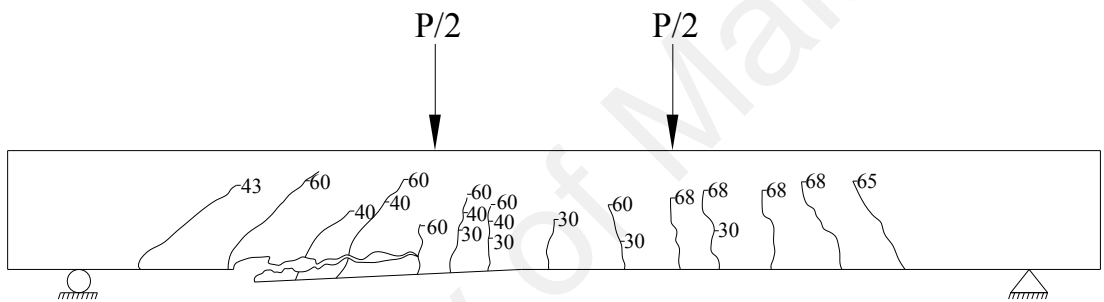
Beam no	$S_{r,max}$ (mm)	$S_{r,min}$ (mm)	$S_{r,mean}$ (mm)	No. Cracks
Control	140	50	84	16
N1.6F	160	65	110	14
N1.6S	173	53	101	13
N1.8F	180	67	107	16
N1.8S	183	77	120	17
N1.9F	110	53	81	21
N1.9S	139	65	103	16

The cracks and the crack propagation path at different load levels were marked on the surface of the beam during testing. Figure 4.12 illustrated the characteristic crack pattern of the control beam and strengthened beams which were documented during the experiment. The primary cracks at the maximum moment regions were vertical and with the load increment several inclined cracks were seen owing to the influence of shear

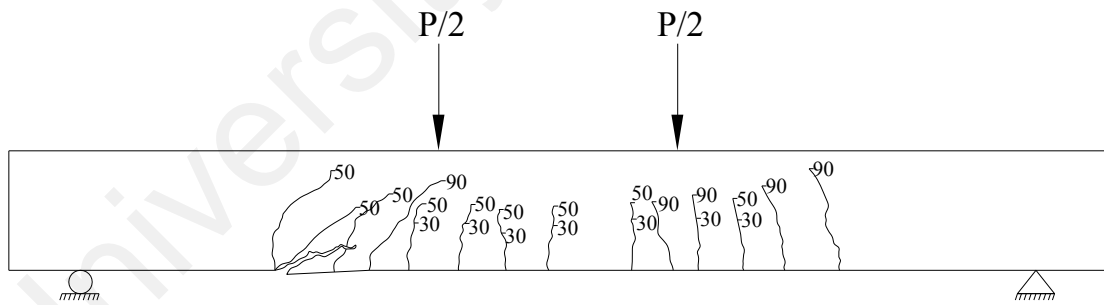
forces on the principal tensile stresses. A few number of vertical cracks were visualized at the shear span zone which started to incline due to the combined flexural-shear effects in the zones with larger bending moment.



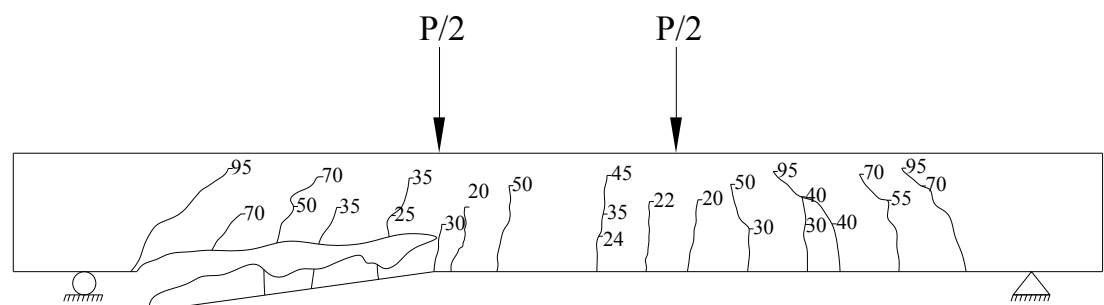
(a) Control



(b) N1.6F

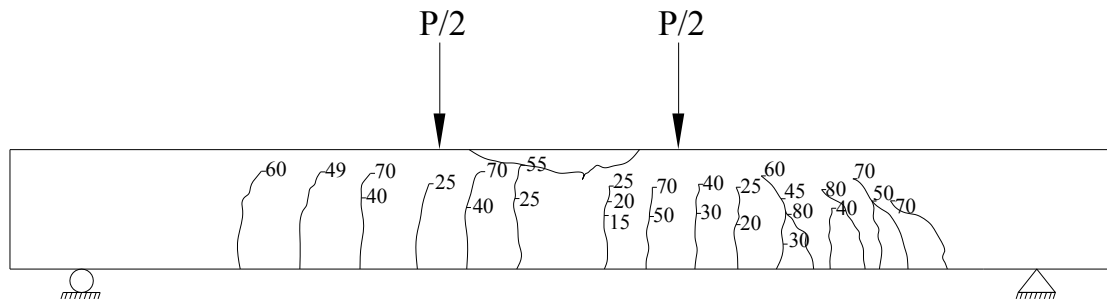


(c) N1.6S

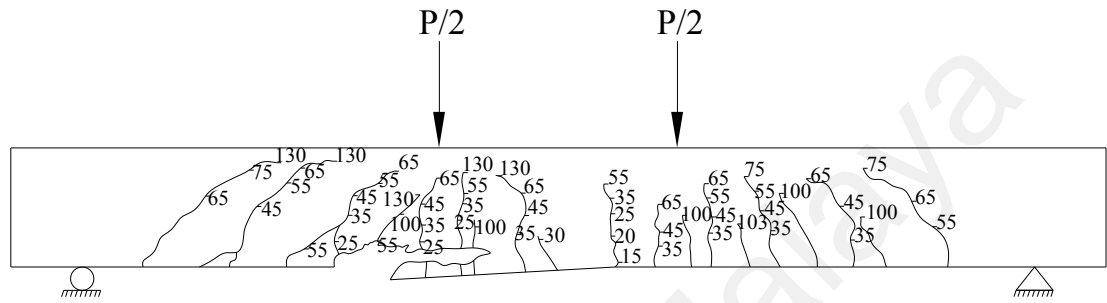


(d) N1.8F

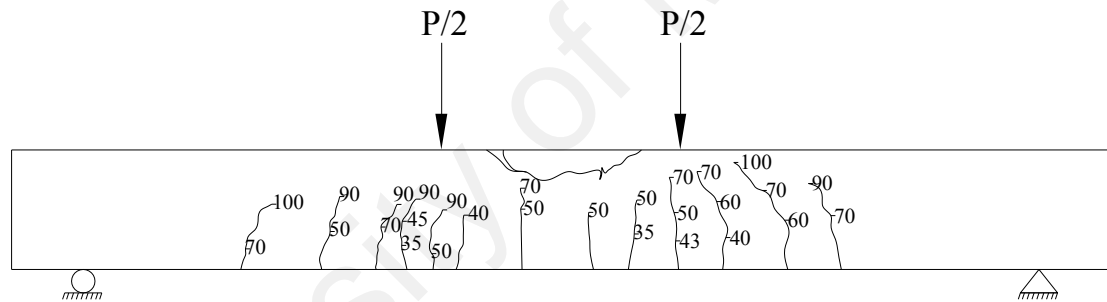
Figure 4.12: Crack pattern of the NSM strengthened beams



(e) N1.8S



(f) N1.9F



(g) N1.9S

Figure 4.12, continued: Crack pattern of the NSM strengthened beams

From Figure 4.13 and Figure 4.14, it can be seen that the crack width of the first crack was around 0.04 to 0.06 mm for most of the strengthened beam specimens except N1.6F (0.1 mm) and N1.9S (0.1mm). The control beam's first crack width was 0.093 mm. The first crack loads for both N1.6F and N1.9S were higher compared to their counterparts with the same bonded length (N1.6S and N1.9F respectively). The N1.9S strengthened beam showed a 117% increment in 1st crack load compared to the control beam.

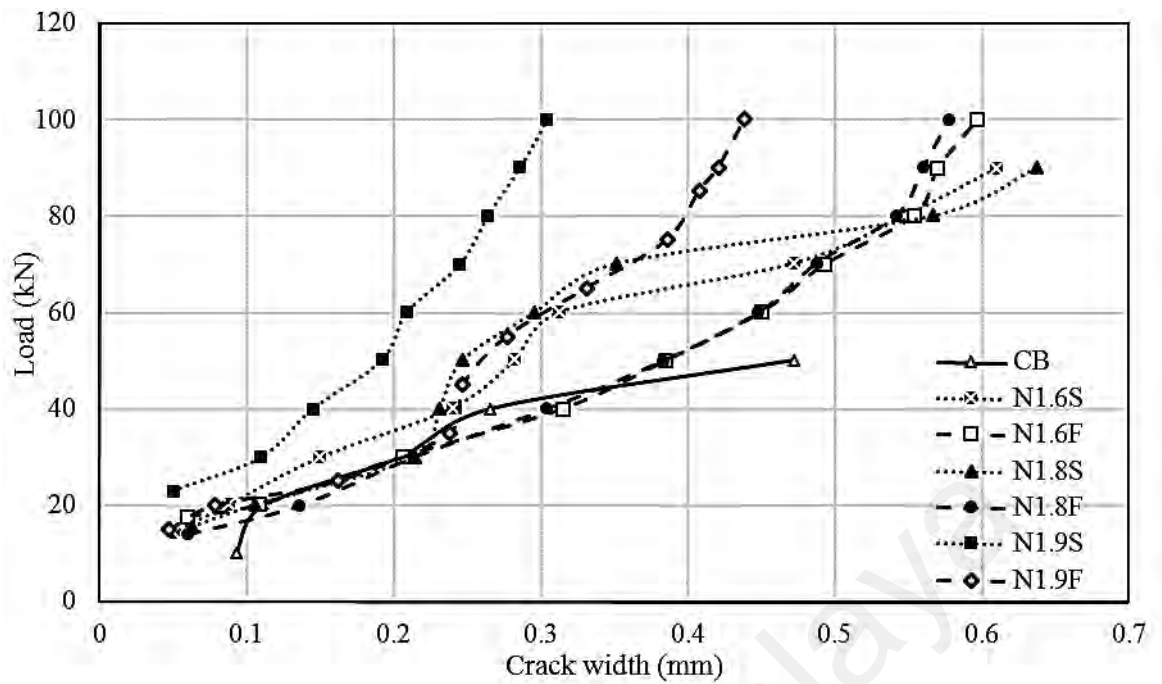


Figure 4.13: Load versus crack width of NSM strengthened RC beams

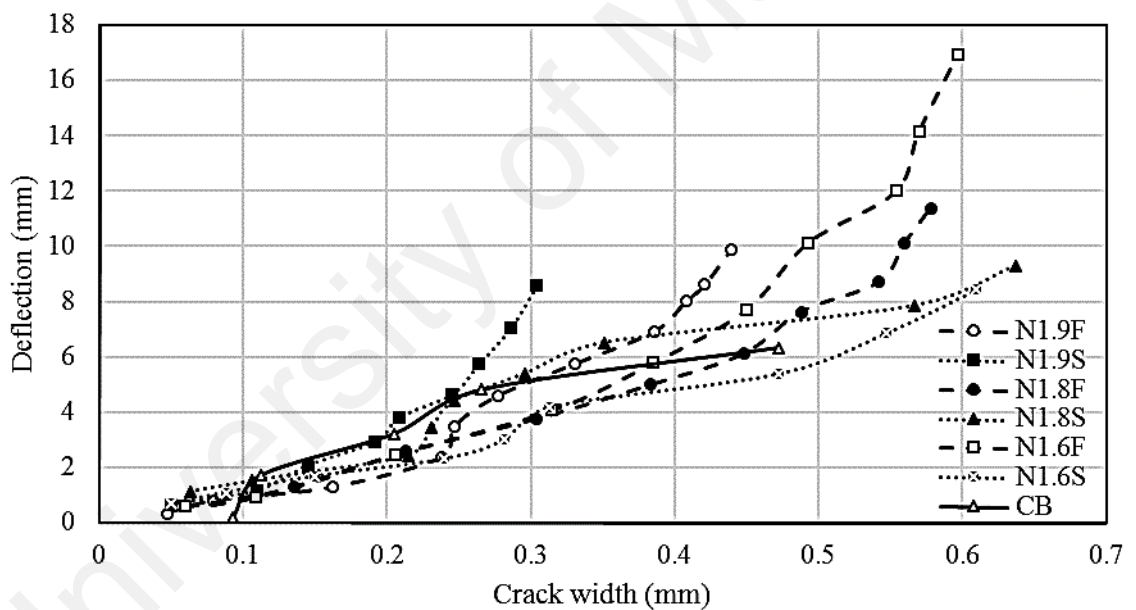


Figure 4.14: Deflection versus crack width of NSM strengthened RC beams

If the NSM materials (steel or CFRP) are compared on the basis of their cracking performance against load, it can be seen that the overall behavior at the ultimate point is similar for both the steel and CFRP strengthened beams when bond lengths are 1600 and 1800 mm. However, steel strengthened beams exhibited better performance at the beginning and middle of the load-crack width curve. Longer bond length (1900 mm) in the same NSM material group (steel/CFRP) resulted in superior performance compared

to the shorter bond lengths (1600 mm or 1800 mm). The progression of the crack widths in beams with strengthening bond lengths of 1600 mm and 1800mm were similar in nature within the same material group.

The N1.6F beam showed the highest deflection among the beam specimens with a load of 100 kN and crack width of 0.6 mm. Increasing the CFRP length reduced deflection and crack width, as can be seen in Figure 4.14. All beams strengthened with NSM steel exhibited less deflection for crack width compared to their NSM CFRP counterparts with the same bond length. A dramatic improvement in crack width was noticed in the N1.9S beam, which had a crack width of only 0.3 mm, compared to the N1.9F beam, which had a crack width of 0.44 mm, at the 100 kN load point. The N1.9S beam also displayed the least deflection for crack width among the strengthened beams (Figure 4.14). The enhanced performance of the N1.9S beam over other beams is due to superior bonding and comparatively enhanced stiffness properties (Hosen et al., 2014; Rahal & Rumaih, 2011).

Figure 4.15 described the different measurements of crack width at first crack and service loading. According to ACI 318-11, the service load deflection ($\text{span}/480$) for the beam specimens was found to be 4.17 mm. After analysis, the corresponding service load and its associated crack width was determined. During testing the crack width was measured with the help of digital crack microscope at different load. At first crack, N1.9F, N1.9S, and N1.6S beams showed almost same width which was around 0.05 mm. The crack width of 1st crack load for N1.8F, N1.8S and N1.6F was 0.05 mm. All the strengthened beams showed less crack width at the first crack load compared to the control beam which was 0.09 mm. During service load, N1.9F, N1.9S and N1.8S showed about 0.25 mm crack width which was lesser than other strengthened beams. N1.9S showed the least crack width of 0.23 at the service load level. N1.8F, N1.6F and

N1.6 S beams failed prematurely due to the debonding failure. So, prior to failure the crack width was growing bigger rapidly as mentioned by Frosch (1999). That may be the possible reason behind such higher crack width compared to the others.

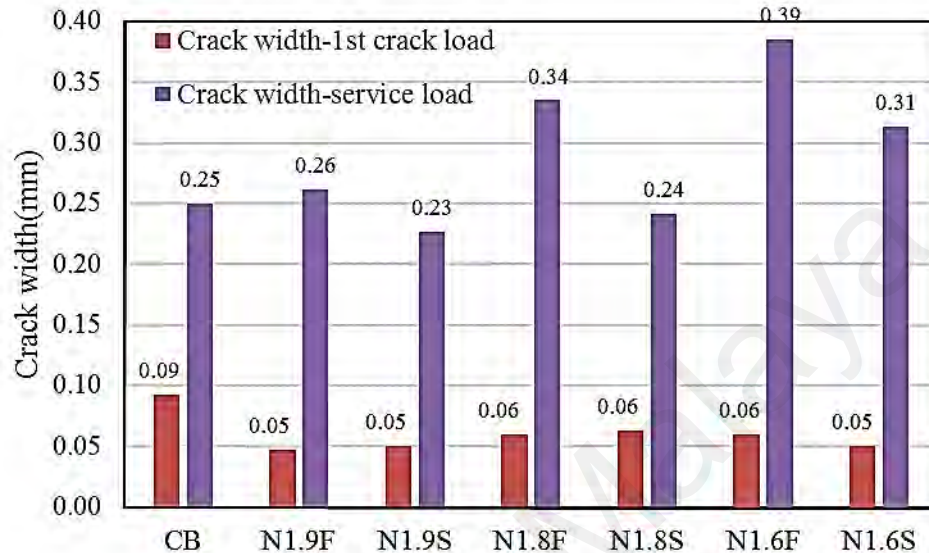


Figure 4.15: Crack width at 1st crack and service load of NSM strengthened beams

4.1.2.5 Ductility Analysis

Ductility is regarded as one of the principal safety parameters of any structures. The ductility of any structural element is its capability to withstand inelastic deformation prior to ultimate failure without substantial lack in resistance or strength capacity (ISIS, 2008).

Table 4.3: Summary of different ductility index of NSM beams

Beam ID	Deflection ductility			Energy ductility			Deformability	
	Δ_y (mm)	Δ_u (mm)	μ_d	E_y (kN-mm)	E_u (kN-mm)	μ_E	Δ_f (mm)	μ_{Δ_f}
CB	7.70	24.70	3.21	263.93	1227.75	4.65	49.91	6.48
N1.9F	10.70	19.20	1.79	647.98	1674.62	2.58	21.11	1.97
N1.9S	10.00	12.40	1.24	677.26	931.06	1.37	31.42	3.14
N1.8F	13.00	18.60	1.43	805.04	1475.05	1.83	22.02	1.69
N1.8S	10.80	16.80	1.56	606.66	1195.43	1.97	43.33	4.01
N1.6F	8.50	13.60	1.60	424.23	930.93	2.19	14.90	1.75
N1.6S	8.30	9.40	1.13	455.52	554.77	1.22	13.25	1.60

It has a significant function to redistribute the stresses from one critical element to another of any statically indeterminate structures (Jeong, 1994). The ductility behavior in FRP strengthened structures is of great concern to researchers as the FRP product does not have any specific yield point and its stress strain response is linear elastic.

Table 4.3 showed the deflection ductility, energy ductility and deformability along with their indices. Conventionally, ductility can be determined from the load-deflection diagram which is basically a ratio of the last deflection at ultimate point to the deflection at the primary yield point of the internal steel reinforcement (Zou, 2003). From literature it has been found that the ductility of any beam reduces with the increasing amount of its internal reinforcement irrespective of steel or CFRP until it reaches the ultimate point (Rasheed et al. 2010). Besides, maintaining the same reinforcement ratio, ductility of any beam can be enhanced by increasing the compressive strength of the applied concrete up to a certain limit and thereafter it decreases as f'_c increases (Ashour, 2000).

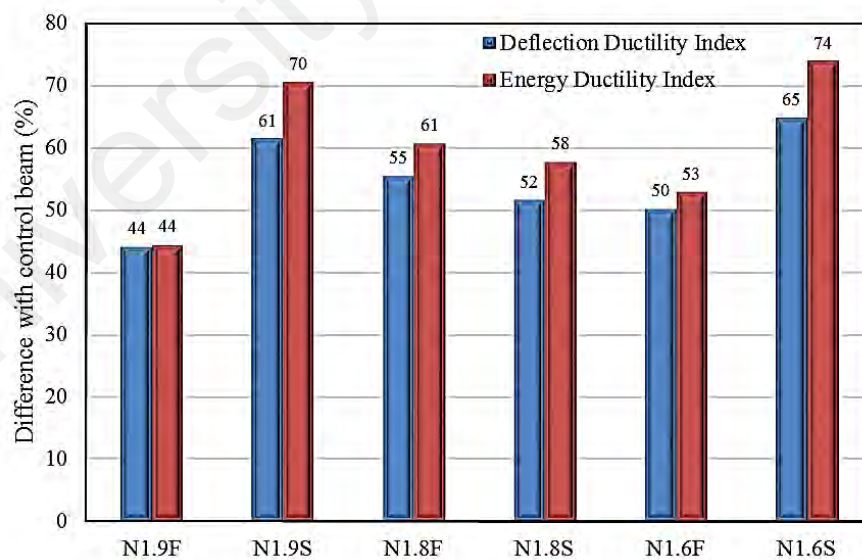


Figure 4.16: Various ductility index of NSM strengthened RC beam

The study has measured the indexes of deflection ductility, energy ductility and the deformation ductility of the control as well as the strengthened RC beams. The

deflection ductility index can be defined as the ratio of the ultimate deflection (Δ_u) to the deflection (Δ_y) at yield load (equation 4.4).

$$\mu_{\Delta u} = \frac{\Delta_u}{\Delta_y} \quad (4.4)$$

Table 4.3 and Figure 4.16 demonstrated the calculation of the strengthened beam's deflection ductility and its percentile difference compared to the control beam. The deflection ductility index of control beam was the highest among all beams due to its pure flexure failure mode where the ratio of deflection at ultimate to yield was the maximum. The stiffer load-deflection response of the strengthened beams induced a less ultimate to yield deflection ratio which led to a lower ductility index. In Figure 4.16, the deflection ductility index of N1.9F, N1.9S, N1.8F, N1.8S, N1.6F and N1.6S beams were reduced by 44%, 61%, 55%, 52%, 50%, and 65%, respectively, compared to control beam and the less percentile values mean the more ductile behavior of beam, as those values represented the difference between the control and the respective strengthened beams. The CFRP NSM strengthened beam showed better ductility performance compared to their steel NSM counterpart. It was due to increased deflection of the CFRP strengthening bar measured during the test. In the structures where the internal steel was replaced by the CFRP bar, this large deflection was a major concern which was addressed by several researchers. As the modulus of elasticity of CFRP was comparatively lesser than the strengthened steel bar, the stiffness of CFRP NSM beams was lessened and deflection was increased accordingly (Hollaway, 2010).

Thomsen et al. (2004) described the ductility index based on energy in the equation 4.5 which was a ratio between the energy (E_u) at ultimate state (the area under the load-mid span deflection curve up to ultimate displacement) and the energy E_y at yield state (the area under the load- deflection curve up to yield displacement).

$$\mu_E = \frac{E_u}{E_y} \quad (4.5)$$

This index gave indication about the evolution of fracture work on the tested specimens (Gopalaratnam & Gettu, 1995; Hosen et al., 2016). Figure 4.16 showed the percentile variance of the energy ductility index of NSM beams with the control one and the detail data was listed in Table 4.3 where the NSM beams showed less energy ductility index than control beam. The energy ductility indexes of N1.9F, N1.9S, N1.8F, N1.8S, N1.6F and N1.6S beams were reduced by 44%, 70%, 61%, 58%, 53%, and 74%, respectively, compared to the control beam. The percentile variation of deflection ductility and energy ductility is almost close to each other for the NSM strengthened beams. The outcome is expected as the CFRP NSM beams showed more deflection and its ultimate load capacity was more than the steel NSM beams. Hence the energy absorption capacity of CFRP NSM beams was higher according to the equation 4.5.

The Deformability index can be expressed as the ratio of deflection at failure of the beam to the deflection at the yield load (equation 4.6) (El-Hacha & Gaafar, 2011).

$$\mu_{\Delta_f} = \frac{\Delta_f}{\Delta_y} \quad (4.6)$$

Where Δ_f and Δ_y are the displacement at failure load and yield load, respectively. Table 4.3 presented a comparison of the ductility and deformability indexes of the strengthened beam specimens with those of the control specimen. Figure 4.17 depicted the deformability index of NSM strengthened beams with the control beam.

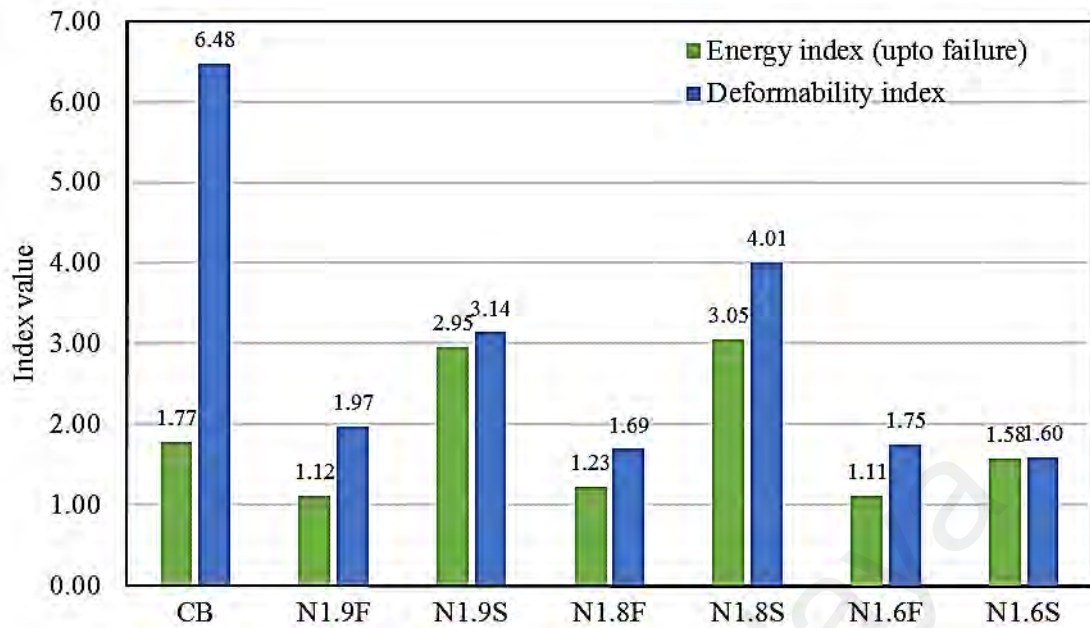


Figure 4.17: Deformability and energy index of NSM strengthened beams

In this same diagram (Figure 4.17), another energy index was provided which was the ratio between the total energy (E_{tot}) up to the full failure of the beam (the total area of the load-mid span deflection curve) and the energy (E_y) at yield state (the area under the load- deflection curve up to yield displacement). It was found in this index that N1.9S and N1.8S was 66% and 72% more than the control beam, respectively. The other CFRP strengthened beams (N1.9F, N1.8F and N1.6F) along with N1.6S beam demonstrated 37%, 31%, 38% and 11% less values compared to the control one. It was noted that the N1.9S, N1.8S and control beams failed due to flexure failure whereas the other beams failed prematurely with concrete cover separation. For that reason, those two steel NSM beams experienced large deflection beyond their ultimate point. In contrast, those debonded CFRP NSM beams failed immediately after reaching their ultimate point. Henceforth, this energy indexes for N1.9F, N1.8F, N1.6F and N1.6S were lower than that of the control beams (Darain et al., 2015).

4.1.2.6 Stiffness Assessment

Stiffness is the paramount feature of RC structures as the deflection and curvature of it changes under applied load due to the variation of stiffness. Stiffness can be

characterized as the product of modulus of elasticity and moment of inertia. The modulus of elasticity is a mechanical property of concrete which is significantly influenced by the proportion and quality of the constituent material like binder, aggregates and water (Aïtcin & Mehta, 1990). In an RC section the moment of inertia is continuously changing which is more pronounced during the formation of 1st cracks and the yielding of tension steel. The stiffness shifts under different levels of loading at 1st crack and yield point can be clearly visualized in a moment -stiffness diagram. Hence, different researchers proposed to use the gross moment of inertia (I_g) before the appearance of any crack. After the appearance of first crack, the effective moment of inertia (I_{eff}) should be used and at the full crack formation of the beam it is recommended to use the cracked moment of inertia (I_{cr}) at the cracked transformed section of the beam.

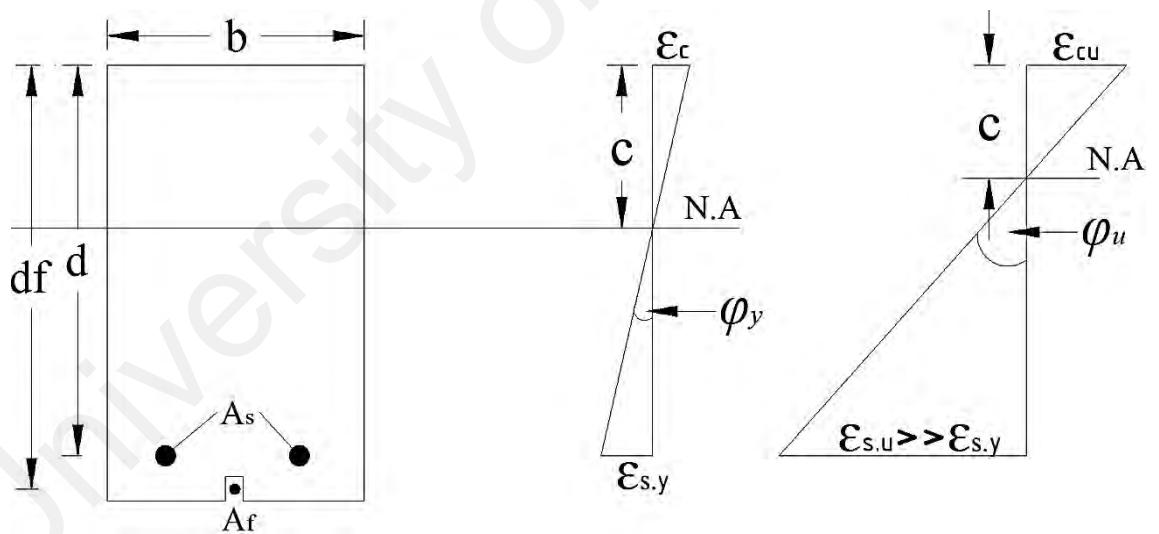


Figure 4.18: Yield and ultimate curvature of the NSM strengthened beam

During the transformation from un-cracked to cracked stages, the stiffness shifts cause first moment redistribution. Due to the yield load, one or more cross-section(s) achieve(s) the yield moment. The yield zone having no strengthening materials develops critical cross-section with plastic deformation which eventually forms a plastic hinge. The non-plastic zone carries the increasing load and the plastic hinge maintains the

constant or slightly increasing bending moment. The zone with the NSM strengthening material carry higher bending stiffness and a limited plastic deformation is visible. Significant load is carried by the yield zone and the further development of plastic hinges is delimited.

The RC beam section greatly varies with the un-cracked and cracked stages due to the applied load. From the displacement data coming from three different LVDTs along the beam length (Figure 3.8), it is possible to calculate the bending stiffness. By using the elastic bending theory in the displacement based equation, it is possible to calculate the experimental bending stiffness through the equation 4.7 (Mohammadhassani et al., 2012).

$$(EI)_{exp} = \frac{Pa(3l^2 - 4a^2)}{48\delta_{exp}} \quad (4.7)$$

Here, $P, l, a,$ and δ_{exp} represent the applied service load, clear span of the RC beam, shear span of the beam and the maximum mid-span experimental deflection at service load, respectively.

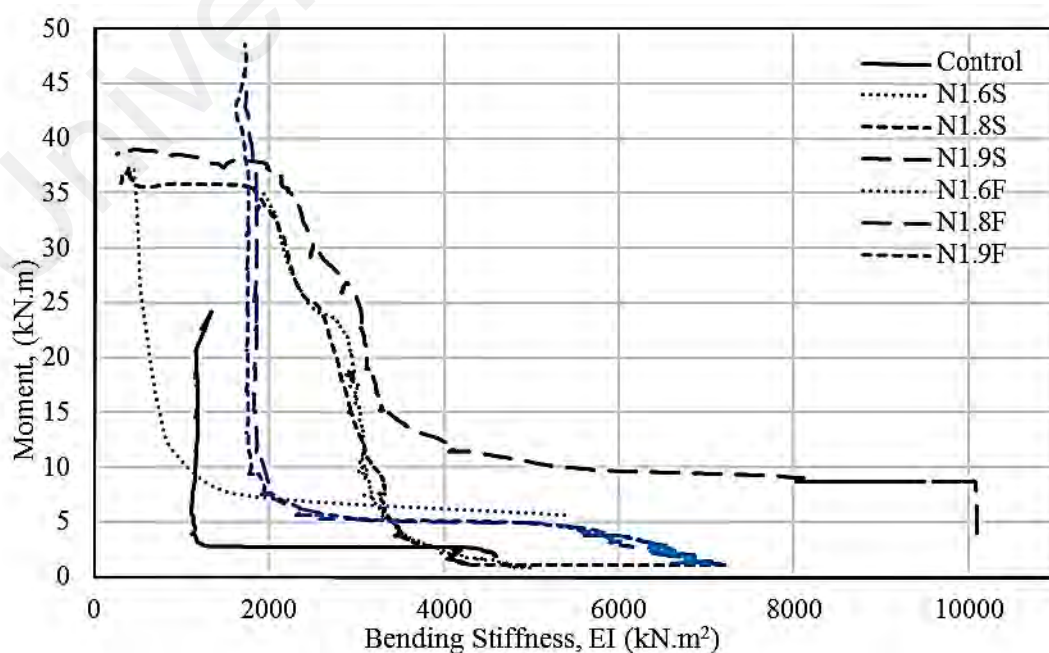


Figure 4.19: Bending stiffness of the control and NSM strengthened beams

Another approach to bending stiffness determination is to evaluate the curvature of the beam at bending due to applied experimental load. For that purpose, the moment-curvature relationship of the RC beam should be developed. There are three approaches to establish this relationship which are as follows: (a) analyze strain of top compression fiber and bottom steel (b) analyze strain of bottom and top steel and (c) analyze strain of top fiber and CFRP bar. During preparation and experimental set-up of the beams, strain gauges were mounted at the internal reinforcement, concrete and the strengthening materials. However, for the simplicity and ease of the work, the first option had been selected to analyze the strain at bottom steel and top concrete compression strain to establish the moment-curvature diagram.

Figure 4.18 demonstrated the yielding and ultimate stage of the strain behavior of the strengthened RC beams using NSM technique. A moment curvature relationship was developed using the extreme tension strain values from the internal steel bar strain gauge and the extreme compression strain gauge values from the top of the mid-span. The curvature φ of the beam was kept changing due to the strain variation of concrete and steel. In figure, the changes were marked at the steel yielding and post-yielding stages where strain of steel was too high and concrete reached to its maximum strain. After getting the curvature, the bending stiffness could be calculated from the experimental results by the equation 4.8 and 4.9 as suggested by Hosen et al. (2016).

$$(EI)_{exp} = \frac{M}{\varphi} \quad (4.8)$$

$$\varphi = \frac{\varepsilon_c + \varepsilon_s}{d} \quad (4.9)$$

Figure 4.19 demonstrated the moment versus bending stiffness diagram, where the steel and CFRP bar had been used as NSM reinforcement. The strengthened beam using steel and CFRP were colored with black and blue, respectively, to understand their

behavior. The overall shape of the moment versus bending stiffness curve was formed like an “L”. For all cases, the NSM strengthening of the RC beam demonstrated an enhanced moment-stiffness relationship compared to the control beam. Initially, the bending stiffness was high as expected due to the un-cracked stage of the beam section. With the increasing application of load, the stiffness was going to decrease and form a knee of the “L” where first crack appeared.

There was no noticeable difference of stiffness after this drastic realignment of the curve though the moment was increased at a steady rate. Except the N1.9S and N1.8S beams, all other beams followed almost a straight line from the first cracking moment to their ultimate point. Those two above mentioned beams showed gradual decrease of stiffness against their increasing moment rate from cracking moment to their yield moment. After this point the curve formed a plateau where their stiffness was decreasing from the yield point to their ultimate failure without any appreciable change of the moment. Please note that, N1.9S and N1.8S beams failed due to concrete crushing before the internal steel yielding (flexure failure), while the other strengthened beams failed due to premature debonding failure.

The control beam showed the same flexure failure like these two beams and its behavior of the moment-stiffness diagram should also perform in the same manner as these beams. However, after the ultimate point, the strain and steel strain gauge data were lost due to the damage of the strain gauge of this control beam. In Figure 4.19, it was depicted that the overall stiffness behavior of steel at initial, first crack, yield and post yielding was better compared to CFRP though their ultimate moment achievement was superior to the steel strengthening material.

4.1.2.7 Strain Measurement

The reduction of ultimate deflection of NSM strengthened beam compared to the control beam was shown in Figure 4.6. The strengthened beams also exhibited the lower compressive strain value which was captured from the strain gauge at the extreme top fiber of the tested beams. To make a justifiable comparison, these strain values were taken at 15 kN, 40 kN and 60 kN. As the service and ultimate loads of the control beam were 39 kN and 64 kN, so the range was taken as 40 kN and 60 kN. Almost all the strengthened beams demonstrated the first crack at 15 kN which was chosen as the lower bound and the 60 kN load was within the service load level of all the strengthened beams.

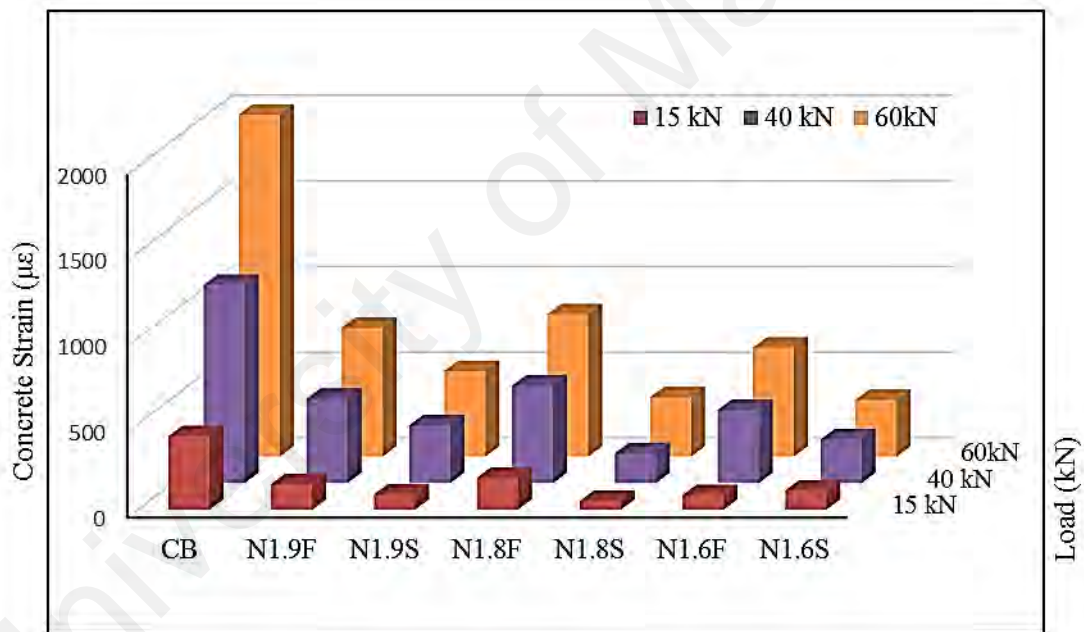


Figure 4.20: Comparison of concrete strain of NSM strengthened beams at 15,40 and 60 kN service load

Figure 4.20 demonstrated the concrete top fiber compression strain at 15, 40 and 60 kN service load level. It is clearly visualized that the concrete strain of the strengthened beams was getting reduced compared to the control beam at all three load levels. The percentile reduction of the NSM strengthened beam compared to the control beam at 60 kN load were 62%, 75%, 58%, 83%, 68% and 83% for N1.9F, N1.9S, N1.8F, N1.8S, N1.6F and N1.6S respectively.

N1.6F and N1.6S beams. The steel NSM beams showed less strain compared to the CFRP NSM beams to this stipulated region.

Figure 4.21 demonstrated the tensile strain of internal steel bar at 15, 40 and 60 kN service load level. It is clearly visualized that the tensile strain of the strengthened beams was getting reduced compared to the control beam at all three load levels. The percentile reduction of the NSM strengthened beam compared to the control beam at 60 kN load were 61%, 74%, 69%, 76%, 86% and 81% for N1.9F, N1.9S, N1.8F, N1.8S, N1.6F and N1.6S beams. The steel NSM beams showed less strain compared to the CFRP NSM beams to this stipulated region.

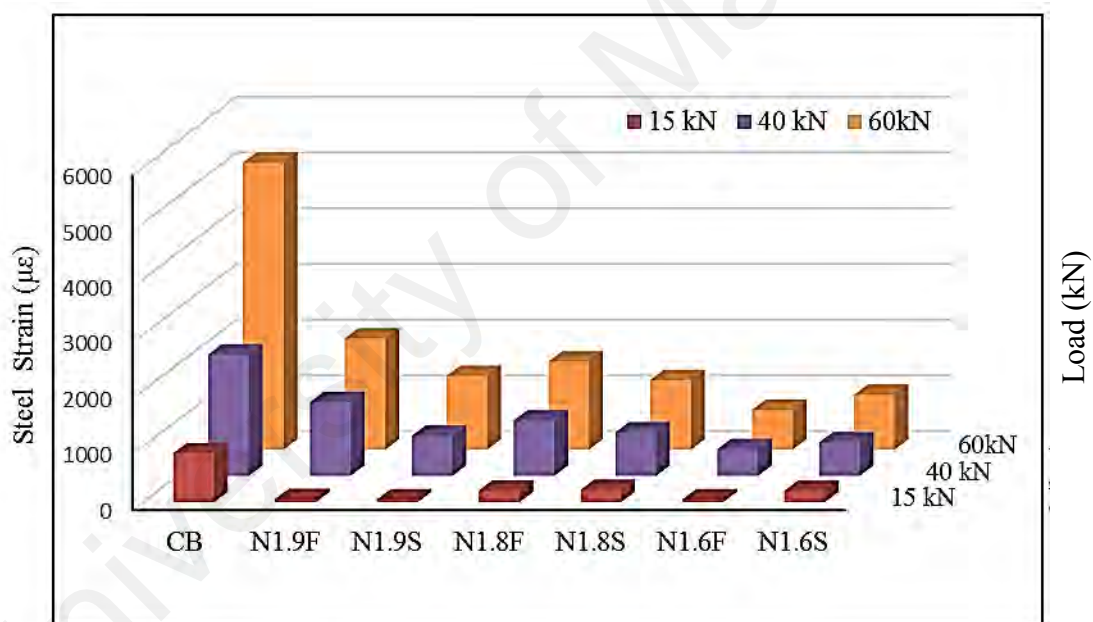


Figure 4.21: Comparison of steel strain of NSM strengthened beams at 15,40 and 60 kN service load

Figure 4.22 demonstrated the tensile strain collected from the strain gauge at the central portion of the NSM steel and CFRP strengthening bar. From the graph, the steel bar and the CFRP can be easily distinguished by their load-strain response. The steel bar portrayed almost the elastic-perfectly plastic behavior, whereas the CFRP demonstrated increasing linear elastic after yielding actions.

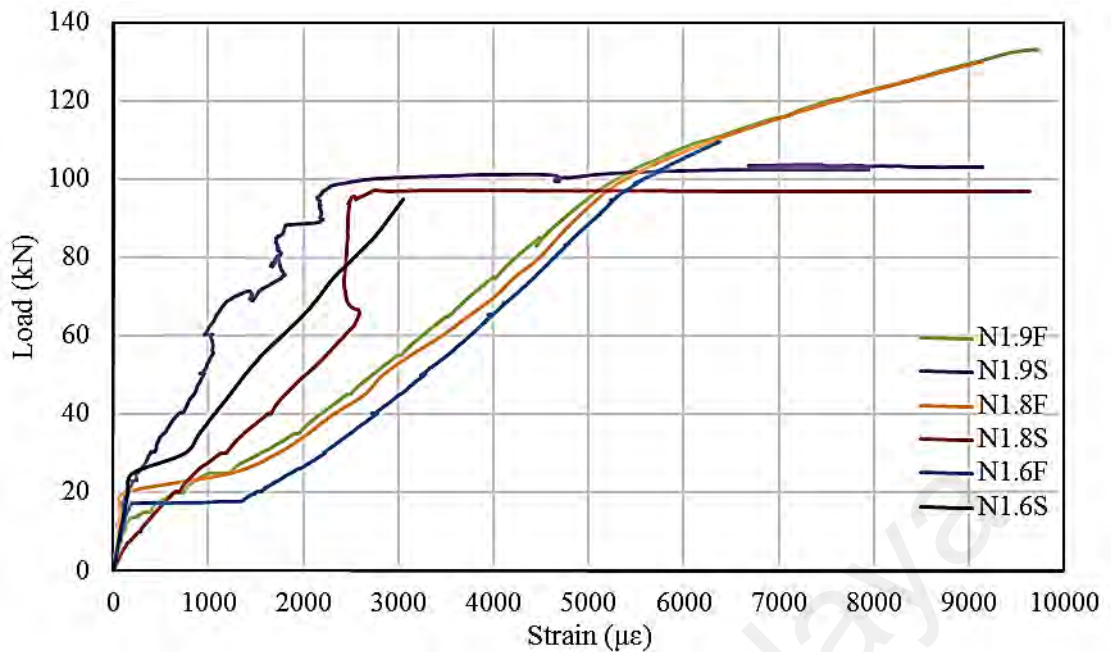


Figure 4.22: Tensile strain at NSM CFRP and steel bar

Except the N1.6S, all other beams achieved the tensile strain more than 6000 $\mu\epsilon$. The maximum tensile strain of N1.9F, N1.9S, N1.8F, N1.8S, N1.6F and N1.6S were 9724 $\mu\epsilon$, 9148 $\mu\epsilon$, 9120 $\mu\epsilon$, 9643 $\mu\epsilon$, 6377 $\mu\epsilon$ and 3044 $\mu\epsilon$, respectively. The steel NSM strengthened beams showed stiffer strain response compare to the CFRP NSM beams. This was due to the greater modulus of elasticity of NSM steel used for strengthening though the ultimate capacity of CFRP NSM beam was higher (De Lorenzis & Teng, 2007).

4.1.3 Control Beam for Group B, C and D

The control beam explained in this section was counted as a reference beam to assess the strengthened beams of Group-B, C and D. Two 3300 mm long beams were tested to get the flexural behavior of the control beam. Finally, control beam 1 was chosen to compare the result with the strengthened beam. All the beams were designed to be under-reinforced with a steel ratio of 0.0085. The beams were tested under four-point bending load in Instron universal testing machine using load control mode at a rate of 5 kN/min until it reaches to the yield point. The machine controller was then changed to

displacement mode at a rate of 2 mm/min up to the full failure of the beam. The load-deflection diagram of the two control beams is shown in Figure 4.23.

The load deflection curves of the control beams showed a bi-linear response up to the yielding stage (Figure 4.23). Beyond this region the behavior of the specimens was totally nonlinear. After the yielding point the curve was becoming flat to some extent and the ultimate failure was initiated. After the ultimate point its deflection was increasing and concrete crushing appeared at the top compression zone. After forming a perfect concrete wedge shape the machine was stopped.

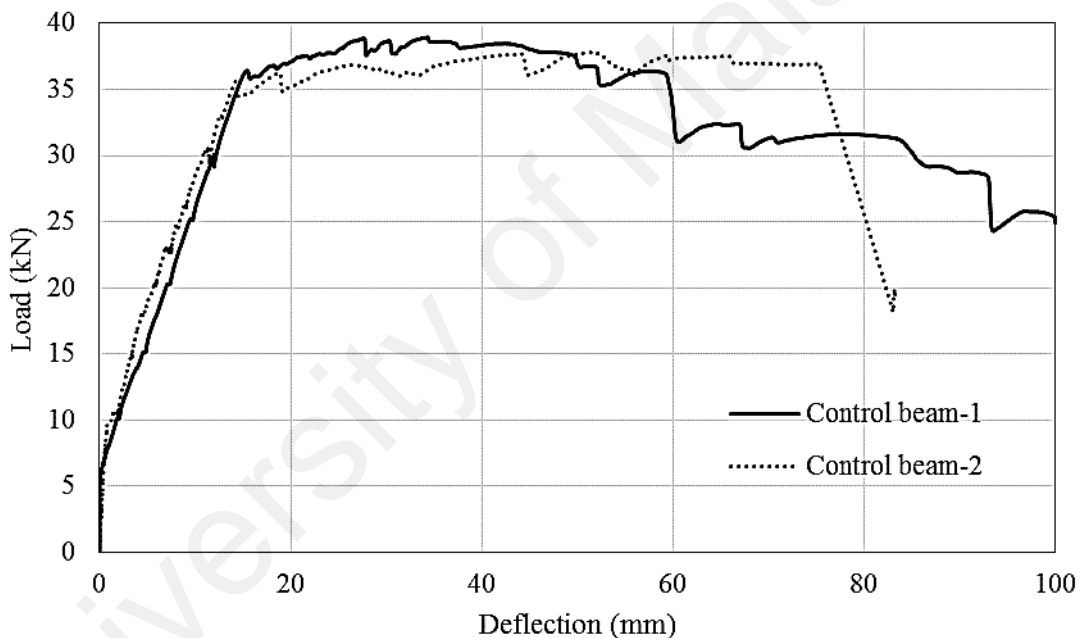
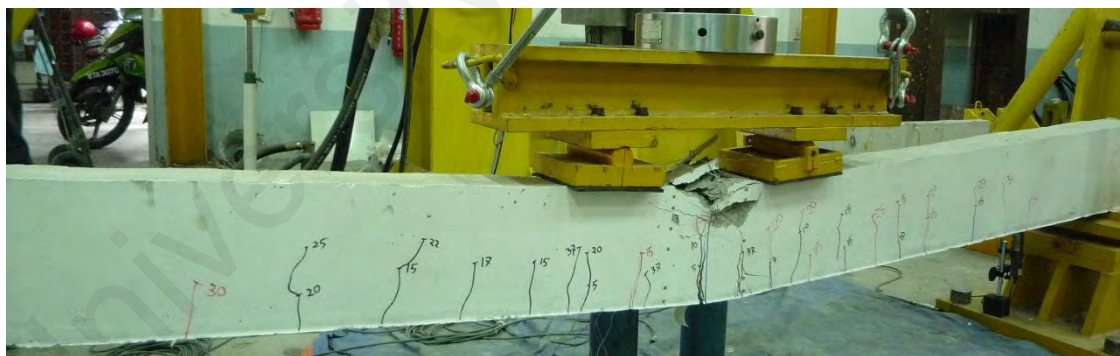


Figure 4.23: Load-deflection curve of control beams for Group B, C and D

The diagram in Figure 4.23 followed a typical RC beam's load deflection curve. The curve can be subdivided into three parts. First crack appeared at 5 kN and 4.8 kN for the control beam 1 and 2, respectively. The 1st portion of the curve could be distinguished until first crack which indicated a stiffer response followed by an elastic linear path up to the yield point. Both the control beams showed the same response until their internal steel reached their yield point at 36.29 kN and 35.4 kN (Figure 4.23). After crossing the yield point, the 3rd portion of the curve maintained a plateau up to the ultimate capacity

at 38.95 kN and 37.5 kN for the corresponding control beam 1 and 2. Beyond this point both the beams demonstrated concrete crushing failure (Figure 4.24) at the top mid-span portion and the load-deflection curve was moving downward which exhibited a softening behavior followed by the formation of wedge at the compression zone. The internal steel strain and concrete strain values were described with the corresponding strains of the strengthened beams at the respective section to make better comparisons among them.

Both the beams had similar characteristics of the load-deflection and the strain value of steel and concrete. However, the ultimate load capacity of control beam 1 is higher than control beam 2. If the control beam 2 was considered as the reference, then the difference of control and strengthened beam would be higher. Therefore, to make a reasonable comparison with the strengthened NSM beam justifiable, control beam 1 was chosen as the reference control beam for this study.



(a) control beam 1



(b) control beam 2

Figure 4.24: Failure modes of control beams for Group B, C and D

4.1.4 Externally Bonded Strengthening with CFRP Fabric

Table 4.4 demonstrated the summary of the experimental findings of the EB strengthened RC beams. Only test variable was the thickness of the CFRP fabric (single

and double layer) which was externally bonded at beam soffit. This series was designed to compare its result with the proposed CEBNSM beams. It listed the corresponding load and deflection of first crack, yield and ultimate capacity of the control and EB strengthened beams along with their failure modes. If there was a comparison with the control beam, the addition of the CFRP fabric at the beam soffit enhanced the load carrying capacity by 70% and 100% at 1st crack load as well as 17% and 37% at yield load for EBP1 and EBP2 respectively.

The ultimate load capacity was increased by 24% and 48% for the EBP1 and EBP2 compared to the control beam. From the result it is evident that strengthening with the CFRP fabric improved the flexural performance of the RC beam though the failure behavior for both of the beams demonstrated premature delamination failure.

Table 4.4: Summary of experimental test results of EB beams

Beam ID	P_{cr} (kN)	Δ_{cr} (mm)	P_y (kN)	Δ_y (mm)	P_u (kN)	Δ_u (mm)	Failure mode
CB	5	0.5	36	15	39	34.3	Flexure
EBP1	8.5	0.9	42.3	16.7	48.2	26.8	Delamination
EBP2	10.5	1.9	49.7	17.9	57.8	26.2	Delamination

*Where P_{cr} = first crack load; P_y = yield load; P_u = ultimate load; Δ_{cr} = deflection at 1st crack; Δ_y = deflection at yield of steel; Δ_u = mid-span deflection at ultimate load.

4.1.4.1 Load Deflection Curve

Figure 4.25 showed the load versus mid-span deflection of control and externally bonded RC beam. The figure depicted the trilinear response behavior for the EB strengthened RC beam which can be divided into three distinct regions. These are (a) elastic region, (b) concrete cracking to steel yielding region and (c) steel yielding to ultimate failure region. The first linear elastic region ends until the 1st cracking of concrete (8.5 and 10 kN). After conversion to moment, it can be addressed as cracking moment, M_c.

The 2nd phase continued up to the yielding of the internal steel bar where a change of slope demarked this curve. Within this region new cracks appeared and widths were getting wider in old cracks. The increase of effective pre-yield stiffness was not significant for these two beams. It was increased by 4.5% and 14.2% for EBP1 and EBP2 comparing with the control beam. The number of cracks stabilized at yielding moment M_y .

At third phase after the steel yielding, the curve slightly changed its slope from M_y to the ultimate moment M_u due to stiffness variation of the strengthened beam. Due to the delamination of the CFRP fabric a dramatic decrease of the curve could be figured out which ended at the level of the normal RC beam capacity range (Ritchie et al., 1991). After this the deflection of beam was increasing with gradual decrement of load like a normal RC beam.

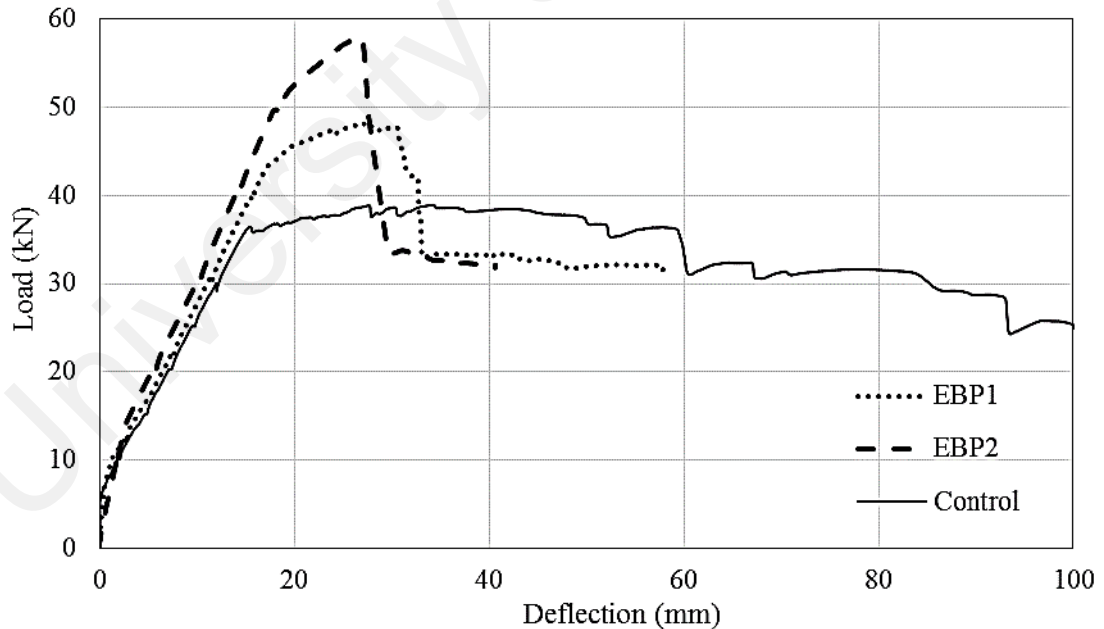


Figure 4.25: Load-deflection curve of EB strengthened beams

4.1.4.2 Cracking Behavior

Figure 4.26 represented the ratios of minimum to average and maximum to average crack spacing of the control and EB strengthened RC beams. The average values of the

maximum and minimum ratios were 1.39 and 0.71, respectively, which agreed well with the predicted value in equation 4.2 and 4.3.

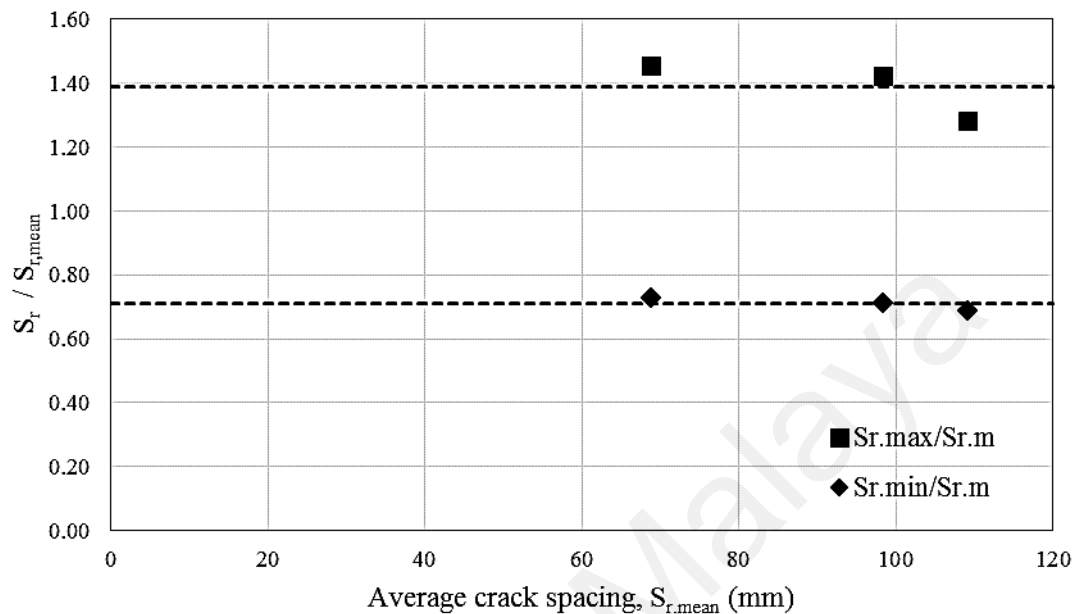


Figure 4.26: Crack spacing details of control and EB strengthened beams

Table 4.5 showed the maximum, minimum and average crack spacing along with the number of cracks appeared on the EB strengthened RC beams. The minimum and maximum crack spacing was observed as 50 and 100 mm for the beam EBP1 and EBP2 respectively. The average crack spacing maintained a range between 69 mm and 98 mm. The EBP1 beam demonstrated 29 number of cracks and the EBP2 beam showed 21 number of cracks.

Table 4.5: Experimental maximum, minimum and average crack spacing of EB beams

Beam no	$S_{r,max}$ (mm)	$S_{r,min}$ (mm)	$S_{r,mean}$ (mm)	No. Cracks
Control	140	75	109	21
EBP1	100	50	69	29
EBP2	140	70	98	21

The first crack width was 0.021 mm, 0.055 mm and 0.037 mm for the control, EBP1 and EBP2 beams which appeared at 5 kN, 8.5 kN and 10 kN load. The load versus crack

width in Figure 4.27 demonstrated the decreasing trend of crack width of the EB strengthened beam compared to the control beam.

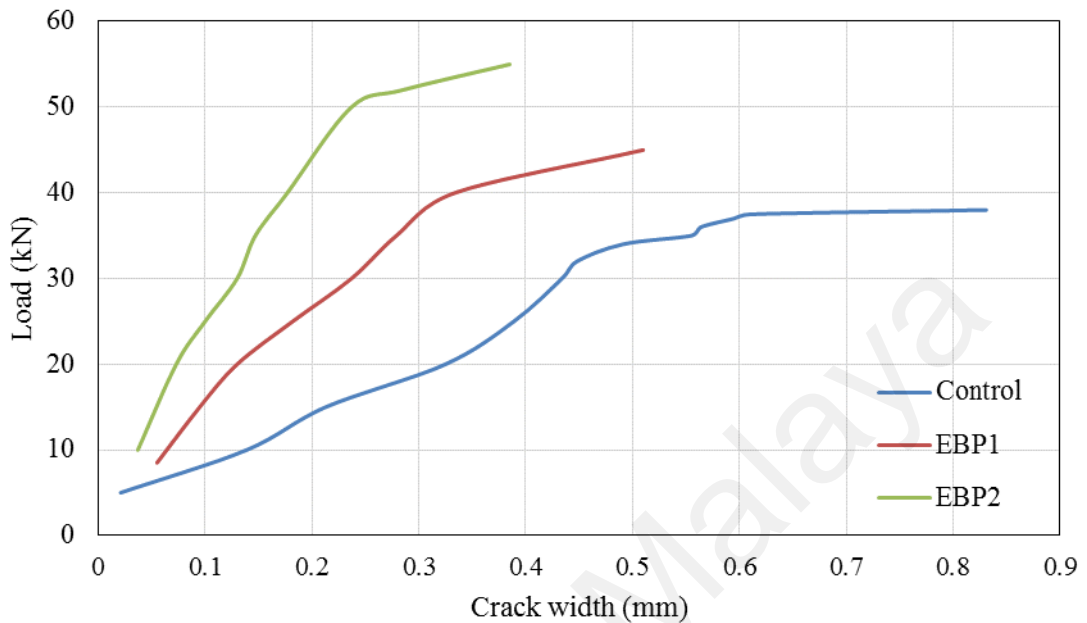


Figure 4.27: Crack width details of control and EB strengthened beams

For the sake of comparison, if 35 kN was considered, the control, EBP1 and EBP2 beams revealed 0.555 mm, 0.279 mm and 0.147 mm crack widths respectively. There was a considerable reduction to the crack width of those EB strengthened beams compared to the control one. It should be noted that this load (35 kN) was very close to the yield load of the control beam which was the basis to select it. Among these two strengthened beams, EBP2 beams displayed better crack width resistance due to its increased area of strengthening reinforcement which eventually developed more flexural stiffness. Similar behavior was observed by Ritchie et al. (1991).

4.1.4.3 Failure Modes

The failure modes of the EB strengthened beams were shown in Figure 4.28. Both the EBP1 and EBP2 beams demonstrated premature debonding failure. During test, the EBP1 beam showed a continuing rise of load-deflection relation until it reached its yield point (42.3 kN). Later at 45 kN load, a lot of cracking sound was taking place

originating from the CFRP fabric. It indicated the impending occurrence of local debonding failure. At a load of 48.2 kN, the CFRP reinforcement delaminated at the end of the CFRP fabric with tremendous energy release. As the machine was not stopped, it continued its deflection increment and ultimately began the failure process of the concrete at top mid-span region.

The EBP2 beam consisted of two layers of CFRP fabric where the cutoff point of the second layer was terminated away from the first layer end point by a distance of 100 mm at both ends. After crossing the yield limit of the beam at 49.7 kN very fine cracks appeared at the concrete cover just above the CFRP fabric layer and popping sound emitted after 52 kN load. The CFRP fabric delaminated suddenly with huge bursting sound which started from the fabric curtailment location towards the mid-span. This phenomenon was supported by the findings of Rahimi and Hutchinson (2001).



(a) EBP1 beam



(b) EBP2 beam

Figure 4.28: Failure modes of EB strengthened beams

The machine was continuing its displacement increment. With a small increase of load the curve again maintained the decreasing trend. At the bottom of the mid-span, small portion of the concrete cover was detached parallel to the level of internal steel with the CRRP fabric. The concrete at the compression zone at top mid-span started crushing like a typical RC beam phenomena.

4.1.4.4 Strain Measurement

Figure 4.29 showed the tensile strain of internal steel bar of the control and the EB strengthened RC beams documented at the center tension zone of the bar. From the graph it was possible to locate the first crack, yield and ultimate point through the slope variation at those respective load levels. The control beam showed the typical elastic perfectly plastic behavior, whereas the strengthened beams demonstrated the increasing linear elastic response after yield point. The EBP2 beam demonstrated a stiffer strain value with a strain hardening response before reaching to the ultimate load capacity of the beam. However, it displayed a sudden and abrupt descending branch at the load-strain curve.

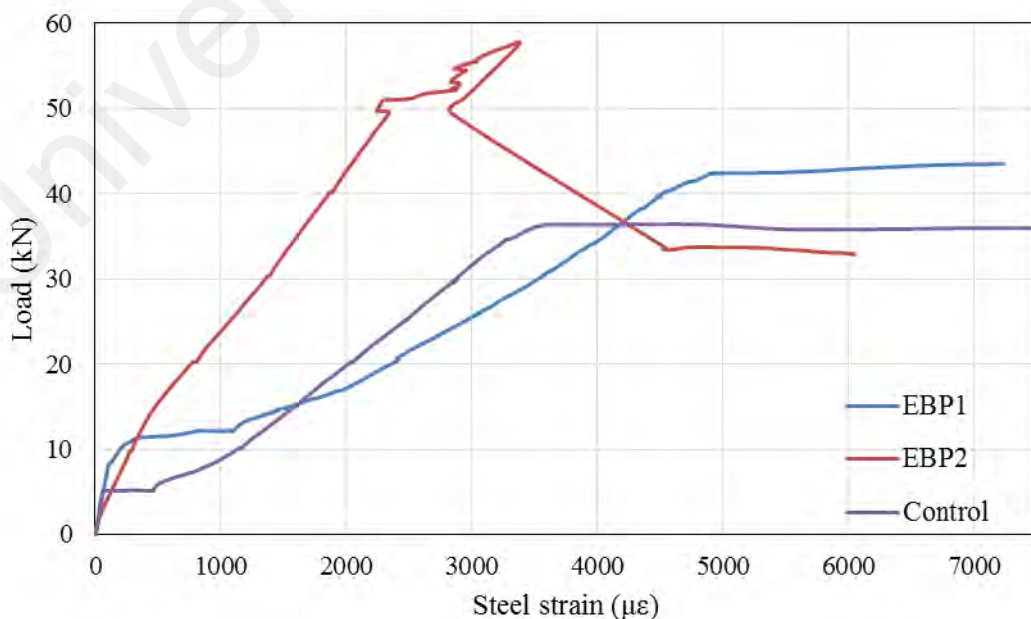


Figure 4.29: Steel tensile strain of control and EB strengthened beams

The strain profile of externally bonded CFRP fabric was described in the Figure 4.30 and Figure 4.31. The strain gauges were installed on the exterior surface along the length from mid-span to the end of the externally bonded beams. The strain readings were plotted at 1st crack, service, yield and ultimate load of the respective beams. Here, the service load was considered as 60% of the ultimate capacity of the corresponding beam. Both the beams showed a linear variation of strains under different load variations. The maximum strain was recorded as 7898 $\mu\epsilon$ and 6694 $\mu\epsilon$ for the EBP1 and EBP2 beams.

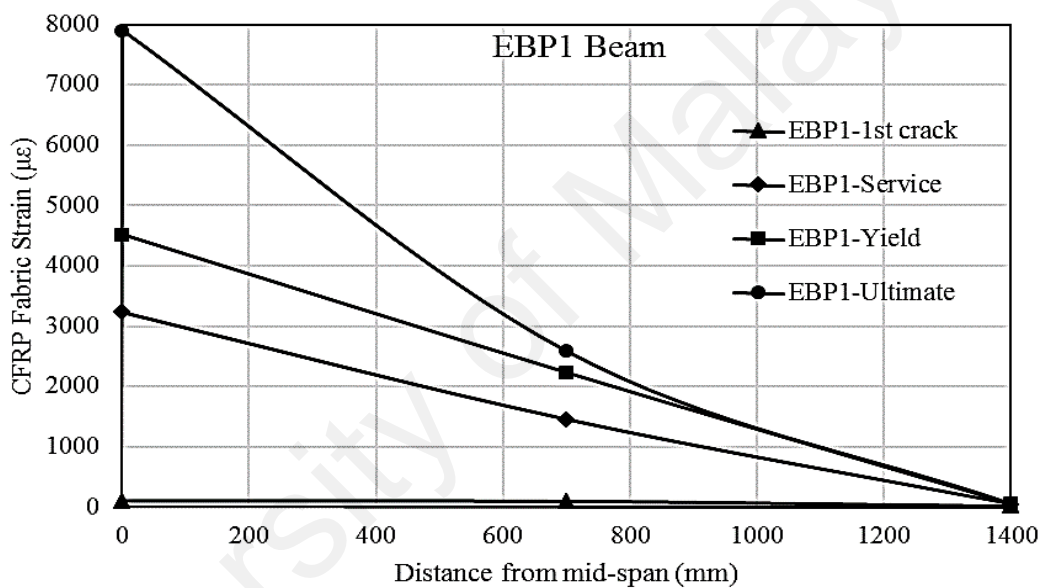


Figure 4.30: CFRP fabric tensile strain profile of EBP1 beam

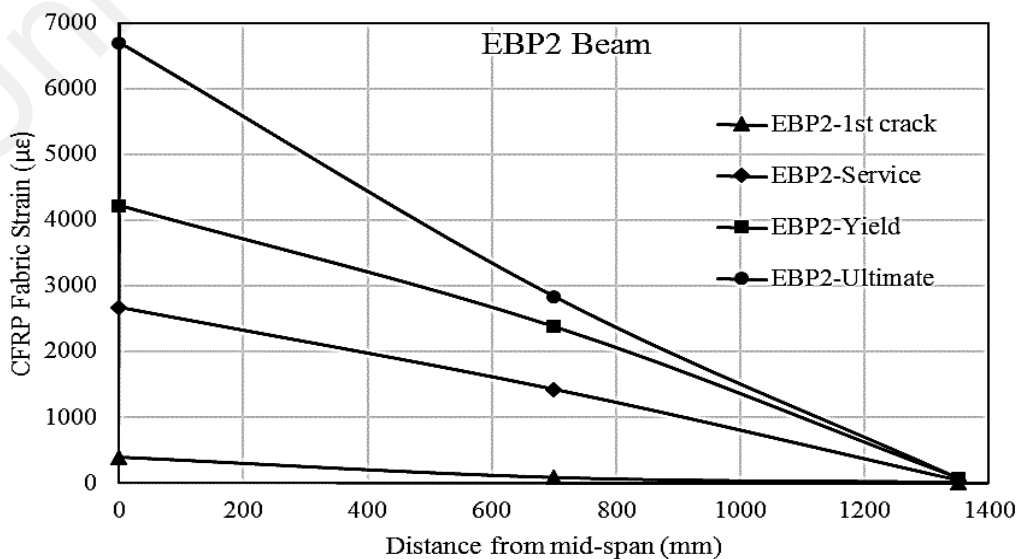


Figure 4.31: CFRP fabric tensile strain profile of EBP2 beam

4.1.5 CEBNSM-B Technique with CFRP and Steel NSM Bar

The experimental results of CEBNSM-B strengthened RC beams are tabulated below (Table 4.6). These beams were strengthened with steel or CFRP bar inside the NSM groove and CFRP fabric bonded at the soffit. The main test variables were the type of NSM bar (CFRP and steel bar), bar diameter (8 mm and 10 mm), thickness of CFRP fabric layer (1 and 2 layer) and anchorage (with and without) at the cutoff point of the EB CFRP fabric. The results are expressed in terms of their first cracking load, yield load and ultimate load capacity. Their corresponding deflection and percentage of load increment due to strengthening were also listed in the Table 4.6.

4.1.5.1 Load Carrying Capacity

Table 4.6 demonstrated the gist of the experimental finding of the total ten (10) number of CEBNSM-B strengthened RC beams. It is evident that the addition of the strengthening material to the RC beams caused superior load carrying capacity, reduction of ultimate deflection and less possibility of debonding problem. The ultimate load capacity was increased by 82%, 32%, 97%, 77%, 110%, 60%, 124%, 118%, 170% and 152% for the CBC8P1, CBS8P1, CBC8P2, CBS8P2, CBC10P1, CBS10P1, CBC10P2, CBS10P2, CBC10P2A and CBS10P2A strengthened beams, respectively, compared to the control beam. The corresponding first crack load and yield load of the beams improved significantly after strengthening. The yield point was determined from the stiffness variation in the load-deflection curve as well as the internal steel yielding point from the corresponding load-steel strain diagram. The average increment of ultimate capacity was 102% compared to control beam, though the corresponding ultimate deflection was less to the control beam. This enhanced ultimate capacity showed the superior performance of the strengthened beams over the control specimen as like the findings of other researchers (Lim, 2009; Rahman et al., 2015).

Table 4.6: Summary of experimental test results of CEBNSM-B beams

Beam ID	Pcr (kN)	Δ_{cr} (mm)	Py (kN)	Δ_y (mm)	Pu (kN)	Δ_u (mm)	Failure modes
CB	5	0.5	36	15.0	39	34.3	FFC
CBC8P1	11	1.5	50	14.9	71	39.7	FFF
CBS8P1	8	1.9	50	20.0	51	22.9	FFF
CBC8P2	13	1.9	55	15.2	77	31.3	FFF
CBS8P2	12	2.4	60	23.2	69	40.8	FFC
CBC10P1	13	1.6	54	16.6	82	43.3	FFF
CBS10P1	8	1.8	55	17.0	62	29.2	FFC
CBC10P2	15	2.3	69	23.7	87	42.7	CFD
CBS10P2	14	2.9	65	18.0	85	37.9	CFD
CBC10P2A	16	2.8	80	24.7	105	47.9	FFC
CBS10P2A	15	2.3	63	18.0	98	45.9	FFC

*Where Pcr = first crack load; Py = yield load; Pu = ultimate load; Δ_{cr} = deflection at 1st crack; Δ_y = deflection at yield of steel; Δ_{max} = mid-span deflection at failure load, FFC = flexural failure (concrete crushing after steel yielding); FFF= Flexure failure due to FRP rupture; CFD = CFRP fabric delamination

Figure 4.32 depicted the percentile increment of 1st crack, yield and ultimate load of the strengthened beam compared to the control beam. It can be easily understood that the 1st crack load had been tremendously improved using the CEBNSM-B technique.

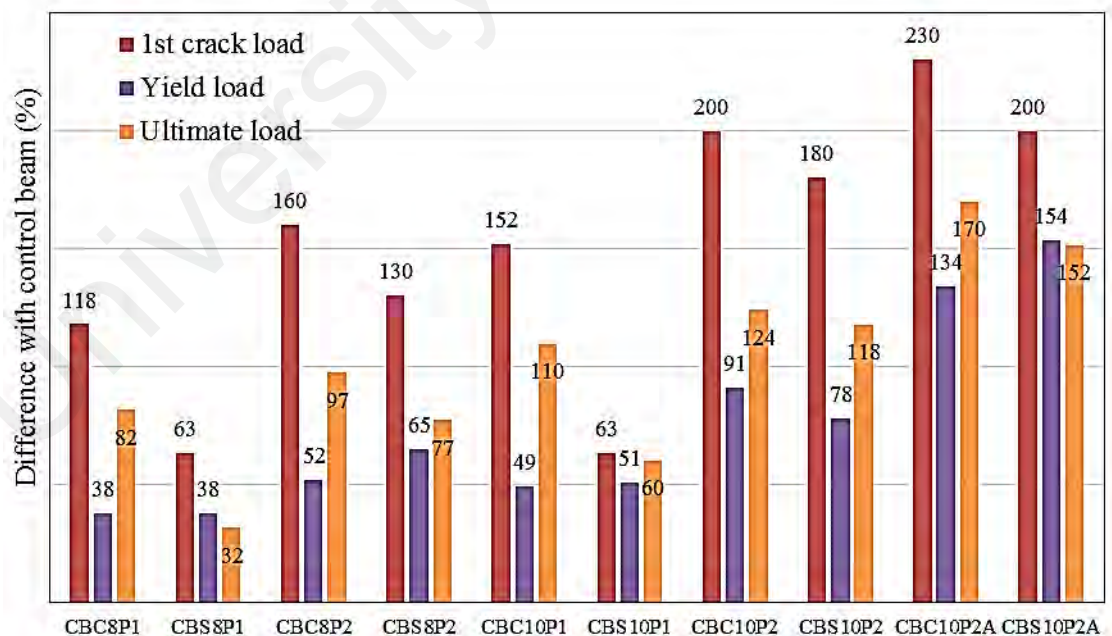


Figure 4.32: Percentile increment of different load levels of CEBNSM-B beams over the control RC beam

The average increment of yield load capacity was 60% compared to the control beam and its trend showed the lowest gain over the corresponding 1st and ultimate capacity of

those strengthened beams. The ultimate capacity was improved more than 100% for most of the cases. Usually the beams with higher area of strengthening material portrayed an enhanced ultimate load carrying capacity as noticed by Lim (2009).

4.1.5.2 Load Deflection Curve

The load deflection relationship of the control and strengthened RC beam is depicted in Figure 4.33. The unstrengthened RC beam showed the usual behavior with cracking and yield point followed by a nonlinear steadily decreased branch at the post yielding stage. The load-deflection diagrams for the CEBNSM-B strengthened beams using CFRP NSM materials demonstrated a nearly tri-linear response up to the ultimate load. The first segment of the curve of these CBC series beams were varied linearly with negligible deflection up to the 1st cracking. Strengthening technique contributed to the increment of the 1st crack load for all strengthened beams.

The second phase was the post cracking to yielding of internal reinforcement of the beams. In this stage a considerable stiffness improvement was noticed in strengthened beams compared to the unstrengthened control beam. At this stage, the internal steel reinforcement and the NSM bar carried the tensile stresses of the beam. The average pre-yield stiffness increment of the strengthened beam was 31% compared to the control beam. The CBC8P2 showed maximum 50% more pre-yield stiffness than the control beam. CFRP bar prevented further increment of flexural cracks, which increased the moment of inertia of the cracked section as noticed by Barros et al. (2006).

The third portion of the load deflection behavior extended from yielding up to failure, and this portion exhibited better improvement in terms of strength and stiffness. In this post-yield stage, due to yielding of the tension steel, most of the tension stresses were resisted by the NSM reinforcement and the EB CFRP fabric. The strengthened beams demonstrated 83% more average pre-ultimate stiffness increment than the control

beam. Again, CBC8P2 showed maximum post-yield stiffness around 116% more than the control beam. The anchored CBC10P2A and CBS10P2A beams demonstrated 93% and 88% stiffness increment. Similar behavior was confirmed by other researchers (Alam & Jumaat, 2012; Hosen et al., 2015). Table 4.6 and Figure 4.32 summarized the carrying capacity and deflection under different load levels along with their percentage of increase of 1st crack, yield and ultimate load.

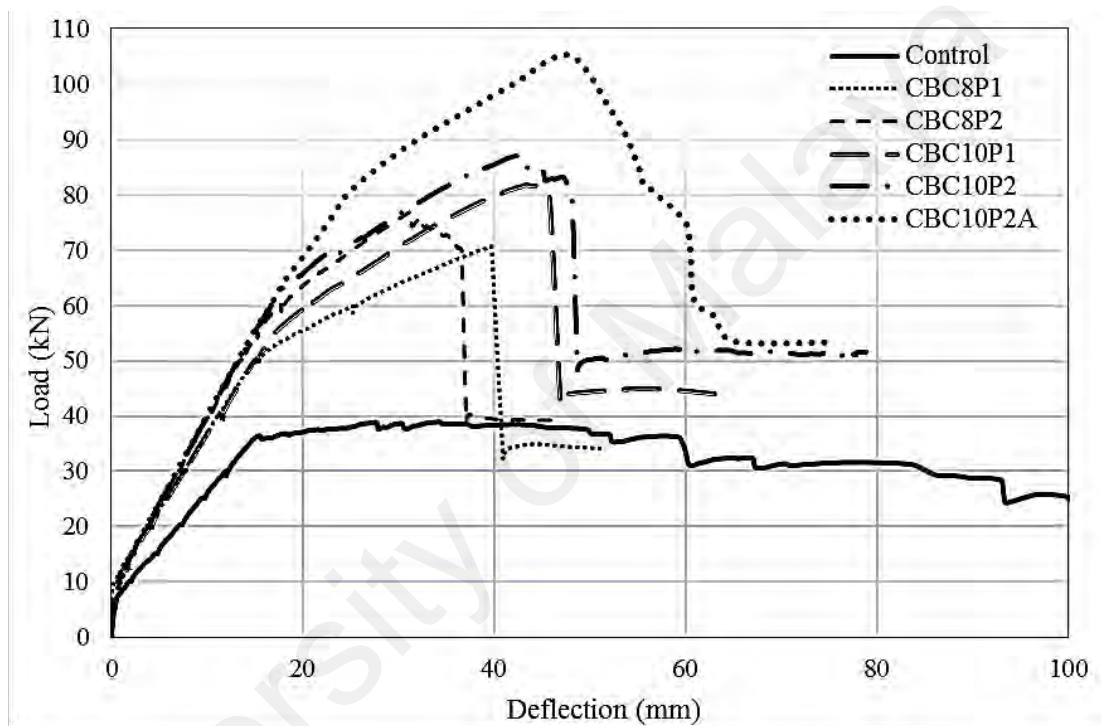


Figure 4.33: Load-deflection curve of CEBNSM-B strengthened beams with CFRP bar

Figure 4.34 showed the load-deflection relationship of the CEBNSM-B beams with steel NSM reinforcement. The load-deflection curves of these CBS series beams were slightly different from the CBC series beam, though both series depicted a tri-linear relationship in the diagram. At the ultimate capacity to the post peak region, the CBS series beams had shown a smooth transition which seemed almost flat unlike the sharp decrement of the CBC series beam. Apart from the phenomena, the CBS series beams also possessed three distinct regions similar to CBC series beams which included pre-cracking, pre-yielding and post-yielding stages.

The CBS8P1 and CBS8P2 beams showed less stiffness at the pre-yielding stage compared to the other strengthened beam, though, overall stiffness increment of CBS series beam was higher than the control beam. Due to the linear elastic behavior of the NSM CFRP bar and EB CFRP fabric, the post peak response of the load-deflection curve of CBC series beams was quite drastic and a dramatic decrement was noticed irrespective of the FRP fracture (flexure failure) or premature (debonding) failure. On the contrary, the post peak response of the CBS series was quite dissimilar to the CBC series which showed a gradually decreasing branch after the ultimate capacity of the beam. This was due to the NSM steel bar which was supposed to show more ductile response unlike the CFRP bar. Both CBC10P2 and CBS10P2 beams demonstrated premature debonding failure which may be due to the additional area of reinforcement furnished at the NSM and EB part as noticed by other researchers (Rahal & Rumaih, 2011; Soliman et al., 2010).

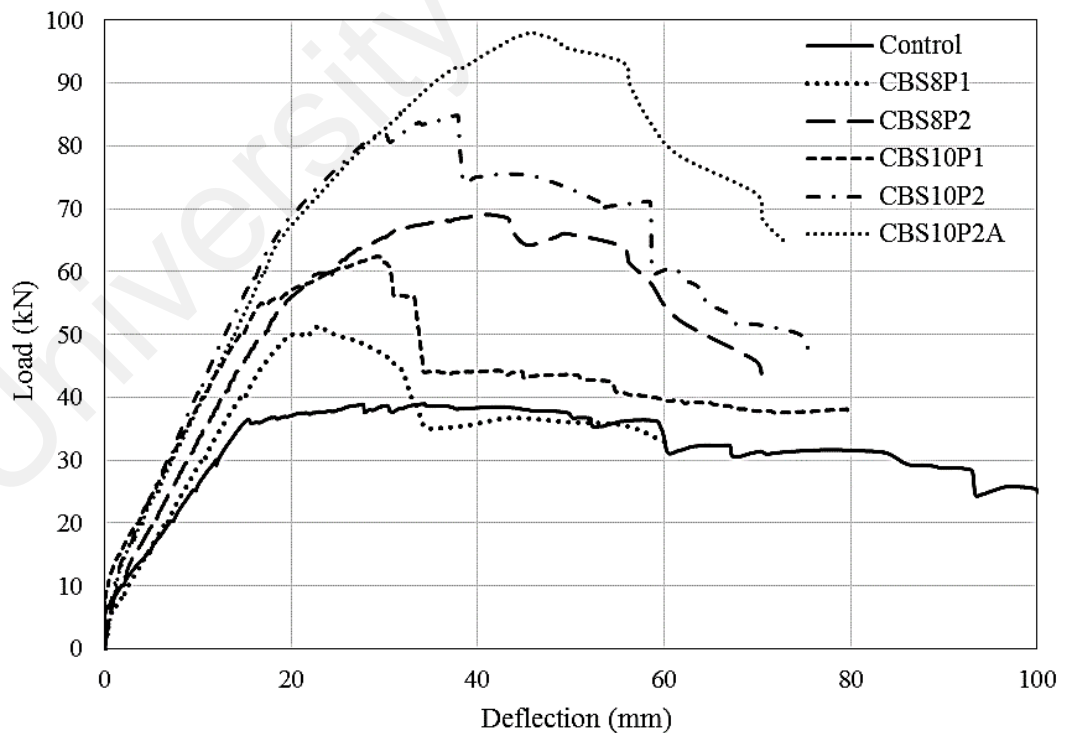


Figure 4.34: Load-deflection curve of CEBNSM-B beams with steel bar

Figure 4.35 shows the deflection reduction of the CEBNSM-B beams at 15 kN, 36.29 kN and 38.95 kN load. The last two loads were the yield and ultimate load of the

control beam. For better comparison, 15 kN load was added which was the 1st crack load for most of the strengthened beams. From the figure, it is clearly evident that the deflection was reduced at these load level. However, at 38.95 kN load the difference was more pronounced compared to the other load level. From the load-deflection diagram, it could be understood that the CBC series showed more deflection at their corresponding ultimate load compared to the CBS series due to the lower modulus of elasticity of the CFRP NSM bar. Darain et al (2016), Almussallam et al. (2013) and Sharaky et al. (2013) mentioned about similar behavior.

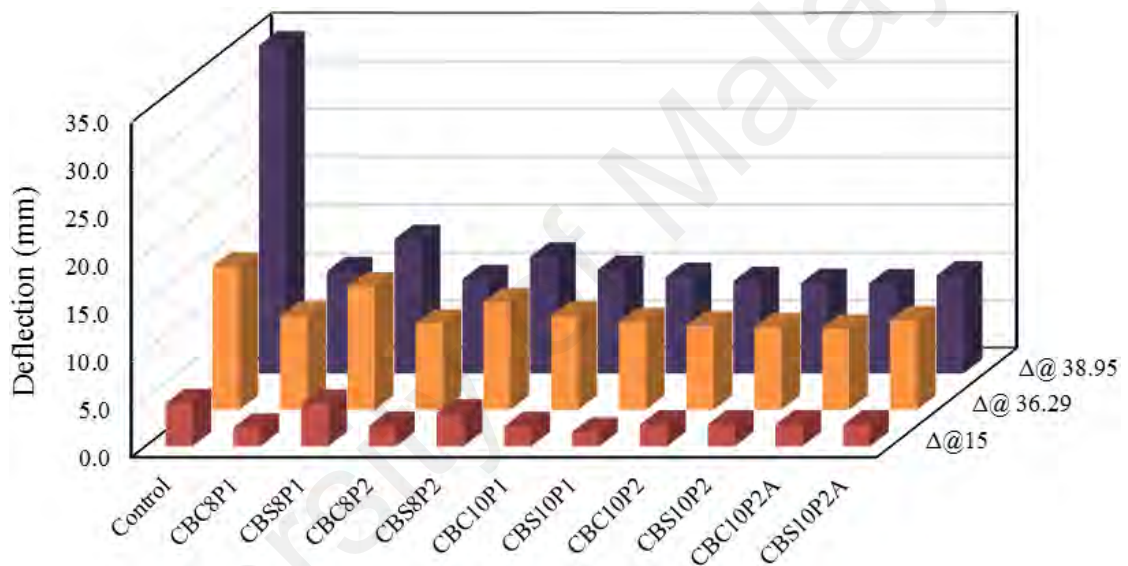


Figure 4.35: Deflection reduction of CEBNSM-B strengthened beam

4.1.5.3 Failure Modes

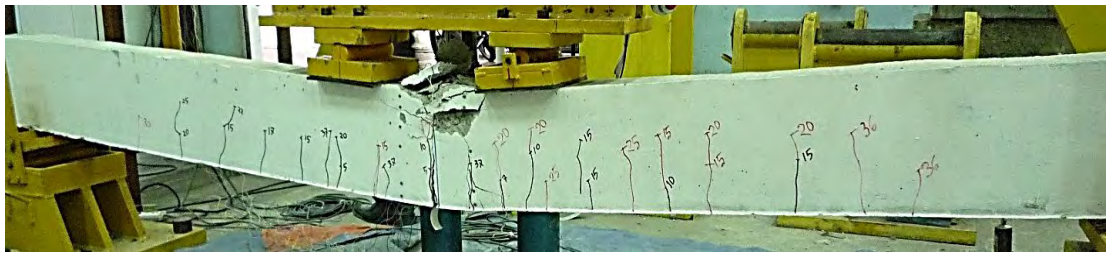
Except CBC10P2 and CBS10P2, all the CEBNSM-B beams without anchorage showed EB CFRP fabric fracture at the bottom tensile mid-span area or concrete crushing after steel yielding at the top compression zone which was the manifestation of flexure failure mode. Both the 8 mm and 10 mm diameter CFRP bars inside the NSM groove with single layer of CFRP fabric showed CFRP fracture in the middle except the CBC10P2 beam which demonstrated debonding failure. For the CBS series beams, CBS8P2 and CBS10P1 beams failed due to crushing of concrete after yielding of the

internal steel bar. CBS8P1 beam failed due to the fabric fracture at tensile zone and CBS10P2 beam failed due to debonding.

The CBC10P2 and CBS10P2 beams exhibited the premature debonding failure. After yielding of the internal reinforcement, cracking noise was detected in the same way as it happened with other CEBNSM-B beams. At this stage, the CFRP fabric was stretched under high tensile strain which was the maximum at the mid-span. Numerous tiny new cracks developed at the interface of the fabric and concrete cover which were expanding. At the maximum moment zone, the primary flexural crack was getting wider and outside this zone, flexural-shear cracks were developed rapidly. With naked eye, it was visible that the CFRP fabric could not maintain its curvature with the beam and was losing its compatibility with the concrete surface. Suddenly with a bursting sound the CFRP fabric failed prematurely. The failure process was abrupt and it was not possible to locate the origination of the debonding failure of CFRP fabric. During delamination of CFRRP fabric, there was no sign of NSM failure. After that, the load was resisted by only the NSM reinforcement which maintained almost invariable load increment with increasing deflection as mentioned by Hawileh et al. (2014). A concrete crushing failure was marked at this stage and the machine was stopped.

Another two beams were assessed with the same strengthening arrangement as CBC10P2 and CBS10P2 with two layers of U-CFRP wrap at the CFRP fabric cut-off location. The beams were afterwards named as CBC10P2A and CBS10P2A. Both the beams had survived against the IC debonding failure and showed the concrete crushing failure after steel bar yielding. Similar failure mode was reported by Darain et al. (2016) and Hosen et al. (2015). However, tiny cracks were developed at the maximum moment region during and after the concrete crushing process. At the end of the test, one large flexure-shear crack developed to both of these anchored beams. The CBS10P2A beam

exhibited two large flexure-shear cracks which started from the bottom of shear span towards the concrete compression wedge zone.



(a) Control beam



(b) CBC8P1 beam



(c) CBC8P2 beam



(d) CBC10P1 beam



(e) CBC10P2 beam

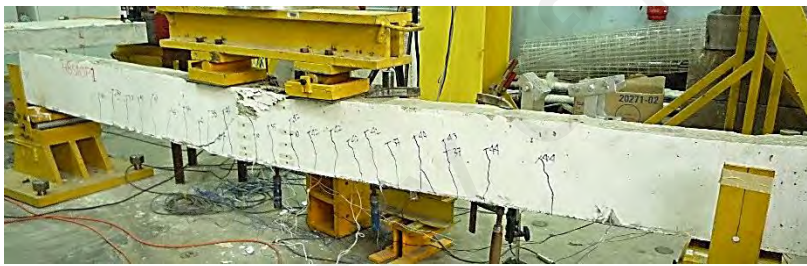
Figure 4.36: Failure modes of CEBNSM-B beams (a) to (k)



(f) CBS8P1 beam



(g) CBS8P2 beam



(h) CBS10P1 beam



(i) CBS10P2 beam

Figure 4.36, continued: Failure modes of CEBNSM-B beams (a) to (k)



(j) CBC10P2A



(k) CBS10P2A

Figure 4.36, continued: Failure modes of CEBNSM-B beams (a) to (k)

The CFRP fabric was placed at the soffit of the beam, so it experienced the maximum tensile stress at the center point of the mid-span. The NSM reinforcement was covered with concrete and was placed at least 8 mm from the extreme bottom fiber. Consequently the CFRP fabric played a dominant role to contribute the ultimate flexural capacity as well as the failure modes. When maximum tensile strain in fabric reaches close to the rupture strain of the CFRP before attaining the maximum strain in concrete (0.003), the beam failed due to rupture of CFRP fabric. Before that, reinforcing steel in the tension area reached the plastic range.

Conversely, for concrete crushing failure, concrete compressive strain reached the maximum after the internal steel yielded and the CFRP fabric service strain did not attain its ultimate strain. CBS8P2, CBS10P1, CBC10P2A and CBS10P2A exhibited this type of flexure failure where concrete crushed after the steel yielding. Similar failure

was observed by other researchers (De Lorenzis & Teng, 2007; Motavalli & Czaderski, 2007).

4.1.5.4 Cracking Behavior

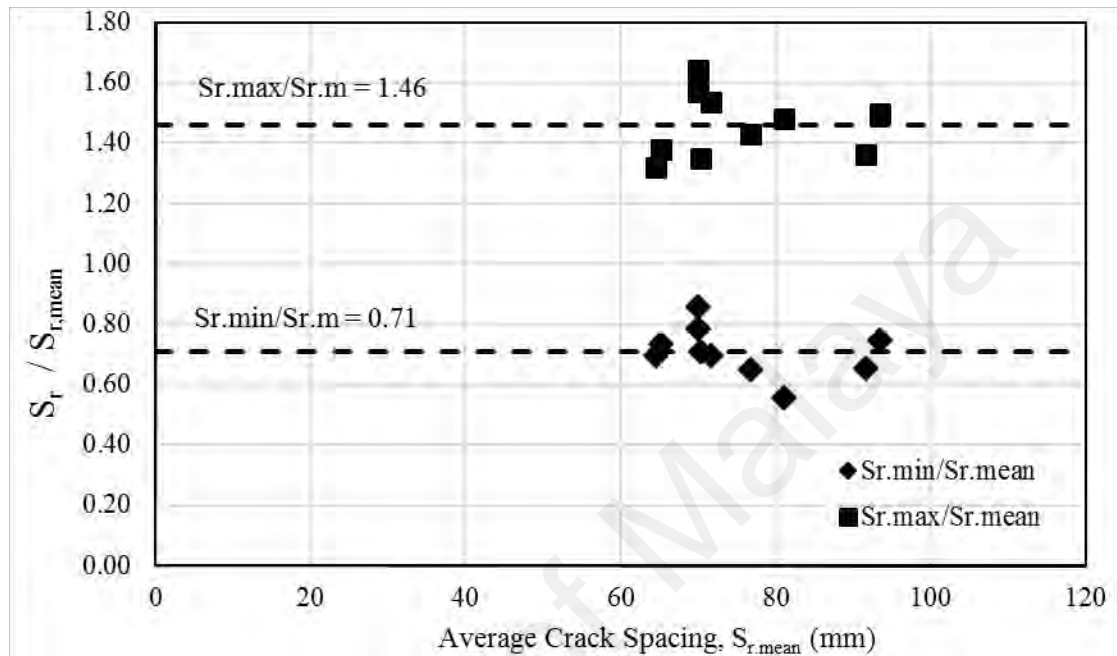


Figure 4.37: Crack spacing details of control and CEBNSM-B beams

Figure 4.37 represented the ratios of minimum to average and maximum to average crack spacing of the control and CEBNSM-B strengthened RC beams. The average values of the maximum and minimum ratios were 1.46 and 0.71, respectively, which agreed well with the predicted value in equation 4.2 and 4.3.

Table 4.7 showed the maximum, minimum and average crack spacing along with the number of cracks appeared on the tested beams. The minimum, maximum and mean crack spacing of the strengthened beams were observed as 45, 140 and 75 mm respectively. The average crack spacing of CEBNSM-B beams maintained a range between 64 mm and 94 mm whereas the average spacing of control beam was 109 mm.

The number of cracks appeared on the strengthened beam was almost same and its average was around 32 compared to 21 cracks on control beam. The CBC8P1 beams demonstrated the highest number of cracks (39 nos.), whereas the CBS10P1 showed the

least cracks (23 nos.). The strengthened beams displayed many cracks of small width, while the unstrengthened beam had fewer cracks of greater width. During deformation of beam due to applied loads, the strengthening material in strengthened beams created a tensile force that equalized the internal bending forces so that less deformation occurred compared to the unstrengthened beam (Wight et al., 2001).

Table 4.7: Experimental maximum, minimum and average crack spacing of CEBNSM-B beams

Beam no	S _{r,max} (mm)	S _{r,min} (mm)	S _{r,mean} (mm)	No. Cracks
CB	140	75	109	21
CBC8P1	85	45	64	39
CBS8P1	125	60	92	24
CBC8P2	110	50	77	31
CBS8P2	120	45	81	27
CBC10P1	95	50	70	38
CBS10P1	140	70	94	23
CBC10P2	90	48	65	34
CBS10P2	110	50	72	34
CBC10P2A	110	60	70	33
CBS10P2A	115	55	70	35

The average 1st crack load for the CEBNSM-B strengthened beams were 12.5 kN which was 150% more than the control beam's cracking load (5 kN). This was a tremendous improvement in perspective of serviceability requirement. The load at first crack was important because after the first crack, full interaction between the reinforcement and the concrete was lost, resulting in reduced stiffness of the beam. If the first crack occurs early, the beam usually shows greater deflection and larger crack widths (Barris et al., 2013). Larger crack widths are especially problematic in field situations where the environmental elements can penetrate through large cracks and damage the reinforcing bars, leading to deterioration of a structure. Thus, higher first crack load and smaller crack widths are desirable to improve the durability of structures as suggested by Wight et al. (2001).

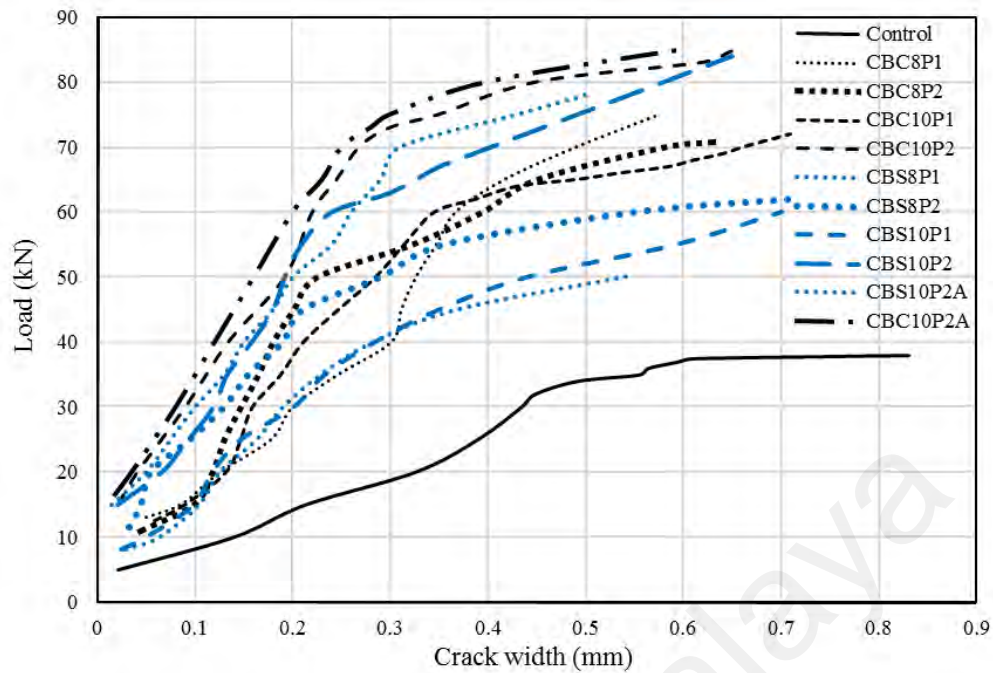


Figure 4.38: Load vs. crack width diagram of CEBNSM-B beams

Figure 4.38 showed the trend of crack width development under monotonic load. The CBC and CBS series beams were demarked with black and blue color in the load versus crack curve to distinguish them easily. The 1st crack loads for control and CEBNSM-B beams were tabulated in Table 4.6 and their percentile increments with respect to control beam were plotted in Figure 4.32 . It could be easily understood from Figure 4.38 that the trend of development of crack width was decreasing compared to the control beam. It was also revealed that up to the yielding of the beam, the formation of crack width was stiffer which widened faster beyond this region as stiffness of beam reduced.

As the 1st crack, yield and ultimate load are different in each beam, so, it would be easier to consider a single load to compare the crack width of different beams. As 35 kN load was very close to the yield load of the control beam, it would be easier to compare the crack width with this value. At 35 kN load, 0.56 mm crack width was developed in control beam. The corresponding crack widths formed at this load were 0.17, 0.23, 0.25, 0.16, 0.19, 0.23, 0.11, 0.13, 0.10, and 0.13 mm for the beams CBC8P1, CBS8P1, 0.16, 0.19, 0.23, 0.11, 0.13, 0.10, and 0.13 mm for the beams CBC8P1, CBS8P1,

CBC8P2, CBS8P2, CBC10P1, CBS10P1, CBC10P2, CBS10P2, CBC10P2A, CBS10P2A, respectively.

The average crack width formed at 35 kN load for the strengthened beams was 0.17 mm which was 70% lesser than the control beam's crack width (0.56%). A strengthening technique can be declared efficient if a good bond relationship is established with its substrate. At that position, more tension force is transferred to the concrete between cracks. Less slip took place between concrete and reinforcements with the increase in the concrete contribution in tension, hence less value of total elongation between them and consequently resulting in less crack width as reported by Allam et al. (2012).

The 1995 version of the ACI-318 code included provisions for crack control based on crack width limits of 0.4 mm and 0.33 mm for interior and exterior applications, respectively. A permissible crack width of between 0.4-0.53 mm was chosen by Frosch (1999). A service load steel stress of $0.6f_y$ was assumed, and simplified design curves were generated based on this assumption. Barris et al. (2013) chose and analyzed the FRP RC experimental beam's crack width of 0.5 to 0.7 mm according to the ACI 440.1R-06 and CAN/CSA-S806. Among these code requirements, 0.33 mm (ACI-318) was the most conservative value and for the comparison purposes the load corresponding to this crack width would be determined which was listed in the Table 4.8. The service load (60% of the ultimate load) and its corresponding crack width were also worked out in this table. Even though the service load of strengthened beams was higher, their corresponding service crack width was lesser than the control beam. The average load of the strengthened beams at the 0.33 mm crack width was 59.5 kN. This mean value represented a load corresponding to an average 76% of their corresponding ultimate load capacity.

Table 4.8: Service load and corresponding crack width of CEBNSM-B beams

Beam ID	P _{cr} (kN)	P _{serv} (kN)	w _{serv} (mm)	Load (kN) at w _k =0.33 mm	% of P _u
Control	5.0	23.4	0.34	22	56
CBC8P1	10.9	42.5	0.18	56	79
CBS8P1	8.2	30.8	0.17	43	84
CBC8P2	13.0	46.1	0.31	54	70
CBS8P2	11.5	41.5	0.19	53	77
CBC10P1	12.6	49.0	0.28	58	71
CBS10P1	8.2	37.4	0.25	44	71
CBC10P2	15.0	52.4	0.19	74	85
CBS10P2	14.0	50.9	0.19	66	78
CBC10P2A	16.5	63.1	0.21	76	72
CBS10P2A	15.0	58.8	0.25	71	72

Here, P_{cr}= 1st crack load, P_{serv}= Service load (60% of the ultimate load), w_{serv}= crack width at service load, and w= crack width.

4.1.5.5 Ductility Analysis

Table 4.9 exhibited the deflection ductility, energy ductility and deformability of the CEBNSM-B beams along with their indexes. The deflection ductility index can be defined as the ratio of the ultimate deflection (Δ_u) to the deflection (Δ_y) at yield load (equation 4.4).

Table 4.9: Summary of different ductility index of CEBNSM-B beams

Beam ID	Deflection ductility			Energy ductility			Deformability	
	Δ_y (mm)	Δ_u (mm)	μ_d	E _y (kN-mm)	E _u (kN-mm)	μ_E	Δ_f (mm)	μ_{Δ_f}
CB	15.0	34.3	2.3	391.6	1043.9	2.7	100.0	6.7
CBC8P1	14.9	39.7	2.7	445.1	1967.2	4.4	51.0	3.4
CBC8P2	15.2	31.3	2.1	481.9	1561.6	3.2	46.0	3.0
CBC10P1	16.6	43.3	2.6	528.0	2390.8	4.5	64.1	3.9
CBC10P2	18.0	37.9	2.1	957.7	2544.0	2.7	78.9	4.4
CBS8P1	20.0	22.9	1.1	557.0	714.9	1.3	60.3	3.0
CBS8P2	23.2	40.8	1.8	841.0	1988.8	2.4	70.5	3.0
CBS10P1	17.0	29.2	1.7	554.2	1294.9	2.3	79.7	4.7
CBS10P2	23.7	42.7	1.8	664.3	2213.4	3.3	75.5	3.2
CBC10P2A	24.7	47.9	1.9	1133.0	3311.3	2.9	75.0	3.0
CBS10P2A	18.0	45.9	2.6	627.7	2965.4	4.7	73.2	4.1

The deflection ductility index of control beam was the highest among all beams due to its pure flexure failure mode where the ratio of deflection at ultimate to yield was the maximum. The stiffer load-deflection response of the strengthened beams induced a lesser ultimate to yield deflection ratio which led to a lower ductility index except CBC8P1, CBC10P1 and CBS10P2A beams which showed some little enhancement.

The percentile variation of various ductility indexes of strengthened beams compared to the control beam is exhibited in the Figure 4.39. The energy ductility index of CBC8P1, CBC8P2, CBC10P1, CBS10P2, CBC10P2A and CBS10P2A beams were increased by 66%, 22%, 70%, 25%, 19% and 77%, respectively.

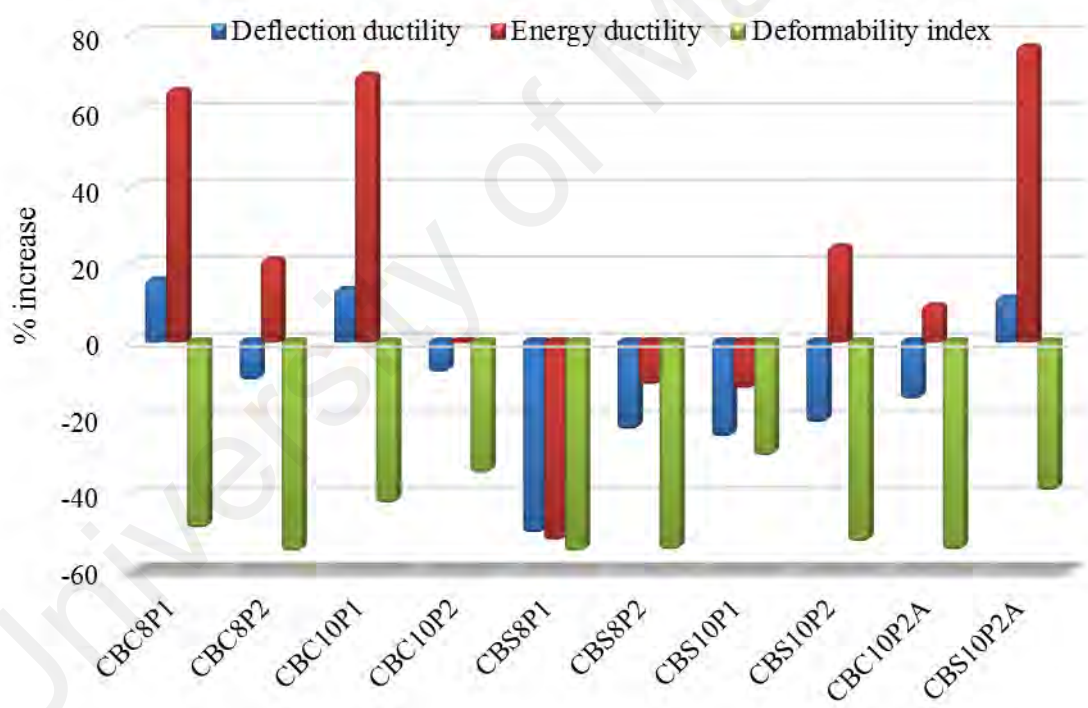


Figure 4.39: Various ductility index for CEBNSM-B beams

The CBC10P2 beam showed no variations of ductility whereas CBS8P1, CBS8P2 and CBS10P1 decreased by 52%, 11% and 12% compared to the control beam energy ductility. The outcome was expected as the CBC series beams showed more deflection and its ultimate load capacity was more than the CBS series beams. Hence the energy absorption capacity of CBC series beams was higher according to the equation 4.5.

The Deformability index can be expressed as the ratio of deflection at failure of the beam to the deflection at the yield load (equation 4.6) (El-Haccha and Rizkalla, 2013). Figure 4.39 depicts the deformability indexes of strengthened beams which were lower than the control beam. This is due to the fact that the control beam demonstrated a huge deflection for its pure flexural failure due to concrete crushing before steel yielding.

4.1.5.6 Stiffness Assessment

Stiffness is one of the dominant characteristics of RC structures since change of its value with the applied load influences the deflection and curvature of any structure. It depends greatly on the cracking, loading level, thickness of bonded material and adhesive.

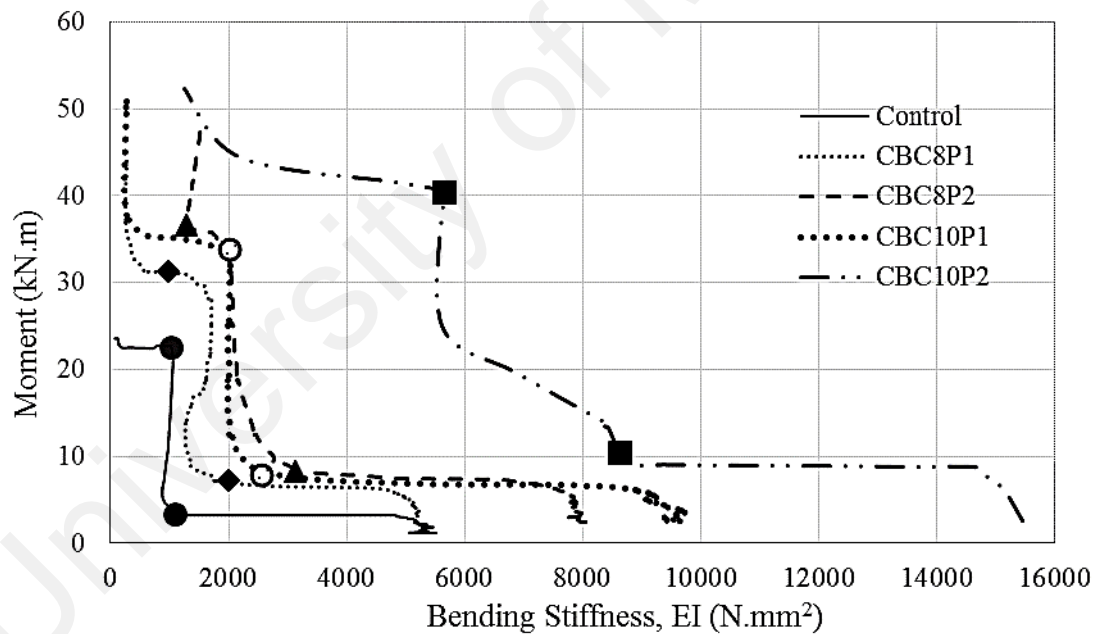


Figure 4.40: Bending stiffness of CFRP bar strengthened CEBNSM-B beams

Stiffness can be characterized as the product of modulus of elasticity and moment of inertia of that section. Bending stiffness is easily defined for a true homogenous material, like steel, but for reinforced concrete the estimate is tougher as it is controlled by cracking, creep, shrinkage, and load history (Swamy et al., 1987). In an RC section the moment of inertia is continuously changing. It is termed as the effective

moment of inertia (I_{eff}) after exceeding the cracking moment (M_{cr}) instead of using gross moment of inertia (I_g). For the full crack formation of the beam the I_{eff} should be referred to as the cracked moment of inertia (I_{cr}) of the cracked transformed section. Besides, with the formation of flexural cracks, the neutral axis also keeps changing its position which is also a big challenge for proper estimation of bending stiffness.

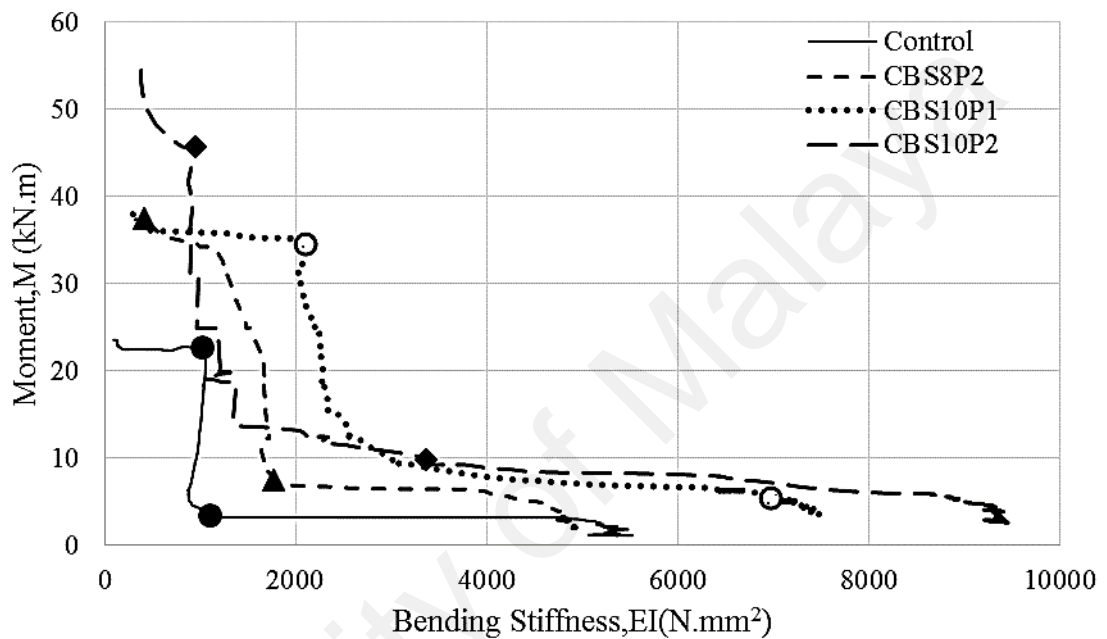


Figure 4.41: Bending stiffness of steel bar strengthened CEBNSM-B beams

For the analysis, curvature and neutral axis location was accounted with the help of the tensile and compression strain value of steel and concrete from their respective strain gauges. Figure 4.18 and equation 4.8 and 4.9 can be referred to calculate the bending stiffness of the beams. A moment curvature relationship was developed using the extreme tension strain values from the internal steel bar strain gauge and the extreme compression strain gauge values from the top of the mid-span.

Figure 4.40 and Figure 4.41 depicts the moment versus bending stiffness diagram, where the CFRP and steel bar had been used as NSM reinforcement. For clarity the CBC and CBS series beams were plotted in different diagrams. The first crack and the yielding of the beams were marked in the diagram. The overall shape of the moment

versus bending stiffness curve was like an “L”. For all cases, the CEBNSM-B beams demonstrated a superior moment-stiffness relationship compared to the control beam as expected. Initially, the bending stiffness was high as expected due to the un-cracked stage of the beam section. The initial stiffness of the control beam was 5512 N.mm². The initial stiffness of the CBC series beams were 5203, 8042, 9653, and 15453 N.mm² for the CBC8P1, CBC8P2, CBC10P1, and CBC10P2 beams. For CBS8P2, CBS10P1, and CBS10P2 beams the initial stiffness were 4885, 7475 and 9428 N.mm².

With the increasing application of load, the stiffness was going to decrease and form a knee of the “L” where first crack appeared. This first crack stiffness of the control beam was 1105 N.mm². The intermediate stiffness at first crack of the CBC series beams were 2008, 3142, 2553, and 8637 N.mm² for the CBC8P1, CBC8P2, CBC10P1, and CBC10P2 beams. For CBS8P2, CBS10P1, and CBS10P2 beams the first crack stiffness were 1173, 6968 and 3365 N.mm². There was no noticeable difference of stiffness after 1st crack and there was a drastic realignment of the curve. It formed almost a straight vertical line where the moment was increased at a steady rate. The CBC10P2 beam showed a gradual decreasing stiffness with the increasing moment capacity from the cracking moment to their yield moment.

At the yield moment, the stiffness of the control beam was 1032 N.mm². The stiffness at yield moment of the CBC series beams were 983, 1292, 2002, and 5656 N.mm² for the CBC8P1, CBC8P2, CBC10P1, and CBC10P2 beams. For CBS8P2, CBS10P1, and CBS10P2 beams the yield stiffness were 421, 2095 and 949 N.mm². After crossing the point the CBC series beams showed almost constant decrease of stiffness with negligible moment increment. Then, again the moment capacity was increasing without any appreciable change of stiffness up to the failure. The CBS series

beams showed a very gradual decrease of stiffness without increasing the moment capacity until their failure.

4.1.5.7 Strain Measurement

Figure 4.42 portrayed comparison of the compressive strain of CEBNSM-B strengthened beams with the control beam which was recorded from the strain gauge at the extreme top fiber of the tested beams. The strengthened beams exhibited lower strain value compared to the control beam. To make a justifiable comparison, these strain values were taken at 15 kN, 30 kN and 39 kN. As the service and ultimate loads of the control beam were 26 kN and 39 kN, so the last two loads were taken as 30 kN and 39 kN. Almost all the strengthened beams demonstrated the first crack at 15 kN which was chosen as the lower bound.

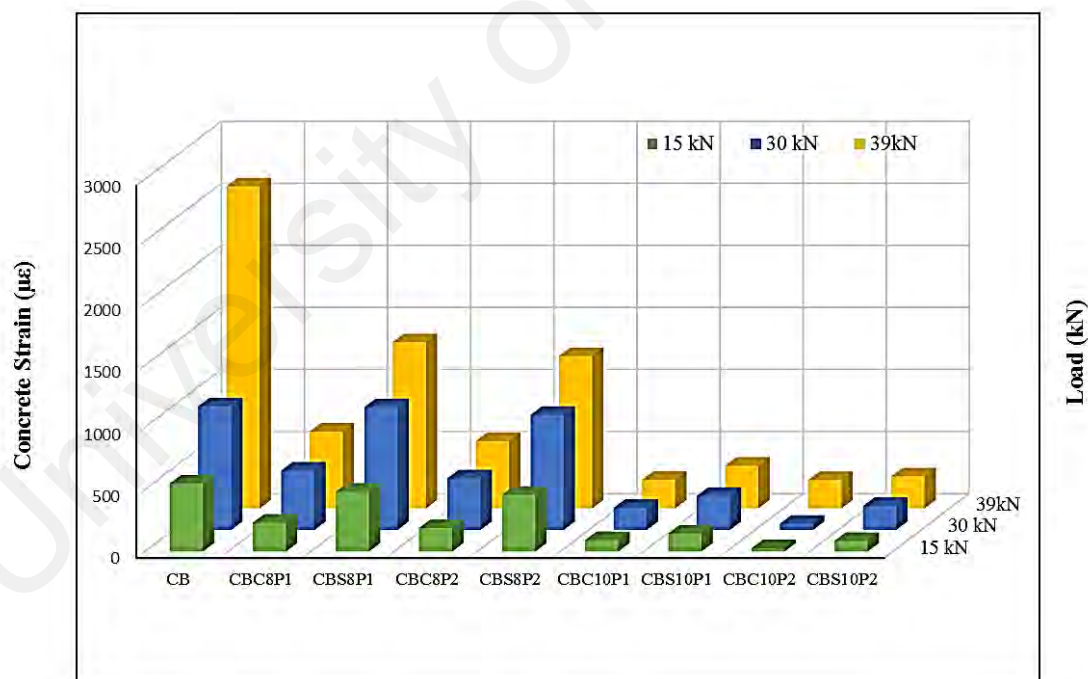


Figure 4.42: Comparison of concrete strain of CEBNSM-B beam at 15, 30 and 39 kN service load

It is clearly visible from Figure 4.42 that the concrete strain of the strengthened beams was getting reduced compared to the control beam at all three load levels. The highest reduction was noticed at 39 kN load which was the ultimate load for the control

beam. The percentile reduction of the CEBNSM-B strengthened beams compared to the control beam at 39 kN load were 76%, 48%, 79%, 53%, 91%, 87%, 1% and 90% for CBC8P1, CBS8P1, CBC8P2, CBS8P2, CBC10P1, CBS10P1, CBC10P2, and CBS10P2 beams. The maximum strain value measured before crushing of the concrete was 2597 $\mu\epsilon$ (0.002597) for the control beam. The highest compressive strain was recorded in CBS10P2 beam which was 2803 $\mu\epsilon$ (0.002803). From load-strain relationship it was found that the curve was getting stiffer with the increasing area of strengthening materials and the strain became less accordingly.

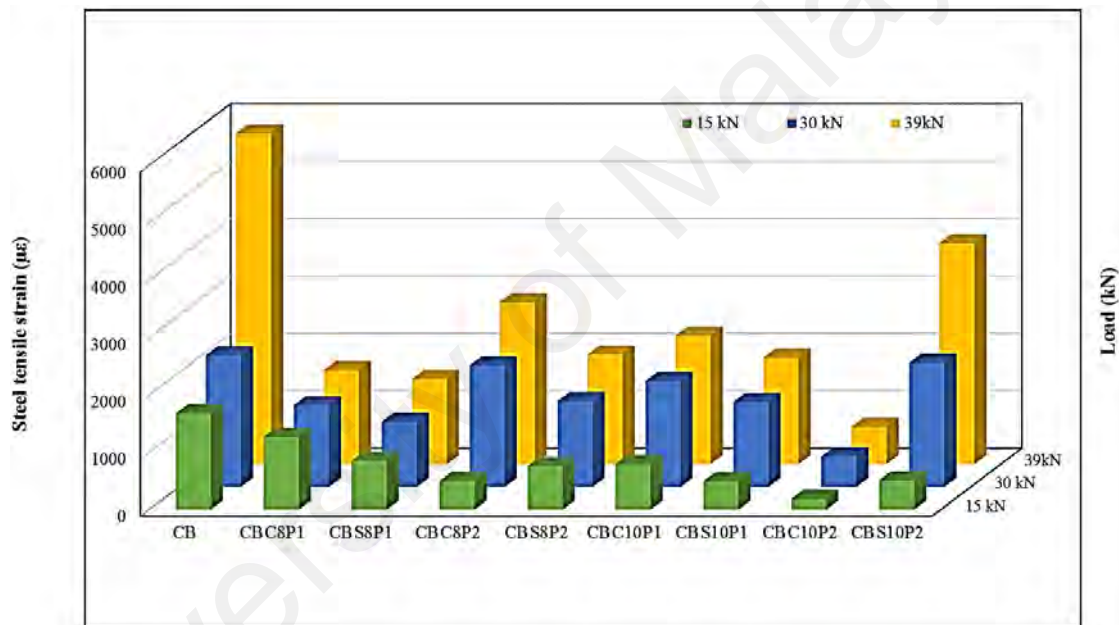


Figure 4.43: Comparison of steel tensile strain of CEBNSM-B beam at 15, 30 and 39 kN service load

Figure 4.43 compared the tensile strain of internal steel bar at 15, 30 and 39 kN service load levels. It is clearly visible that the tensile strain of the strengthened beams was getting reduced compared to the control beam at these three load levels. The percentile reduction of the CEBNSM-B strengthened beams compared to the control beam at 39 kN load was 72%, 74%, 51%, 67%, 61%, 68%, 89%, and 33% for CBC8P1, CBS8P1, CBC8P2, CBS8P2, CBC10P1, CBS10P1, CBC10P2, and CBS10P2 beams.

Figure 4.44 showed the load versus tensile strain variation of the CFRP NSM bar at its middle point where the strain was supposed to be maximum. The diagram showed the typical linear elastic variation of load strain which is the main characteristic of a CFRP bar. The tensile strain of CBC10P1 and CBC10P1 beam had moved further in an elastic fashion after reaching their yield point. The strain gauges were spoiled after reaching the strain which is depicted in the figure.

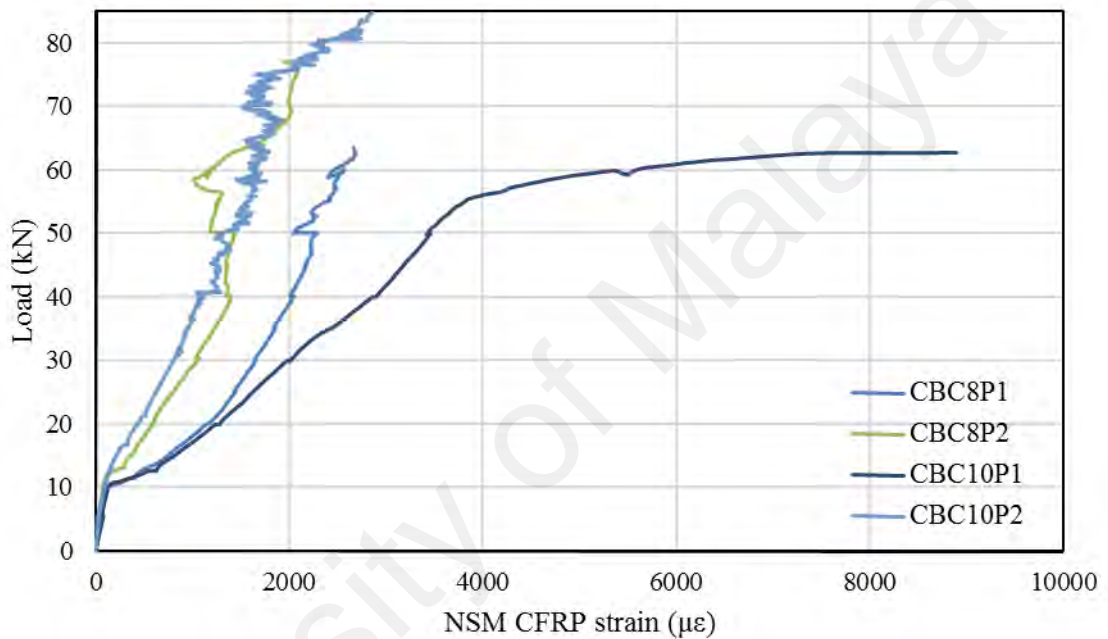


Figure 4.44: NSM CFRP strain of CEBNSM-B beams

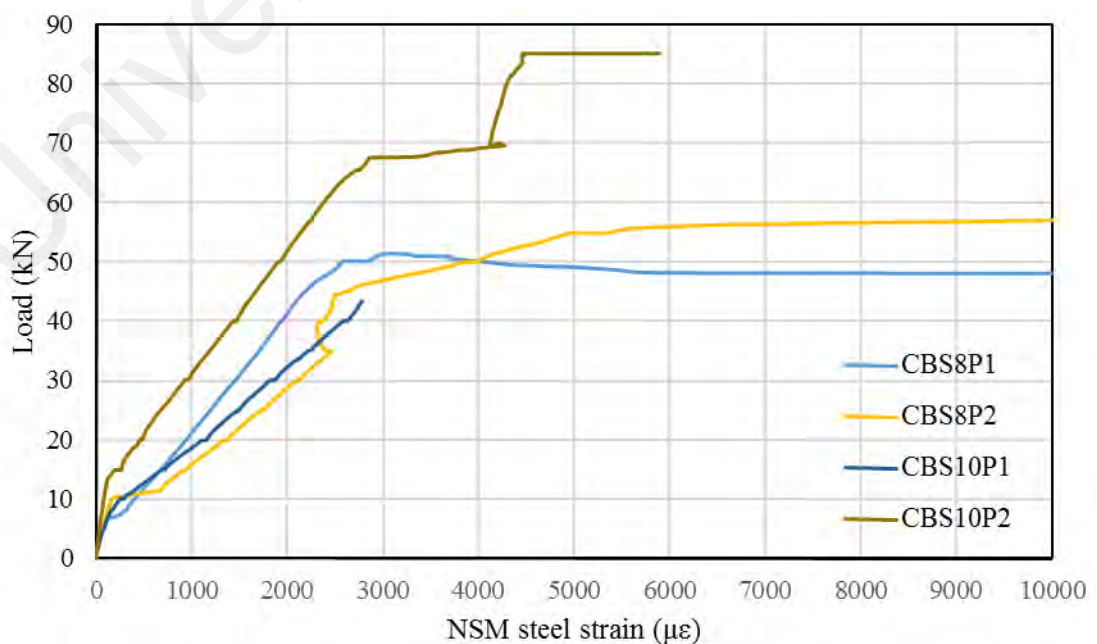


Figure 4.45: NSM steel strain of CEBNSM-B beams

Figure 4.45 showed the load versus tensile strain variation of the steel NSM bar at its middle point where the strain was supposed to be maximum. The diagram showed the typical linear elastic plastic variation of load strain which is the main characteristic of a steel bar. Except CBS10P1 beam, all other beams demonstrated the plastic strain after reaching their yield point. The strain gauges of CBS10P1 and CBS10P2 beams were spoiled after reaching the strain depicted in the Figure 4.45.

4.1.6 CEBNSM-S Technique with CFRP Strip

The experimental outcomes of CEBNSM-S strengthened RC beams are organized in the Table 4.10 below. These beams were strengthened with CFRP strip inside the NSM groove and CFRP fabric bonded at the beam soffit. The main test variables were the number of NSM CFRP strip (1, 2, 3 and 4 nos.), number of grooves (single or double), dimension of the groove (5 mm × 25 mm and 10 mm × 25 mm) and thickness of EB CFRP fabric layer (1 and 2 layer). The results are documented in terms of their first cracking load, yield load and ultimate load capacity with their corresponding deflection and pre-yield stiffness. The percentage of load increment due to strengthening was also presented in the Table 4.6.

4.1.6.1 Load Carrying Capacity

Table 4.6 synopsis the experimental findings of the CEBNSM-S strengthened RC beams. Addition of the CFRP strip and fabric to the RC beams caused superior load carrying capacity, reduction of ultimate deflection and avoidance of debonding problem.

The ultimate load capacity was increased by 51%, 126%, 96%, 81%, 135%, and 176% for the CS1G1P2, CS2G2P2, CS2G1P1, CS2G2P1, CS3G3P1 and CS4G2P1 strengthened beams, respectively, compared to the control beam. The corresponding first crack load and yield load of the beams improved significantly after strengthening. The yield point was determined from the stiffness variation in the load-deflection curve

as well as the internal steel yielding point from the corresponding load-steel strain diagram.

Table 4.10: Summary of experimental test results of CEBNSM-S beams

Beam ID	Per (kN)	Δ_{cr} (mm)	Py (kN)	Δ_y (mm)	Ke (kN/m)	Pu (kN)	Δ_u (mm)	Failure modes
CB	5	0.5	36	15.0	2419.3	39	34.3	FFC
CS1G1P2	10	1.2	50	19.5	2538.5	59	32.9	FFC
CS2G2P2	13	1.3	60	20.9	2870.8	88	45.8	FFF
CS2G1P1	17	2.7	62	17.2	3601.4	77	25.1	FFC
CS2G2P1	11	1.0	61	20.5	2975.6	71	30.9	FFC
CS3G3P1	14	2.1	61	18.4	3315.2	92	44.4	FFC
CS4G2P1	17	1.9	71	19.3	3699.5	108	41.5	FFC

*Where Per = first crack load; Py = yield load; Pu = ultimate load; Δ_{cr} = deflection at 1st crack; Δ_y = deflection at yield of steel; Δ_{max} = mid-span deflection at failure load, FFC = flexural failure due to concrete crushing after steel yielding; FFF= Flexure failure due to FRP rupture

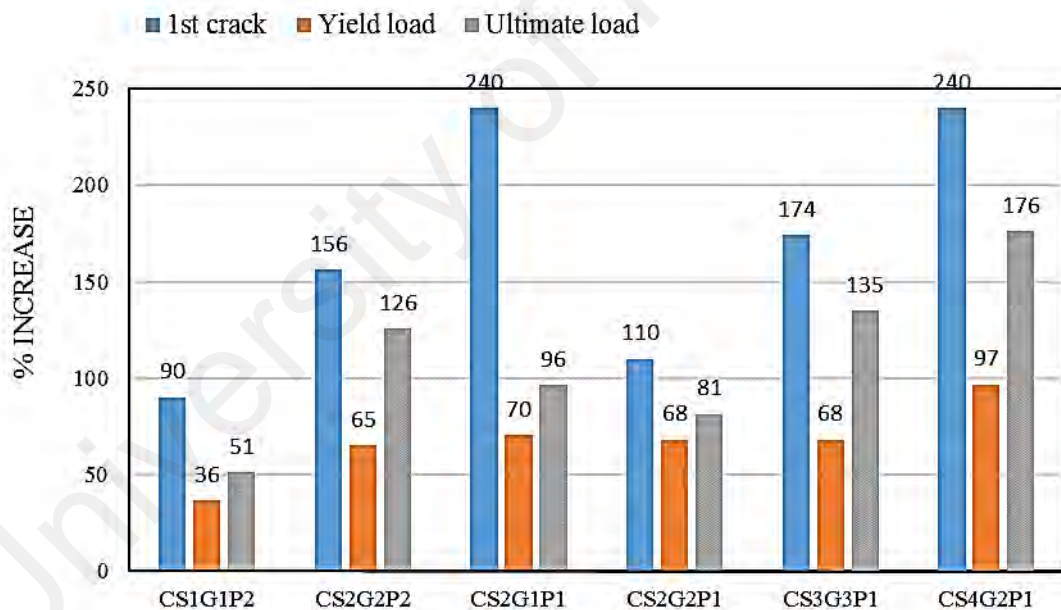


Figure 4.46: Percentile increment of different load levels of CEBNSM-S beams

Figure 4.46 depicted the percentile increment of 1st crack, yield and ultimate load of the strengthened beams compared to the control beam. It can be easily understood that the 1st crack load had been tremendously improved using the CEBNSM-B technique. Moderate increment was visualized for yield load, though the ultimate capacity was improved an average of 102%. Usually the beams with higher area of strengthening

material portrayed an enhanced ultimate load carrying capacity. The increased bond surface of NSM CFRP strips as well as externally bonded fabric increased the load capacity of the strengthened beams as reported by Hassan and Rizkalla (2003).

4.1.6.2 Load Deflection Curve

The load-deflection diagrams for the CEBNSM-S strengthened beams using NSM CFRP strip demonstrated almost a tri-linear response (Figure 4.47). The first segment of the curve varied linearly with negligible deflection up to the 1st cracking. However, strengthening technique increased the 1st crack load for all strengthened beams.

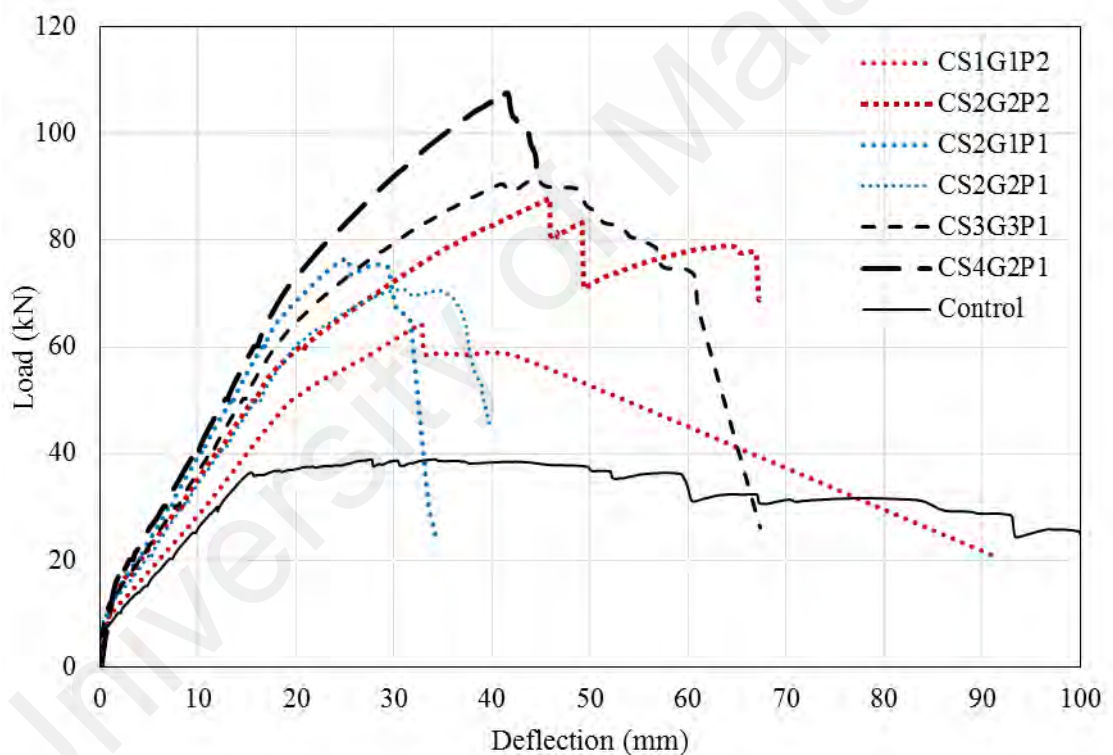


Figure 4.47: Load-deflection curve of CEBNSM-S beams

The second phase was the post cracking to yielding of the internal reinforcement of the beams. In this stage, a considerable stiffness improvement was noticed in strengthened beams compared to the control beam. At this stage, the internal steel reinforcement and the NSM strip carried the tensile stresses of the beam. The CS2G1P1 and CS4G2P1 showed maximum pre-yield stiffness of 49% and 53% more than the control beam. Whereas, the other beams showed an average stiffness increment of 21%.

The beam which had two strips in single groove showed superior stiffness compared to other strengthened beams.

The third portion of the load deflection behavior extended from yielding up to failure, and this portion displayed superior improvement of strength and stiffness compared to control beam. In this post-yield stage, due to yielding of the tension steel, most of the tension stresses were resisted by the NSM CFRP strip and the EB CFRP fabric. The CS2G1P1 showed maximum post-yield stiffness around 168% more than the control beam. Table 4.10 and Figure 4.46 summarized the carrying capacity and deflection under different load levels along with their percentage of increase of 1st crack, yield and ultimate load.

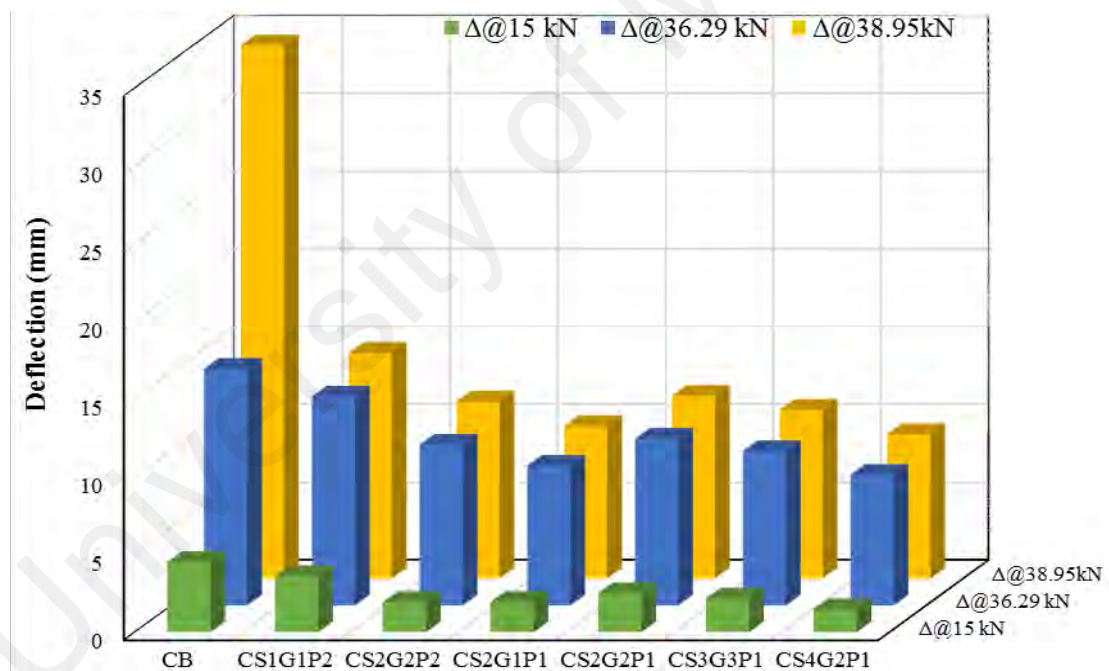


Figure 4.48: Deflection reduction of CEBNSM-S beams

Figure 4.48 demonstrated the deflection of CEBNSM-S beams at 15 kN, 36.29 kN and 38.95 kN service loads. The last two loads were the yield and ultimate load of the control beam. For most of the strengthened beams the first crack appeared round 15 kN which was the justification to use this value as the lower bound. At all these three load levels, deflection was reduced considerably which was clearly visible in the Figure 4.48.

However, at 38.95 kN load, the difference was more prominent compared to the other load level. At 38.95 kN load the deflection was reduced by 58%, 67%, 71%, 66%, 68% and 73% for CS1G1P2, CS2G2P2, CS2G1P1, CS2G2P1, CS3G3P1 and CS4G2P1 beams compared to the control beam. CS2G1P1 and CS4G2P1 showed the highest value of deflection reduction. It should be noted that these two beams were strengthened with two strips in a single groove. Their stiffness also seemed to be higher which was the probable reason for reducing deflection. This behavior was also experienced by other researchers (Hassan & Rizkalla, 2003; Hassan, T. K. & Rizkalla, S. H., 2004).

4.1.6.3 Failure Modes

Figure 4.49 demonstrated the failure modes of CEBNSM-S beams. All these beams except CS2G2P2 showed flexure failure where concrete failed at the compression after the yielding of internal steel bar. The externally bonded CFRP fabric of CS2G2P2 beam fractured at the mid-span. It was again gaining strength after 70 kN load then the concrete started crushing at the top mid-span compression zone. The steel strain of that beam was checked and it was clearly seen that the internal steel yielded before the fabric fracture.

The CS1G1P2 beam failed due to concrete crushing before steel yielding. After developing a full compression wedge at the top mid-span compression zone, the flexural crack at the maximum moment region was growing more. Due to the increasing application of displacement by the Instron machine, the crack was getting wider and several other flexural-shear cracks accompanied that one, though the CFRP fabric remained intact.

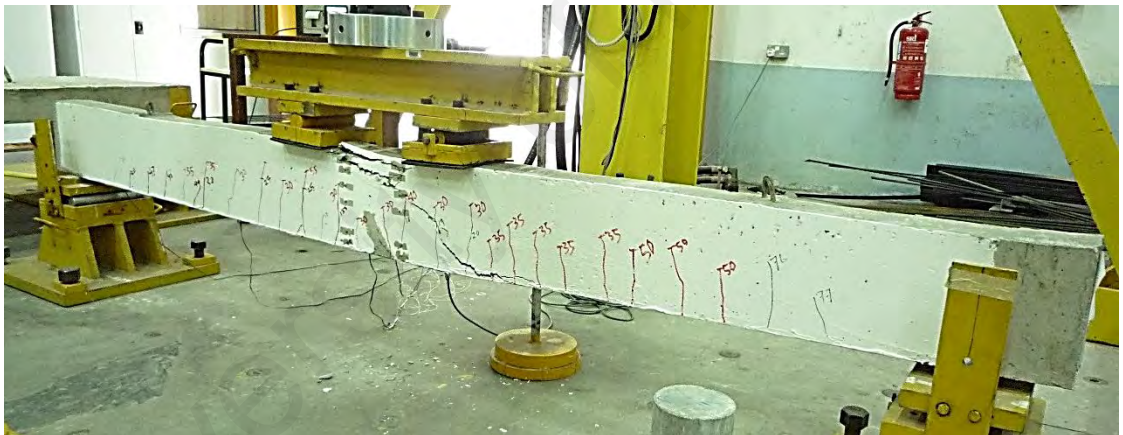
The CS2G1P1, CS2G2P1, CS3G3P1, CS4G2P1 beams had shown the concrete crushing failure after yielding of internal steel bar. After the development of cracking moment, tiny flexural cracks were developed at the maximum moment region.



(a) CS1G1P2



(b) CS2G2P2



(c) CS2G1P1



(d) CS2G2P1

Figure 4.49: Failure modes of CEBNSM-S beams



(e) CS3G3P1



(f) CS4G2P1

Figure 4.49, continued: Failure modes of CEBNSM-S beams

With the application of load, more flexural and flexure-shear cracks were developed at the beam surface and the old cracks were getting wider. The strain at the concrete compression zone reached their maximum limit while the flexural cracks were enlarged at the maximum moment region (Babaeidarabad et al., 2014). The compression wedge was becoming more prominent and the concrete softening behavior was revealed with a gradual decreasing branch at the load-deflection curve. At the end of the increasing displacement application by the Instron machine, several cracks changed the direction and were growing wider as also noticed by Ali et al. (2008).

4.1.6.4 Cracking Behavior

Figure 4.50 represents the ratios of minimum to average and maximum to average crack spacing of the control and CEBNSM-S strengthened RC beams. The average values of the maximum and minimum ratios were 1.44 and 0.72, respectively, which agreed well with the predicted value in equation 4.2 and 4.3.

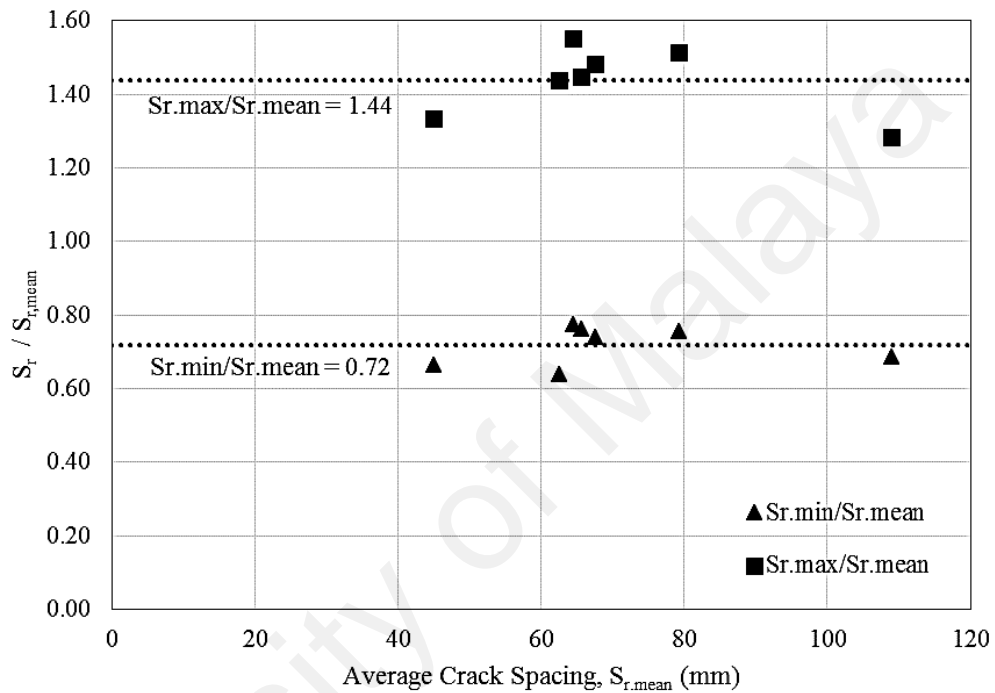


Figure 4.50: Crack spacing details of control and CEBNSM-S beams

Table 4.11 showed the maximum, minimum and average crack spacing along with the number of cracks appeared on the tested CEBNSM-S beams. The minimum, maximum and mean crack spacing of the strengthened beams were observed as 30, 120 and 70 mm respectively.

Table 4.11: Experimental maximum, minimum and average crack spacing of CEBNSM-S beams

Beam no	$S_{r,max}$ (mm)	$S_{r,min}$ (mm)	$S_{r,mean}$ (mm)	No. Cracks
CB	140	75	109	21
CS1G1P2	90	40	63	32
CS2G2P2	95	50	66	30
CS2G1P1	120	60	79	28
CS2G2P1	60	30	45	41
CS3G3P1	100	50	68	31
CS4G2P1	100	50	64	36

The average crack spacing of CEBNSM-B beams maintained a range between 45 mm and 79 mm whereas the average spacing of control beam was 109 mm. The number of cracks appeared on the strengthened beams were almost same and its average was around 33 compared to 21 cracks on control beam. The CS2G2P1 beams demonstrated the highest number of cracks (41 nos.), whereas the CS2G1P1 showed the least cracks (28 nos.). The strengthened beams displayed many cracks of small width, while the unstrengthened beam had fewer cracks of larger width. During deformation of beam due to applied loads, the strengthening material in strengthened beams created a tensile force that equalizes the internal bending forces so that less deformation occurs compared to the unstrengthened beam (Wight et al. 2001).

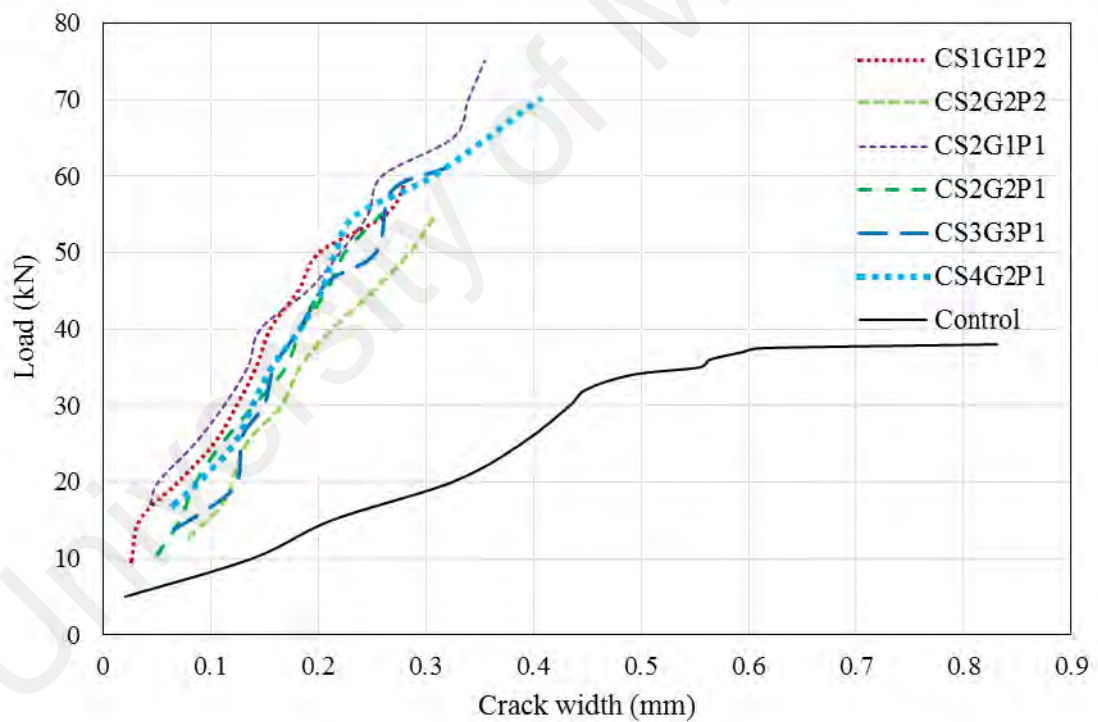


Figure 4.51: Load vs. crack width diagram of CEBNSM-S beams

Figure 4.51 showed the trend of crack width development under monotonic load of CEBNSM-S beams. It can be easily understood from Figure 4.51 that the trend of development of crack width was decreasing compared to the control beam. The crack width of control beam at 1st crack load was 0.021 mm. The corresponding 1st crack

widths were 0.027 mm, 0.08 mm, 0.044 mm, 0.05 mm, 0.066 mm, and 0.066 mm for the CS1G1P2, CS2G2P2, CS2G1P1, CS2G2P1, CS3G3P1 and CS4G2P1 beam, respectively.

As the 1st crack, yield and ultimate load is different in each beam, so, it would be easier if a single load is considered to compare the crack width of different beams. As 35 kN load was very close to the yield load of the control beam, hence it could be easier to compare the crack width with this value. At 35 kN load, 0.56 mm crack width was developed in control beam. The corresponding crack widths formed at this load were 0.14 mm, 0.18 mm, 0.14 mm, 0.17 mm, 0.16 mm, and 0.16 mm for the beam CS1G1P2, CS2G2P2, CS2G1P1, CS2G2P1, CS3G3P1 and CS4G2P1 beam respectively. These strengthened beams showed a decrement of the crack width by 74%, 67%, 76%, 69%, 71%, and 72% compared to the control beam.

The average 1st crack load for the CEBNSM-S strengthened beams was found as 13.4 kN which was 168% higher than the 1st crack load of control beam. Whereas, the mean value of crack width at 1st crack was 0.055 mm which was 164% lesser than the control beam's crack width (0.021 mm). Higher first crack load and smaller crack widths are the signs of superior serviceability and very much desirable to enhance the durability of any RC structures as suggested by Allam et al. (2012).

4.1.6.5 Ductility Analysis

Table 4.12 exhibited the deflection ductility, energy ductility and deformability of the CEBNSM-S beams along with their indexes. The deflection ductility index can be defined as the ratio of the ultimate deflection (Δ_u) to the deflection (Δ_y) at yield load (equation 4.4). The deflection ductility index of control beam was the highest among all beams due to its pure flexure failure mode where the ratio of deflection at ultimate to

yield was the maximum. The stiffer load-deflection response of the strengthened beams induced a less ultimate to yield deflection ratio which led to a lower ductility index.

Table 4.12: Summary of different ductility index of CEBNSM-S beams

Beam ID	Deflection ductility			Energy ductility			Deformability	
	Δy (mm)	Δu (mm)	μd	E_y (kN-mm)	E_u (kN-mm)	μE	Δf (mm)	$\mu_{\Delta f}$
CB	15.0	34.3	2.3	391.6	1043.9	2.7	100.0	6.7
CS1G1P2	19.5	32.9	1.7	537.9	1318.3	2.5	91.2	4.7
CS2G2P2	20.9	45.8	2.2	755.7	3394.3	4.5	67.6	3.2
CS2G1P1	17.2	25.1	1.5	598.3	1156.3	1.9	34.2	2.0
CS2G2P1	20.5	30.9	1.5	708.4	1406.9	2.0	39.8	1.9
CS3G3P1	18.4	44.4	2.4	636.0	2708.9	4.3	67.3	3.7
CS4G2P1	19.3	41.5	2.2	774.7	2807.8	3.6	44.6	2.3

Energy ductility which is a ratio between the energy (E_u) at ultimate state and the energy E_y at yield state showed increased ductility index for CS2G2P2, CS3G3P1 and CS4G2P1 beams about 69%, 60% and 36% , respectively, compared to the control beam. Other strengthened beams showed a bit less energy ductility index compared to the control one. The deformability ductility index was also less for the CEBNSM-S beams compared to the control beam. This was due to the fact that the unstrengthened control beam showed typical flexure failure (concrete crushing after steel yielding) where the deflection was the maximum at failure compared to other strengthened beams. After failure of EB CFRP fabric, in case of CEBNSM strengthened beam, the Instron machine was stopped. However, the beam could go for further increment of deflection as the applied load would be resisted by the NSM system and subsequently by the internal steel until their ultimate failure.

4.1.6.6 Stiffness Assessment

Stiffness is the capacity to withstand bending or deflection due to applied load and is also termed as flexural rigidity. It is a fundamental matter of interest while considering

the serviceability performance of concrete structures. Improved stiffness attributes to greater ultimate strength of a structural member and also has an effect on other structural properties such as deflection, ductility and cracking behavior. It depends greatly on the cracking, loading level, thickness of bonded material and adhesive.

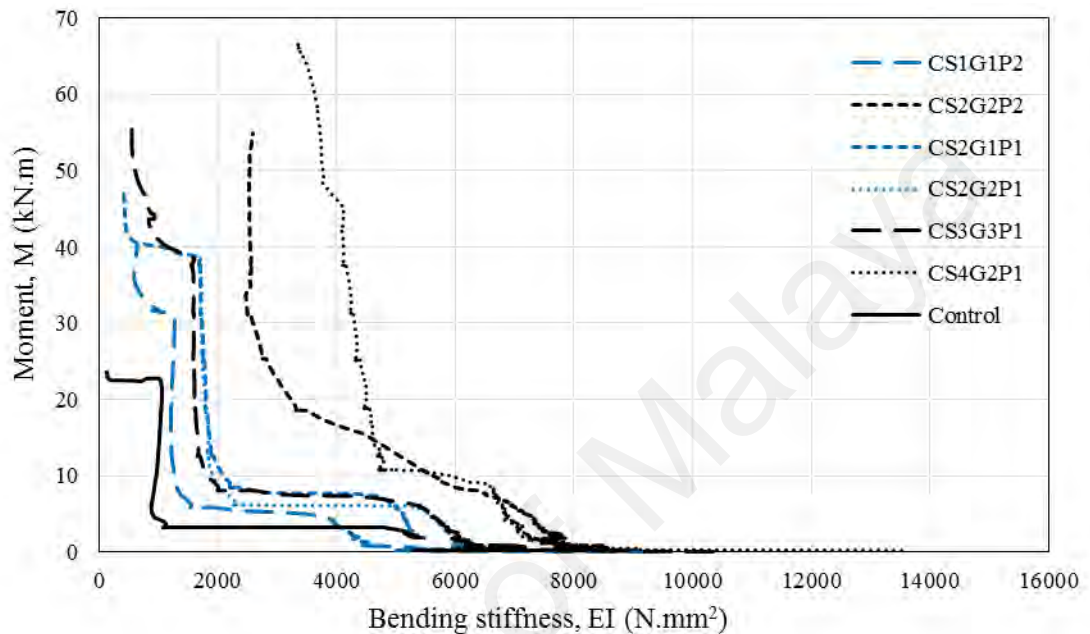


Figure 4.52: Bending stiffness variation of CEBNSM-S beams

For the analysis, curvature and neutral axis location was accounted with the help of the tensile and compression strain value of steel and concrete from their respective strain gauges. Figure 4.18 and equation 4.8 and 4.9 can be referred to calculate the bending stiffness of the beams. A moment curvature relationship was developed using the extreme tension strain values from the internal steel bar strain gauge and the extreme compression strain gauge values from the top of the mid-span.

Figure 4.52 depicts the moment versus bending stiffness diagram, where the CFRP strip was used as NSM reinforcement. The overall shape of the moment versus bending stiffness curve was like an “L”. For all cases, the CEBNSM-S beams demonstrated a superior moment-stiffness relationship compared to the control beam as expected. Initially, the bending stiffness was high as expected due to the un-cracked stage of the

beam section. The initial stiffness of the control beam was 5512 N.mm². The initial stiffness of the CEBNSM-S beams were 9406, 8689, 5299, 6685, 10347, and 13527 N.mm² for the CS1G1P2, CS2G2P2, CS2G1P1, CS2G2P1, CS3G3P1 and CS4G2P1 beam respectively.

With the increasing application of load, the stiffness was going to decrease and form a knee of the “L” where first crack appeared. This first crack stiffness of the control beam was 1105 N.mm². The intermediate stiffness at first crack of the CEBNSM-S beams were 1532, 6399, 2052, 2276, 2007 and 5469 N.mm² for CS1G1P2, CS2G2P2, CS2G1P1, CS2G2P1, CS3G3P1 and CS4G2P1 beams, respectively. There was no noticeable difference of stiffness after 1st crack and there was a drastic realignment of the curve. It formed almost a straight vertical line where the moment was increased at a steady rate. The CS2G2P2 and CS4G2P1 beam showed a gradual decreasing stiffness with the increasing moment capacity from the cracking moment to their yield moment.

At the yield moment, the stiffness of the control beam was 1032 N.mm². The stiffness at yield moment of the CEBNSM-S beams were 1262, 2557, 1689, 1718, 1600, and 4116 N.mm² for the CS1G1P2, CS2G2P2, CS2G1P1, CS2G2P1, CS3G3P1 and CS4G2P1 beam respectively. After crossing the point the strengthened beams showed gradual decrease of stiffness with steady moment increment until their failure.

4.1.6.7 Strain Measurement

Figure 4.53 demonstrated the concrete top fiber compression strain at 15, 30 and 39 kN service load levels. It is clearly visualized that the concrete strain of the strengthened beams was getting reduced compared to the control beam at all three load levels. The percentile reduction of the concrete strain value of CEBNSM-S beam compared to the control beam at 39 kN load were 50%, 60%, 62%, 63%, 57%, and 69% for the CS1G1P2, CS2G2P2, CS2G1P1, CS2G2P1, CS3G3P1 and CS4G2P1 beam

respectively. The average percentile reduction of the strengthened beams was 60%. The CS4G2P1 beams showed the maximum reduction, though its ultimate strain was the top among all beams.

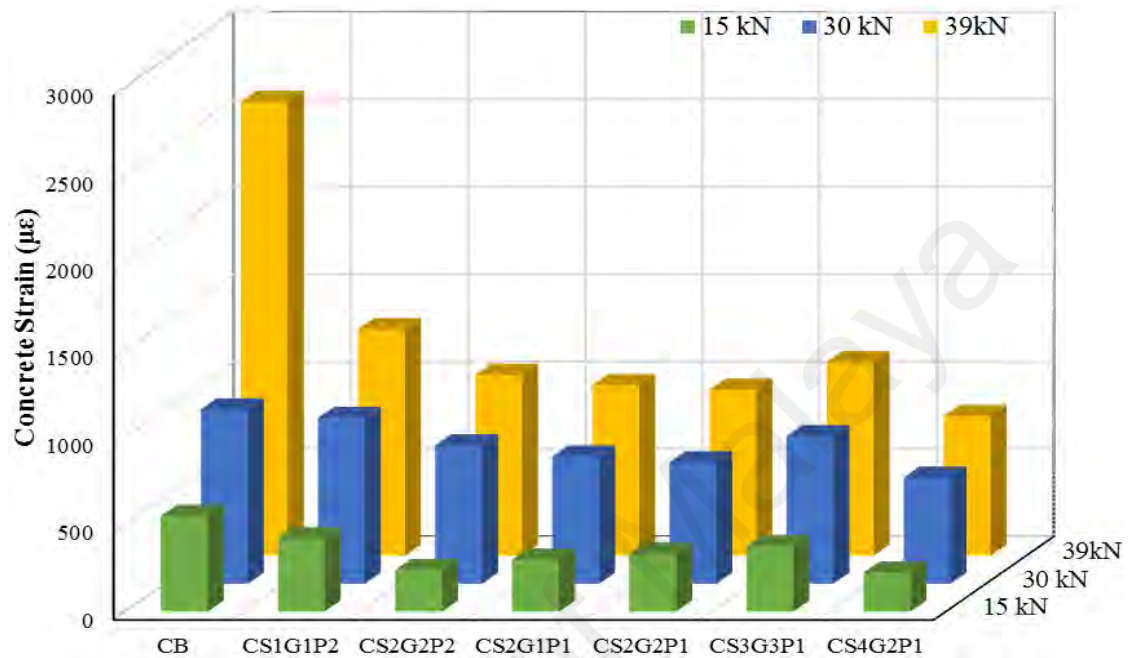


Figure 4.53: Comparison of concrete strain of CEBNSM-S beam at 15, 40 and 60 kN service load

Figure 4.54 demonstrated the tensile strain collected from the strain gauge at the center of the internal steel bar. From the graph, the control and CEBNSM-S beams can be distinguished by their tensile strain against load response. The steel bar of control beam portrayed almost the elastic-perfectly plastic behavior, whereas the CEBNSM-S beams demonstrated increasing linear elastic behavior after yielding occurred. The CS2G2P2 and CS4G2P1 beams showed very stiff linear elastic behavior where the load sharply increased without any significant strain variations.

Figure 4.55 demonstrated the tensile strain of internal steel bar at 15, 30 and 39 kN service load levels. It is clearly visualized that the tensile strain of the strengthened beams was getting reduced compared to the control beam at all three load levels. The percentile reduction of the CEBNSM-S strengthened beam compared to the control

beam at 39 kN load were 36%, 83%, 58%, 56%, 54%, and 92% for the CS1G1P2, CS2G2P2, CS2G1P1, CS2G2P1, CS3G3P1 and CS4G2P1 beams, respectively.

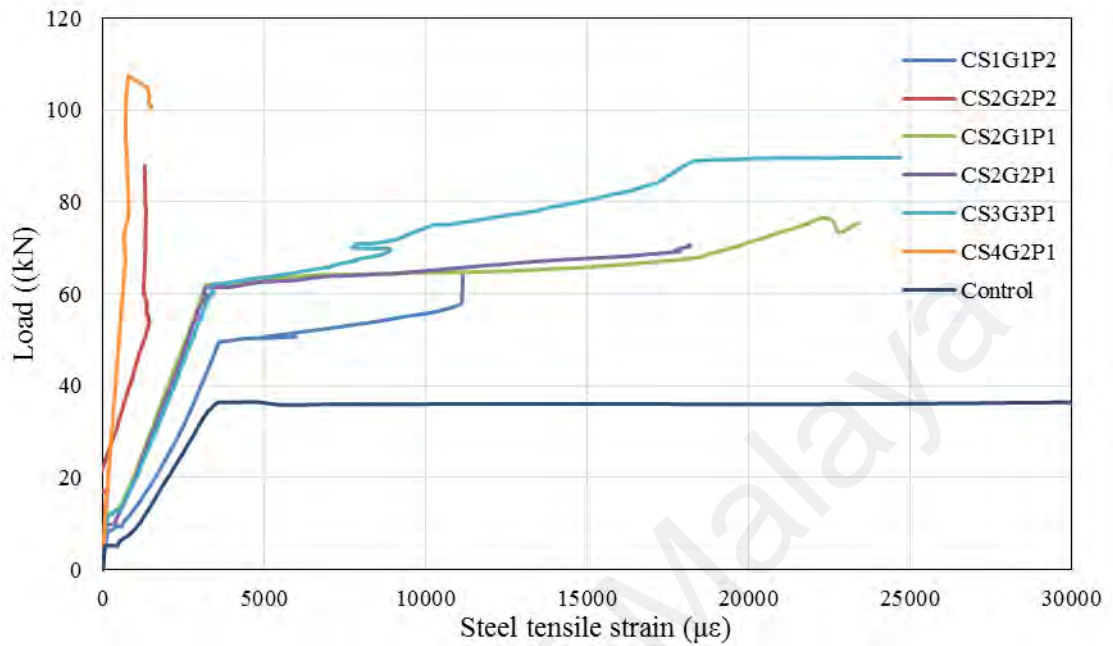


Figure 4.54: Load-steel strain curve of CEBNSM-S beams

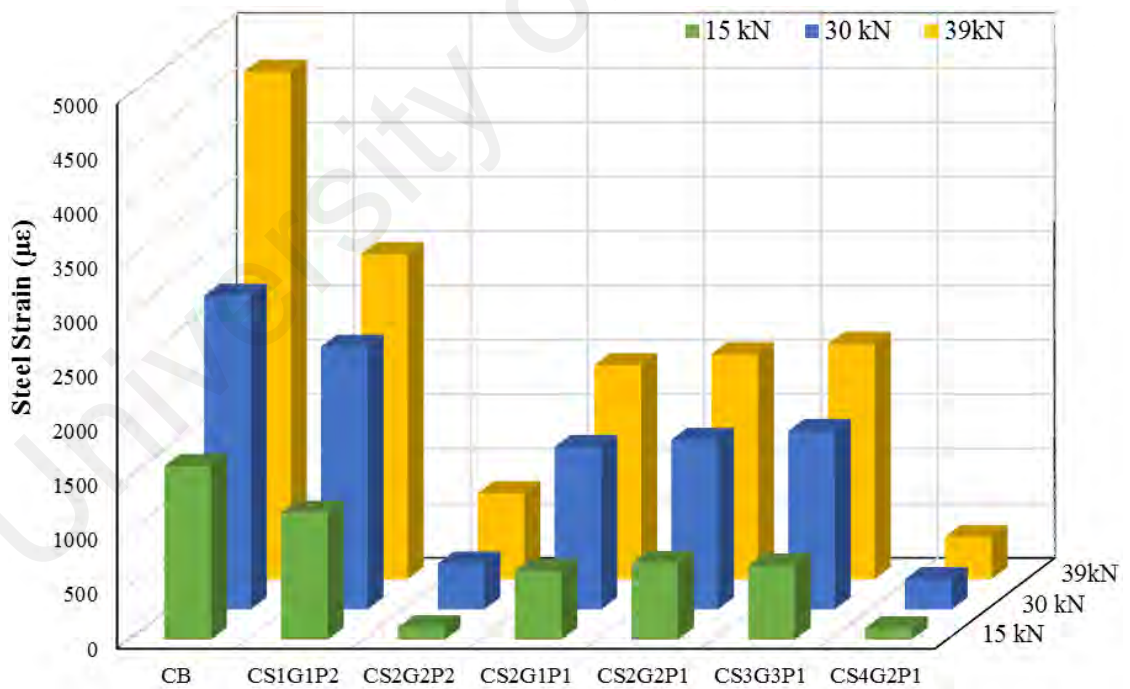


Figure 4.55: Comparison of steel tensile strain of CEBNSM-S beam at 15, 40 and 60 kN service load

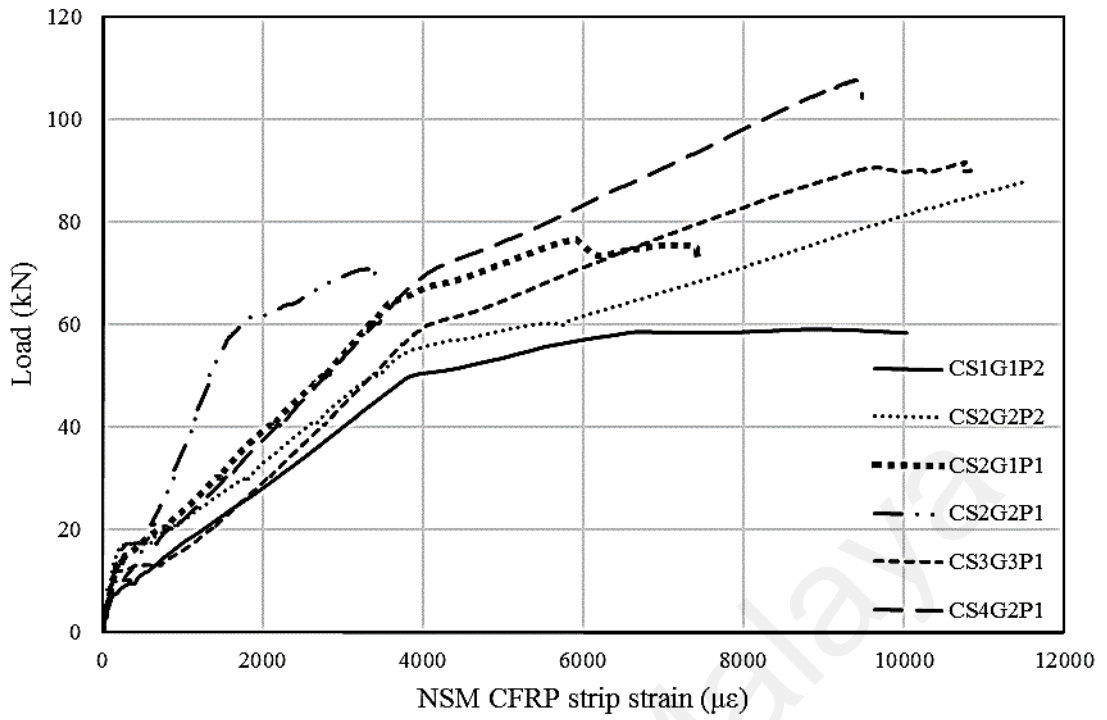


Figure 4.56: NSM CFRP strip strain of CEBNSM-S beams

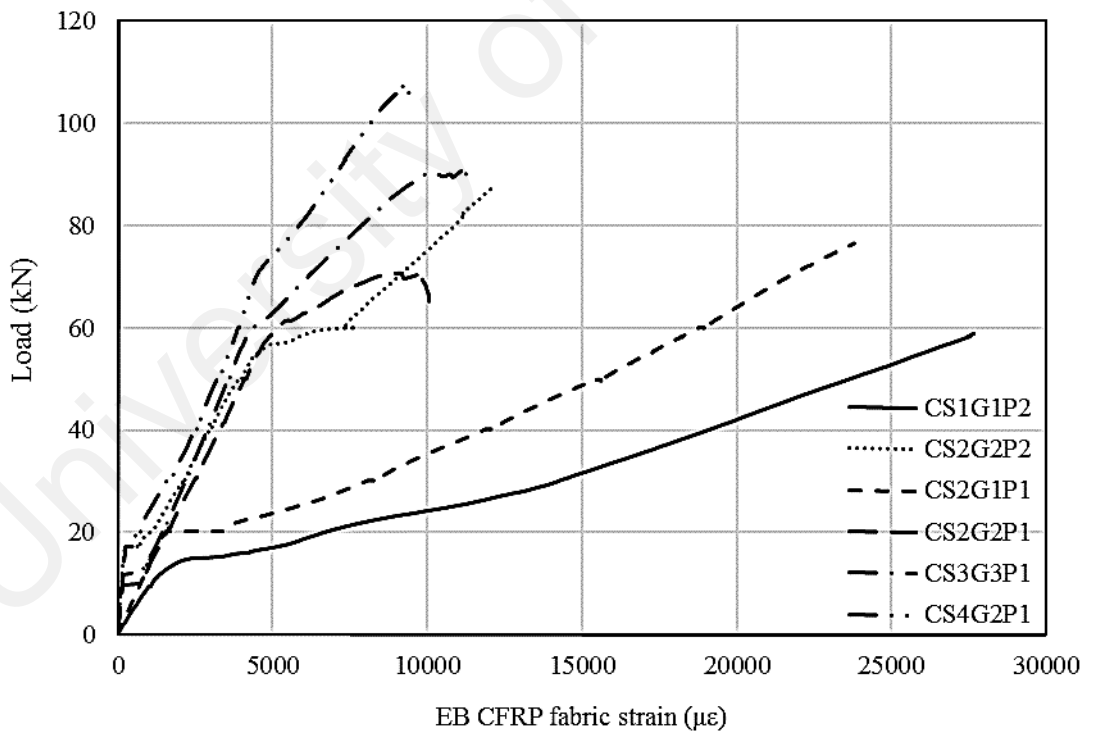


Figure 4.57: EB CFRP fabric strain of CEBNSM-S beams

4.2 Parametric Analysis of Experimental Results

4.2.1 NSM Strengthened Beam

4.2.1.1 Effect of Bond Length

Figure 4.58 compared the effect of bond length in the NSM strengthened RC beam. 1600 mm, 1800 mm and 1900 mm bond lengths were used for both CFRP and steel NSM bars. From Figure 4.58, it was clear that the ultimate capacity of the CFRP and steel strengthened beams was enhanced noticeably. For CFRP material, the beams with 1800 mm and 1900 mm bond length showed 19.5% and 21.6% increment compared to the beam using 1600 mm bond length. For steel, 5.8% and 10.3% increase was noticed for the beams with 1800 mm and 1900 mm bond length compared to the 1600 mm beam.

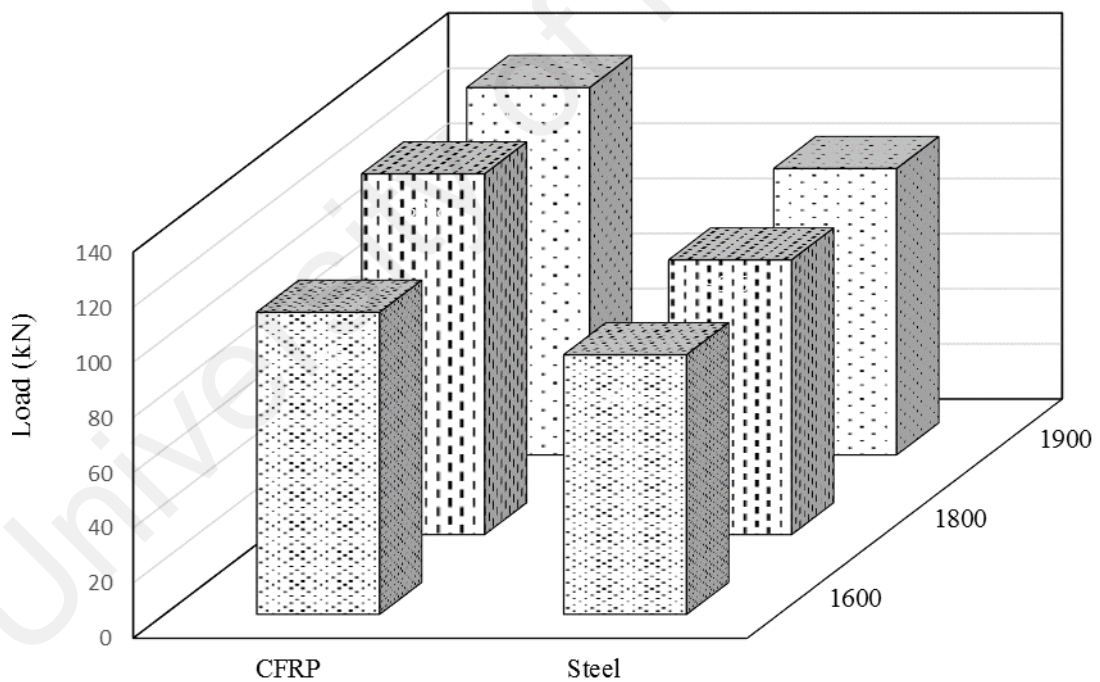


Figure 4.58: Effect of bond length of NSM bar

However, the steel NSM beam with 1800 mm and 1900 mm bond length showed flexure failure (concrete crushing before steel yielding) unlike other beams where concrete cover separation failure was occurred. The 1800 mm bond length was 90% of the clear span (2000 mm). So, for this case 1800 mm steel NSM showed good bond capacity due to its deformed surface characteristics. However, different researchers

found different bond length, though almost all the cases the material was CFRP and debonding occurred at the final stage.

4.2.1.2 Effect of Strengthening Materials

The effect of steel and CFRP as NSM strengthening material can be explained with the Figure 4.58. The NSM CFRP strengthened beam with 1600 mm, 1800 mm and 1900 mm bond length demonstrated 16.4 %, 31.3% and 28.3% increase of the ultimate capacity compared to the same bond length of the NSM steel strengthened beam.

4.2.2 CEBNSM-B Strengthened Beam

4.2.2.1 Effect of Area of Strengthening Materials

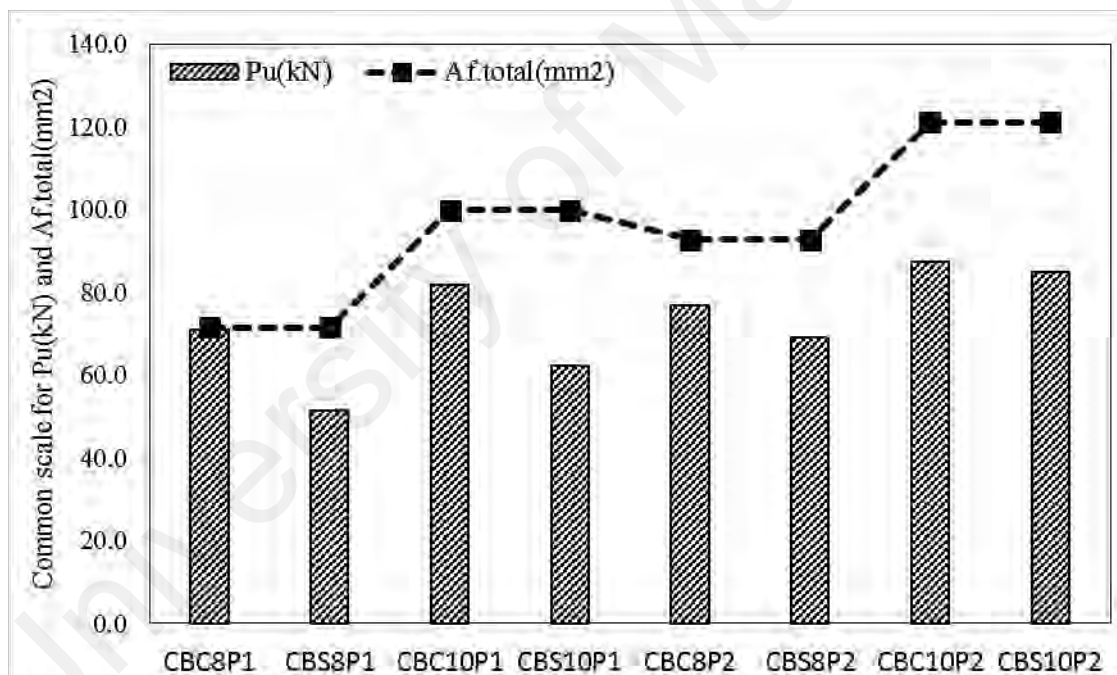


Figure 4.59: Effect of area of CEBNSM-B strengthening materials

Figure 4.59 exhibits the ultimate capacity of different CEBNSM-B beams with their corresponding area of strengthening materials. It was evident that the capacity of beam increased with the increment of the strengthening area. In this figure, it was possible to create two groups with same area of EBR materials. The first four beams with one layer CFRP fabric consisted of 8 and 10 mm diameter NSM CFRP and steel bar. For example, the CBC8P1 and CBS8P1 beams have same area of strengthening materials

(71.5 mm²) but CBC8P1 beam showed 38% more ultimate capacity than the steel NSM CBS8P1 beam. This trend was factual for other cases among the CEBNSM-B beams.

4.2.2.2 Effect of NSM Materials

Figure 4.60 displayed the comparative breakdown of the effect of steel and CFRP as NSM strengthening material on CEBNSM-B beams. The CBC8P1, CBC10P1, CBC8P2, and CBC10P2 beams which consisted of NSM CFRP bar demonstrated 38%, 30.9%, 11.3% and 2.9% ultimate capacity compared to their counterpart beams which were strengthened with steel NSM bars. It should be noted that the percent of ultimate capacity increment of CEBNSM-B beams was reduced with the increasing amount of total strengthening material.

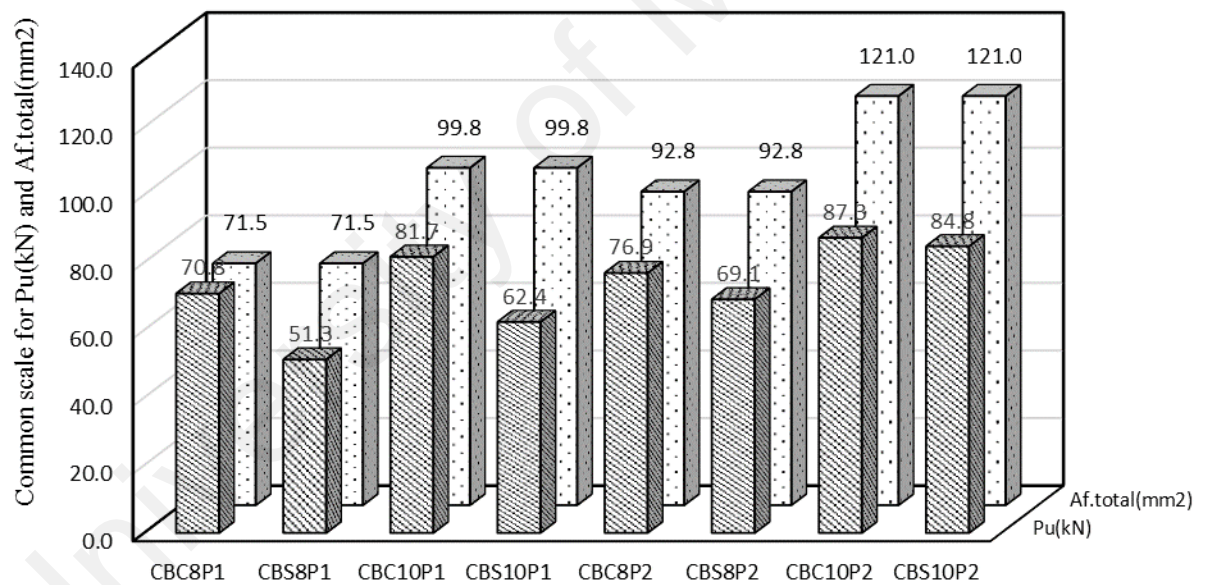


Figure 4.60: Effect of NSM strengthening materials on CEBNSM-B beams

4.2.2.3 Effect of EB CFRP Thickness

Figure 4.61 showed the effect of EB CFRP fabric thickness on CEBNSM-B beams. Only EB CFRP fabric area was provided in this figure along with the ultimate capacity. Among these eight beams, each pair consisted of same NSM diameter (8 or 10 mm) but variable thickness of one or two layers of CFRP fabric. Among the whole group, the single layered CBC8P2, CBS8P2, CBC10P2, and CBS10P2 beams showed 8.6%,

34.7%, 6.9% and 35.9% enhanced ultimate capacity compared to the double layered CBC8P1, CBS8P1, CBC10P1, and CBS10P1 beams, respectively. The beams having NSM steel bars with 2 ply CFRP fabric showed superior strength compared to their CFRP NSM counterpart beams.

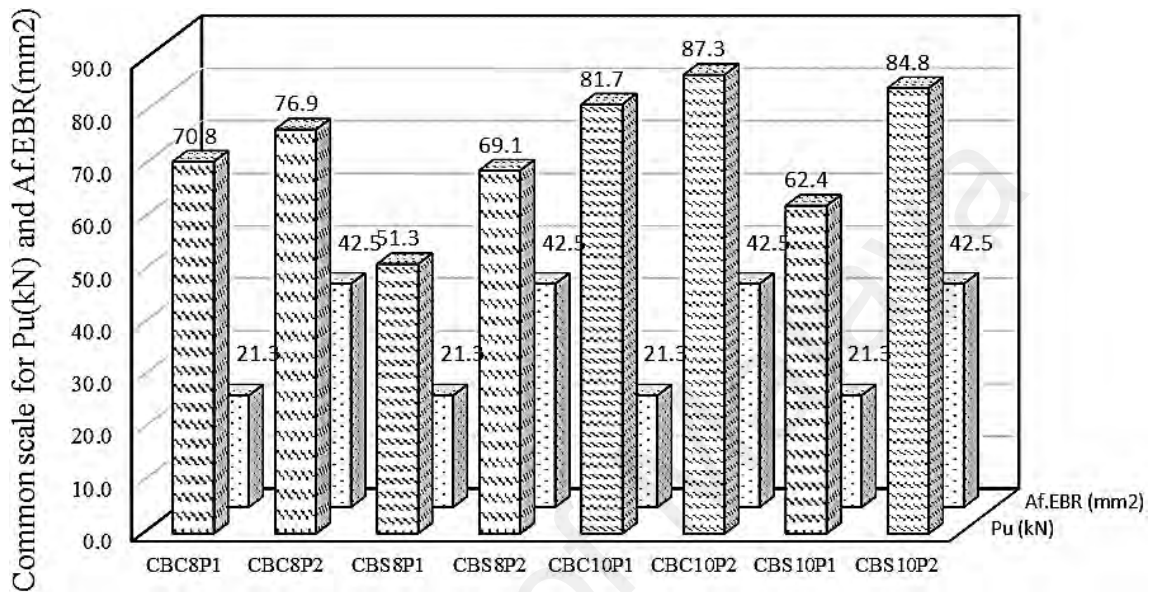


Figure 4.61: Effect of EB CFRP fabric thickness on CEBNSM-B beams

4.2.2.4 Effect of NSM Diameter

CFRP and steel NSM bar was used to strengthen the RC beam with 8 mm and 10 mm diameter bar. Figure 4.62 shows only the area of the NSM bar and their effect on enhancing the ultimate strength of CEBNSM-B beam.

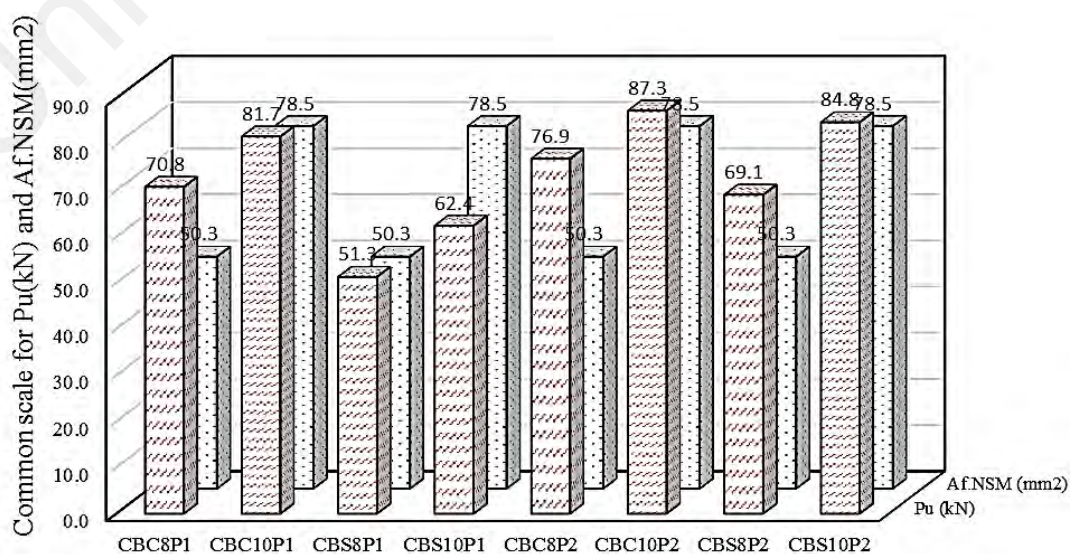


Figure 4.62: Effect of variable diameter of NSM bar on CEBNSM-B beams

From the above figure, it could be easier to group the first four and the last four beams according to the same thickness of EB CFRP fabric. Within the group the diameter of NSM bar was variable. Obviously the beam having 10 mm diameter NSM bar showed more enhanced strength than the 8 mm diameter beams. The CBC10P1, CBS10P1, CBC10P2, and CBS10P2 beams showed 15.4%, 21.6%, 13.5% and 22.7% raised ultimate capacity than the CBC8P1, CBS8P1, CBC8P2, and CBS8P2 beams respectively.

4.2.2.5 Effect of U-Wrap Anchorage

Figure 4.63 showed the effect of U-Wrap anchorage on the CEBNSM-B beams where EBP2 beams were considered as the reference. The beams with double layered CFRP fabric plus 10 mm NSM bar were further strengthened at their fabric curtailment location with two layer CFRP fabric to avoid premature debonding. The CBC10P2A and CBS10P2A beams displayed 81.8% and 69.6% enhanced ultimate capacity compared to the EBP2 beam which also had the same double layer CFRP fabric at its beam soffit. Furthermore, CBC10P2A and CBS10P2A beams failed due to flexure unlike the beams CBC10P2 and CBS10P2 which failed due to premature debonding failure.

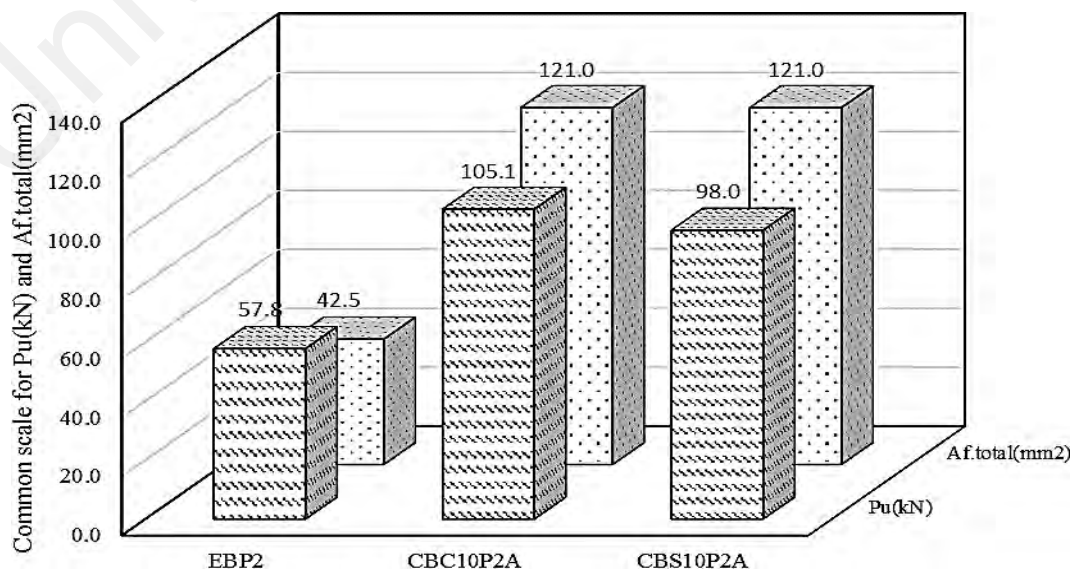


Figure 4.63: Effect of U-Wrap anchorage on CEBNSM-B beams

4.2.3 Comparison between EB and CEBNSM-B beams

To compare the performance of the CEBNSM-B beams, two RC beams were strengthened with one and two layer of EB CFRP fabric. Figure 4.64 shows the difference between the ultimate capacity of EBP1 and one layered CEBNSM-B beams. The CBC8P1, CBS8P1, CBC10P1 and CBS10P1 beams illustrated the enhanced strength of 47%, 6%, 70% and 29% than that of EBP1 beam. The total strengthening reinforcement area for EB CFRP layer was same for all the strengthened beams as 21.3 mm². However, the CEBNSM-B beams with steel NSM bar showed less enhancement due to the lower tensile strength of the steel bar.

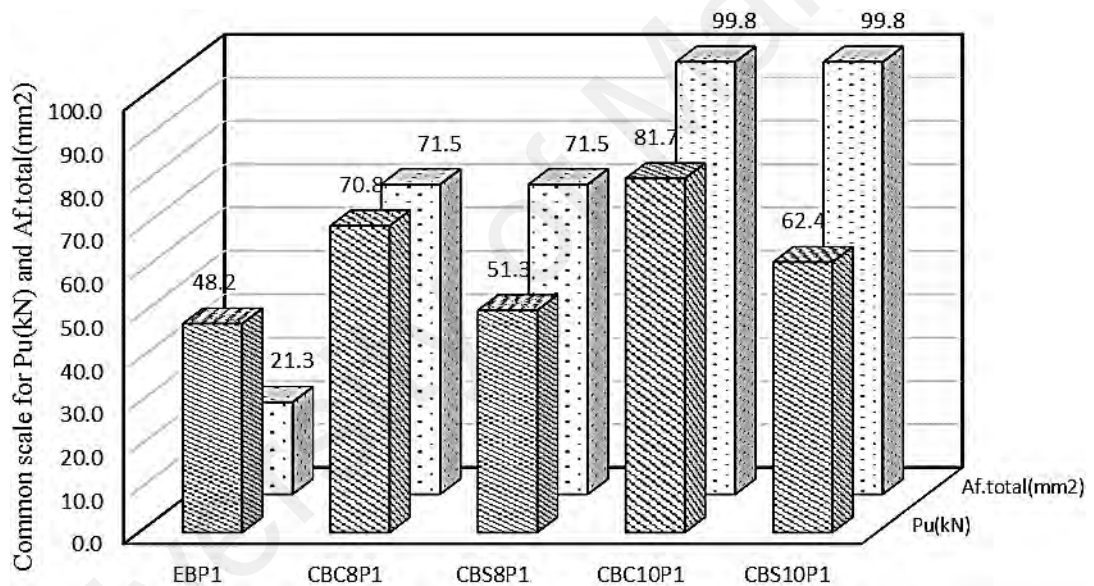


Figure 4.64: Comparison between EBP1 and single ply CEBNSM-B beams

Figure 4.65 depicts the comparison between the EBP2 and double layered CEBNSM-B beams. Within this group, the CBC8P2, CBS8P2, CBC10P2 and CBS10P2 beams demonstrated greater ultimate strength of 33%, 20%, 51% and 47% than that of EBP1 beam. The average trend of increasing strength of these groups were almost same, though the double layered beams with steel NSM bar (CBS8P2 and CBS10P2) demonstrated better performance than the single layered CBS8P1 and CBS10P1 beams.

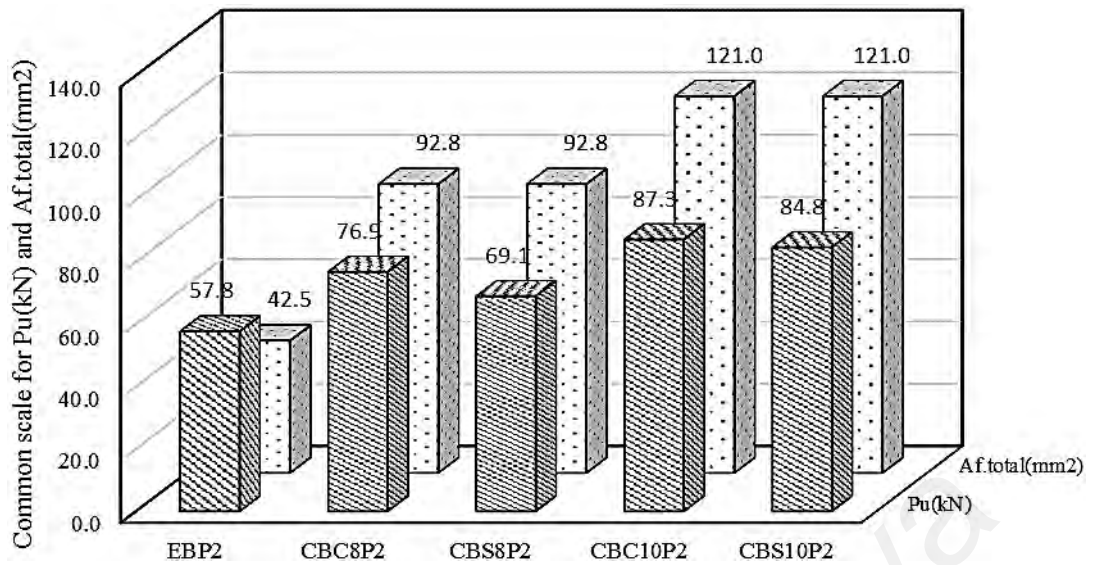


Figure 4.65: Comparison between EBP1 and double ply CEBNSM-B beams

4.2.4 CEBNSM-S Strengthened Beam

4.2.4.1 Effect of Area of Strengthening Materials

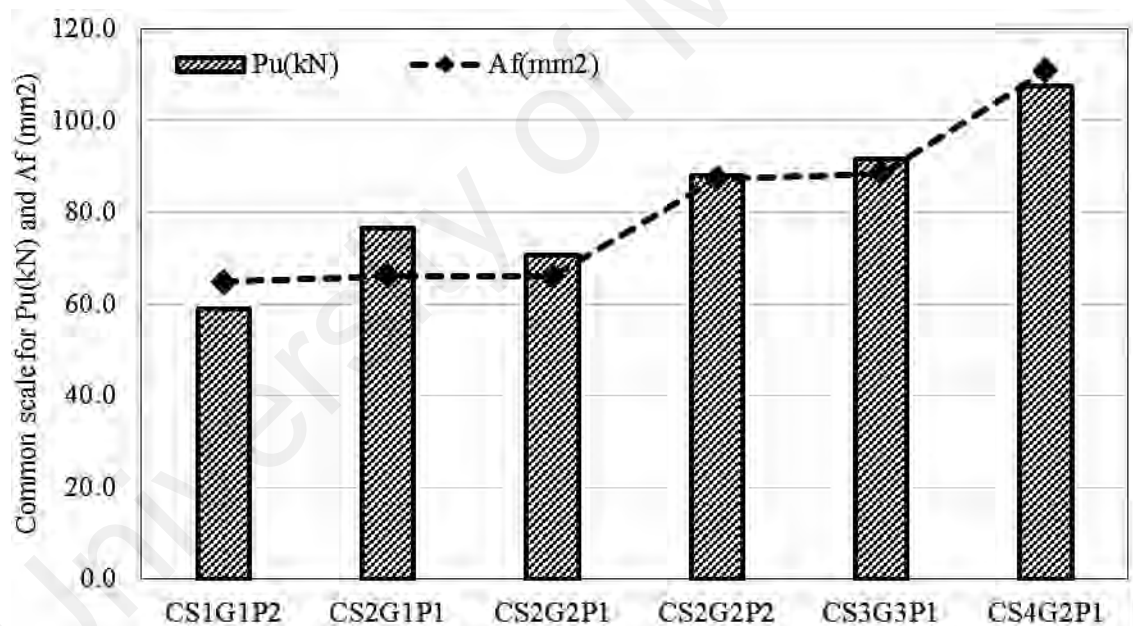


Figure 4.66: Effect of area of strengthening materials on CEBNSM-S beams

Figure 4.66 presents the ultimate strength of various CEBNSM-S beams with their area of strengthening constituents. It was manifested that the strength of beam increased with the increase of the area of strengthening materials. One interesting finding was identified among the CS2G1P1 and CS2G2P1 beams where the strengthening area was same, though CS2G1P1 beams showed 8% rise of ultimate capacity over CS2G2P1.

4.2.4.2 Effect of Number of Groove

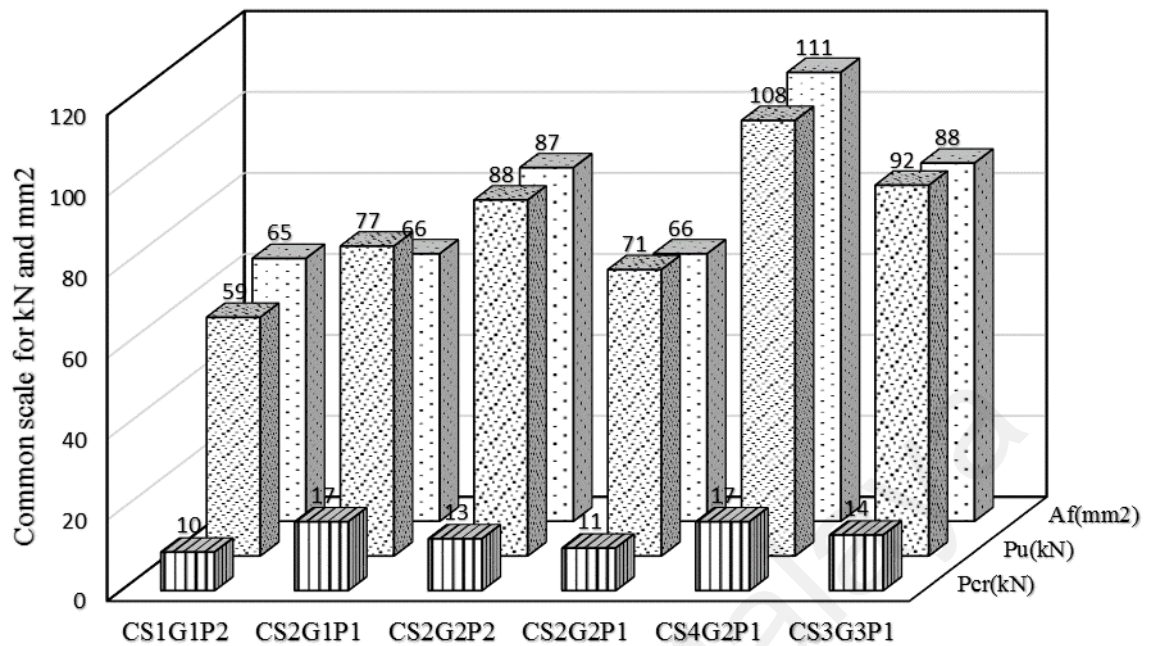


Figure 4.67: Effect of number of groove on CEBNSM-S beams

Figure 4.67 reports the effect of number of groove on the strengthened beams. Basically, increasing groove number implied more strengthening area which supposedly enhanced the ultimate capacity of the strengthened beam. However, this statement encountered contradiction when more than one CFRP strips were placed in a single groove.

4.2.4.3 Effect of Groove Dimension

Two types of groove dimension were used in this study: a) 5mm × 25mm and b) 10 mm × 25mm. Parretti and Nanni, 2004 and Blaschko, 2003 recommended a minimum depth of the groove as 1.5 times the height of the strip and 3 mm larger than the height of FRP strip, respectively. According to the reference, the height of the groove for this study was fixed at 25 mm. Blaschko, 2003 proposed the minimum groove as CFRP strip thickness plus 3 mm for adhesive layer thickness. Parretti and Nanni, 2004 suggested a minimum groove width as three times the FRP strip thickness. According to their recommendations, the groove width for single FRP strip was selected for this study as 5 mm to stay in a safer position by rounding off the decimal places of dimension for ease

of the groove preparation process. In case of two strips inside a single groove, the width was extended to 10 mm. In this configuration, both the strips got a side clearance of 3 mm for adhesive layer along with a clear distance of 1.2 mm between two adjacent FRP strips. In this study, CS2G1P1 and CS4G2P1 beams consisted of double strips in a single groove and the rest were maintaining the single strip inside a groove.

From Figure 4.66 and Figure 4.67, it is revealed that in spite of having almost same strengthening area CS2G1P1 and CS3G3P1 beams displayed 8% and 4.5% increase of ultimate capacity than that of CS2G2P1 and CS2G2P2 beams. Besides, the 1st cracking load for CS2G1P1 and CS3G3P1 was also improved considerably compared to their counterpart beams. Besides, CS4G2P1 beam which consisted two grooves where double strips were placed in single groove displayed the best flexural performance among the CEBNSM-S beams. These results exhibit the superior performance of these beams consisting of double CFRP strips in a single groove.

4.2.5 Comparison between EB and CEBNSM-S beams

Figure 4.68 represents the comparison between the EBP1 and single layered CEBNSM-S beams. Maintaining the same EB CFRP area of 21.3 mm², the CS2G1P1, CS2G2P1, CS3G3P1 and CS4G2P1 beams displayed enhanced flexural capacity of 59%, 47%, 90% and 123% compared to the EBP1 beam. Figure 4.69 reported the difference of the ultimate capacity between the EBP2 and single layered CEBNSM-S beams. Only CS1G1P2 and CS2G2P2 beams were strengthened with double layer CFRP fabric which showed 53% and 105% increment of ultimate strength over EBP2 beams.

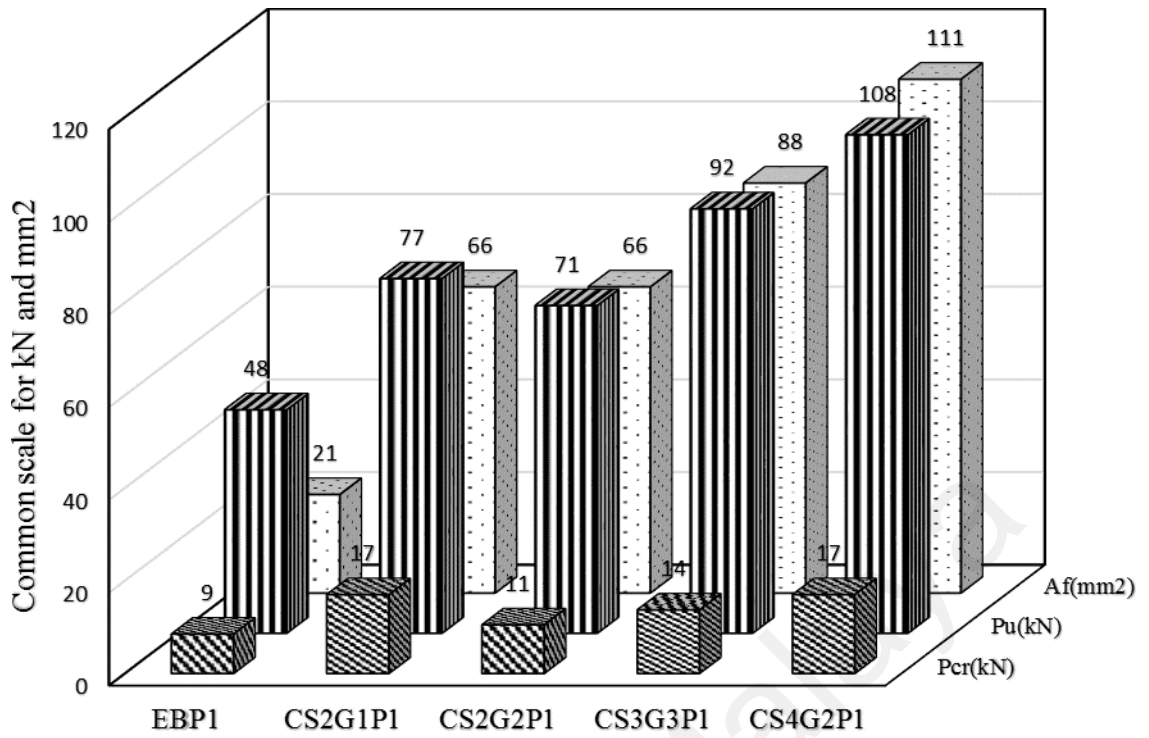


Figure 4.68: Comparison between EBP1 and single ply CEBNSM-S beams

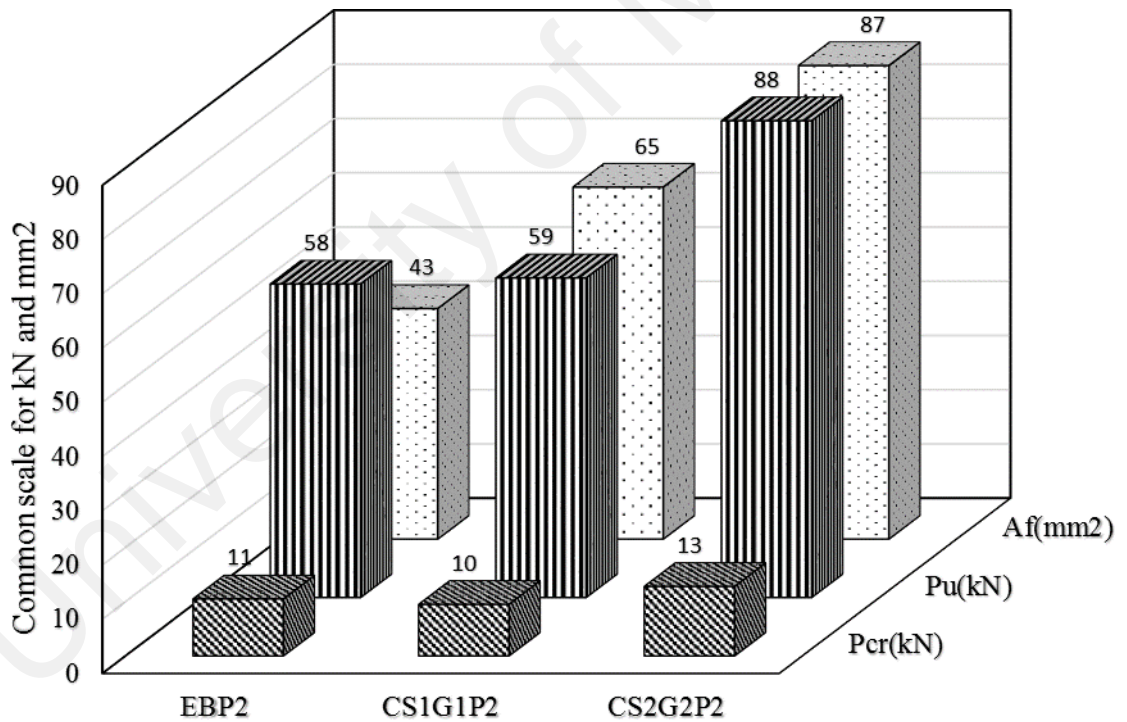


Figure 4.69: Comparison between EBP2 and double ply CEBNSM-S beams

4.2.6 Comparison between CEBNSM-B and CEBNSM-S beams

It is possible to compare the CEBNSM-B and CEBNSM-S beams having NSM CFRP bar or strip. Having a strengthening area of 66 mm², one CEBNSM-S beam (CS2G1P1) showed 240% and 96% increase of the 1st crack and ultimate load capacity

compare to the control beam. In contrast, a CEBNSM-B beam (CBC8P1) with 71.52 mm² exhibited 118% and 82% of increase of the 1st crack and ultimate load capacity compare to the control beam. Similar case was happened to CS3G3P1 (88.45 mm²) and CBC8P2 (92.77 mm²) beams, where their 1st crack and ultimate load capacity was increased by 174%, 135%, 160% and 97% respectively for these two beams respectively compare to the control beam. So, even with more strengthening area the CEBNSM-B showed less increment of load capacity compare to the CEBNSM-S beams.

If crack width is considered, it is possible to measure the crack width of the above mentioned beam at 60 kN load which was close to the service load. These four beams were considered as their strengthening area was close to each other within their respective groups. At 60 kN load, the crack width of CBC8P1 and CS2G1P1 was found 0.4 mm and 0.26 mm. In addition, CBC8P2 and CS3G3P1 demonstrated 0.37 mm and 0.28 mm crack width respectively. As a result, for both case the CEBNSM-S showed less crack width at the same load level compare to the CEBNSM-B beam.

The results revealed that the ultimate capacity was increased considerably for both these techniques. Comparing with NSM and EBR techniques, CEBNSM technique showed a promising possibility to apply to the underperforming structure to increase their capacity. The proposed CEBNSM technique significantly increased the first crack load compared to the unstrengthened and the other strengthening techniques. Most interestingly, the failure mode had changed for most of the instances from debonding to flexure failure which was a remarkable contribution of this technique.

4.3 Analytical Prediction Approach

4.3.1 Deflection Prediction

In early RC designs, serviceability issues were dealt with indirectly. However, serviceability is now considered to be a major issue in designing a structure. Among the two limit states (strength and serviceability), the serviceability limit state refers to the performance of structures under normal service loads and is concerned with the uses and/or occupancy of structures. Serviceability is measured by considering the magnitudes of deflections, cracks, and vibrations of structures. In general, ACI 318-05 provisions for deflection control are concerned with deflections that occur at service levels under immediate and sustained static loads. The present study only concentrates on short term or immediate deflection.

The deflection of simply supported beam under two-point loading can be computed by using equation 4.10.

$$\Delta = \frac{P}{24E_c I_e} a(3L^2 - 4a^2) \quad (4.10)$$

Where, P is the applied load on the beam, a is shear span, L is beam span and $E_c I_e$ is the flexural stiffness of the beam which is product of elastic modulus, E_c , and moment of inertia, I_e . The last two variables are subject to change during the course of loading. In concrete beam test, the modulus of elasticity will vary due to load increase. This is caused by the inelastic stress-strain behavior of concrete beyond the elastic limits, while the moment of inertia will vary when cracks on the beam occur due to the tensile strain greater than the cracking strain of concrete (Charkas et al., 2003). The cracked zones in a concrete beam are ineffective in resisting stresses originating from applied loads and moments. Therefore, cracking of concrete decreases the resistance of a concrete beam to loading, leading to greater deformation in the beam. The decrease in the second moment of area of a concrete beam during the course of loading is taken into account by the

effective moment of inertia approach (Akmaluddin, 2011). Changing variation of the effective moment of inertia is summarized in Figure 4.70

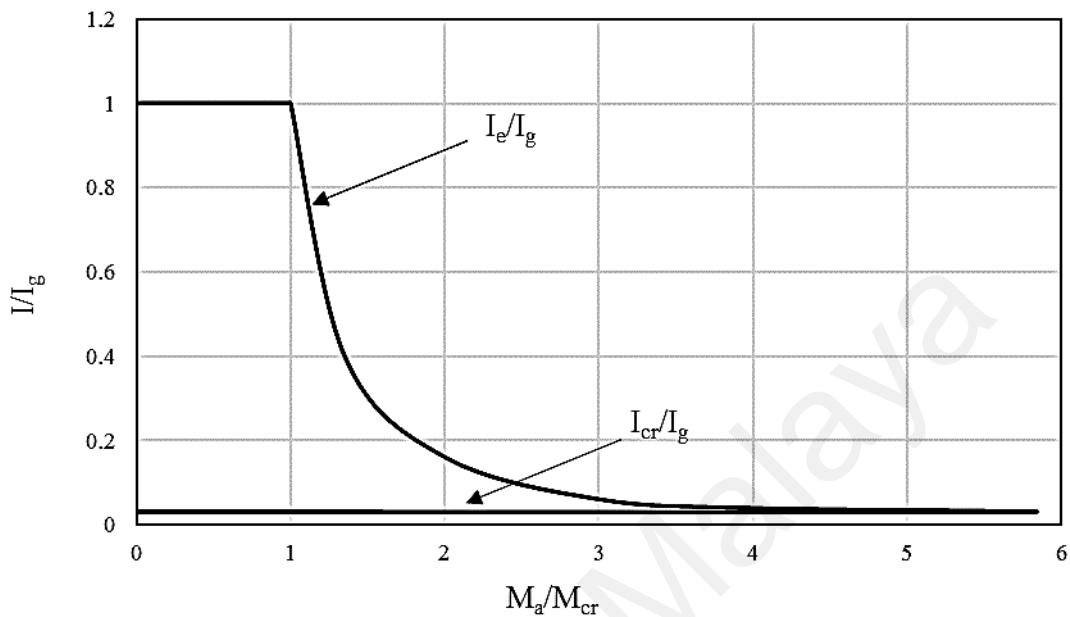


Figure 4.70: Typical moment of inertia variation with various moment

By referring to the Figure 4.70, when the maximum moment (M_a) in a beam does not exceed the cracking moment (M_{cr}), the beam is in the un-cracked condition therefore I is taken as I_g . This is shown by a linear line of I_e/I_g equal to 1 in Fig. 4.70. Once M_a bigger than M_{cr} , the overall moment of inertia of a concrete beam decreases gradually from the un-cracked moment of inertia (I_g) to the fully-cracked moment of inertia (I_{cr}). This gradual decrease is taken into consideration by the effective moment of inertia approach (I_e).

The empirically calibrated Branson's equation represents the transition from uncracked gross moment of inertia (I_g) to the transformed moment of inertia (I_{cr}). ACI 318-99 (1999) adopted this Eqs. (4.11) for effective moment of inertia (I_e) to estimate the immediate deflection of steel reinforced RC beams.

$$I_e = I_{cr} + (I_g - I_{cr}) \left(\frac{M_{cr}}{M_a} \right)^3 \quad (4.11)$$

Here, M_a is the service moment and M_{cr} is the cracking moment. However, researchers have found that this equation. (4.11) overestimates the I_e of a FRP reinforced beam due to the linear elastic behavior of FRP material. Gao et al. (1998) proposed a modified version of Branson's Eqs. (4.12-4.13) for FRP reinforced beams.

$$I_e = I_{cr} + (\beta_d I_g - I_{cr}) \left(\frac{M_{cr}}{M_a} \right)^3 \quad (4.12)$$

$$\beta_d = \alpha_b \left[\frac{E_f}{E_s} + 1 \right] \quad (4.13)$$

Here, α_b is a bond dependent coefficient and ACI recommends its value be 0.5 for all FRP bar types until a more precise value is determined from further research.

The Italian guideline (CNR, 2006) has suggested that the curvature diagram of the FRP reinforced member be integrated following the proposed Eurocode 2 model. Non-linear analysis can be used to consider this diagram by considering both the tension stiffening and cracking of the concrete. The deflection f can be calculated using the following Eqs. (4.14).

$$f = f_1 \beta_1 \beta_2 \left(\frac{M_{cr}}{M_{max}} \right)^m + f_2 \left[1 - \beta_1 \beta_2 \left(\frac{M_{cr}}{M_{max}} \right)^m \right] \quad (4.14)$$

Where, f_1 = deflection of the uncracked section; f_2 = deflection of the transformed cracked section; $\beta_1 = 0.5$, which is the value of FRP bar bond properties; β_2 = coefficient used for the duration of loading (1 for short term and 0.5 for long term or cyclic loading); M_{max} = maximum moment; M_{cr} = cracking moment; and m = a coefficient equal to 2.

To avoid inelastic deformations of RC members with non-prestressed external FRP reinforcement, the existing internal steel reinforcement should be prevented from

yielding under service load levels, especially for members subjected to cyclic loads. For this reason, ACI has set two Eqs. (4.15)-(4.16) for the stress in steel and concrete under service loading (ACI 440.2R-08, 2008). They are as follows:

$$f_{s,s} \leq 0.80f_y \quad (4.15)$$

$$f_{c,s} \leq 0.45f'_c \quad (4.16)$$

The stress level in the steel reinforcement can be calculated based on a cracked-section analysis of the FRP-strengthened reinforced concrete section (Figure 4.71), as indicated in the following Eqs. (4.17):

$$f_{s,s} = \frac{\left[M_s + \varepsilon_{bi} A_f E_f \left(d_f - \frac{kd}{3} \right) \right] (d - kd) E_s}{A_s E_s \left(d - \frac{kd}{3} \right) (d - kd) + A_f E_f \left(d_f - \frac{kd}{3} \right) (d_f - kd)} \quad (4.17)$$

Here, M_s is equal to the moment due to all sustained loads (dead loads and the sustained portion of the live load) plus the maximum moment induced in a fatigue loading cycle. Under service loading conditions, within the elastic response range of the member, the FRP stress level can be computed using the following Eqs. (4.18).

$$f_{f,s} = f_{s,s} \left(\frac{E_f}{E_s} \right) \frac{d_f - kd}{d - kd} - \varepsilon_{bi} E_f \quad (4.18)$$

4.3.2 Deflection Prediction Model for NSM Strengthened RC beam

The proposed model is formulated upon sectional analysis and strain compatibility (Al-Mahmoud, F. et al., 2009; El-Mihilmy & Tedesco, 2000). The following assumptions were made in this model: (1) plane sections remain plane after bending, (2) the strains in the reinforcement and concrete are directly proportional to the distance from the neutral axis, (3) there is no slip between the NSM bars and the concrete, (4) the maximum compressive strain in the concrete is 0.003, and (5) the tensile strength of the concrete is neglected.

The calculation procedure to predict the load-deflection of beam specimen (control and strengthened) beam is as follows:

- i. Assume a given external applied load on the beam.
- ii. Calculate the external moment.
- iii. Assume a strain at the compression fiber of the concrete.
- iv. Assume the neutral axis depth.
- v. Calculate the strains in the tension steel, NSM steel and steel/CFRP reinforcement by using triangular rule.
- vi. Calculate stresses and forces in the compression concrete, tension steel, and NSM steel bar.
- vii. Evaluate force equilibrium equations. If not in equilibrium, change the neutral axis depth in step (iv) and repeat steps (iv) to (vii) until in equilibrium.
- viii. If the forces are equilibrium, calculate internal moment by taking moment at concrete compressive force level.
- ix. Compare the calculated internal moment to the external moment obtained in step (ii). If not equal, change the assume strain in step (iii) and repeat steps (iii) to (ix).
- x. If external moment is equal to internal moment, calculate the deflection using equation 4.10.
- xi. Calculate the deflection and record the load and deflection data.
- xii. Apply the load increment and repeat steps 2 to 10 until failure.

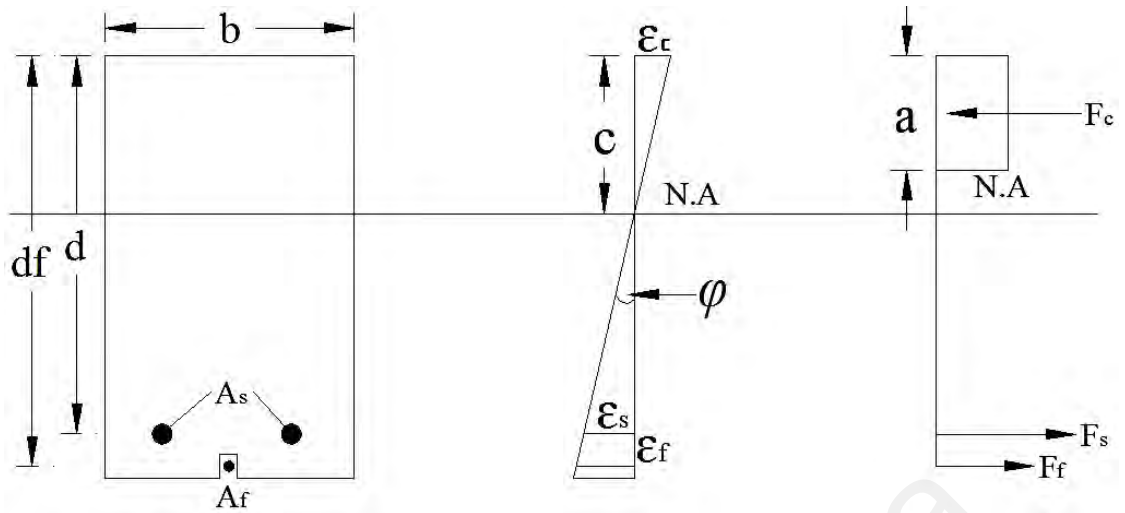


Figure 4.71: Strain and stress distribution of NSM strengthened beam

The ultimate load capacities of the strengthened beams were determined by the strain compatibility and force equilibrium requirements, as demonstrated in Figure 4.71. The iteration procedure was adopted to achieve equilibrium. The following equations (4.19 to 4.25) were used to calculate the moment and ultimate load of the strengthened beams.

The strain of the NSM bar at failure

$$\varepsilon_f = \varepsilon_{cu} \frac{d_f - c}{c} = 0.003 \frac{d_f - c}{c} \quad (4.19)$$

The stress of the NSM bar at failure

$$f_f = E_f \varepsilon_f = E_f \times 0.003 \frac{d_f - c}{c} \quad (4.20)$$

Under Equilibrium condition

$$F_c = F_s + F_f \quad (4.21)$$

$$0.85f'_c b \beta = A_s f_y + A_f E_f \times 0.003 \frac{d_f - c}{c} \quad (4.22)$$

(4.23)

$$(0.66f'_c b)c^2 + (0.003E_f A_f - A_s f_y)c - (0.003E_f A_f d_f) = 0$$

The resulting moment of the NSM strengthened RC beam

$$M_n = A_s f_y \left(d - \frac{a}{2} \right) + A_f f_f \left(d_f - \frac{a}{2} \right) \quad (4.24)$$

(4.25)

$$P_u = \frac{2M_u}{a}$$

Where b is the width of the beam, h is the depth of the beam, d is the distance between the top fiber of the concrete and the center of gravity of the tension steel bars, d_f is the distance between the top fiber of the concrete and the center of gravity of the NSM bar, c is the depth of the neutral axis, ϵ_{cu} is the ultimate strain at the top fiber of the concrete, ϵ_s is the strain in the tension steel, ϵ_f is the strain in the NSM reinforcement, f'_c is the compressive strength of the concrete, A_s is the area of tension steel, A_f is the area of the NSM reinforcement, f_y is the yield strength of the tension steel bar, f_f is the tensile strength of the CFRP NSM bar, F_c is the total compressive force of the concrete, F_s is the tensile force of the tension steel, F_f is the tensile force of the side NSM reinforcement, a is the shear span length, M_n is the nominal moment, and P is the ultimate load.

The load versus mid-span deflection curves for the RC beams strengthened with NSM CFRP bars can be divided into three distinct linear phases (Al-Mahmoud, F. et al., 2009; Charkas et al., 2003; El-Mihilmy & Tedesco, 2000), as follows:

1. Pre-cracked segment ($P < P_{cr}$)
2. Cracking segment ($P_{cr} \leq P \leq P_y$)
3. Post-cracking segment ($P_y < P < P_u$)

Where P , P_{cr} , P_y and P_u constitute the service load, cracking load, first yield load of the tension reinforcement, and ultimate load, respectively.

1. Un-cracked phase: Elastic equations are applied to determine the deflection of the strengthened beams utilizing the gross transformed moment of inertia I_g , which contains the contribution of the S-NSM CFRP bars. Therefore, deflection of the un-cracked stage can be calculated using equation 4.10.

2. Cracking phase: When applied, load P is greater than the cracking load P_{cr} , the section of the concrete in the locality of the mid-span cracks, then the flexural stiffness of the beam reduces. In a lower moment location, where there are no cracks in the concrete, the moment of inertia is almost equal to the gross transformed moment of inertia I_g . Where the tension cracks are located, the moment of inertia of that section is almost equal to the transformed cracked moment of inertia I_{cr} . The moment of inertia lies between the two values of I_g and I_{cr} . When the tensile forces develop between the concrete and cracks, then the flexural rigidity, EI , refers to tension stiffening. In this period, the beam no longer has a constant moment of inertia along its length, and the effective moment of inertia I_e is used. To determine the effective moment of inertia I_e the following equation (4.26) is used.

$$I_e = I_{cr} \left[1 + \left(1 - \frac{M}{M_y} \right)^3 \right] \quad (4.26)$$

Therefore, deflection of the cracked stage can be calculated using equation 4.10.

3. Post-cracking phase: In this phase, the deflection by curvature along the beam length is determined; to calculate the curvature by linear interpolation between the curvatures at first yield of tension reinforcing steel ϕ_y and the ultimate curvature ϕ_u (equation 4.27 to 4.29). The depth of neutral axis and ultimate moment can be obtained

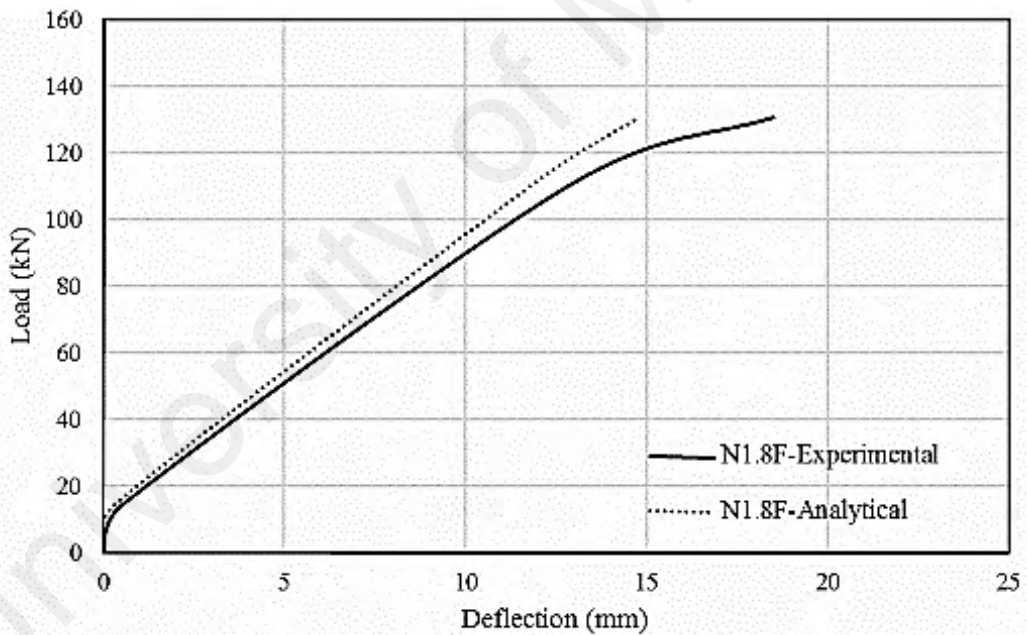
for the ultimate load capacity section. Therefore, deflection of the cracked stage can be calculated using equation 4.10.

$$\varphi_u = \frac{\varepsilon_{cu}}{c} \quad (4.27)$$

$$\varphi = \varphi_y + \frac{(M - M_y)}{(M_n - M_y)} (\varphi_u - \varphi_y) \quad (4.28)$$

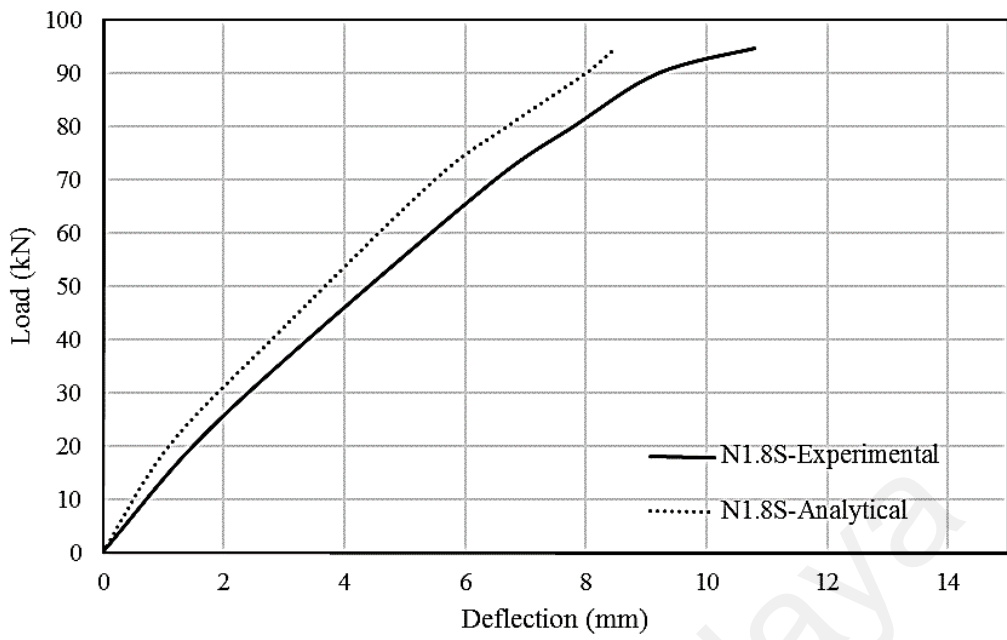
$$I_e = I_{cr} + (I_g - I_{cr}) \left(\frac{M_{cr}}{M_a} \right)^3 \quad (4.29)$$

Figure 4.72 portrays a graphical assessment of the experimental and analytical load-mid-span deflection curves. The relationship between the experimental and analytical results shows very good agreement for all specimens.

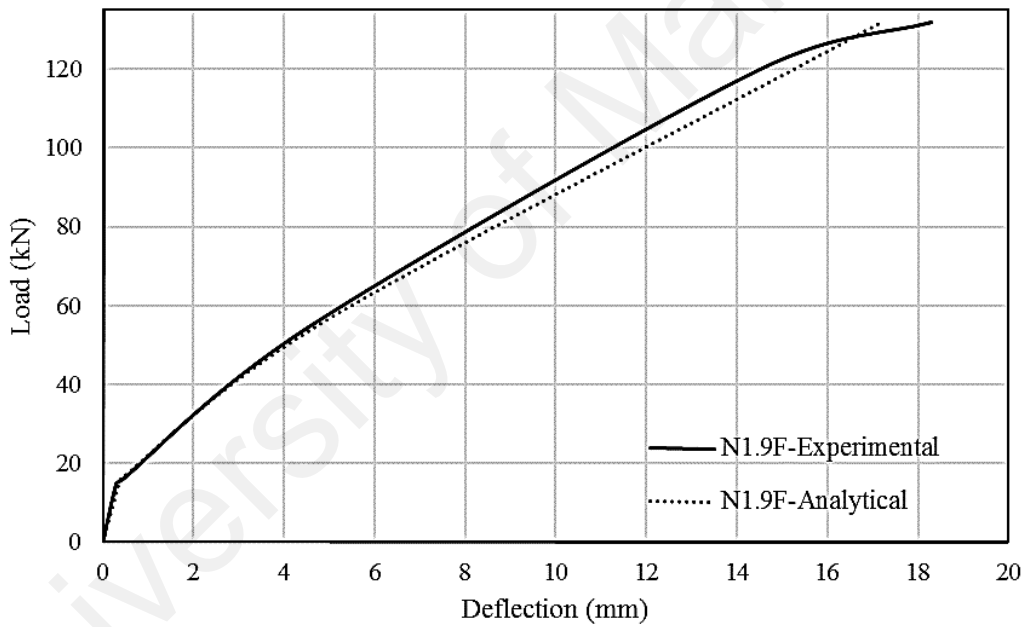


(a) N1.8F beam

Figure 4.72: Experimental and analytical load-deflection diagram of N1.8F, N1.8S, N1.9F and N1.9S beams

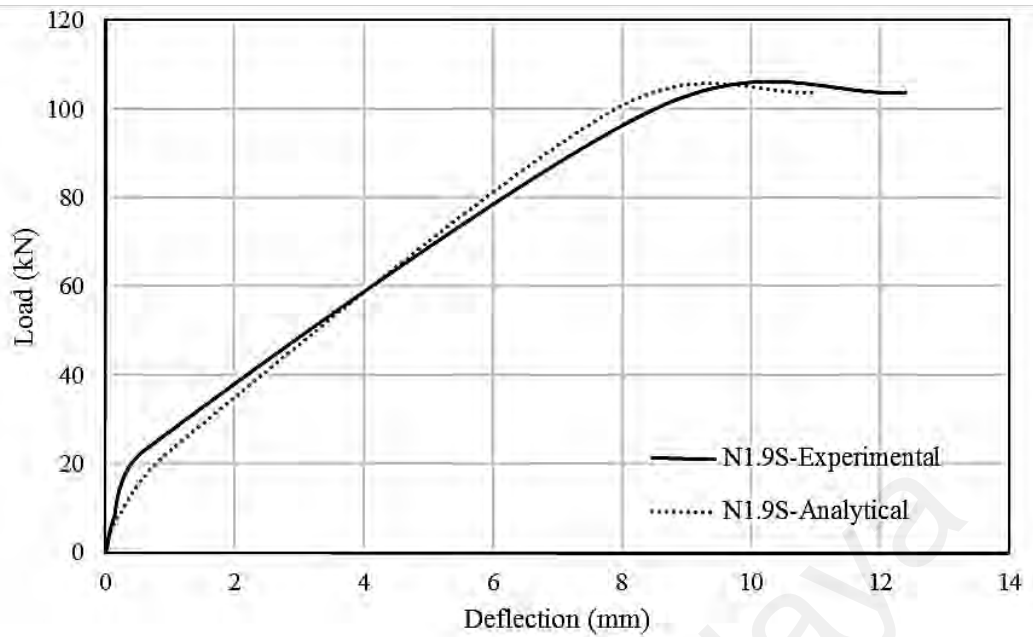


(b) N1.8S beam



(c) N1.9F beam

Figure 4.72, continued: Experimental and analytical load-deflection diagram of N1.8F, N1.8S, N1.9F and N1.9S beams



(d) N1.9S beam

Figure 4.72, continued: Experimental and analytical load-deflection diagram of N1.8F, N1.8S, N1.9F and N1.9S beams

4.3.3 Optimum Bond Length of NSM Bar

Figure 4.73 showed the bending moment diagram for four point bending load. To avoid failure of beam due to debonding it is suggested to extend the NSM bar until the point where the moment is equal to the moment resisting capacity of beam by internal bar (M_s) as shown in Figure 4.73 (Alam & Jumaat, 2012). Therefore, from the geometrical analysis, it is possible to find out the critical length of the NSM bar (L_c).

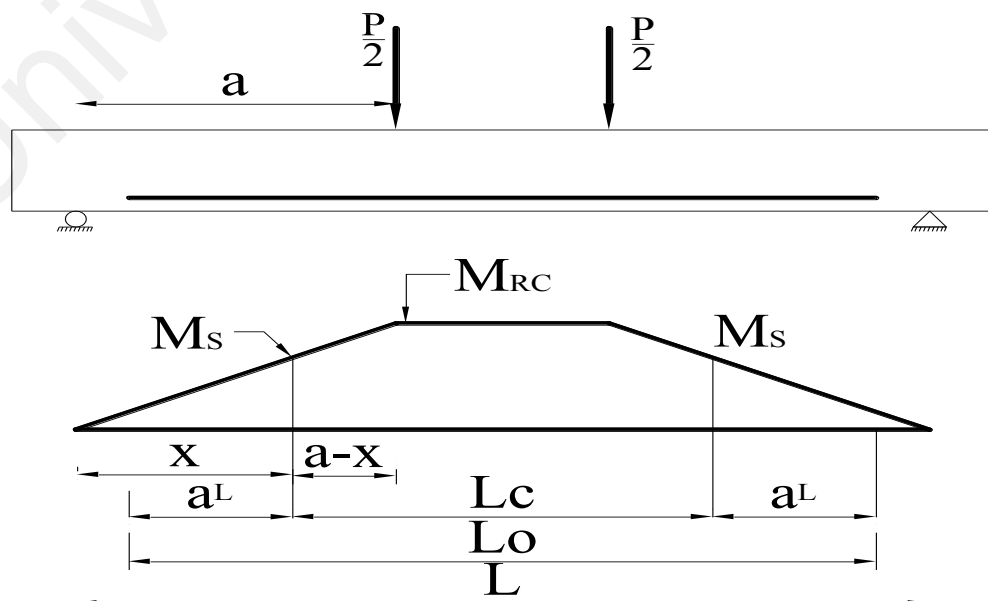


Figure 4.73: Bending moment diagram with optimum length of NSM bar

From the moment diagram in the Figure 4.73, it is possible to find out the value of x (equation 4.30 and 4.32).

$$\frac{x}{a} = \frac{M_s}{M_{RC}} \quad (4.30)$$

$$x = \frac{M_s a}{M_{RC}} \quad (4.31)$$

Thus the critical length of strengthening NSM bar (equation 4.31)

$$L_c = L - 2x = L - 2\left(\frac{M_s a}{M_{RC}}\right) \quad (4.32)$$

Where L_c = critical length of NSM bar, L = beam span, M_s = moment resisting capacity of beam by internal reinforcement, M_{RC} = Maximum moment resisting capacity of beam based on crushing of concrete and a is the shear span of the beam.

Anchorage length based on BS8110 can be added with the critical length to obtain the optimum length of the NSM bar for safety (equation 4.33).

$$L_o = L_c + 2a_L = L - 2\left(\frac{M_s a}{M_{RC}}\right) + 2a_L \quad (4.33)$$

4.3.4 Crack Width

According to ACI, allowable crack width in FRP reinforced structures is wider than that in steel reinforced concrete beams as FRP is a corrosion resistant material. The well-known Gergely and Lutz (1973) crack width equation is mainly used for steel reinforced structures and requires modification when applied to FRP reinforced members (Gao et al., 1998). The original Gergely-Lutz Eqs. (4.34) with SI units is as follows.

$$w = 0.0113\beta_h f_s^3 \sqrt{d_c A} \quad (4.34)$$

Here, the crack width w is expressed in mm. Wang and Salmon (1992) pointed out the fact that instead of stress in the tensile reinforcement, strain is the guiding factor that

varies proportionately with crack width. Based on this concept, the Gergely-Lutz equation has been modified by replacing the steel strain ε_s with the FRP strain, $\varepsilon_f = \frac{f_f}{E_f}$. A bond quality coefficient k_b is also introduced to the Eqs. (4.35)-(4.36), which becomes as follows.

$$w = \frac{2.2}{E_f} \beta_n k_b f_f \sqrt[3]{d_c A} \quad (4.35)$$

$$f_f = M_s \frac{n_f d (1 - k)}{I_{cr}} \quad (4.36)$$

Here, $K_b < 1$ (when FRP bond behavior is superior to steel); $K_b = 1$ (when FRP bond behavior is similar to steel); $K_b > 1$ (when FRP bond behavior is inferior to steel); $E_f =$ modulus of elasticity of FRP (MPa); $\beta_n =$ ratio of the distance between the neutral axis and the tension face to the distance between the neutral axis and the centroid of reinforcement; $f_f =$ stress level in FRP (MPa); $d_c =$ thickness of cover from the tension face to the center of the closest bar (mm); $A =$ the effective tension area of concrete around the main reinforcement divided by the number of bars (mm^2). The ACI committee recommends a value of 1.2 for deformed FRP bars, if K_b is unknown. Euro Code 2 (2004) has proposed an expression for calculating the characteristic value of crack width. The Eqs. (4.37) is as follows.

$$w_k = S_{r,max} (\varepsilon_{sm} - \varepsilon_{cm}) \quad (4.37)$$

Maximum crack spacing can be calculated from the following Eqs. (4.38),

$$S_{r,max} = 3.4c + 0.425k_1k_2 \frac{\phi}{\mu_s} \quad (4.38)$$

The difference between the mean steel and the concrete strain between cracks can be calculated using Eqs. (4.39),

$$\varepsilon_{sm} - \varepsilon_{cm} = \frac{\sigma_s}{E_s} - k_t \left[\frac{f_{ctm} A_{c,eff}}{E_s A_s} + \frac{f_{ctm}}{E_{cm}} \right] \quad (4.39)$$

Where, k_t = factor of load duration; $A_{c,eff}$ = effective area of concrete in tension; k_1 = bond coefficient; k_2 = type of loading; ϕ = diameter of bar; μ_s = ratio of the internal steel reinforcement to the effective area of concrete in tension. In the updated Eurocode 2, the bond relationship is present only in the crack spacing formulation, in a simplified way by the coefficient k_l , while in the tension stiffening term ($\varepsilon_{sm} - \varepsilon_{cm}$) the concrete tensile strength appears and the surface type of bars is neglected (Ceroni & Pecce, 2009).

University of Malaysia

CHAPTER 5: ARTIFICIAL INTELLIGENCE TECHNIQUE

The contemporary systems are complex in nature and tough to predict the actual behavior. It is a real challenge to develop a precise prediction model even though the fundamental mechanics are known, since the solution is sometimes expensive due to its complex nature or the uncertainties involved into the system. To overcome this problem, soft computing technique provides an alternative solution. The concept of artificial intelligence began to materialize by Professor Lotfi Zadeh with his revolutionary fuzzy logic theory. The AI based solutions are simple, rapid but precise as it accommodates the prevalent imprecision of the real world. Therefore, AI technique helps in utilizing the allowance for imprecision, dubiety and fractional truth so that pliancy, robustness, cheaper resolution and improved rapport with realness can be achieved. Several soft computing techniques are popular such as fuzzy logic inference system, adaptive neuro fuzzy inference system (ANFIS), artificial neural network and genetic algorithm etc. The present research concentrates only on the Fuzzy Logic Expert System (FLES).

5.1 Fuzzy Logic Expert System (FLES)

Human being, unlike a conventional machine, can subconsciously address to any problem with all its features of ambiguity and uncertainty. Humans can acquire information through experience which might not be precise and could be qualitative or vague as they are able to reason, infer and deduce new knowledge. Professor Lotfi Zadeh, who is respected as the founder of fuzzy logic theory had developed fuzzy set theory. It can capture the uncertainty, linked with the human cognitive procedure, such as thinking and reasoning. This approach provides an inference morphology that allows imprecise human cognitive competences to be harnessed to knowledge based systems. It is intelligent to handle numerical data and linguistic knowledge concurrently by means

of membership function. The fuzzy set theory is the contributory part of FLES which is based on fuzzy *if-then* rules and fuzzy *reasoning*. The fuzzy logic can be applied when:

- Organized information is available.
- A theoretical model is undiscovered or irresolvable.
- The method is significantly non-linear.
- There is deficiency of accurate sensor data.
- It is applied in generic decision-making problems.

Possible difficulties in applying fuzzy logic arise from the following:

- If knowledge is subjective.
- For high dimensional inputs, the increase in the required number of rules is exponential.
- If the expert feels any difficulties such as: structuring the knowledge properly, too aware of their expertise or if they try to hide knowledge etc.

Fuzzy logic is considered as one of the influential technologies in the embedded microcontroller of different processing plant, machine, electronic equipment, computer chips; even NASA operated automated space docking using this technique. It is also used for navigation of robots and auto focusing of cameras.

5.2 Basic Theory of FLES

Fuzzy set theory is the basic behind the fuzzy logic. Zadeh (1965) mentioned it as a broad view of the classical set theory and the classical logic is also known as Boolean logic, crisp logic or binary. As the fuzzy set is developed from the generalization of the classical one, it can be said that the theory of classical set is a subset of the fuzzy sets theory. In another sense, theory of classical set comprises partial event of the more usual fuzzy set theory. Unlike the “crisp logic”, which is operated with binary logic, fuzzy

logic variables are not constrained within a clearly defined boundary of the range 0 and 1.

Fuzzy subset can be distinguished by a membership function (MF) that is equal to the identity function of a classical set. To understand the fuzzy set concept let us work out an example related with hot temperature ($^{\circ}\text{C}$). To detect whether the temperature (x) is either a member or non-member of the set 'hot' (A), thus the membership $\mu_A(x)$ of x into A is given by:

$$\mu_A(x) = 1 \text{ if } x \text{ is totally in } A;$$

$$\mu_A(x) = 0 \text{ if } x \text{ is not in } A;$$

$$0 < \mu_A(x) < 1 \text{ if } x \text{ is partly in } A.$$

Hot temperature might be expressed as 'temperature more than 40°C '. This argument can be stated in the structure of a classical set as *hot temperature* = $\{x|x \geq 40\}$. In Figure 5.1, it is possible to see the sharp limit enforced by the crisp sets. However, in the fuzzy set approach, the idea of degree of membership is employed which makes the provision to exist any value between 0 and 1. A fuzzy set A of a universe of discourse X (the limit over which the varying extents) is categorized by a membership function $\mu_A(x): X \rightarrow [0,1]$ which connects with each element x of X a number $\mu_A(x)$ in the interval $[0, 1]$, with $\mu_A(x)$ representing the degree of membership of x in A . Figure 5.2 displays fuzzy sets with a degree of membership that allows fuzzy boundaries to be defined.

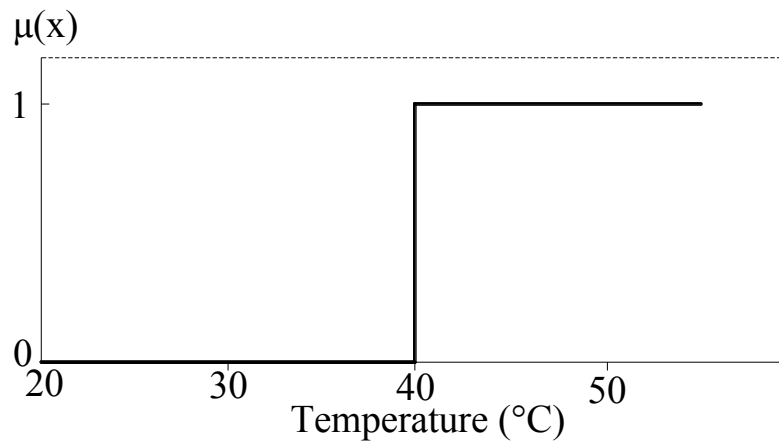


Figure 5.1: Crisp set for hot temperature

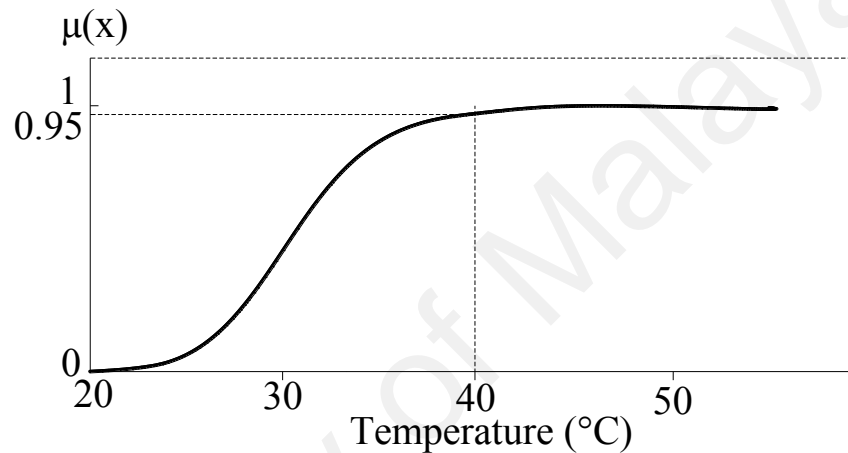


Figure 5.2: Fuzzy set for hot temperature

The MF curve describes the way that every single point in the input space is represented to a membership value between 0 and 1. The grade of membership is expressed as the degree of belonging of an element to a particular set. The input space is sometimes referred to as the universe of discourse (Shukla, 2000; Zadeh, 1965). The MF is typically symbolized by μ_A . For a part x of X , the value $\mu_A(x)$ is termed as the membership degree of x in the fuzzy set. The membership degree $\mu_A(x)$ quantifies the grade of membership of the element x to the fuzzy set. The values between 0 and 1 characterize fuzzy members, which belong to the fuzzy set only partially. The Fuzzy Logic includes 11 built-in membership functions. These 11 functions are, in turn, built from several basic functions: piecewise linear functions, the Gaussian distribution function, the sigmoid curve, and quadratic and cubic polynomial curves.

The memberships with piecewise linear function are the simplest. Among the categories triangular function is mostly used due to its simplicity and rigorousness. Basically, this choice of the membership function depends on the nature of the work (Zhao & Bose, 2002).

Figure 5.3 and Figure 5.4 showed the typical triangular and trapezoidal MF for better understanding of their characteristics. A triangular MF is described in Figure 5.3 by three parameters a , b and c given by the expressions in equation 5.1; where the parameters a and c locate the feet of the triangle and the parameter b locates the peak.

$$f(x, a, b, c) = \max \left\{ \min \left(\frac{x-a}{b-a}, \frac{c-x}{c-b} \right), 0 \right\} \quad (5.1)$$

A trapezoidal MF is described in Figure 5.4 by four parameters a , b , c and d given by the expressions in equation 5.2; where the parameters a and d locate the feet of the trapezoid and b and c locate the shoulder.

$$f(x; a, b, c, d) = \max \left\{ \min \left(\frac{x-a}{b-a}, 1, \frac{d-x}{d-c} \right), 0 \right\} \quad (5.2)$$

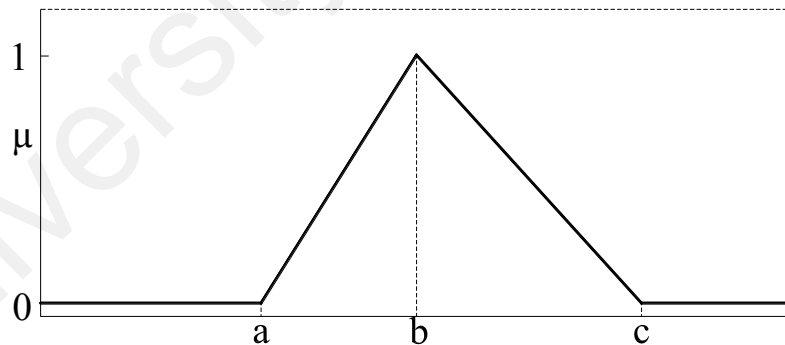


Figure 5.3: Triangular membership function for input variables

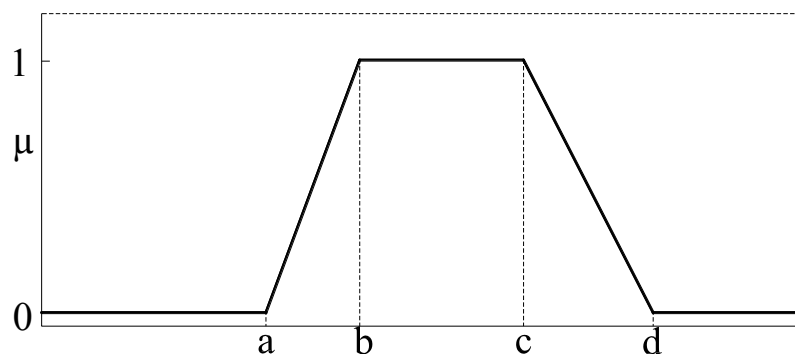


Figure 5.4: Trapezoidal membership function for input variables

Fuzzy logic approach can be subdivided into two categories: a) model based and b) knowledge based approach. The model based method refers to the development of a theoretical model supported by gathering of data, and quantification of the data into numerals to match the output with a target. The second one is knowledge based approach which is depicted in the flow diagram of Figure 5.5; where input is needed for building a hypothesis from the expert's opinion either in linguistic terms or in number. In the current study, this approach has been used where the real experimental observation is used as the expert knowledge to determine the relationship which affects the results.

There are three principal types of fuzzy system, namely:

- i. Mamdani fuzzy system: This system is also recognized as the linguistic fuzzy system. This system is appropriate for human input and it achieved widespread acceptance due to its intuitive characteristics.
- ii. Singleton Fuzzy system: This system simplifies the defuzzification process of a linguistic system by limiting the output to a singleton membership function. There is no numerical integration in this process which reduces the computation time for evaluation and learning of fuzzy system.
- iii. Takagi-Sugeno Fuzzy system: This system has the similarity like Mamdani approach in many aspects. The most related parts are the first two operations where the inputs are fuzzified and applied by the operator. However, the basic difference exists in their output membership functions where the Takagi-Sugeno is either constant or linear. This technique is computationally efficient and good for mathematical analysis. It performs well with the adaptive and optimized techniques.

In this research the basic Mamdani type fuzzy logic expert system (FLES) is considered which basically comprises of four principal components. They are: (1) Fuzzification – which takes crisp numeric inputs and converts them into the fuzzy form needed by the decision-making logic, (2) Rule base – which holds a set of *if-then* rules, that quantify the knowledge that human experts have amassed about solving a specific problem, (3) Inference – which creates the control actions according to the information provided by the fuzzification module and by applying knowledge, and (4) Defuzzification – which calculates the actual output, i.e. converts fuzzy output into a precise numerical value (crisp value).

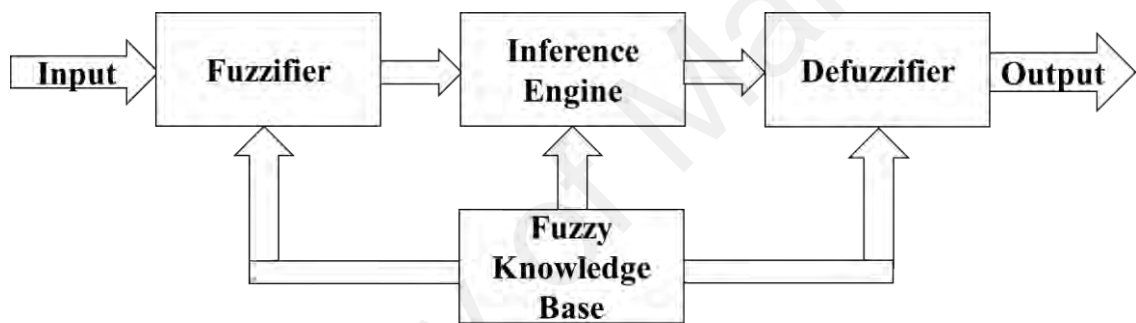


Figure 5.5: Flow chart of knowledge based approach

5.2.1 Fuzzification

The fuzzification takes crisp numeric inputs and converts them into the fuzzy form needed by the decision-making logic. The first task in fuzzification interfaces is the selection of input and output variables. After that all input and output numeric variables have to be defined in linguistic terms such as low, medium, high and so on. Subsequently, membership functions for all input and output variables have to be formed. The central concept of fuzzy set theory is membership functions, which represent numerically to what degree an element belongs to a set. A membership function is typically a curve that converts the crisp numerical value of input variable into the fuzzy number within a range from 0 to 1, representing the belongingness of the input to a fuzzy set. There are different forms of membership functions such as triangle,

trapezoid, and Gaussian functions. The selection of membership functions and their formations are based on system knowledge, expert's appraisals, and experimental conditions.

5.2.2 Rule base

The rule base holds a set of *if-then* rules that quantify the knowledge that human experts have amassed about solving a specific problem. Moreover, fuzzy rules are the heart of the fuzzy expert system which determines the relationship between input-output of the model. This performs as a source to the decision making logic. Moreover, it consists of a data base and a rule base. In the fuzzy knowledge base system, knowledge is represented by *if-then* rules. Fuzzy rules consist of two parts: an antecedent part stating conditions on the input variables and a consequent part describing the corresponding values of output variables. For instance, in the case of three inputs P, Q, and R, and one output Z, which have the linguistic variables of very low, medium, and low medium for P, Q and R respectively and medium for Z, then development of fuzzy inference rules can be demonstrated as follows:

If P is very low and Q is medium, and R is low medium then Z is medium.

5.2.3 Inference

The Inference creates the control actions according to the information provided by the fuzzification module and by applying knowledge. It plays a central role in a fuzzy logic model due to its ability to create human decision making and deduce fuzzy control actions as per the information provided by the fuzzification module by applying knowledge about how to control the process best. Three types of fuzzy inference systems (FIS) have been widely employed in various applications: Mamdani, Sugeno and Tsukamoto fuzzy models (Cevik, 2011). The differences between these three fuzzy inference systems are due to the consequences of their fuzzy rules, and thus their

aggregation and defuzzification procedures differ accordingly (Jang et al., 1997). The Mamdani-type FIS uses the technique of defuzzification of a fuzzy output and has output membership functions (Mamdani & Assilian, 1975). This FIS is widely accepted for capturing expert knowledge (Kaur & Kaur, 2012). The Mamdani-type FIS describes the expertise in more intuitive, and more human like manner. Most commonly, the Mamdani max-min fuzzy inference mechanism is used because it ensures a linear interpolation of the output between the rules.

For instance, in case of tree-inputs and single-output fuzzy inference system, it can be shown in Figure 5.6 below.

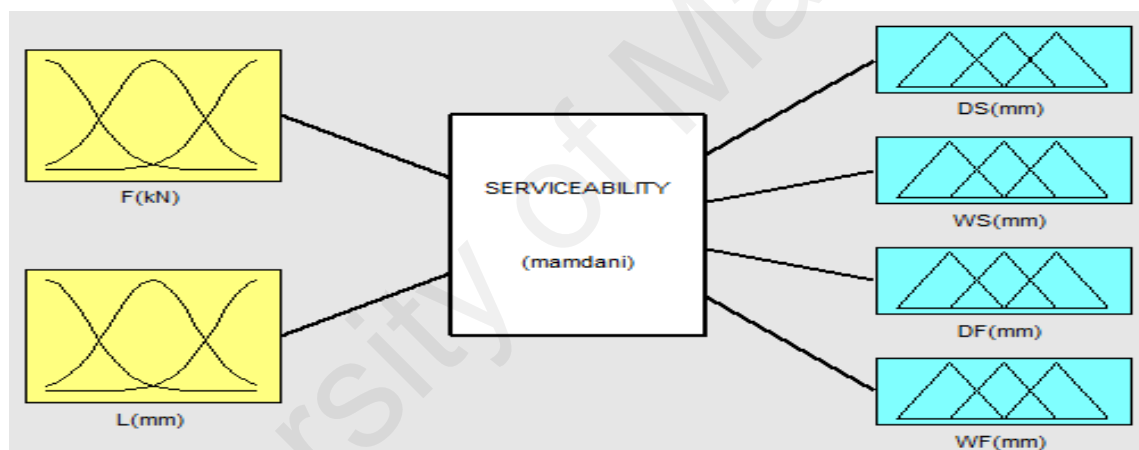


Figure 5.6: Fuzzy inference mechanisms

where applied load (F) and rod length (L) are in input side and deflection for steel bar strengthened beams (DS), crack width for steel bar strengthened beams (WS), deflection for CFRP bar strengthened beams (DF) and crack width for CFRP bar strengthened beams (WF) are on output side.

5.2.4 Defuzzification

The defuzzification calculates the actual output, i.e. converts fuzzy output into a precise numerical value (crisp value). The conversion of a fuzzy set to a single crisp output on which action can be taken is called defuzzification. The defuzzification

interface combines the conclusions reached by the decision-making logic and converts the fuzzy output into a precise crisp numeric value. There are several methods of defuzzification, such as centroid, center of sum, mean of maxima and left-right maxima. Most commonly, the center of gravity (centroid) defuzzification method is used, since this operator assures a linear interpolation of the output between the rules.

5.3 Serviceability Prediction Model Using FLES

5.3.1 FLES Model Development

The Fuzzy Logic Expert System (FLES) offers an effective solution for a simple and rapid, yet reliable and accurate alternative method to predict serviceability of NSM strengthened structures as it depends on expert knowledge. Other artificial intelligence techniques such as artificial neural networks and genetic algorithms require extensive experimental results to optimize parameters, which is a challenging, labor intensive and time consuming process. Conversely, FLES uses expert appraisals as well as a logical system closer to human reasoning rather than extensive experimental results.

The basic configuration of a FLES comprises of four principal components (Passino et al., 1998). They are known as fuzzification, rule base, inference and defuzzification.

In the FLES model created for this study there are two input parameters, applied load (F) and rod length (L). From the laboratory investigation it has been experienced that these two parameters could significantly influence four output parameters: deflection for steel bar strengthened beams (DS), crack width for steel bar strengthened beams (WS), deflection for CFRP bar strengthened beams (DF) and crack width for CFRP bar strengthened beams (WF) (Table 2). Actually, the input parameters of F and L might be less or more in simulating the intensity and magnitude of load and rod length. The load varied within the range from 0 to 100 kN and the rod length varied between 1600 mm and 1800 mm. In this instance, eleven linguistic variables for Load (F) and four

linguistic variables for Length (L) were considered. For fuzzification, the input variable F was given eleven possible linguistic variables, namely very very low (VVL), very low (VL), low (L), High low (HL), low medium (LM), medium (M), high medium (HM), medium high (MH), high (H), very high (VH), and very very high (VVH), and for input variable L four linguistic variables were used, very low (VL), low (L), medium (M), and high (H). The linguistic variables used for the output variables were Level 1 to 12 for DS and DF, and Level 1 to 16 for WS and WF, respectively. If more input variables were considered the fuzzy inference rules would become more complex and vice versa. Therefore, the number of input variables was reasonable to achieve suitable output from the proposed model. A Mamdani max-min inference approach and the center of gravity defuzzification method were applied as these operators assure a linear interpolation of the output between the rules (Hossain et al., 2012). Figure 4 displays the fuzzy inference system in the case of two inputs and four outputs. The units of the input and output variables are kN for F and mm for L, DS, WS, DF and WF. A total of 44 fuzzy inference rules were formed based on expert knowledge and past experience. Some of the rules are shown in Table 5.1. An example is illustrated here concerning how the values of the last four columns of fuzzy inference rules (Table 5.1) are determined.

Rule 1: If applied force (F) is very very low (VVL), and rod length (L) is very low (VL) then deflection for steel bar strengthened beams (DS) is level 1 (L1), crack width for steel bar strengthened beams (WS) is level 1 (L1), deflection for CFRP bar strengthened beams (DF) is level 1 (L1), and crack width for CFRP bar strengthened beams (WF) is level 1 (L1).

Rule 36: If applied force (F) is high (H), and rod length (L) is high (H) then deflection for steel bar strengthened beams (DS) is level 7 (L7), crack width for steel bar strengthened beams (WS) is level 8 (L8), deflection for CFRP bar strengthened

beams (DF) is level 9 (L9), and crack width for CFRP bar strengthened beams (WF) is level 10 (L10).

Table 5.1: Fuzzy inference rules

Rule no.	Input variables		Output variables			
	<i>F</i>	<i>L</i>	<i>DS</i>	<i>WS</i>	<i>DF</i>	<i>WF</i>
1	VVL	VL	L1	L1	L1	L1
....
7	VL	M	L2	L1	L2	L1
....
12	L	H	L2	L2	L3	L3
....
18	M	L	L4	L7	L5	L8
....
25	VHM	VL	L6	L9	L9	L12
....
36	H	H	L7	L8	L9	L10
....
44	VVH	H	L9	L8	L10	L11
There are 44 fuzzy inference rules. Rule no 1, 7, 12, 18, 25, 36 and 44 have been shown in this table for example.						

There is a level of membership for each linguistic word that applies to an input variable. Fuzzifications of the input variables were made by using the following equations 5.3 to 5.8:

$$F(i_1) = \begin{cases} i_1; & 0 \leq i_1 \leq 100 \\ 0; & \text{otherwise} \end{cases} \quad (5.3)$$

$$L(i_2) = \begin{cases} i_2; & 1600 \leq i_2 \leq 1900 \\ 0; & \text{otherwise} \end{cases} \quad (5.4)$$

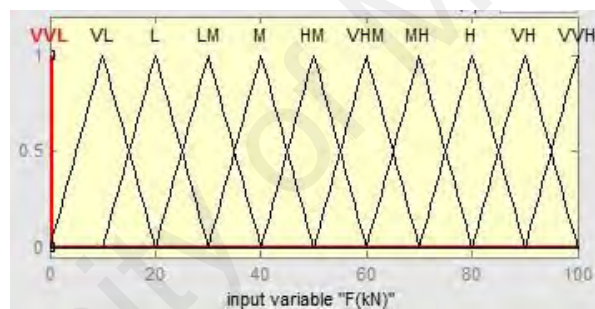
$$DS(o_1) = \begin{cases} o_1; & 0 \leq o_1 \leq 16 \\ 0; & \text{otherwise} \end{cases} \quad (5.5)$$

$$WS(o_2) = \begin{cases} o_2; & 0 \leq o_2 \leq 0.64 \\ 0; & \text{otherwise} \end{cases} \quad (5.6)$$

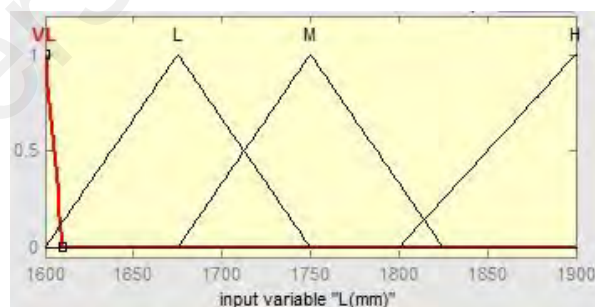
$$DF(o_3) = \begin{cases} o_3; & 0 \leq o_3 \leq 16 \\ 0; & \text{otherwise} \end{cases} \quad (5.7)$$

$$WF(o_4) = \begin{cases} o_4; & 0 \leq o_4 \leq 0.64 \\ 0; & \text{otherwise} \end{cases} \quad (5.8)$$

Where, i_1 is the first input variable load (F), i_2 is the second input variable length (L) and o_1 , o_2 , o_3 and o_4 are the output variables DS , WS , DF and WF respectively. Prototype triangular fuzzy sets for the fuzzy variables were set up using MATLAB Fuzzy Toolbox. Among the many membership functions, triangular, trapezoidal, piecewise linear and Gaussian are those mostly used. These membership functions are chosen based on the researcher's past experience and ease of application. Moreover, the triangular membership functions provide a faster and easier solution, since in the symmetric condition, the center of gravity is at the apex of the triangle, which makes computational calculation easier (Mendel, 1995). The membership values obtained from the above formulas are shown in Figure 5.7 for two input variables.



a) Input variable “F (kN)”



b) Input variable “L (mm)”

Figure 5.7: Membership functions of input variables a) load – F (kN) and b) NSM length – L (mm)

To demonstrate the fuzzification process, linguistic expressions for the triangular membership functions can be described using following equation 5.9:

$$\mu_{triangle}(x, c_1, c_2, c_3) = \left\{ \begin{array}{ll} 0; & x \leq c_1 \\ \frac{x - c_1}{c_2 - c_1}; & c_1 \leq x \leq c_2 \\ \frac{c_3 - x}{c_3 - c_2}; & c_2 \leq x \leq c_3 \\ 0; & x \geq c_3 \end{array} \right\} \quad (5.9)$$

Where, x is the input and output variable; c_1 , c_2 and c_3 are the coefficients of membership functions.

Linguistic expressions and membership functions of load (F) and length (L) obtained from the developed rules and above formula (Eq. 5.10, 5.11) for HM and H are presented as follows:

$$\mu_{HM}(F) = \left\{ \begin{array}{ll} \frac{i_1 - 40}{50 - 40}; & 40 \leq i_1 \leq 50 \\ \frac{60 - i_1}{60 - 50}; & 50 \leq i_1 \leq 60 \\ 0; & i_1 \geq 60 \end{array} \right\} \quad (5.10a)$$

$$\mu_{HM}(F) = \{0/40 + 0.5/45 + 1/50 + \dots + 0.5/55 + 0/60\} \quad (5.10b)$$

$$\mu_H(L) = \left\{ \begin{array}{ll} 0; & i_2 \leq 1800 \\ \frac{i_2 - 1800}{1900 - 1800}; & 1800 \leq i_2 \leq 1900 \\ 1; & i_2 \geq 1900 \end{array} \right\} \quad (5.11a)$$

$$\mu_H(L) = \{0/1800 + 0.5/1850 + \dots + 1/1900\} \quad (5.11b)$$

Similarly, the linguistic expressions and membership functions of other parameters could be calculated.

Rajasekaran and Pai (2011) has reported that in many conditions, for a system whose output is fuzzy, it can be simpler to receive a crisp decision if the output is represented as a single scalar quantity. At this stage, the output membership values are multiplied by their corresponding singleton values and then are divided by the sum of the membership values to calculate $Output^{crisp}$ as follows (equation 5.12):

$$Output^{crisp} = \frac{\sum_i b_i \mu(i)}{\sum_i \mu(i)} \quad (5.12)$$

Where, b_i is the position of the singleton in the i th universe, and $\mu(i)$ is equal to the firing strength of the truth values of rule i .

5.3.2 Numerical Error Determination

The predictive ability of the developed system was also investigated using mathematical and statistical methods. In order to establish the relative error (ε) of the structure, the subsequent equation 5.13 was used:

$$\varepsilon = \sum_{i=1}^n \left| \frac{y_i - \hat{y}_i}{y_i} \right| \frac{100\%}{n} \quad (5.13)$$

In addition, the goodness of fit (η) of the predictive system was calculated as follows (equation 5.14):

$$\eta = \sqrt{1 - \frac{\sum_{i=1}^n (y_i - \hat{y}_i)^2}{\sum_{i=1}^n (y_i - \bar{y})^2}} \quad (5.14)$$

Where, n is the number of interpretations, y_i is the measured value, \hat{y}_i is the predicted value, and \bar{y} is the mean of measured values. The relative error provides the difference between the predicted and measured values and in a perfectly accurate

system that should be equal to zero. The goodness of fit provides the ability of the developed system and its highest value is 1.

5.3.3 Results of FLES Model

The fuzzy logic expert model has been developed based on the input variables applied load (F) and rod length (L). The operation of the developed fuzzy logic model is shown in Figure 9. The final outputs – deflection for steel bar strengthened beams (DS), crack width for steel bar strengthened beams (WS), deflection for CFRP bar strengthened beams (DF) and crack width for CFRP bar strengthened beams (WF) of the fuzzy logic system – are verified using MATLAB Fuzzy Toolbox (Figure 9). The output results can be verified by changing the input values in the MATLAB® rule viewer. For example, if the applied load (F) is 50 kN and the rod length (L) is 1900 mm, then all forty-four fuzzy rules are assessed concurrently to determine the fuzzy outputs deflection for steel bar strengthened beams (DS), crack width for steel bar strengthened beams (WS), deflection for CFRP bar strengthened beams (DF), and crack width for CFRP bar strengthened beams (WF), respectively. However, some of the rules remain obsolete as ‘fuzzy and’ function has been used in the antecedent part of the fuzzy rules and they do not produce any output fuzzy set. The outputs of the active fuzzy rules are then aggregated to obtain a final output fuzzy set, which is finally defuzzified using the center of gravity defuzzification method to create the crisp outputs (DS) of 3 mm, WS of 0.2 mm, DF of 3.5 mm and WF of 0.256 mm, respectively, as shown in Figure 5.8.

Using MATLAB, the fuzzy control surfaces were developed as shown in Figure 5.9 and Figure 5.10. These figures visually depict how the fuzzy logic operates dynamically over time. The images show the relationship between load (F) and length (L) on the input side and deflection and crack width on the output side for steel and FRP bars. The surface plots shown in Figure 5.9 and Figure 5.10 depict the impact of load (F) and

length (L) on deflection and crack width. The plots were used to verify the rules and the membership functions and to see if they are appropriate and whether modifications are necessary to improve the output.

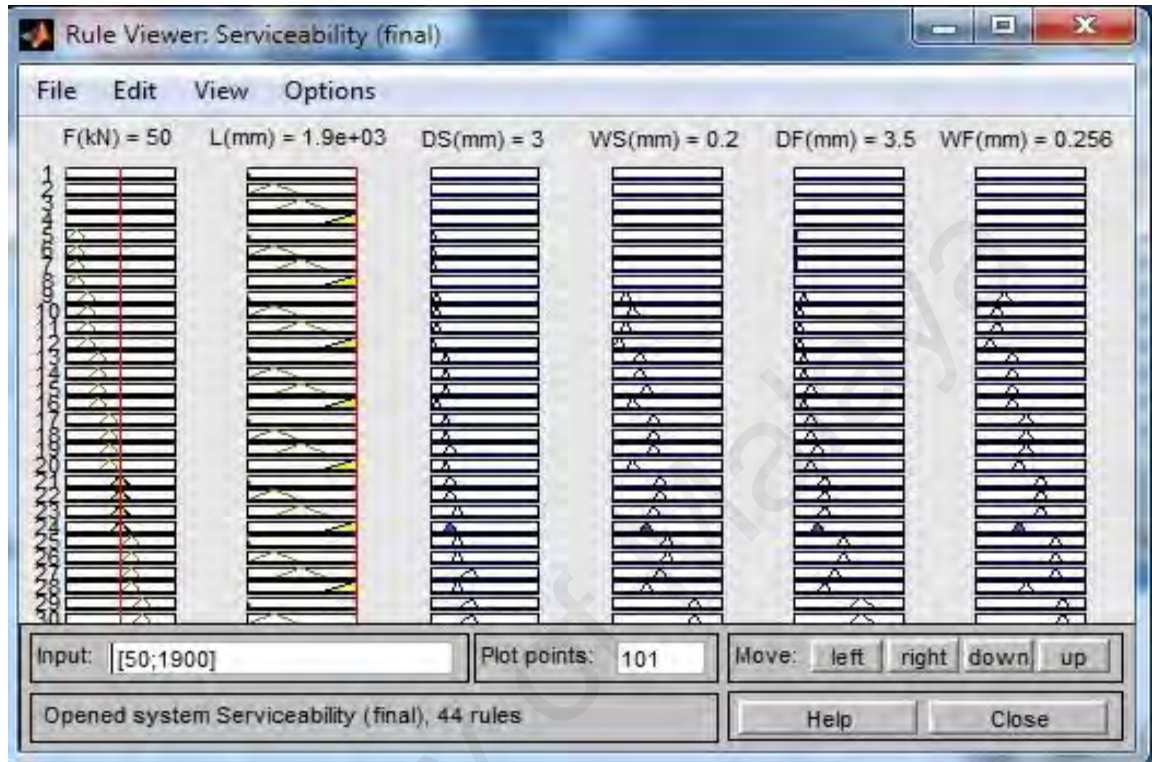
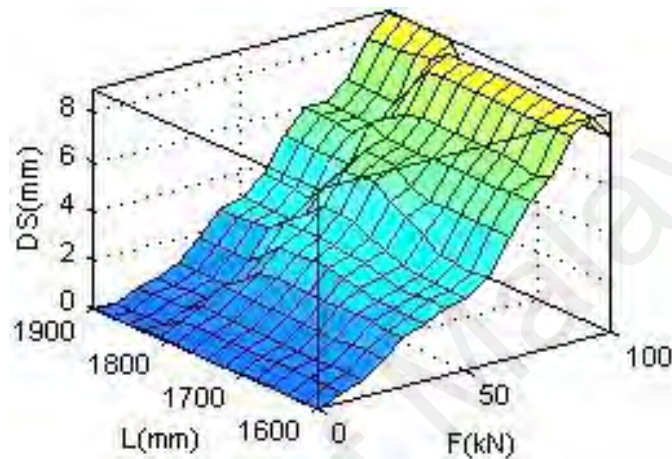


Figure 5.8: Rule viewer of fuzzy inference system

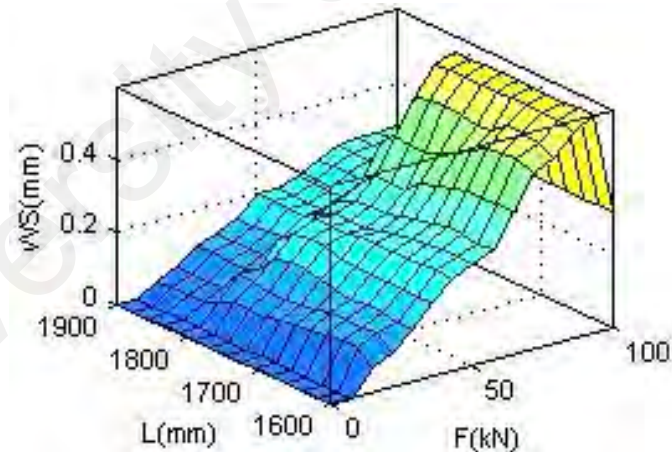
In the present study, F from 0-100 kN and L from 1600-1900 mm were used as input and deflection and crack width from 0-16 mm and 0-0.64 mm, respectively, were used as output for both types, steel bar (Type A) and CFRP bar (Type B), to develop the fuzzy model. After developing the model, the deflection and crack width for both types were predicted from the control surfaces (Figure 5.9 and Figure 5.10).

The surface plot in Figure 5.9(a) shows that as the applied load (F) increases, there is a concomitant increase in deflection (D) as expected. Deflection increases slowly at first as applied load increases until a certain value and reaches its peak when the applied load and bar length are both at their maximum levels, although the effect is less prominent at the higher levels of bar length since the stiffness of the beam becomes higher. Consequently, deflection is lower for the lower levels of applied load and bar length,

which is as expected. It is, therefore, important to keep the load distribution at optimum levels to get minimal deflection, and bar length should be sufficient to maintain normal operating conditions. Similar patterns were also observed in the other surface plots. Thus, the developed fuzzy model can aid in the selection of significant input parameters and their required levels for RC elements to achieve a targeted level of serviceability.



(a) Deflection (DS)

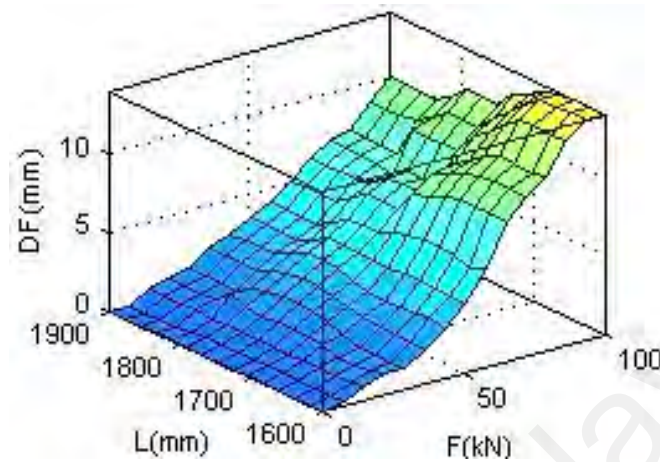


(b) Crack width (WS)

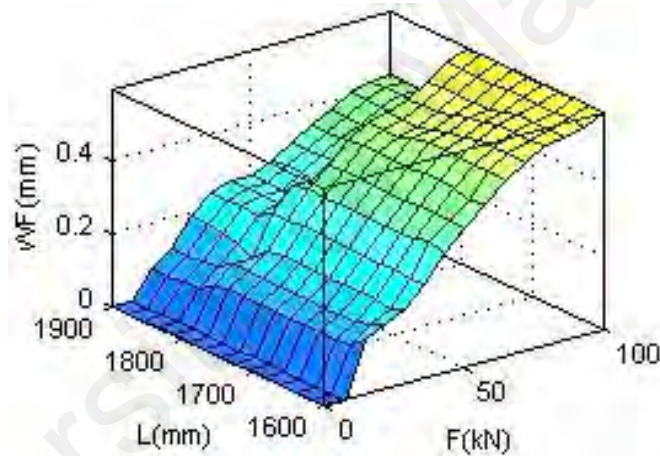
Figure 5.9: Control surfaces for steel bar

Using the input variables F as 50 kN and L as 1900 mm, the output values obtained from the developed fuzzy logic model for deflection and crack width in steel bar (Type A) and FRP bar (Type B) were DS as 3 mm, WS as 0.2 mm, DF as 3.5 mm and WF as 0.256 mm. The experimental values obtained for the same load condition and bar length were 2.946 mm, 0.192 mm, 4.1 mm, and 0.268 mm, respectively. However, it is worth

noting that this demonstration is limited in that if there are more than two inputs it becomes difficult to visualize the surface.



(a) Deflection (DF)

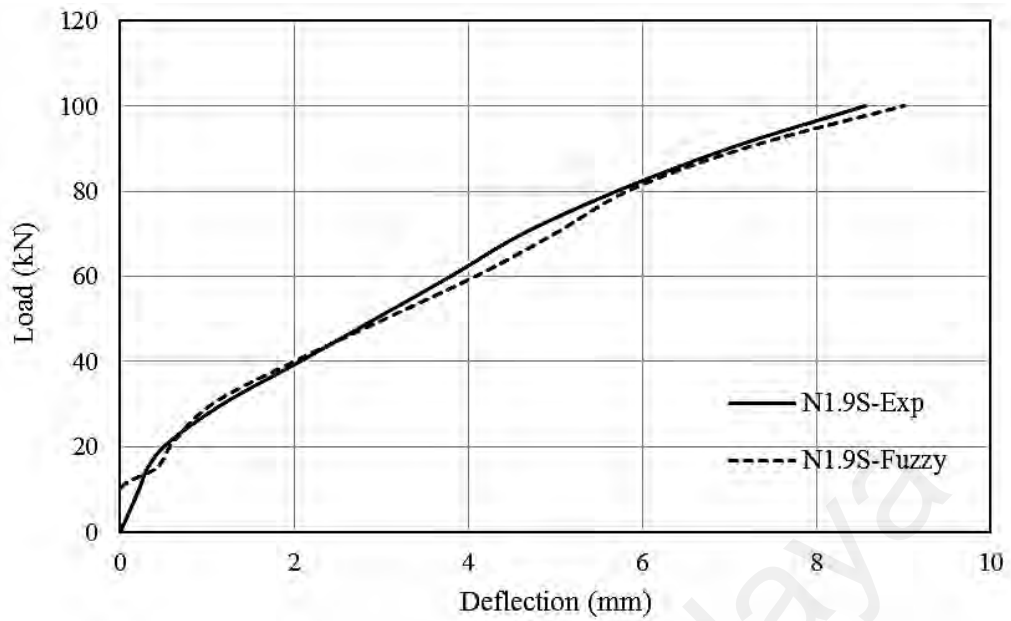


(b) Crack width (WF)

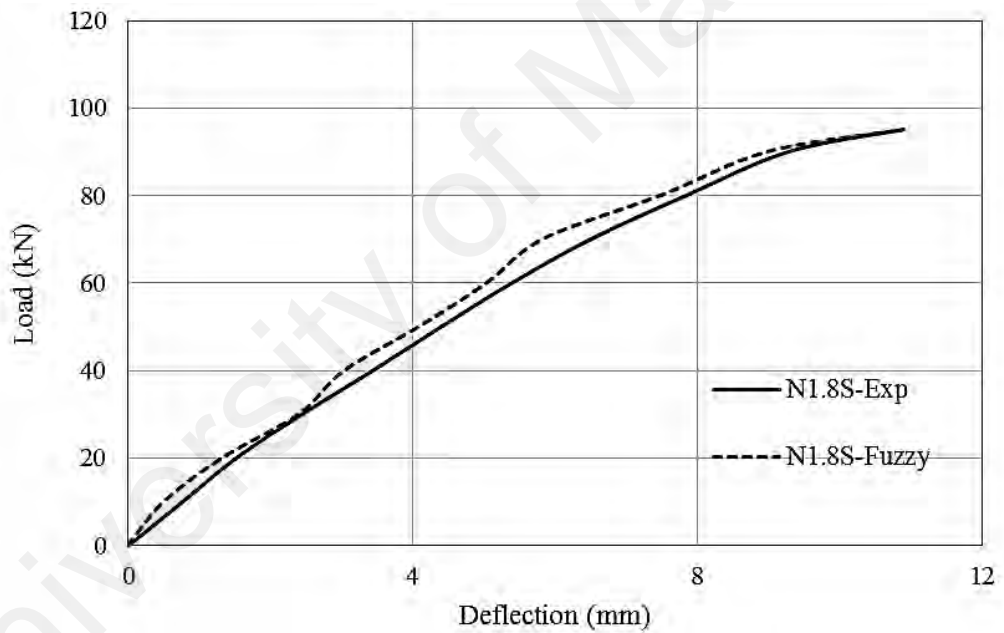
Figure 5.10: Control surfaces for CFRP bar

5.3.4 Model Validation

Figure 5.11 and Figure 5.12 display a comparison between the experimental and the FLES predicted output for the deflection of N1.9S, N1.9F, N1.8S and N1.8F beams. For NSM steel strengthened beams, the highest ultimate failure was around 100 kN, which is lower than the highest ultimate strength of NSM CFRP strengthened beams (around 130kN).



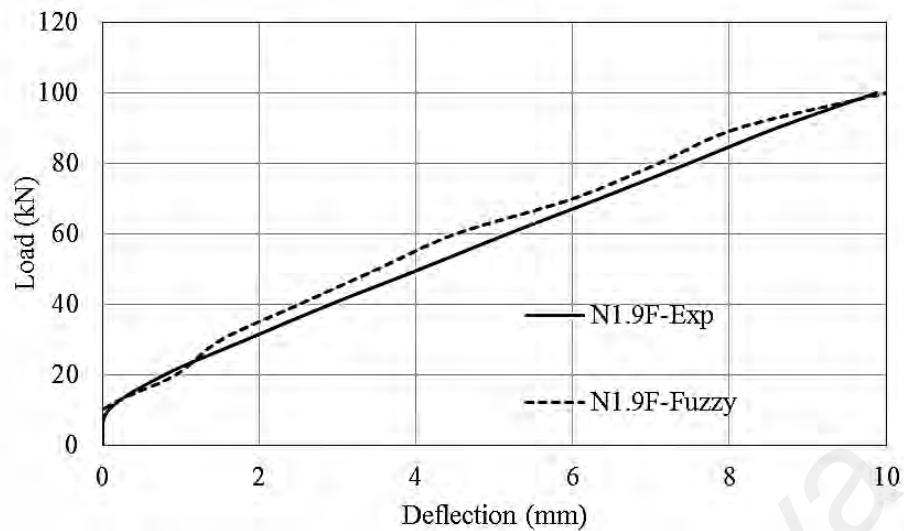
(a) N1.9S beam



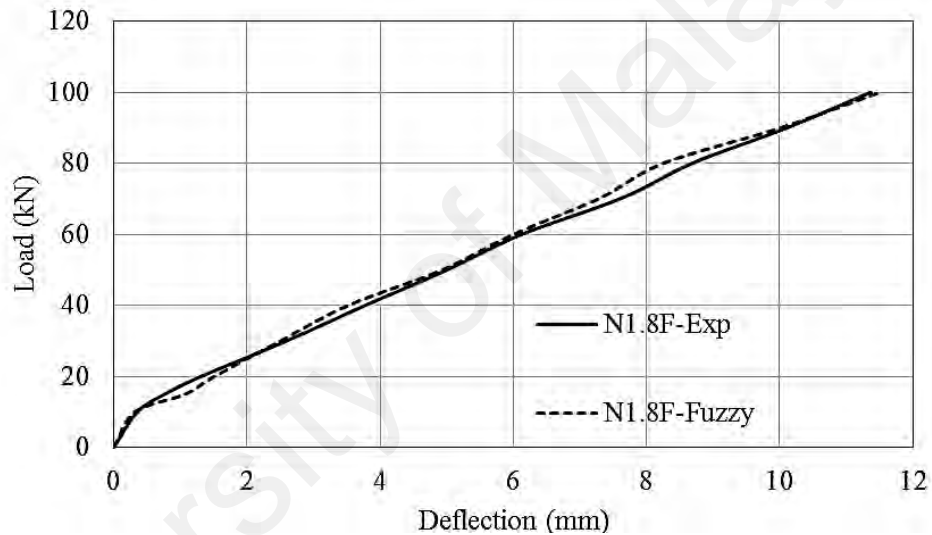
(b) N1.8S beam

Figure 5.11: Experimental and predicted load deflection graphs for NSM steel beams

For comparison purposes in order to maintain similarity and avoid complicating the input data for the FLES, the maximum load range was considered as 100kN for both steel and CFRP strengthened beams with 1800 mm and 1900 mm bonded length. From the figures it can be clearly seen that there is an good agreement between the experimental deflection values and the fuzzy predicted deflection output for these NSM strengthened beams.



(a) N1.9F beam



(b) N1.8F beam

Figure 5.12: Experimental and predicted load deflection graphs for NSM CFRP beams

This study uses limited experimental data to verify this model. It would be better if more data from other research works were used to validate the model. The variation in length is one of the important parameters in this test. However, only three types of length were used in this research to avoid the testing of huge experimental specimens in the laboratory. For precise work, more variations in length can help to increase the efficiency of the model. Basically, a small number of parameters and more membership functions provide greater accuracy when using a fuzzy mode.

CHAPTER 6: FINITE ELEMENT MODELLING

The finite element method (FEM) can be defined as a method of approximation to continuum problem which is divided into a finite number of interconnected parts or elements. The behavior of an element is specified with finite number of parameters. A displacement function is associated with each finite element. Each interlinked element is connected, directly or indirectly, to all other elements by means of shared interfaces, with nodes and/or borderline and/or surfaces. If every single element follows the same rule of the standard discrete problem, then the system will act as a complete one and its solution is finite. The behavior of a particular node in a structure can be revealed with the known stress-strain relationship of the material that constitutes the structure. The total set of equations describing the behavior of each node results in a series of algebraic equations best expressed in matrix notation.

6.1 Basic Steps of FEM

Two methods are applied in FEM, namely a) force or flexibility method and b) displacement or stiffness method. The first approach assumes that the forces are unknown and the equilibrium with other associated equations are used to develop the governing equations. The second approach assume that the displacement at the node is unknown. Another compatibility condition is that the element connected through a common node before loading will remain connected after loading with deformation. Hence, the governing equation in terms of displacement can be deduced from the equilibrium equation and the relating force to displacement. The following steps should be followed to solve any problem related with FEM:

Step 1: Discretize and Select the Element Types

In this step, the structure should be separated into an equivalent system of numerous

finite elements with linked nodes and a selection of most appropriate element type. There are several types of elements, namely a) primary line element (bar or truss and beam element); b) two dimensional element (triangular and quadrilateral) and c) tetrahedral and hexahedral brick element). If the geometry or loading are symmetric around an axis, then axisymmetric element is used which is developed by rotating a triangle or quadrilateral about a fixed axis.

Step 2: Select a Displacement Function

A suitable displacement function is chosen for each element. For a two-dimensional element, the displacement function is a function of the coordinates in its plane (say, the x-y plane).

Step 3: Define the Strain/Displacement and Stress/Strain Relationships

Stress-strain or strain-displacement are the important relations to derive the equation for each finite element; say, in the x direction we have strain ϵ_x related to displacement u by equation 6.1.

$$\epsilon_x = \frac{du}{dx} \quad (6.1)$$

Step 4: Derive the Element Stiffness Matrix and Equations

With direct equilibrium method the nodal force and displacement are obtained by the stiffness matrix and the corresponding element equation. Another simpler way is to use a work or energy method to form the stiffness matrix and equations for two- and three-dimensional elements. The principle of virtual work (using virtual displacements), the principle of minimum potential energy, and Castigliano's theorem are methods frequently used for the purpose of derivation of element equations. One more method named weighted residuals (popular is the Galerkin's method) are suitable for working up

the element equations. The method produces the similar results as the energy method. It is especially useful when a functional such as potential energy is not readily available. The weighted residual methods allow the finite element method to be applied directly to any differential equation.

The basic stiffness matrix (equation 6.2) is as follows (equation 6.3)

$$\begin{Bmatrix} f_1 \\ f_2 \\ f_3 \\ \vdots \\ f_n \end{Bmatrix} = \begin{bmatrix} k_{11} & k_{12} & k_{13} & \dots & k_{1n} \\ k_{21} & k_{22} & k_{23} & \dots & k_{2n} \\ k_{31} & k_{32} & k_{33} & \dots & k_{3n} \\ \vdots & & & & \vdots \\ k_{n1} & & & \dots & k_{nn} \end{bmatrix} \begin{Bmatrix} d_1 \\ d_2 \\ d_3 \\ \vdots \\ d_n \end{Bmatrix} \quad (6.2)$$

$$\{f\} = [k]\{d\} \quad (6.3)$$

Where $\{f\}$ is the vector of element nodal forces, $[k]$ is the element stiffness matrix, and $\{d\}$ is the vector of unknown element nodal degrees of freedom or generalized displacements, n .

Step 5: Assemble the Element Equations to Obtain the Global or Total Equations and Introduce Boundary Conditions.

The discrete element equations produced in step 4 can be combined together by means of superposition method (direct stiffness method) which originated from nodal force equilibrium to get the overall equations for the entire structure. The matrix format of the concluding accumulated or global equation is equation 6.4

$$\{F\} = [K]\{d\} \quad (6.4)$$

Step 6: Solve for the Unknown Degrees of Freedom (or Generalized Displacements).

Modifying the equation 6.4 with changing boundary condition, a new set of equation (equation 6.5) can be developed along with the corresponding matrix as

$$\begin{Bmatrix} F_1 \\ F_2 \\ F_n \end{Bmatrix} = \begin{bmatrix} K_{11} & K_{12} & K_{1n} \\ K_{21} & K_{22} & K_{2n} \\ K_{n1} & K_{n2} & K_{nn} \end{bmatrix} \begin{Bmatrix} d_1 \\ d_2 \\ d_n \end{Bmatrix} \quad (6.5)$$

Where n is total number of unknown nodal degrees of freedom of the structure. These equations can be solved for the d 's by using an elimination method (such as Gauss's method) or an iterative method (such as Gauss-Seidel's method).

Step 7: Solve for the Element Strains and Stresses

Significant secondary numbers of strain and stress (or moment and shear force) can be attained for the structural stress-analysis problem.

Step 8: Interpret the Results

The final aim is to understand and explore the outcomes for use in the design/analysis. To analyze or design a structure, it is very important to identify the location maximum stress and deformation.

6.2 FEM Model Construction of CEBNSM-B beams

Numerical study was performed with the Finite Element Method (FEM). An FEM software named ABAQUS[®] was used to develop a three dimensional (3D) model for analyzing the control and strengthened RC beam. The numerical study was conducted to validate the experimental results in terms of load-deflection behavior and strain distribution across the concrete-CFRP substrate. The numerical output will be investigated to assess the flexural behavior and other important parameters to assess the efficacy of the strengthening.

The RC beam models consisted of the similar geometric attribute, material characteristics, and boundary conditions identical to the experimented simply supported

RC beam. Two rigid steel supports (one is a hinge and the other is a roller support) were placed at bottom to transmit the applied loads and decrease the stress concentration. Concrete plastic behavior in compression was defined by means of the renowned Saenz, 1964 model. Concrete damage plasticity model was applied to simulate the perfect inelastic damage behavior of concrete in tension and compression together. The descending branch of concrete stress-strain curve subjected to tension was utilized to explain the tension stiffening, strain-softening, and reinforcement (RF) interaction with concrete. Elastic–brittle failure behavior was considered for the NSM CFRP strengthening bar in tension as well as the zero strength and stiffness in compression. An interface was considered between the NSM and filling epoxy materials as well as between the steel reinforcement and concrete. Consistent constitutive models relevant to reinforcement and concrete are simulated in the ABAQUS environment. The input material properties and constitutive models are briefly reviewed in the subsequent sections.

6.2.1 Material Properties and Constitutive Laws

6.2.1.1 Concrete

There are several options to simulate the concrete cracks and crushing behavior in Abaqus, namely: a) smeared crack model; b) brittle crack model, and c) damaged plasticity model. The present research was motivated to use the damaged plasticity model due to its high possibility of convergence compared to other models. Besides, it has a good capability to characterize the inelastic behavior of concrete in tension and compression as well as damage characteristics. The model assumes that the tensile cracking and compressive crushing are the dominant failure mechanisms. Stiffness degradation and continuum damage mechanics approach are used to model the crack propagation.

Figure 6.2 shows the axial compression behavior of concrete where the stress-strain response is linear until it reaches the initial yield σ_{c0} . From the initial yield to the ultimate stress σ_{cu} , the plastic regime can be characterized as a stress hardening response followed by strain softening. It is presumed that the uniaxial stress-strain relationship can be changed into stress versus plastic-strain curves (Equation 6.6 and 6.7).

$$\sigma_t = \sigma_t(\tilde{\varepsilon}_t^{pl}, \dot{\tilde{\varepsilon}}_t^{pl}, \theta, f_i) \quad (6.6)$$

$$\sigma_c = \sigma_c(\tilde{\varepsilon}_c^{pl}, \dot{\tilde{\varepsilon}}_c^{pl}, \theta, f_i) \quad (6.7)$$

where the subscripts t and c refer to tension and compression, respectively; $\tilde{\varepsilon}_t^{pl}$ and $\tilde{\varepsilon}_c^{pl}$ are the equivalent plastic strains, $\dot{\tilde{\varepsilon}}_t^{pl}$ and $\dot{\tilde{\varepsilon}}_c^{pl}$ are the equivalent plastic strain rates, θ is the temperature, and f_i , ($i = 1, 2, \dots$) are other predefined field variables.

The d_t and d_c are the two damage variables that characterize the elastic stiffness degradation. It is assumed that these two variables are the functions of plastic strains, temperature, and field variables (equations 6.8 and 6.9).

$$d_t = d_t(\tilde{\varepsilon}_t^{pl}, \theta, f_i); \quad 0 \leq d_t \leq 1 \quad (6.8)$$

$$d_c = d_c(\tilde{\varepsilon}_c^{pl}, \theta, f_i); \quad 0 \leq d_c \leq 1 \quad (6.9)$$

In Abaqus, the damage variables are able to pick out the values from zero (undamaged material) to one that is fully damaged. If, the material undamaged elastic stiffness is E_0 , then the stress-strain relationships due to uniaxial tension and compression will be, respectively (equations 6.10 and 6.11):

$$\sigma_t = (1 - d_t)E_0(\varepsilon_t - \tilde{\varepsilon}_t^{pl}) \quad (6.10)$$

$$\sigma_c = (1 - d_c)E_0(\varepsilon_c - \tilde{\varepsilon}_c^{pl}) \quad (6.11)$$

In Abaqus, several parameters need to be given to develop the damaged plasticity model. They are: plastic damage parameters, Poisson's ratio, elastic modulus,

description of tensile and compressive behavior. The five plastic damage parameters are the dilation angle, the flow potential eccentricity, the ratio of initial equibiaxial compressive yield stress to initial uniaxial compressive yield stress, the ratio of the second stress invariant on the tensile meridian to that on the compressive meridian and the viscosity parameter that defines viscoplastic regularization.

It is important to develop the interface relation between rebar and concrete, which can be modeled using the tension stiffening approach. It can simulate load transfer across the cracks through the rebar. Moreover, it permits the model to simulate strain-softening behavior of cracked concrete. There are two ways to specify the tension stiffening in concrete: a) post failure stress-strain relation; b) fracture energy cracking criterion. To avoid the mesh sensitivity problem, the fracture energy method of Hillerborg et al. (1976) can be applied rather than the post failure stress-strain relation. This approach assumes the total of energy (G_F) to wide open a unit area of crack as a material property (Figure 6.3).

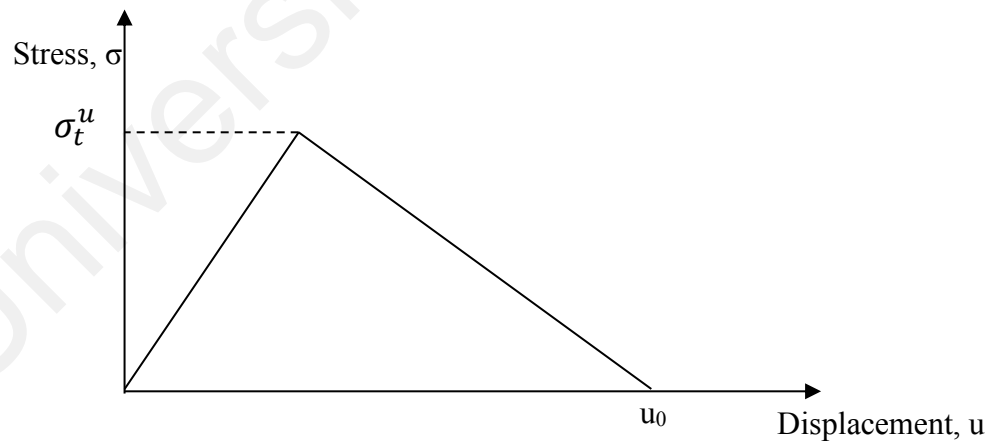


Figure 6.3: Fracture energy cracking model (Abaqus documentation)

The concrete compressive strain ε_o corresponding to the peak stress f'_c is usually 0.002 – 0.003, under uniaxial compression. The ACI Committee 318 (Committee, 2011) recommended a demonstrative value and this analysis incorporates it as $\varepsilon_o = 0.003$.

Under uniaxial compressive stress, the Poisson's ratio ν_c of concrete is 0.15 – 0.22, though an illustrative value of 0.19 or 0.20 was used by (Nilson, 1982). In this modelling, the Poisson's ratio of concrete was considered as $\nu_c = 0.20$. The uniaxial tensile strength of concrete f'_t in equation 6.12 was taken in this study as 4.5 (Hu et al., 2004).

$$f'_t = 0.33\sqrt{f'_c} \text{ MPa} \quad (6.12)$$

The modulus of elasticity of concrete E_c in equation 6.13 is vastly correlated to its compressive strength and can be calculated from the empirical formula (Committee, 2011).

$$E_c = 4700\sqrt{f'_c} \text{ MPa} \quad (6.13)$$

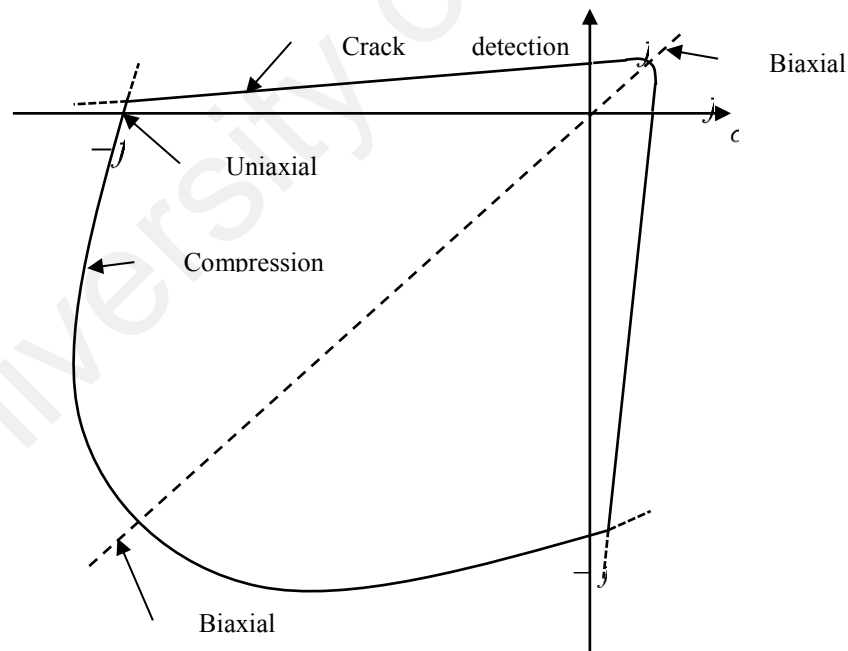


Figure 6.4: Plane stress concrete failure surface (Abaqus documentation)

The failure strengths of concrete are observed different form under multiaxial combinations. Moreover, under multiple stress conditions, the maximum strength envelope to be mostly independent of load path (Kupfer et al., 1969). A Mohr-Coulomb

genre compression surface with a crack detection surface is employed in ABAQUS to model the concrete failure surface (Figure 6.4).

6.2.1.2 Internal Steel Bar

The steel reinforcement stress–strain curve was assumed to be elasto-plastic as shown in Figure 6.5. Several parameters are needed to specify the stress-strain property such as modulus of elasticity (E_s), Poisson’s ratio (ν) and yield stress (f_y). The modulus of elasticity and Poisson’s ratio of internal steel was considered as 200 GPa and 0.3, respectively, in this study. In Abaqus, the reinforcement was considered as an equivalent uniaxial material all over the element section and the bond-slip influence between concrete and steel was not considered. The constitutive behavior of the reinforcement, the cross-sectional area, position, spacing and orientation of reinforcement were modeled considering their actual behavior during experiment.

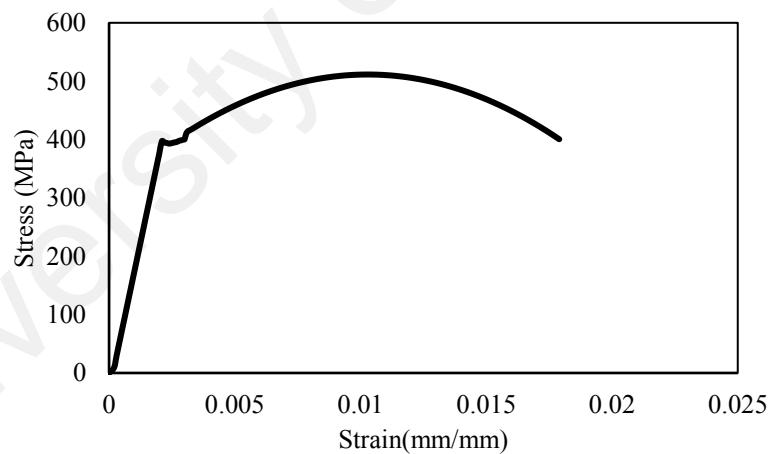


Figure 6.5: Elasto-plastic model for reinforcement

6.2.1.3 FRP

The CFRP composites were assumed to behave linear elastic material. Its stress-strain response is linear elastic until it reach the failure strain. For model development, the value of modulus of Elasticity, Poisson’s ratio and tensile strength of CFRP are taken as 165 GPa, 0.3 and 2400 MPa respectively. CFRP is an orthotropic material

which is reflected in the present numerical study. However, very negligible difference was shown when it was analyzed with isotropic linear elastic assumption.

6.2.1.4 CFRP-Concrete Interface

An important task is to define and model the interface between CFRP and concrete. The FRP-concrete interface can be modeled using the perfect bond or cohesive model. The perfect bond model demonstrated a bit overestimation of ultimate load and stiffness compared to the experimental output. However, regarding the convergence issue and the computation capability this approach is more convenient. On the other hand, the cohesive model describes surfaces of separation and defines their relations by identifying a relative deviation at each contact point. The model can be described by the parameters, initial stiffness, shear strength, fracture energy and curve shape of the bond slip model. The adhesive properties are important inputs for this model. So, the initial stiffness, shear strength and fracture energy as a function of adhesive and concrete properties are needed to simulate the model (equation 6.14 to 6.16). However, this approach is complex in nature and convergence is the main issue to run the simulation.

$$\text{Initial Stiffness, } K_0 = 0.16 \frac{G_a}{t_a} + 0.47 \quad (6.14)$$

$$\text{Shear strength, } \tau_{max} = 1.46 G_a^{0.165} f_{ct}^{1.033} \quad (6.15)$$

$$\text{Fracture energy, } G_f = 0.52 f_{ct}^{0.26} G_a^{-0.23} \quad (6.16)$$

Here, t_a is the adhesive thickness in mm, G_a is the adhesive modulus in GPa and f_{ct} is the tensile strength of concrete in MPa.

6.2.2 Model Geometry

The concrete beam were modeled as 3D solid elements to simulate the actual behavior of tested RC beams. For this reason, 8-node reduced integration solid hexahedron elements were considered to model concrete. These elements have three degrees of freedom at each node. Single point volume integration is carried out by

Gaussian quadrature. The biggest advantage of using solid elements with one-point integration is the substantial savings in computer time though they need to control the zero energy modes. Undesirable hourglass modes tend to have periods that are typically much smaller than the periods of the structural response, and they are often observed to be oscillatory. One way of resisting undesirable hourglassing is with a viscous damping or small elastic stiffness capable of stopping the formation of the irregular modes but having an insignificant effect on the stable global modes. In ABAQUS software, three-dimensional algorithms for controlling the hourglass modes are typically used.

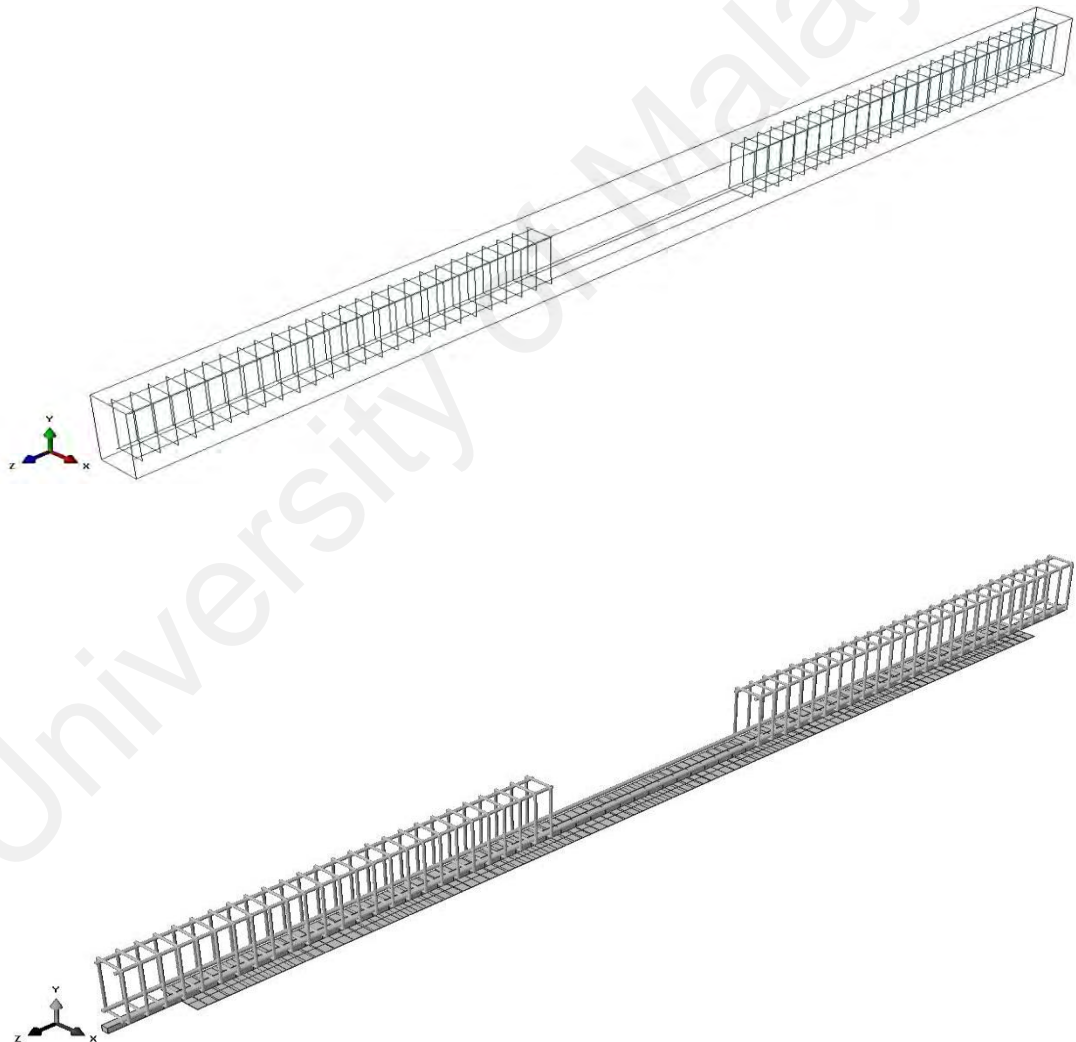


Figure 6.6: 3D non-linear finite element model of reinforcements

The longitudinal steel and strengthening bars as well as the transverse ties were modelled using 2-node truss elements (Figure 6.6). The truss elements have three degrees of freedom at each node, translations in x , y , and z directions. The difference

between the beam and the truss elements is that the former has stiffness associated with the deformation of the beam's axis while the latter has only axial stiffness. The numerical convergence study showed that further decrease in the mesh size has little effect on the numerical results but leads to the risk of computer memory overflow and substantially increases the computing time. Figure 6.7 shows the typical mesh of CEBNSM strengthened beam. The FE analysis was based on perfect bond assumption between steel bars and surrounding concrete.

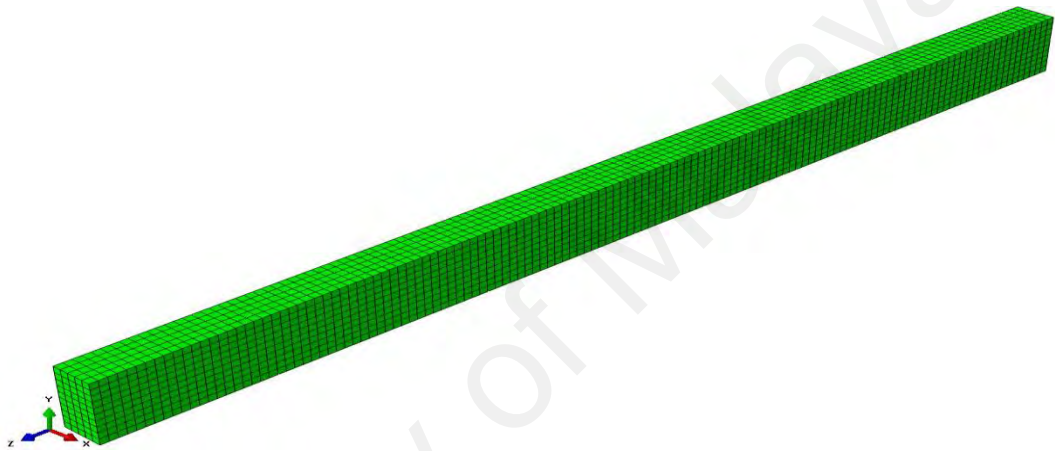


Figure 6.7: 3D finite element mesh of RC strengthened specimen

The Element definition consists of:

- assigning an element number to the element;
- defining individual elements by specifying their nodes;
- grouping elements into element sets;
- creating elements from existing elements

The Abaqus model has been defined in terms of an assembly of part instances. In such a model almost all elements must belong to a part or part instance. The only exceptions are mass, rotary inertia, capacitance, connector, spring, and dashpot elements, which can belong to a part or to the assembly. Element numbers are unique within a part, part instance, or the assembly; but they can be repeated in different parts or part instances.

The solid 8-node linear brick element, C3D8R was used for concrete material which reduced integration with hourglass control. In addition, for steel reinforcement, a 2-node straight truss element, T3D2 was used to linear interpolate the position and displacement.

6.2.3 Loads

The loading types available for static analysis are explained here. In Abaqus, concentrated nodal forces or moments can be applied to the displacement or rotation degrees of freedom. To simulate the model, distributed pressure forces or body forces was applied in the body mass (Figure 6.8). In the real experiment, four point bending load was applied to the control as well as the strengthened beams. Load control mode was maintained with a rate of 5 kN/minute up to the yield point of the tested beam. When the applied load crossed the yield point, the load control mode of Instron machine was changed the position control mode with a rate of 3 mm/minute until failure of the experimented beam. For simulating the exact loading application appropriate amplitude was chosen within the specified time domain.

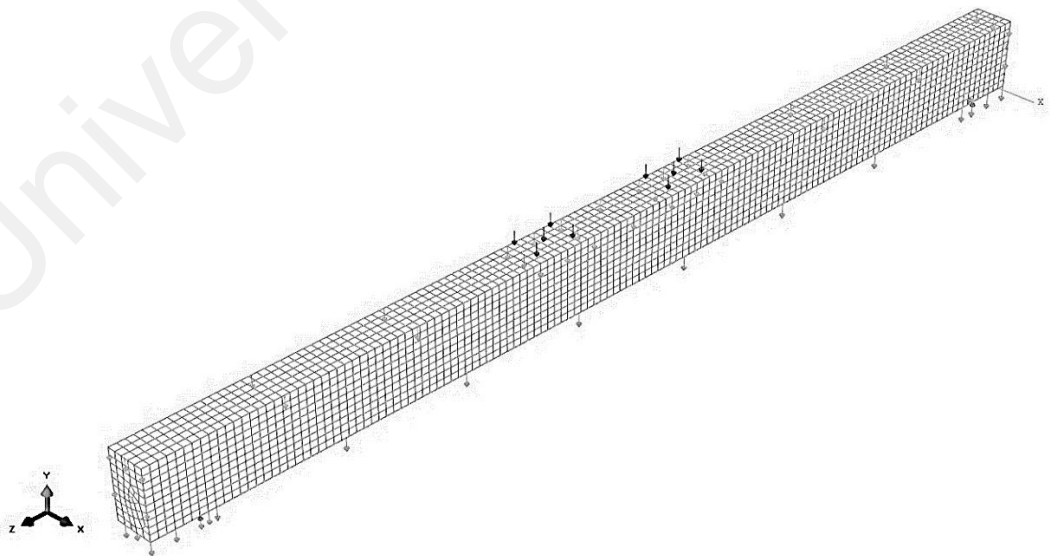


Figure 6.8: Applied Loading in the model

6.2.4 Mesh Sensitivity Analysis

A convergence of results is achieved when an adequate number of elements are used in the model. Previous results showed that very fine or coarse caused trouble to obtain the convergence and often produced erroneous results. The results obtained from a fine mesh were more accurate. An even finer mesh gave almost the same result as the previous mesh but more time was needed for computations.

Control beam was chosen to perform a mesh sensitivity analysis was performed to assess the convergence of the solution and to determine the appropriate mesh density. Only the mesh density of the concrete elements was considered in this mesh sensitivity analysis while the number of elements of steel for main reinforcement and stirrups were kept sufficiently fine for all models. Since most of the beam volume consists of concrete, and due to the fact that concrete elements experience cracking and damage evolution, changing their mesh density would have a greater effect on the deflection, consequently the strains, as compared with the linear elastic materials. Three FEM models were simulated with 25, 35 and 45 mesh size for the sensitivity study.

Table 6.1: Mesh sensitivity analysis for FEM model with different mesh size

Element size	No. of element	No. of nodes	No. of variables	CPU time (sec)
25	7804	9988	29964	3:40
35	3864	5050	15150	2:25
45	2518	3282	9846	0:15

Table 6.1 demonstrated the model output for these three different mesh sizes. The number of total element, nodes and variables were recorded according to the developed model. The CPU time was the approximate time of the model for completing the task if

there was no error or any divergence issue. Another two models were created with 15 and 20 mesh size to verify the experimental result. However, both the model failed which did not converge and gave error sign.

Figure 6.9 demonstrated the load-deflection behavior of the experimental and FE analysis for different mesh sizes. From result it could be easily understood the efficacy of the finer mesh sizes. The 25 mesh size presented good agreement with the experimental result compared to the other beams. The coarser mesh (45) model deviate much at the pre-ultimate to the ultimate point with compare to the experimental beam.

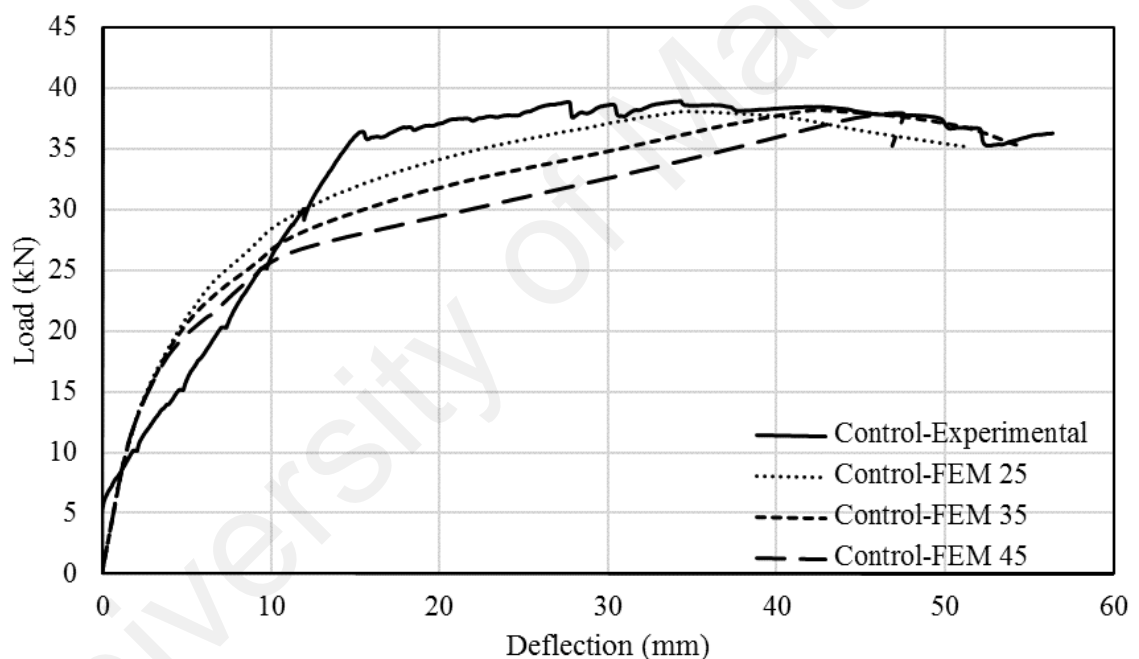


Figure 6.9: Comparison between the experimental and FE analysis for different mesh sizes

Figure 6.10 exhibited the surface contour plot of the tensile damage behavior the control beam model with 25, 35 and 45 mesh size. The finer mesh size displayed more cracks and finely dispersed cracks compared to the coarser mesh size (45). Considering the accuracy issue, 25 mesh size was taken into account for developing the FEM model for the strengthened RC beam.

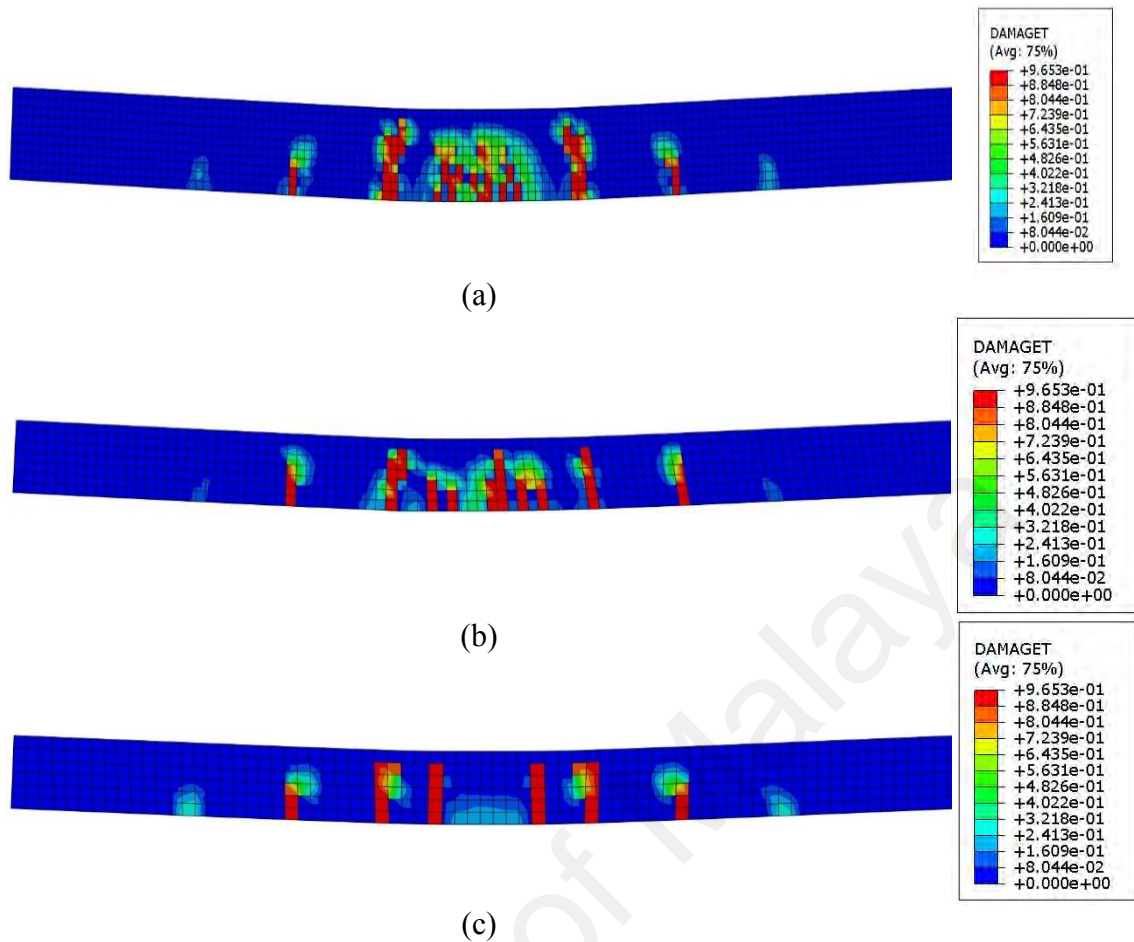


Figure 6.10: Tensile damage behavior of control beam with (a) 25, (b) 35 and (c) 45 mesh size

6.3 Results of FEM simulation of CEBNSM-B beams

The numerical analysis was performed to verify the experimental results in terms of load-deflection behavior and strain distribution of the strengthening materials. The commercial finite element program ABAQUS® was used to develop three dimensional (3D) model for analyzing the control and strengthened RC beam. Their input material properties, associated constitutive models, model geometry and loading pattern was briefly discussed to simulate the unstrengthened and strengthened RC beams. The following first section demonstrated the FEM simulated results of load-deflection and strain variation of the different element of the NSM strengthened RC beams. Therefore, the subsequent chapter presented the comparison between the experimental and FEM output in terms of the load-deflection and strain variation.

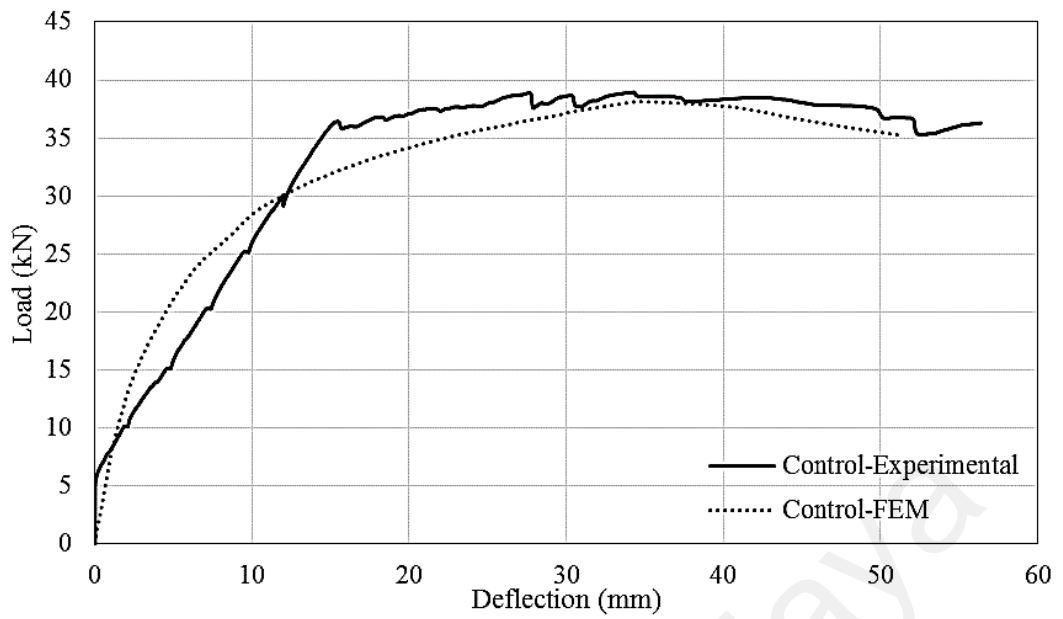
6.3.1 Load-deflection Comparison

Table 6.2 compared the load-deflection relationship obtained from the FEM simulated output for CEBNSM-B strengthened RC beams with the experimental results. The ultimate load and deflection obtained from both experimental and FEM investigation was tabulated in the Table 6.2. The difference between the experimental and FEM output was within the acceptable limit (10%).

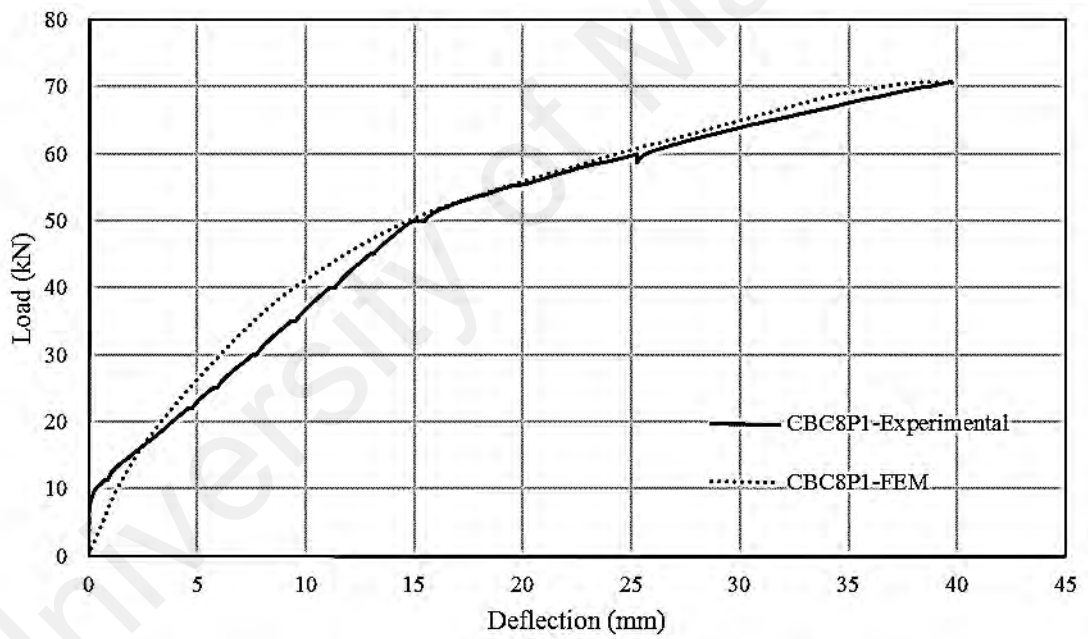
Table 6.2: Comparison between experimental and FEM output for CEBNSM-B beams

Beam ID	$P_{u.exp}$	$\Delta_{u.exp}$	$P_{u.FEM}$	$\Delta_{u.FEM}$	P_{FEM}/P_{exp}	$\Delta_{FEM}/\Delta_{exp}$
Control	39.0	34.3	38	34.6	0.98	1.01
CBC8P1	70.8	39.7	70.8	38.6	1.0	0.97
CBC8P2	76.9	31.3	79.7	36.1	1.0	1.12
CBC10P1	81.7	43.3	82.2	44.5	1.0	1.03
CBC10P2	87.3	42.7	87.6	47.0	1.0	1.10
CBS8P1	69.1	40.8	72.5	38.7	1.05	0.95
CBS8P2	69.1	40.8	72.5	38.7	1.0	1.08
CBS10P1	62.4	29.2	65	32.8	1.0	1.10
CBS10P2	84.8	37.9	77	42.6	0.9	1.10

Figure 6.11 presented the load-deflection behavior of control and NSM strengthened RC beam. The comparison clearly revealed the effectiveness of the developed FEM model. Both the simulated deflection and load conformed to the experimental values.

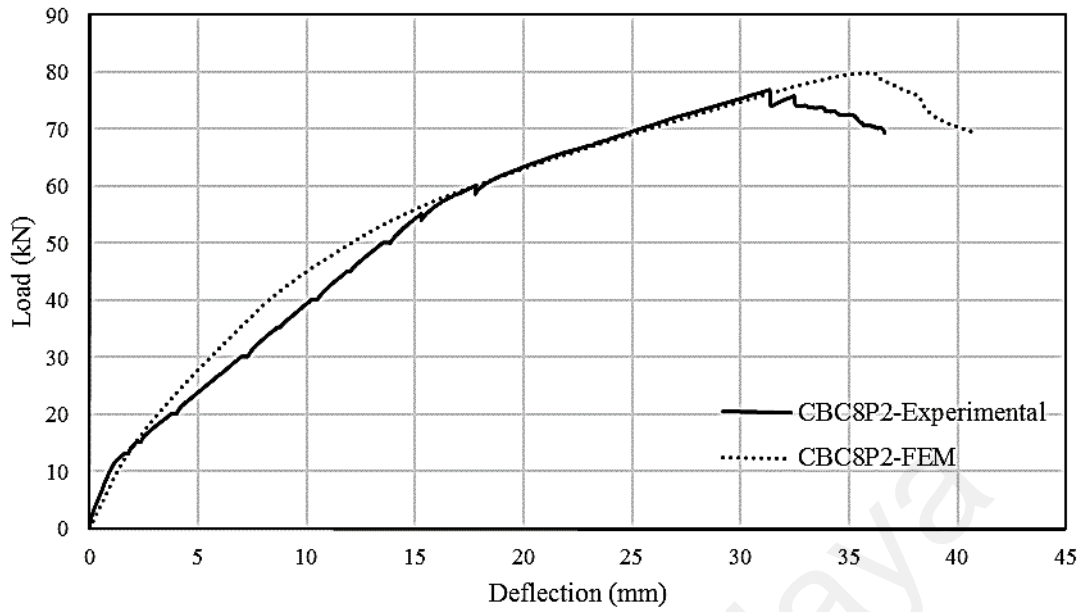


(a) Control

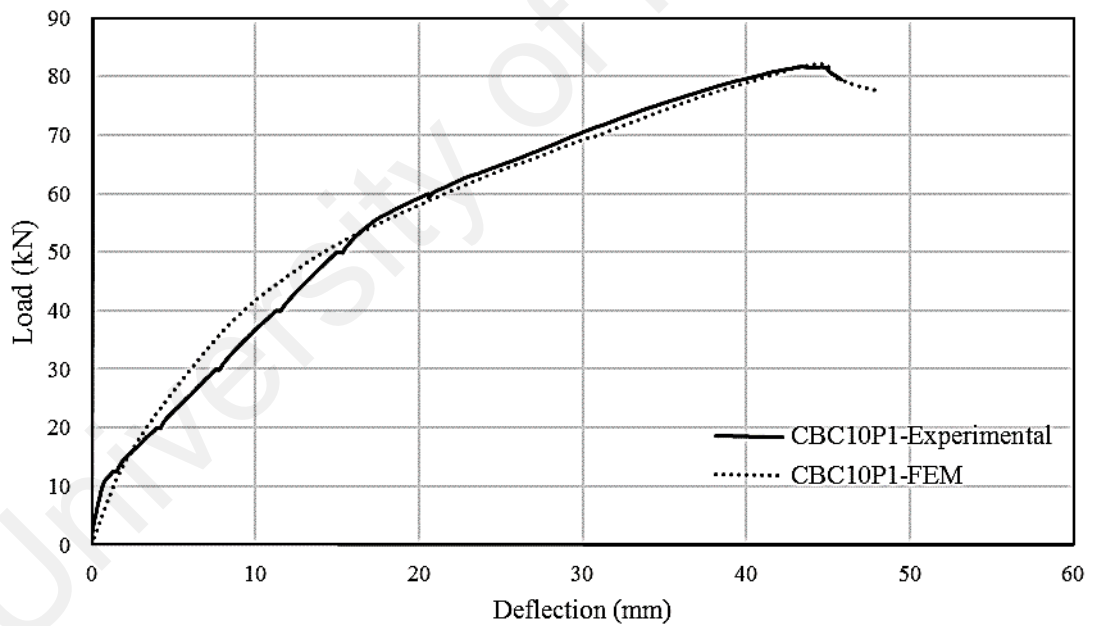


(b) CBC8P1 beam

Figure 6.11: Comparison between experimental and FEM load-deflection behavior for control and CEBNSM-B strengthened RC beam (a) to (g)

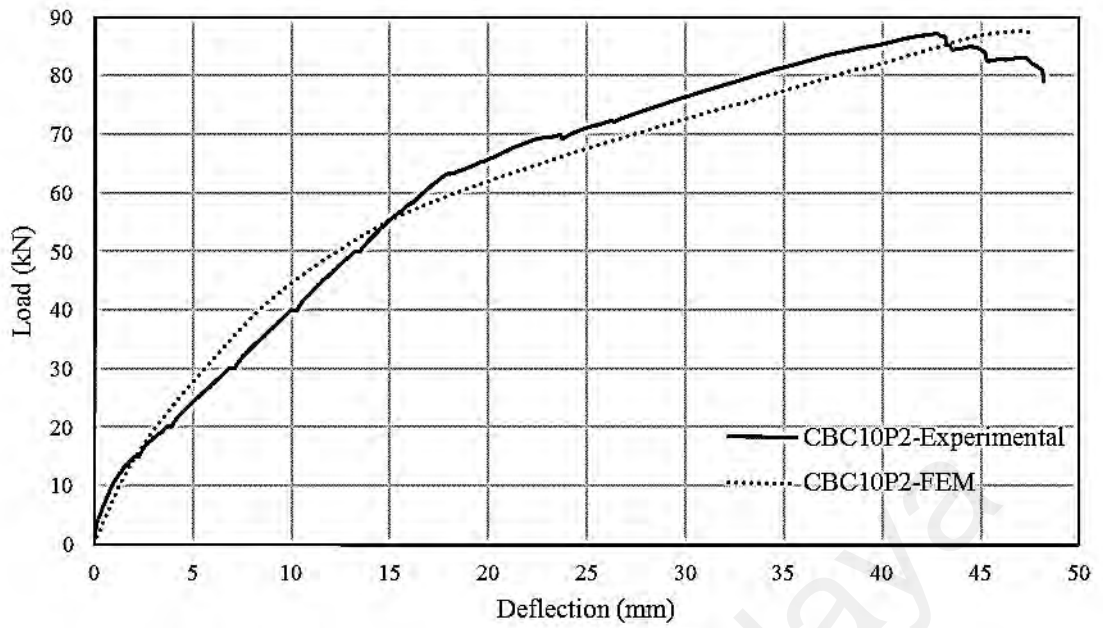


(c) CBC8P2 beam

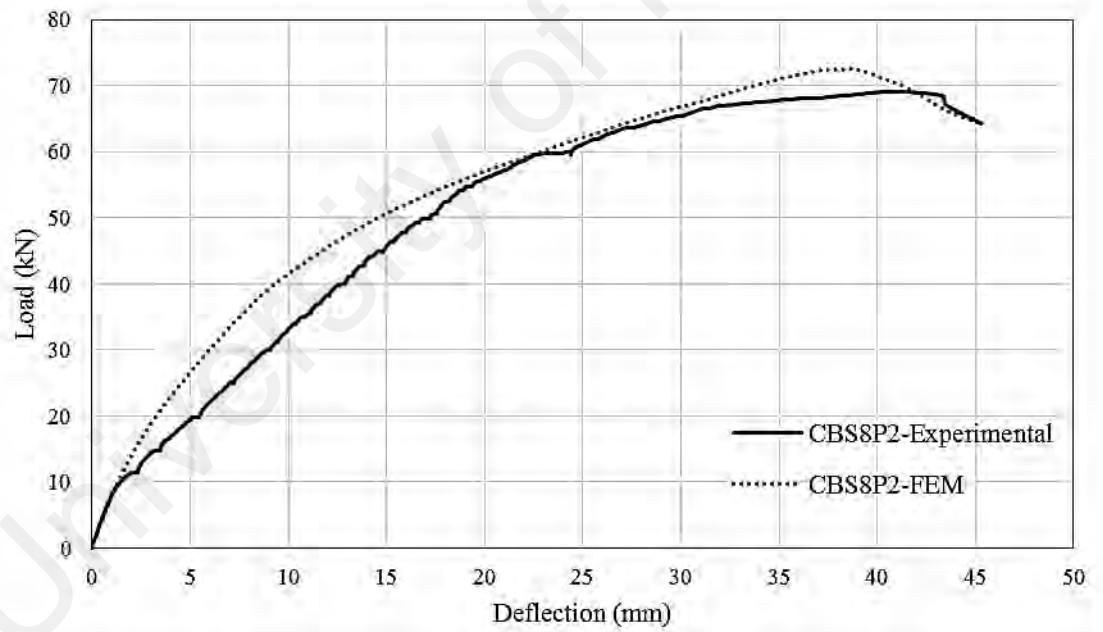


(c) CBC10P1 beam

Figure 6.11, continued: Comparison between experimental and FEM load-deflection behavior for control and CEBNSM-B strengthened RC beam (a) to (g)

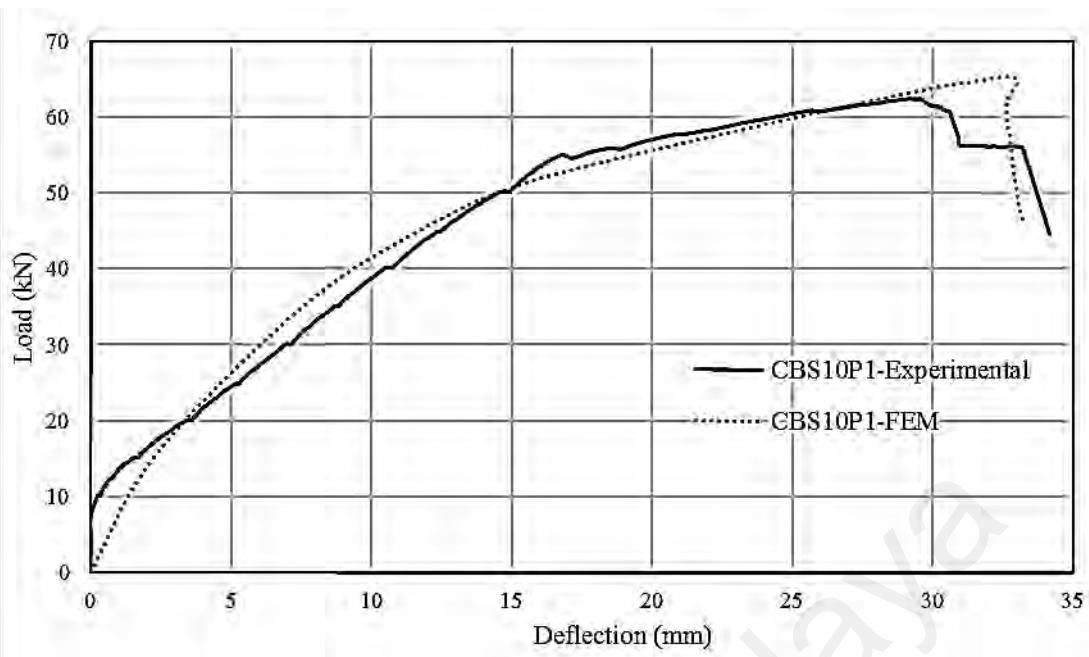


(d) CBC10P2 beam

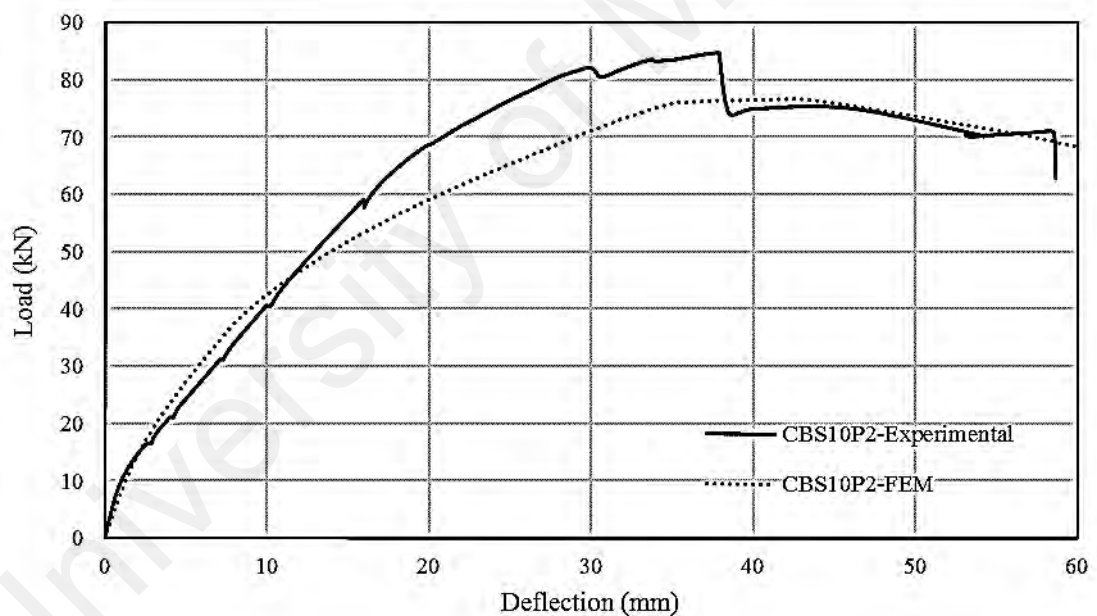


(e) CBS8P2 beam

Figure 6.11, continued: Comparison between experimental and FEM load-deflection behavior for control and CEBNSM-B strengthened RC beam (a) to (g)



(f) CBS101 beam



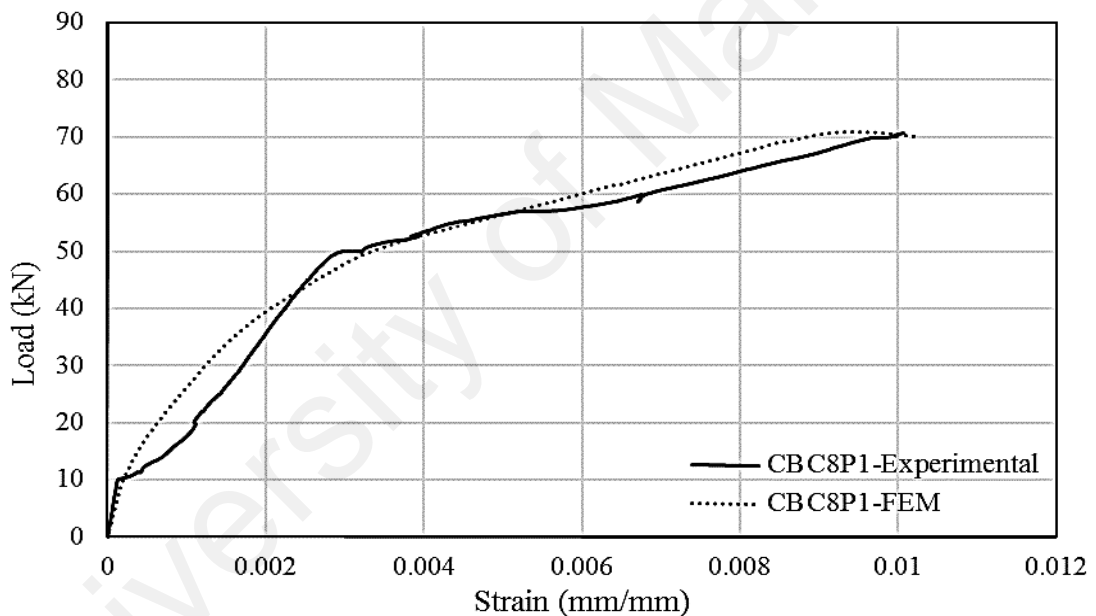
(g) CBS10P2 beam

Figure 6.11, continued: Comparison between experimental and FEM load-deflection behavior for control and CEBNSM-B strengthened RC beam (a) to (g)

The tensile damage behavior of the CEBNSM-B strengthened RC beams were demonstrated at the appendix D1. From the surface contour plot of the strengthened beam, it was possible to locate the location of the crack during failure. The crack evolution and the propagation of the simulated cracks adequately matched with the experimental crack pattern during failure.

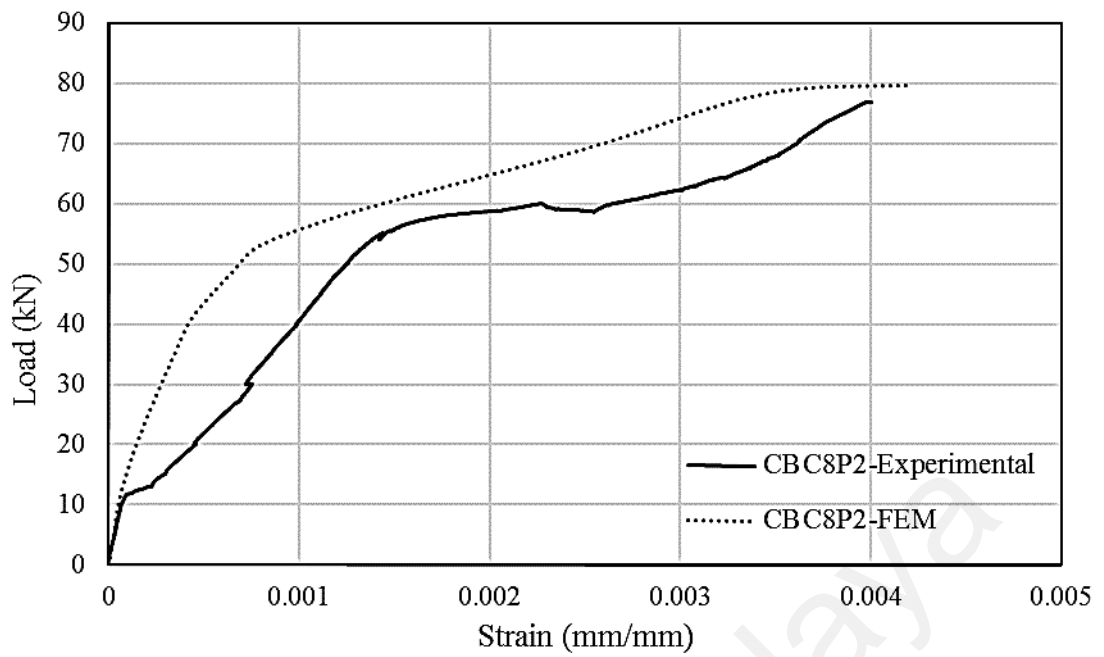
6.3.2 Load-Strain Comparison

Figure 6.12 demonstrated the load-strain behavior of CFRP fabric which was externally bonded at the beam soffit. The strain reading was measured at the mid-span region of the beam where the tensile strain was maximum. As the CFRP fabric was placed at the extreme bottom surface of the beam, so the chance of fabric fracture or debonding possibility is maximum for this strengthening material. The strain reading from FEM showed a good agreement with the experimental values. However, few beams (CBC8P2 and CBC10P1) showed relatively stiffer response compared to the experimental results.

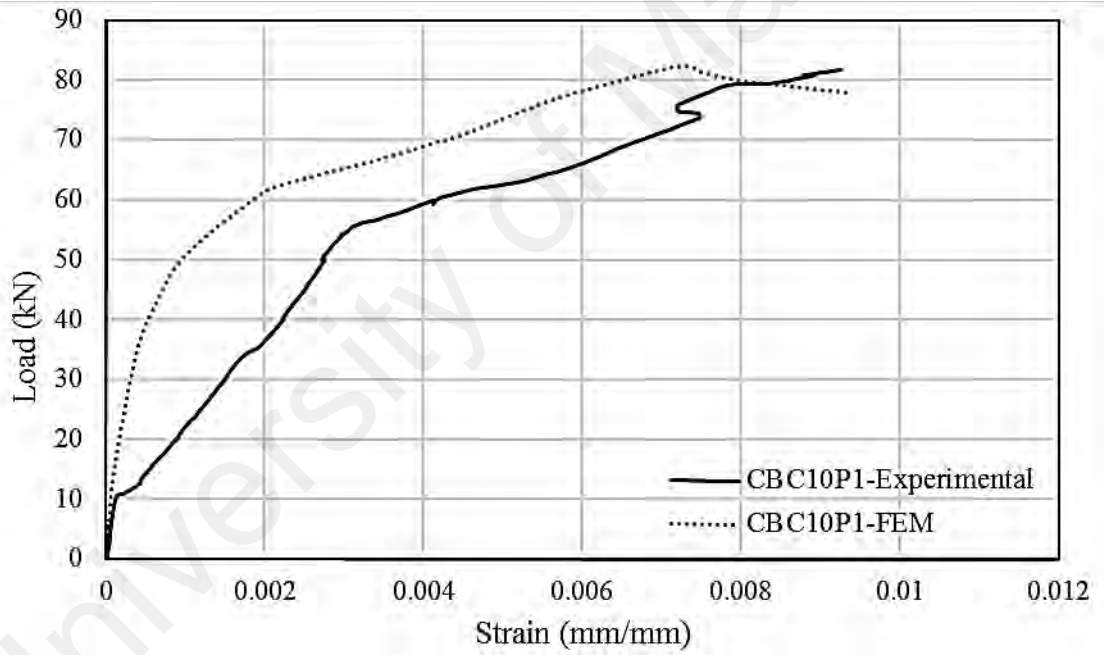


(a) CBC8P1 beam

Figure 6.12: load-strain behavior of CFRP fabric for control and CEBNSM-B strengthened RC beam (a) to (h)

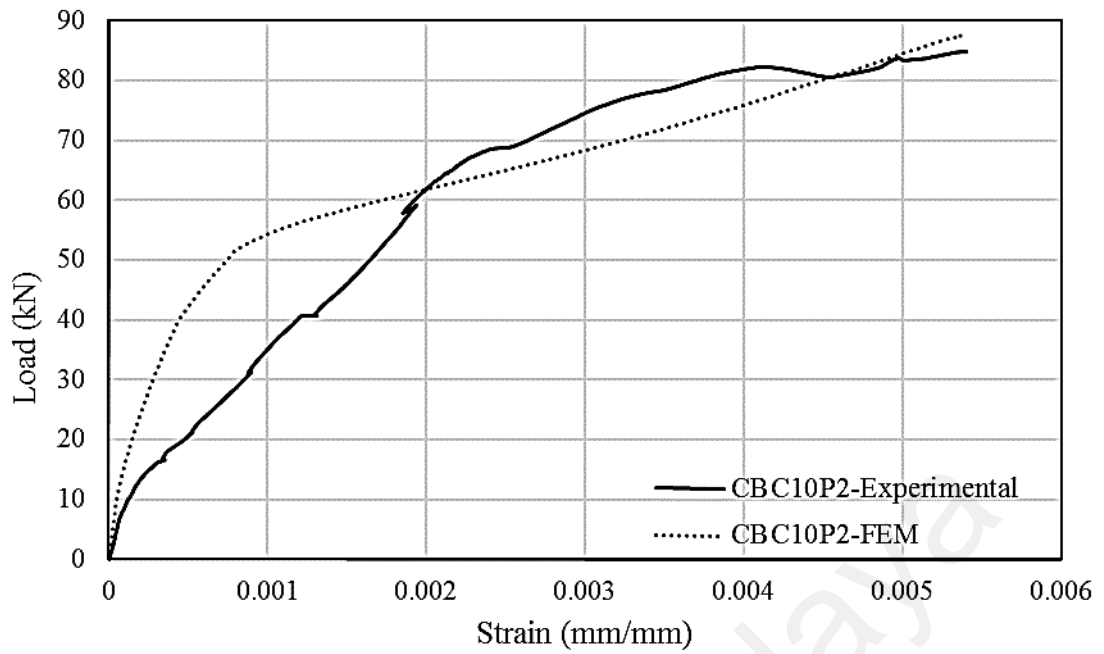


(b) CBC8P2 beam

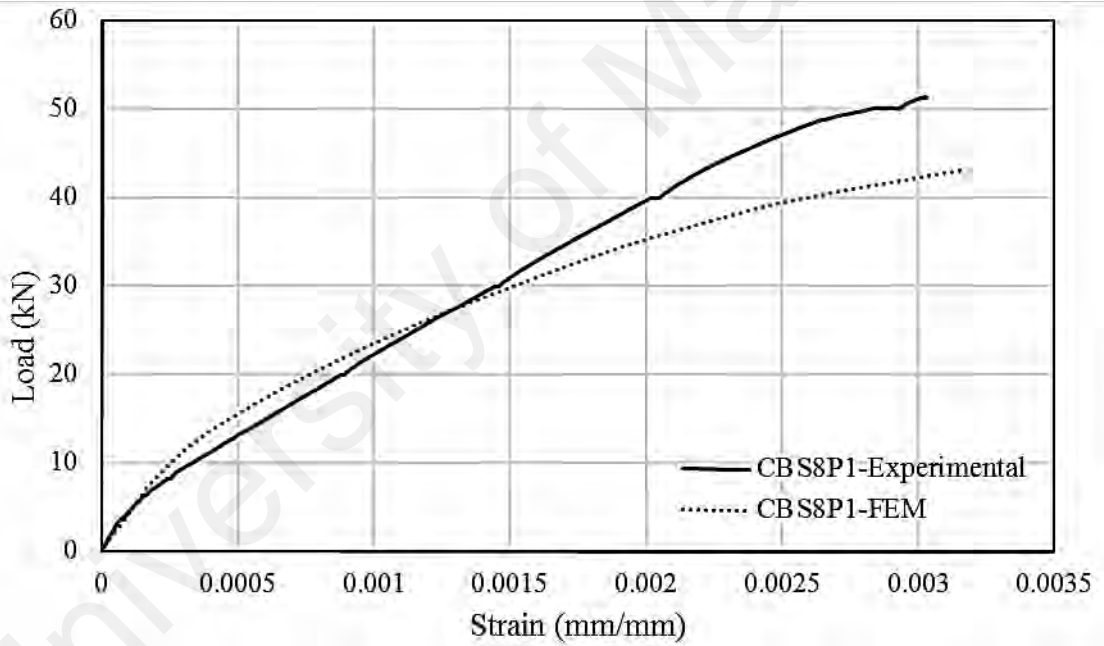


(c) CBC10P1 beam

Figure 6.12, continued: load-strain behavior of CFRP fabric for control and CEBNSM-B strengthened RC beam (a) to (h)

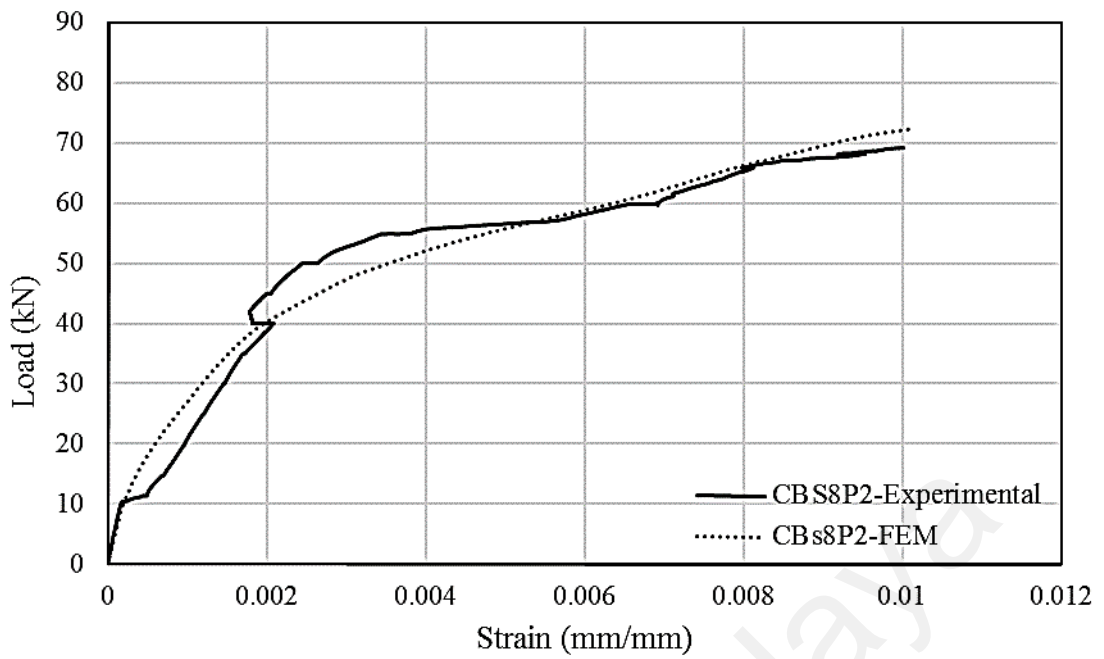


(d) CBC10P2 beam

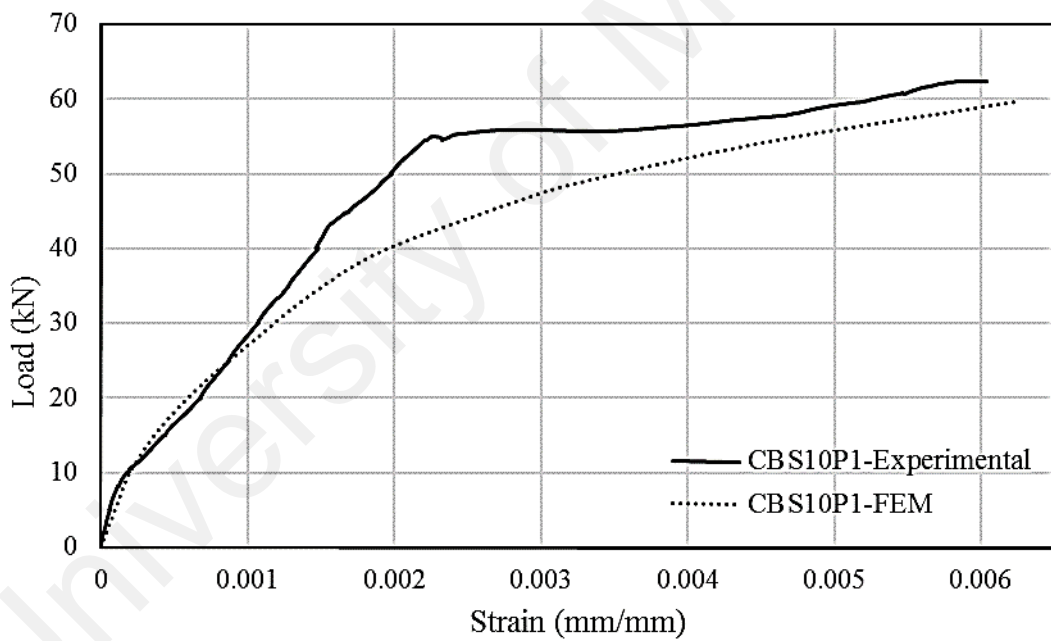


(e) CBS8P1 beam

Figure 6.12, continued: load-strain behavior of CFRP fabric for control and CEBNSM-B strengthened RC beam (a) to (h)

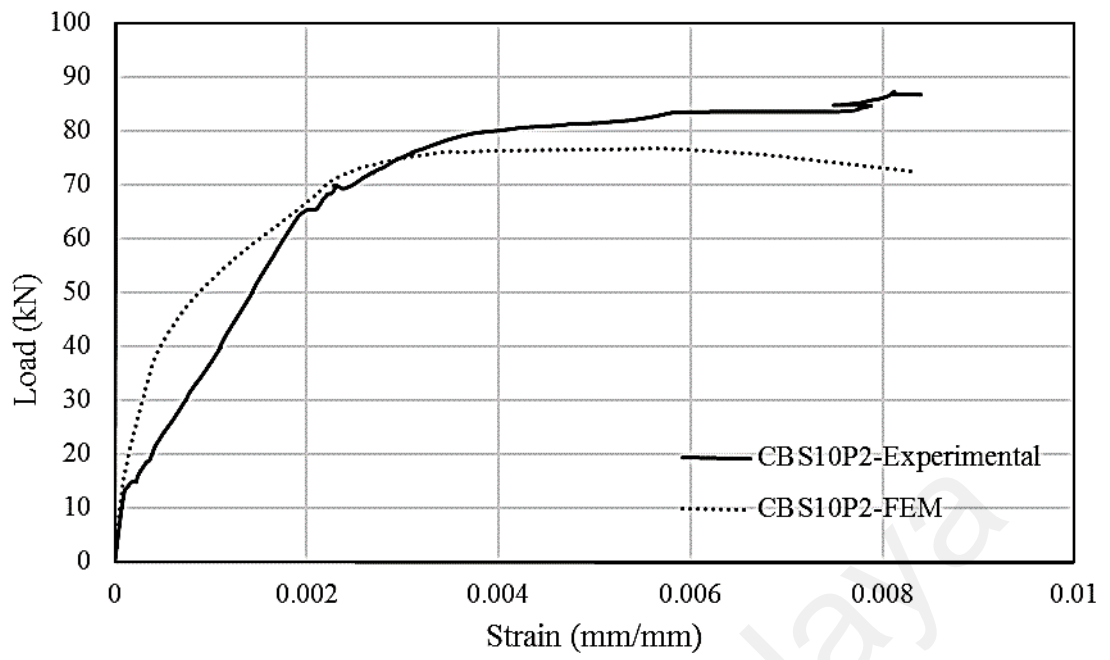


(f) CBS8P2 beam



(g) CBS10P1 beam

Figure 6.12, continued: load-strain behavior of CFRP fabric for control and CEBNSM-B strengthened RC beam (a) to (h)



(h) CBS10P2 beam

Figure 6.12, continued: load-strain behavior of CFRP fabric for control and CEBNSM-B strengthened RC beam (a) to (h)

University of Malaya

CHAPTER 7: CONCLUSIONS

The aim of this study was to develop an effective strengthening solution which will increase the flexural strength of RC beams with less possibility of debonding when cross-sectional width is limited. The proposed CEBNSM strengthening method combined the externally bonded CFRP fabric with near surface mounted reinforcement. According to the test matrix described in Table 3.1, four series of strengthened RC beams were tested. The findings of the study are summarized in the following sections.

7.1 NSM and EBR Strengthened RC Beams

The experimental results of NSM and EBR strengthened beams are summarized as follows:

- i. Debonding failure is a common failure mode for EBR and NSM strengthened beams.
- ii. Steel strengthened NSM beams with larger bond length (1900 mm and 1800 mm) demonstrated flexure failure (concrete crushing after steel yielding).
- iii. Steel NSM beams showed less ultimate capacities but better stiffness and cracking behavior compared to beams with NSM CFRP material.
- iv. Among the strengthened beams with three NSM bond lengths, the longest one performed the best.

7.2 Serviceability Prediction Model Using Fuzzy Logic

The conclusions for serviceability prediction model using FLES are as follows:

- i. The fuzzy logic algorithm accurately predicted the serviceability behavior of the strengthened beams.

- ii. For all parameters, the relative error and the goodness of fit of the predicted values were found to be within the acceptable limit.

7.3 Combined Externally Bonded and Near Surface Mounted RC Beam

The summary of experimental results of CEBNSM strengthened beams are as follows:

- i. Most of the CEBNSM beams failed due to flexure. Their 1st crack load and ultimate capacity were higher than the EBR and NSM strengthened beams.
- ii. For CEBNSM-B beams, externally bonded CFRP fabric was fractured in most cases at mid-span after internal steel yielding, whereas concrete crushing after steel yielding was the dominant failure mode of CEBNSM-S beams.
- iii. CEBNSM-S beams showed higher strength with less deflection, crack spacing and crack width compared to the CEBNSM-B beams.
- iv. Introducing U-Wrap CFRP anchorage to CEBNSM-B beams at the curtailment location of EB fabric changed the failure mode from debonding to flexure failure and their ultimate capacity was enhanced considerably.

7.4 Performance of CEBNSM Strengthened RC Beam

The performances of CEBNSM strengthened RC beams are summarized as follows:

- i. The experimental results of both types of CEBNSM strengthened beams showed an enhanced flexural capacity, stiffness and serviceability behavior. A tremendous improvement was noticed in the case of first crack load.

- ii. A considerable reduction of the deflection was observed for all of the CEBNSM strengthened beams.
- iii. The mean crack spacing and crack width of the CEBNSM strengthened beams were less compared to the control beams. However, the number of cracks appeared more for the strengthened beams compared to the control specimens.

7.5 Finite Element Analysis

The conclusions of FEM study are as follows:

- i. The simulated deflection and strain values from the FEM model matched well with the experimental results.
- ii. The relative error involved in the FEM analysis was less than the accepted limit.
- iii. The simulated tensile damage behavior of the strengthened beams was very similar to the experimental beams.

7.6 Recommendation

During fulfilling the objectives of this study, it was revealed that further research is needed to fully understand the behavior of the CEBNSM strengthened RC structures. Based on the results of this research, several recommendations are drawn to explore for better understanding of this structural strengthening research:

- i. Assessment of the efficacy of the different mechanical anchorage systems and their design procedure to eliminate the debonding failure for the CEBNSM technique.
- ii. Possibility of using CEBNSM technique in the long span pre-stress girder. Life size specimen should be tested to get the actual behavior of the strengthened girder.

- iii. Assessment of the response of the strengthened structures using this technique with repeated loading which is the common loading on the transportation structures.
- iv. Evaluation of the residual static and fatigue capacity of pre-cracked RC structures under different loading condition (service, yield and ultimate loading) and assess their capacity increment after applying the CEBNSM strengthening technique
- v. Evaluation of the durability characteristics of the FRP based CEBNSM strengthening techniques under harsh environmental conditions with or without sustained stress levels.
- vi. Development of the design guidelines of the CEBNSM technique with proper safety factors.

REFERENCE

- ACI 318-99. (1999). Building Code Requirements for Structural Concrete (ACI 318-99) and Commentary (318R-99), Farmington Hills, Mich.
- ACI 440. (2006). Guide for the Design and Construction of Concrete Reinforced with FRP Bars (ACI 440.1 R-06). American Concrete Institute, Detroit, Michigan.
- ACI 440.2R-08. (2008). Guide for the design and construction of externally bonded FRP systems for strengthening concrete structures, Farmington Mills, MI.
- ACI. (2002). Guide for the design and construction of externally bonded FRP systems for strengthening concrete structures. ACI 440.2R-02, ACI, Farmington Hills, Michigan.
- Aïtcin, P.-C., & Mehta, P. K. (1990). Effect of coarse aggregate characteristics on mechanical properties of high-strength concrete. *Materials Journal*, 87(2), 103-107.
- Akmaluddin, A. (2011). Effect of Tensile Reinforcement Ratio on the Effective Moment of Inertia of Reinforced Lightweight Concrete Beams for Short Term Deflection Calculation. *Journal of Engineering and Technological Sciences*, 43(3), 209-226.
- Al-Emrani, M., Haghani, R., Höglind, J., & Björklund, A. (2007). The effect of plate end tapering on the interfacial stresses in adhesively bonded composite elements. Paper presented at the The third international conference on structural engineering, mechanics and computation. Cape Town, South Africa, 10-12 September 2007.
- Al-Mahmoud, F., Castel, A., Francois, R., & Tourneur, C. (2009). Strengthening of RC members with near-surface mounted CFRP rods. *Composite Structures*, 91(2), 138-147. doi: 10.1016/j.compstruct.2009.04.040
- Al-Mahmoud, F., Castel, A., Francois, R., & Tourneur, C. (2011). Anchorage and tension-stiffening effect between near-surface-mounted CFRP rods and concrete. *Cement & Concrete Composites*, 33(2), 346-352. doi: 10.1016/j.cemconcomp.2010.10.016
- Al-Mahmoud, F., Castel, A., François, R., & Tourneur, C. (2009). Strengthening of RC members with near-surface mounted CFRP rods. *Composite Structures*, 91(2), 138-147.
- Al-Mahmoud, F., Castel, A., François, R., & Tourneur, C. (2011). Anchorage and tension-stiffening effect between near-surface-mounted CFRP rods and concrete. *Cement and Concrete Composites*, 33(2), 346-352.
- Alam, M. A., & Jumaat, M. Z. (2012). Experimental Investigations on U- and L-Shaped End Anchored CFRP Laminate Strengthened Reinforced Concrete Beams. *Arabian Journal for Science and Engineering*, 37(4), 905-919. doi: DOI 10.1007/s13369-012-0213-6
- Ali, M., Oehlers, D. J., & Park, S. M. (2001). Comparison between FRP and steel plating of reinforced concrete beams. *Composites Part A: Applied Science and Manufacturing*, 32(9), 1319-1328.
- Ali, M. S. M., Oehlers, D. J., & Griffith, M. C. (2008). Shear transfer across cracks in FRP strengthened RC members. *Journal of Composites for Construction*, 12(4), 416-424. doi: 10.1061/(asce)1090-0268(2008)12:4(416)

- Allam, S. M., Shoukry, M. S., Rashad, G. E., & Hassan, A. S. (2012). Crack width evaluation for flexural RC members. *Alexandria engineering journal*, 51(3), 211-220.
- Almusallam, T. H., Elsanadedy, H. M., Al-Salloum, Y. A., & Alsayed, S. H. (2013). Experimental and numerical investigation for the flexural strengthening of RC beams using near-surface mounted steel or GFRP bars. *Construction and Building Materials*, 40, 145-161. doi: 10.1016/j.conbuildmat.2012.09.107
- Ashour, A. F. (2006). Flexural and shear capacities of concrete beams reinforced with GFRP bars. *Construction and Building Materials*, 20(10), 1005-1015. doi: 10.1016/j.conbuildmat.2005.06.023
- ASTM. (2014). Standard Test Method for Compressive Strength of Cylindrical Concrete Specimens ASTM C39/C39M-14. USA: American Society for Testing and Materials (ASTM) International.
- Aydin, K., & Kisi, O. (2014). Applicability of a Fuzzy Genetic System for Crack Diagnosis in Timoshenko Beams. *Journal of Computing in Civil Engineering*, 29(5), 04014073.
- Babaeidarabad, S., Loreto, G., & Nanni, A. (2014). Flexural strengthening of RC beams with an externally bonded fabric-reinforced cementitious matrix. *Journal of Composites for Construction*, 18(5), 04014009.
- Badawi, M. A. (2007). *Monotonic and fatigue flexural behaviour of RC beams strengthened with prestressed NSM CFRP rods*. (PhD thesis), University of Waterloo.
- Barris, C., Torres, L., Comas, J., & Mias, C. (2013). Cracking and deflections in GFRP RC beams: an experimental study. *Composites Part B: Engineering*, 55, 580-590.
- Barros, J. A., Ferreira, D., Fortes, A. S., & Dias, S. J. E. (2006). Assessing the effectiveness of embedding CFRP laminates in the near surface for structural strengthening. *Construction and Building Materials*, 20(7), 478-491. doi: 10.1016/j.conbuildmat.2005.01.030
- Beber, A., Fihlo, A., & Campagnolo, J. (2001, December 12-15). CFRP in the strengthening of reinforced concrete beams. Paper presented at the FRP Composites in Civil Engineering. Proceedings of the International Conference on FRP composites in Civil Engineering, Hong Kong, China.
- Bizindavyi, L., & Neale, K. (1999). Transfer lengths and bond strengths for composites bonded to concrete. *Journal of Composites for Construction*, 3(4), 153-160.
- Blaschko, M. (2003). Bond behaviour of CFRP strips glued into slits. Paper presented at the 6th International Symposium on FRP Reinforcement for Concrete Structures (FRPRCS-6).
- Bouchikhi, A., Lousdad, A., & Megueni, A. (2010). On the reduce of interfacial shear stresses in fiber reinforced polymer plate retrofitted concrete beams. *Materials & Design*, 31(3), 1508-1515.
- Breña, S. F., & Macri, B. M. (2004). Effect of carbon-fiber-reinforced polymer laminate configuration on the behavior of strengthened reinforced concrete beams. *Journal of Composites for Construction*, 8(3), 229-240.
- Ceroni, F. (2010). Experimental performances of RC beams strengthened with FRP materials. *Construction and Building Materials*, 24(9), 1547-1559. doi: 10.1016/j.conbuildmat.2010.03.008

- Ceroni, F., & Pecce, M. (2009). Design provisions for crack spacing and width in RC elements externally bonded with FRP. *Composites Part B: Engineering*, 40(1), 17-28.
- Cevik, A. (2011). Modeling strength enhancement of FRP confined concrete cylinders using soft computing. *Expert Systems with Applications*, 38(5), 5662-5673.
- Chaallal, O., Mofidi, A., Benmokrane, B., & Neale, K. (2011). Embedded through-section FRP rod method for shear strengthening of RC beams: Performance and comparison with existing techniques. *Journal of Composites for Construction*, 15(3), 374-383. doi: 10.1061/(ASCE)CC.1943-5614.0000174
- Chajes, M. J., Finch, W. W., Januszka, T. F., & Thomson, T. A. (1996). Bond and force transfer of composite material plates bonded to concrete. *ACI Structural Journal*, 93(2), 208-217.
- Charkas, H., Rasheed, H. A., & Melhem, H. (2003). Rigorous procedure for calculating deflections of Fiber-Reinforced Polymer-Strengthened reinforced concrete beams. *ACI Structural Journal*, 100(4).
- Chen, J., & Teng, J. (2001). Anchorage strength models for FRP and steel plates bonded to concrete. *Journal of Structural Engineering*, 127(7), 784-791.
- Chicoine, T. (1997). Conception et analyse d'ancrages sur les poutres renforcées en flexion à l'aide de matériaux composites. Mémoire de maîtrise, Département de génie civil, Université de Sherbrooke, Canada.
- CNR. (2006). Guide for the design and construction of concrete structures reinforced with fiber-reinforced polymer bars. CNR-DT 203/2006. Rome, Italy: Italian National Research Council (CNR).
- Committee, A. (2011). Building code requirements for structural concrete (318-11) and commentary-(318R-11). Detroit Mich. Am. Concr. Inst.
- Darain, K. M., Jumaat, M. Z., Hossain, M. A., Hosen, M. A., Obaydullah, M., Huda, M. N., & Hossain, I. (2015). Automated serviceability prediction of NSM strengthened structure using a fuzzy logic expert system. *Expert Systems with Applications*, 42(1), 376-389.
- Darain, K. M., Jumaat, M. Z., Shukri, A. A., Obaydullah, M., Huda, M. N., Hosen, M. A., & Hoque, N. (2016). Strengthening of RC Beams Using Externally Bonded Reinforcement Combined with Near-Surface Mounted Technique. *Polymers*, 8(7), 261.
- De Lorenzis, L. (2002). *Strengthening of RC structures with near surface mounted FRP rods*. (PhD Thesis), University of Lecce, Italy.
- De Lorenzis, L., & Nanni, A. (2001a). Characterization of FRP rods as near-surface mounted reinforcement. *Journal of Composites for Construction*, 5(2), 114-121.
- De Lorenzis, L., & Nanni, A. (2001b). Shear strengthening of reinforced concrete beams with near-surface mounted fiber-reinforced polymer rods. *ACI Structural Journal*, 98(1), 60-68.
- De Lorenzis, L., & Nanni, A. (2002). Bond between near-surface mounted fiber-reinforced polymer rods and concrete in structural strengthening. *ACI Structural Journal*, 99(2), 123-132.

- De Lorenzis, L., & Teng, J. G. (2007). Near-surface mounted FRP reinforcement: An emerging technique for strengthening structures. *Composites Part B: Engineering*, 38(2), 119-143. doi: <http://dx.doi.org/10.1016/j.compositesb.2006.08.003>
- El-Hacha, R., & Gaafar, M. (2011). Flexural strengthening of reinforced concrete beams using prestressed, near-surface-mounted CFRP bars. *Pci Journal*, 134-151.
- El-Hacha, R., & Rizkalla, S. H. (2004). Near-surface-mounted fiber-reinforced polymer reinforcements for flexural strengthening of concrete structures. *ACI Structural Journal*, 101(5), 717-726.
- El-Hacha, R., & Rizkalla, S. H. (2004). Near-surface-mounted fiber-reinforced polymer reinforcements for flexural strengthening of concrete structures. *ACI Structural Journal*, 101(5).
- El-Mihilmy, M. T., & Tedesco, J. W. (2000). Deflection of reinforced concrete beams strengthened with fiber-reinforced polymer (FRP) plates. *ACI Structural Journal*, 97(5).
- EN, B. (2009). 12390-3: 2009 Testing hardened concrete. Making and curing specimens for strength tests., ISBN, 940137696.
- EN, B. (2009). 12390-5:2009. Flexural Strength of Test Specimens. *Testing Hardened Concrete*, 1-14.
- Eshwar, N., Nanni, A., & Ibell, T. J. (2008). Performance of two anchor systems of externally bonded fiber-reinforced polymer laminates. *ACI Materials Journal*, 105(1), 72-80.
- Euro Code 2. (2004). Eurocode 2: Design of Concrete Structures: Part 1-1: General Rules and Rules for Buildings: British Standards Institution.
- Fanning, P. J., & Kelly, O. (2001). Ultimate response of RC beams strengthened with CFRP plates. *Journal of Composites for Construction*, 5(2), 122-127.
- Ferrier, E., Larbi, A. S., Georgin, J., & Ambroise, J. (2012). New hybrid cement-based composite material externally bonded to control RC beam cracking. *Construction and Building Materials*, 36, 36-45.
- fib. (2001). Externally bonded FRP reinforcement for RC structures Bulletin (Vol. 14, pp. 138). Switzerland: fédération internationale du béton (fib).
- Frosch, R. J. (1999). Another look at cracking and crack control in reinforced concrete. *ACI Structural Journal*, 96, 437-442.
- GangaRao, H. V. S., Vijay, P. V., & Taly, N. (2006). Frequently Asked Questions about Composite Materials *Reinforced Concrete Design with FRP Composites* (pp. 1-18): CRC Press.
- Gao, D., Benmokrane, B., & Masmoudi, R. (1998). A Calculating Method for Flexural Properties of FRP-reinforced Concrete Beam: Department of Civil Engineering, Faculty of Engineering, University of Sherbrooke.
- Garden, H., Hollaway, L., & Thorne, A. (1997). A preliminary evaluation of carbon fibre reinforced polymer plates for strengthening reinforced concrete members. *Proceedings of the Institution of Civil Engineers. Structures and buildings*, 122(2), 127-142.

- Gergely, P., & Lutz, L. A. (1973). Maximum crack width in reinforced concrete flexural members. *ACI Special Publication*, 20, pp. 87-117.
- Godat, A., L'hady, A., Chaallal, O., & Neale, K. (2012). Bond Behavior of the ETS FRP Bar Shear-Strengthening Method. *Journal of Composites for Construction*, 16(5), 529-539.
- Gopalaratnam, V. S., & Gettu, R. (1995). On the characterization of flexural toughness in fiber reinforced concretes. *Cement and Concrete Composites*, 17(3), 239-254.
- Grelle, S. V., & Sneed, L. H. (2013). Review of anchorage systems for externally bonded FRP laminates. *International Journal of Concrete Structures and Materials*, 7(1), 17-33.
- Güler, K., Demir, F., & Pakdamar, F. (2012). Stress–strain modelling of high strength concrete by fuzzy logic approach. *Construction and Building Materials*, 37, 680-684.
- Haghani, R., Al-Emrani, M., & Kliger, R. (2008). Effect of tapering on interfacial stresses in adhesive joints without adhesive fillet. Paper presented at the Fourth International Conference on FRP Composites in Civil Engineering (CICE 2008).
- Hassan, T. (2002). *Flexural performance and bond characteristics of FRP strengthening techniques for concrete structures*. PhD thesis, University of Manitoba, Winnipeg, Manitoba, Canada.
- Hassan, T., & Rizkalla, S. (2002). Flexural strengthening of prestressed bridge slabs with FRP systems. *Pci Journal*, 47(1), 76-93.
- Hassan, T., & Rizkalla, S. (2003). Investigation of bond in concrete structures strengthened with near surface mounted carbon fiber reinforced polymer strips. *Journal of Composites for Construction*.
- Hassan, T. K., & Rizkalla, S. H. (2004). Bond mechanism of near-surface-mounted fiber-reinforced polymer bars for flexural strengthening of concrete structures. *ACI Structural Journal*, 101(6).
- Hassan, T. K., & Rizkalla, S. H. (2004). Bond mechanism of near-surface-mounted fiber-reinforced polymer bars for flexural strengthening of concrete structures. *ACI Structural Journal*, 101(6), 830-839.
- Hassanen, M. A., & Raoof, M. (2001). Design against premature peeling failure of RC beams with externally bonded steel or FRP plates. *Magazine of Concrete Research*, 53(4), 251-262.
- Hawileh, R. A., Rasheed, H. A., Abdalla, J. A., & Al-Tamimi, A. K. (2014). Behavior of reinforced concrete beams strengthened with externally bonded hybrid fiber reinforced polymer systems. *Materials & Design*, 53, 972-982.
- Hillerborg, A., Modéer, M., & Petersson, P.-E. (1976). Analysis of crack formation and crack growth in concrete by means of fracture mechanics and finite elements. *Cement and concrete research*, 6(6), 773-781.
- Hollaway, L. (2010). A review of the present and future utilisation of FRP composites in the civil infrastructure with reference to their important in-service properties. *Construction and Building Materials*, 24(12), 2419-2445.

- Hollaway, L. C., & Leeming, M. (1999). *Strengthening of reinforced concrete structures: Using externally-bonded FRP composites in structural and civil engineering*: Elsevier.
- Hollaway, L. C., & Teng, J.-G. (2008). *Strengthening and rehabilitation of civil infrastructures using fibre-reinforced polymer (FRP) composites*: Elsevier.
- Hosen, M. A., Jumaat, M. Z., Alengaram, U. J., Islam, A., & bin Hashim, H. (2016). Near Surface Mounted Composites for Flexural Strengthening of Reinforced Concrete Beams. *Polymers*, 8(3), 67.
- Hosen, M. A., Jumaat, M. Z., Darain, K. M. U., Obaydullah, M., & Islam, A. S. (2014). *Flexural Strengthening of RC Beams with NSM Steel Bars*. Paper presented at the IICBE International Conference, Kuala Lumpur, Malaysia. www.iicbe.org
- Hosen, M. A., Jumaat, M. Z., & Islam, A. (2015). Inclusion of CFRP-Epoxy Composite for End Anchorage in NSM-Epoxy Strengthened Beams. *Advances in Materials Science and Engineering*, 2015.
- Hossain, A., Rahman, A., & Mohiuddin, A. (2012). Fuzzy evaluation for an intelligent air-cushion tracked vehicle performance investigation. *Journal of Terramechanics*, 49(2), 73-80.
- Hu, H.-T., Lin, F.-M., & Jan, Y.-Y. (2004). Nonlinear finite element analysis of reinforced concrete beams strengthened by fiber-reinforced plastics. *Composite Structures*, 63(3), 271-281.
- Irani, Z., & Kamal, M. M. (2014). Intelligent systems research in the construction industry. *Expert Systems with Applications*, 41(4), 934-950.
- Jalali, M., Sharbatdar, M. K., Chen, J.-F., & Alaei, F. J. (2012). Shear strengthening of RC beams using innovative manually made NSM FRP bars. *Construction and Building Materials*, 36, 990-1000.
- Jang, J., Sun, C. T., & Mizutani, E. (1997). *Neuro-fuzzy and soft computing*. 1997. PTR Prentice Hall.
- Jeong, S.-M. (1994). *Evaluation of ductility in prestressed concrete beams using fiber reinforced plastic tendons*: University of Michigan.
- Kalayci, A. S., Yalim, B., & Mirmiran, A. (2010). Construction tolerances and design parameters for NSM FRP reinforcement in concrete beams. *Construction and Building Materials*, 24(10), 1821-1829. doi: 10.1016/j.conbuildmat.2010.04.022
- Kalfat, R., Al-Mahaidi, R., & Smith, S. T. (2011). Anchorage devices used to improve the performance of reinforced concrete beams retrofitted with FRP composites: State-of-the-art review. *Journal of Composites for Construction*, 17(1), 14-33.
- Kaur, A., & Kaur, A. (2012). Comparison of Mamdani-Type and Sugeno-Type Fuzzy Inference System for Air Conditioning System. *International Journal of Soft Computing and Engineering*, 2(2), 2231-2307.
- Kotynia, R. (2012). Bond between FRP and concrete in reinforced concrete beams strengthened with near surface mounted and externally bonded reinforcement. *Construction and Building Materials*, 32, 41-54.

- Kotynia, R., Abdel Baky, H., Neale, K. W., & Ebead, U. A. (2008). Flexural strengthening of RC beams with externally bonded CFRP systems: Test results and 3D nonlinear FE analysis. *Journal of Composites for Construction*, 12(2), 190-201.
- Kupfer, H., Hilsdorf, H. K., & Rusch, H. (1969). Behavior of concrete under biaxial stresses. Paper presented at the ACI Journal proceedings.
- Lim, D. H. (2009). Combinations of NSM and EB CFRP strips for flexural strengthening of concrete structures. *Magazine of Concrete Research*, 61(8), 633-643. doi: 10.1680/mac.2008.61.8.633
- Lim, D. H. (2010). Shear behaviour of RC beams strengthened with NSM and EB CFRP strips. *Magazine of Concrete Research*, 62(3), 211-220. doi: 10.1680/mac.2010.62.3.211
- Lousdad, A., Megueni, A., & Bouchikhi, A. (2010). Geometric edge shape based optimization for interfacial shear stress reduction in fiber reinforced polymer plate retrofitted concrete beams. *Computational Materials Science*, 47(4), 911-918.
- Lu, X., Teng, J., Ye, L., & Jiang, J. (2007). Intermediate crack debonding in FRP-strengthened RC beams: FE analysis and strength model. *Journal of Composites for Construction*, 11(2), 161-174.
- Maalej, M., & Bian, Y. (2001). Interfacial shear stress concentration in FRP-strengthened beams. *Composite Structures*, 54(4), 417-426.
- Mamdani, E. H., & Assilian, S. (1975). An experiment in linguistic synthesis with a fuzzy logic controller. *International journal of man-machine studies*, 7(1), 1-13.
- Maruyama, K., & Ueda, T. (2001). JSCE design recommendations for upgrading of RC members by FRP sheet. *Proc. FRPRCS-5—Fibre-Reinforced Plastics for Reinforced Concrete Structures*, 441-446.
- Meier, U., & Kaiser, H. (1991). Strengthening of structures with CFRP laminates. Paper presented at the Advanced composites materials in civil engineering structures.
- Mendel, J. M. (1995). Fuzzy logic systems for engineering: a tutorial. *Proceedings of the IEEE*, 83(3), 345-377.
- Mohamed Ali, M. S., Oehlers, D. J., & Seracino, R. (2006). Vertical shear interaction model between external FRP transverse plates and internal steel stirrups. *Engineering Structures*, 28(3), 381-389. doi: <http://dx.doi.org/10.1016/j.engstruct.2005.08.010>
- Mohammadhassani, M., Jumaat, M. Z., Jameel, M., Badiiee, H., & Arumugam, A. M. (2012). Ductility and performance assessment of high strength self compacting concrete (HSSCC) deep beams: An experimental investigation. *Nuclear Engineering and Design*, 250, 116-124.
- Mostofinejad, D., & Shamel, S. M. (2013). Externally bonded reinforcement in grooves (EBRIG) technique to postpone debonding of FRP sheets in strengthened concrete beams. *Construction and Building Materials*, 38, 751-758. doi: 10.1016/j.conbuildmat.2012.09.030
- Motavalli, M., & Czaderski, C. (2007). FRP composites for retrofitting of existing civil structures in Europe: state-of-the-art review. Paper presented at the International Conference of Composites & Polycon., American Composites Manufacturers Association. Tampa, FL, USA.

- Muhamad, R., Mohamed Ali, M., Oehlers, D., & Griffith, M. (2010). The tension stiffening mechanism in reinforced concrete prisms. *Int J Adv Struct Eng*, submitted for publication.
- Nardone, F., Lignola, G. P., Prota, A., Manfredi, G., & Nanni, A. (2011). Modeling of flexural behavior of RC beams strengthened with mechanically fastened FRP strips. *Composite Structures*, 93(8), 1973-1985.
- Nasrollahzadeh, K., & Basiri, M. M. (2014). Prediction of shear strength of FRP reinforced concrete beams using fuzzy inference system. *Expert Systems with Applications*, 41(4), 1006-1020.
- Nilson, A. H. (1982). *State-of-the-art report on finite element analysis of reinforced concrete*. New York, NY: American Society of Civil Engineers: Task Committee on Finite Element Analysis of Reinforced Concrete Structures of the Structural Division Committee on Concrete and Masonry Structures, ASCE.
- Nordin, H., & Täljsten, B. (2006). Concrete beams strengthened with prestressed near surface mounted CFRP. *Journal of Composites for Construction*, 10(1), 60-68.
- Obaidat, Y. (2011). *Structural retrofitting of concrete beams using FRP-debonding issues*. Lund University.
- Ochsendorf, J. (2005). Sustainable engineering: The future of structural design. Paper presented at the Proc., Structures Congress and the Forensic Engineering Symp.: Metropolis and Beyond.
- Oehlers, D. J. (1992). Reinforced concrete beams with plates glued to their soffits. *Journal of Structural Engineering*, 118(8), 2023-2038.
- Oehlers, D. J., Mohamed Ali, M., Haskett, M., Lucas, W., Muhamad, R., & Visintin, P. (2010). FRP-Reinforced concrete beams: unified approach based on IC theory. *Journal of Composites for Construction*, 15(3), 293-303.
- Oller, E., Cobo, D., & Mari, A. (2011). Laminate debonding process of FRP-strengthened beams. *Structure and Infrastructure Engineering*, 7(1-2), 131-146.
- Oudah, F., & El-Hacha, R. (2012). A new ductility model of reinforced concrete beams strengthened using Fiber Reinforced Polymer reinforcement. *Composites Part B: Engineering*, 43(8), 3338-3347. doi: 10.1016/j.compositesb.2012.01.071
- Oudah, F., & El-Hacha, R. (2012). A new ductility model of reinforced concrete beams strengthened using Fiber Reinforced Polymer reinforcement. *Composites Part B-Engineering*, 43(8), 3338-3347. doi: 10.1016/j.compositesb.2012.01.071
- Parretti, R., & Nanni, A. (2004). Strengthening of RC members using near-surface mounted FRP composites: Design overview. *Advances in Structural Engineering*, 7(6), 469-483.
- Passino, K. M., Yurkovich, S., & Reinfrank, M. (1998). *Fuzzy control (Vol. 42)*: Citeseer.
- Rahal, K. N., & Rumaih, H. A. (2011). Tests on reinforced concrete beams strengthened in shear using near surface mounted CFRP and steel bars. *Engineering Structures*, 33(1), 53-62. doi: 10.1016/j.engstruct.2010.09.017

- Rahimi, H., & Hutchinson, A. (2001). Concrete beams strengthened with externally bonded FRP plates. *Journal of Composites for Construction*, 5(1), 44-56.
- Rahman, M. M., Jumaat, M. Z., Rahman, M. A., & Qeshta, I. M. (2015). Innovative hybrid bonding method for strengthening reinforced concrete beam in flexure. *Construction and Building Materials*, 79, 370-378.
- Rajasekaran, S., & Pai, G. V. (2011). *Neural networks, Fuzzy logic and Genetic algorithms*: PHI Learning Private Limited.
- Rasheed, H. A., Harrison, R. R., Peterman, R. J., & Alkhrdaji, T. (2010). Ductile strengthening using externally bonded and near surface mounted composite systems. *Composite Structures*, 92(10), 2379-2390. doi: 10.1016/j.compstruct.2010.03.009
- Razaqpur, A. G., Shedid, M., & Petrina, D. (2011). Behavior of beams strengthened with novel self-anchored near-surface-mounted CFRP bars. *Journal of Composites for Construction*, 15(4), 625-634. doi: 10.1061/(ASCE)CC.1943-5614.0000183
- Reed, M. W., Barnes, R. W., Schindler, A. K., & Lee, H.-W. (2005). Fiber-reinforced polymer strengthening of concrete bridges that remain open to traffic. *ACI Structural Journal*, 102(6), 823.
- Ritchie, P. A., Thomas, D. A., Lu, L.-W., & Connelly, G. M. (1991). External reinforcement of concrete beams using fiber reinforced plastics. *ACI Structural Journal*, 88(4).
- Ritchie, P. A., Thomas, D. A., Lu, L.-W., & Connelly, G. M. (1990). External reinforcement of concrete beams using fiber-reinforced plastics.
- Rizkalla, S., & Hassan, T. (2001). Various FRP strengthening techniques for retrofitting concrete structures. Paper presented at the CICE 2001 Conference proceedings.
- Rosenboom, O., & Rizkalla, S. (2006). Behavior of prestressed concrete strengthened with various CFRP systems subjected to fatigue loading. *Journal of Composites for Construction*, 10(6), 492-502.
- Saxena, P., Toutanji, H., & Noumowe, A. (2008). Failure analysis of FRP-strengthened RC beams. *Journal of Composites for Construction*, 12(1), 2-14.
- Şen, Z. (2010). Rapid visual earthquake hazard evaluation of existing buildings by fuzzy logic modeling. *Expert Systems with Applications*, 37(8), 5653-5660.
- Sena-Cruz, J. (2005). Strengthening of concrete structures with near-surface mounted CFRP laminate strips.
- Sena-Cruz, J., & Barros, J. A. (2004). Modeling of bond between near-surface mounted CFRP laminate strips and concrete.
- Sena-Cruz, J. M., Barros, J. A. O., Coelho, M. R. F., & Silva, L. F. F. T. (2012). Efficiency of different techniques in flexural strengthening of RC beams under monotonic and fatigue loading. *Construction and Building Materials*, 29, 175-182. doi: 10.1016/j.conbuildmat.2011.10.044
- Sharaky, I. A., Torres, L., Baena, M., & Vilanova, I. (2013). Effect of different material and construction details on the bond behaviour of NSM FRP bars in concrete. *Construction and Building Materials*, 38, 890-902. doi: 10.1016/j.conbuildmat.2012.09.015

- Shehata, I., Cerqueira, E., Pinto, C., & Shehata, L. (2001). Strengthening of RC beams in flexure and shear using CFRP laminate. Thomas Tetford London, 97-106.
- Shukla, K. (2000). Neuro-genetic prediction of software development effort. *Information and Software Technology*, 42(10), 701-713.
- Sikadur®-30. Product Data Sheet-Adhesive for bonding reinforcement. Retrieved May 21, 2016, from: <https://mys.sika.com/dms/...get/...e6dc.../Sikadur-30%202011-10_1.pdf>.
- Smith, S. T., & Teng, J. (2002a). FRP-strengthened RC beams. I: review of debonding strength models. *Engineering Structures*, 24(4), 385-395.
- Smith, S. T., & Teng, J. (2002b). FRP-strengthened RC beams. II: assessment of debonding strength models. *Engineering Structures*, 24(4), 397-417.
- Soliman, S. M., El-Salakawy, E., & Benmokrane, B. (2010). Flexural behaviour of concrete beams strengthened with near surface mounted fibre reinforced polymer bars. *Canadian Journal of Civil Engineering*, 37(10), 1371-1382.
- Spadea, G., Bencardino, F., & Swamy, R. (1998). Structural behavior of composite RC beams with externally bonded CFRP. *Journal of Composites for Construction*, 2(3), 132-137.
- Sun, Z., Wu, G., Wu, Z., & Luo, Y. (2011). Flexural strengthening of concrete beams with near-surface mounted steel-fiber-reinforced polymer composite bars. *Journal of Reinforced Plastics and Composites*, 0731684411427209.
- Sun, Z. Y., Wu, G., Wu, Z. S., & Luo, Y. B. (2011). Flexural strengthening of concrete beams with near-surface mounted steel-fiber-reinforced polymer composite bars. *Journal of Reinforced Plastics and Composites*, 30(18), 1529-1537. doi: 10.1177/0731684411427209
- Swamy, R., Jones, R., & Bloxham, J. (1987). Structural behaviour of reinforced concrete beams strengthened by epoxy-bonded steel plates. *Structural Engineer. Part A*, 65, 59-68.
- Täljsten, B. (1994). Plate bonding strengthening of existing concrete structures with epoxy bonded plates of steel or fibre reinforced plastics.
- Teng, J., De Lorenzis, L., Wang, B., Li, R., Wong, T., & Lam, L. (2006). Debonding failures of RC beams strengthened with near surface mounted CFRP strips. *Journal of Composites for Construction*, 10(2), 92-105.
- Teng, J., Smith, S. T., Yao, J., & Chen, J. (2003). Intermediate crack-induced debonding in RC beams and slabs. *Construction and Building Materials*, 17(6), 447-462.
- Thomsen, H., Spacone, E., Limkatanyu, S., & Camata, G. (2004). Failure mode analyses of reinforced concrete beams strengthened in flexure with externally bonded fiber-reinforced polymers. *Journal of Composites for Construction*, 8(2), 123-131.
- Toutanji, H., Zhao, L., & Zhang, Y. (2006). Flexural behavior of reinforced concrete beams externally strengthened with CFRP sheets bonded with an inorganic matrix. *Engineering Structures*, 28(4), 557-566. doi: <http://dx.doi.org/10.1016/j.engstruct.2005.09.011>
- Triantafillou, T. C. (1998). Shear strengthening of reinforced concrete beams using epoxy-bonded FRP composites. *ACI Structural Journal*, 95(2).

- Triantafillou, T. C., & Plevris, N. (1992). Strengthening of RC beams with epoxy-bonded fibre-composite materials. *Materials and Structures*, 25(4), 201-211.
- Tsai, M., & Morton, J. (1995). The effect of a spew fillet on adhesive stress distributions in laminated composite single-lap joints. *Composite Structures*, 32(1), 123-131.
- Ulaga, T., Vogel, T., & Meier, U. (2003). Bilinear stress-slip bond model: theoretical background and significance. FRPRCS-6-Fibre-reinforced polymer reinforcement for concrete structures.
- Van Gemert, D. (1980). Force transfer in epoxy bonded steel/concrete joints. *International Journal of Adhesion and Adhesives*, 1(2), 67-72.
- Wahab, N., Soudki, K. A., & Topper, T. (2010). Mechanism of bond behavior of concrete beams strengthened with near-surface-mounted CFRP rods. *Journal of Composites for Construction*, 15(1), 85-92.
- Wang, C., & Salmon, C. (1992). *Reinforced concrete design*, 5, 1992: Harper and Row, New York.
- Wight, R., Green, M., & Erki, M. (2001). Prestressed FRP sheets for poststrengthening reinforced concrete beams. *Journal of Composites for Construction*, 5(4), 214-220.
- Wu, G., Wu, Z.-S., Luo, Y.-B., Sun, Z.-Y., & Hu, X.-Q. (2010). Mechanical properties of steel-FRP composite bar under uniaxial and cyclic tensile loads. *Journal of Materials in Civil Engineering*, 22(10), 1056-1066.
- Yost, J. R., Gross, S. P., Dinehart, D. W., & Mildenberg, J. J. (2007). Flexural behavior of concrete beams strengthened with near-surface-mounted CFRP strips. *ACI Structural Journal*, 104(4).
- Yost, J. R., Gross, S. P., Dinehart, D. W., & Mildenberg, J. J. (2007). Flexural behavior of concrete beams strengthened with near-surface-mounted CFRP strips. *ACI Structural Journal*, 104(4), 430-437.
- Zadeh, L. A. (1965). Fuzzy sets. *Information and control*, 8(3), 338-353.
- Zhao, J., & Bose, B. K. (2002). Evaluation of membership functions for fuzzy logic controlled induction motor drive. Paper presented at the IECON 02 [Industrial Electronics Society, IEEE 2002 28th Annual Conference of the].
- Zheng, S.-j., Li, Z.-q., & Wang, H.-t. (2011). A genetic fuzzy radial basis function neural network for structural health monitoring of composite laminated beams. *Expert Systems with Applications*, 38(9), 11837-11842.
- Ziraba, Y., Baluch, M., Basunbul, I., Sharif, A., Azad, A., & Al-Sulaimani, G. (1994). Guidelines toward the design of reinforced concrete (RC) beams with external plates. *Structural Journal*, 91(6), 639-646.